Investigation of RNA degradation in the cyanobacterium *Synechocystis* sp. PCC6803

Inaugural - Dissertation

zur Erlangung des

Doktorgrades der Naturwissenschaften

doctor rerum naturalium

(Dr. rer. nat.)

des Fachbereichs Biologie und Chemie

der Justus- Liebig - Universität Gießen

vorgelegt von

Olga Siadat

1. Gutachter/in: PD Dr. Elena Evguenieva-Hackenberg

Institut für Mikrobiologie und Molekularbiologie

Justus - Liebig - Universität Gießen

2. Gutachter/in: Prof. Dr. Annegret Wilde

Institut für Molekulare Genetik

Albert-Ludwigs-Universität Freiburg

Selbständigkeitserklärung

Ich erkläre: Ich habe die vorgelegte Dissertation selbstständig und ohne unerlaubte fremde Hilfe und nur mit den Hilfen angefertigt, die ich in der Dissertation angegeben habe. Alle Textstellen, die wörtlich oder sinngemäß aus veröffentlichten Schriften entnommen sind, und alle Angaben, die auf mündlichen Auskünften beruhen, sind als solche kenntlich gemacht. Ich stimme einer evtl. Überprüfung meiner Dissertation durch eine Antiplagiat-Software zu. Bei den von mir durchgeführten und in der Dissertation erwähnten Untersuchungen habe ich die Grundsätze guter wissenschaftlicher Praxis, wie sie in der „Satzung der Justus-Liebig-Universität Gießen zur Sicherung guter wissenschaftlicher Praxis“ niedergelegt sind, eingehalten.

_____

Bad Nauheim, den 11.06.2016

Table of contents

Abstract

Cyanobacteria occupy very diverse habitats with rapidly changing environmental conditions, which forces them to develop effective response mechanisms in order to survive. Post-transcriptional control of gene expression, which is mostly determined by the function of regulatory RNA molecules and the RNA degradation apparatus, provides an important mechanism for adaptation to environmental demands. Investigation of major players in RNA degradation and maturation in the model cyanobacterium *Synechocystis* sp. PCC6803, namely homologs of RNase E/G (Rne) and RNase III (Rnc2), was the main focus of the present work. As RNA chaperone Hfq, which facilitates otherwise imperfect sRNA-mRNA base pairing, functions as a post-transcriptional regulator of gene expression in many bacteria, we also studied two Hfq-dependent sRNAs Hpr8 and Hpr10 with a closer look on their degradation patterns.

In order to clarify protein-RNA interactions between studied RNases and their possible RNA targets *in vivo* a genome wide analysis of binding sites for Rne and Rnc2 was performed using individual-nucleotide resolution crosslinking and immunoprecipitation (iCLIP) combined with Solexa high-throughput sequencing. This novel approach confirmed that Rne binds to the stem loop structure in the 5' UTR of *rne* gene and therefore most likely regulates its own synthesis in a similar manner as it has been shown for *E. coli*. Discovery of Rne binding sites within the rRNA precursor between 23S and 5S rRNAs led to the assumption that the maturation of 5S rRNA in *Synechocystis* is analogous to the one in *E. coli*. Conducted *in vitro* cleavage assays and a 3' RACE experiment substantiated this hypothesis and proved the accuracy of results provided by iCLIP method. We also revealed interaction of Rne with a number of sRNAs. *In vitro* cleavage assays were performed to verify Rne-dependent processing of some of the putative targets. Interestingly, we could see a clear pattern in Rne interaction with tRNAs: analysis of the location of the binding site determined that Rne always binds to the anticodon loop of tRNAs; an additional binding site at the variable loop of some tRNAs was also discovered.

Evaluation of Rnc2 binding properties was completed by implementing iCLIP approach as well. Detection of Rnc2 binding sites within rRNAs and tRNAs suggested involvement of this RNase in maturation of their precursors in *Synechocystis* as it has been shown for other bacteria. We could also observe that the two studied RNases Rne and Rnc2 in some cases have binding sites mapped to the same transcripts and therefore might act together. In addition we could demonstrate using *in vitro* cleavage assays that the sRNA Hpr10 is a true substrate for Rnc2. iCLIP experiment revealed a binding site next to a long double-stranded region within this sRNA, where processing most likely occurs. In summary, we could show that the iCLIP method can be used for the study of RNase-RNA interactions in bacteria. Verification of iCLIP data using *in vitro* assays confirmed that several RNAs are true targets of the respective RNases. Clearly, more comprehensive studies are needed in the future to analyse the specific functions of these ribonucleases in post-transcriptional gene regulation.

Zusammenfassung

Cyanobakterien besiedeln sehr vielfältige Habitate, in denen sich Umweltbedingungen sehr schnell ändern können. Dadurch sind Cyanobakterien gezwungen effektive Mechanismen zu entwickeln um sich an die jeweiligen Bedingungen anzupassen. Die posttranskriptionale Regulation der Genexpression, welche überwiegend durch kleine regulatorische RNAs und RNA-Abbau bestimmt wird, stellt einen Mechanismus für die Anpassung an umweltbedingte Veränderungen dar. Die Untersuchung der wesentlichen Enzyme beim RNA-Abbau und der RNA-Reifung im Modelcyanobakterium *Synechocystis* sp. PCC6803, Homologe von RNase E/G (Rne) und RNase III (Rnc2), stellt den Kern dieser Arbeit dar. Da in vielen Bakterien das RNA-Chaperon Hfq eine wichtige Rolle für die posttranskriptionale Regulation der Genexpression durch kleine nicht-kodierende RNAs hat, wurden in dieser Arbeit auch die zwei Hfq-abhängigen sRNAs, Hpr8 and Hpr10, vor allem bezüglich ihres Degradationsmuster näher untersucht.

Für die Darstellung der RNA-Proteininteraktionen zwischen untersuchten RNasen und deren möglichen RNA-Zielen wurde eine genomweite Analyse der Bindungsstellen von Rne und Rnc2 *in vivo* - unter Verwendung der Methode der *Individual Nucleotide Resolution Crosslinking* und *Immunoprecipitation* (iCLIP), kombiniert mit Solexa-High-Throughput-Sequenzierung- durchgeführt. Dieser neuartige Untersuchungsansatz bestätigte, dass Rne an eine Stem-Loop-Struktur der 5' UTR der *rne* mRNA bindet und daher sehr wahrscheinlich die eigene Synthese in einer ähnlichen Weise, wie auch bei *E. coli* bekannt, reguliert. Die Entdeckung von Rne-Bindungsstellen in rRNA-Vorstufen zwischen den 23S und 5S rRNAs führte zur Annahme, dass die Reifung der 5S rRNA in *Synechocystis* analog zu *E. coli* ist. Die durchgeführten *in vitro* Untersuchungen zur Prozessierung der rRNA und ein 3'-RACE-Experiment bestätigten die vorgenannte Hypothese und die Genauigkeit der Ergebnisse, welche durch die iCLIP-Methode erlangt wurden. Zudem wurde eine potenzielle Interaktion zwischen Rne und einigen sRNAs identifiziert und durch *in vitro* Untersuchungen belegt. Interessanterweise wurde ein deutliches Muster in potenziellen Rne-Interaktionen mit tRNAs deutlich: Die Analyse offenbarte, dass Rne an die Antikodon-Schleife verschiedener tRNAs bindet; eine zusätzliche Bindungsstelle an der variablen Schleife einiger tRNAs wurde ebenfalls postuliert.

Die iCLIP-Methode wurde auch für die Identifizierung von Rnc2-RNA-Bindestellen verwendet. Die detektierten Rnc2-Bindungsstellen in rRNAs und tRNAs legen die Beteiligung der RNase III an der Reifung dieser Produkte in *Synechocystis*, wie dies bereits für andere Bakterien bekannt ist, nahe. In dieser Arbeit wird auch ersichtlich, dass die RNasen Rne und Rnc2 teilweise an die gleichen Transkripte binden und daher sehr wahrscheinlich gemeinsam an der Prozessierung verschiedener RNAs beteiligt sind. Zusätzlich wurde durch *in vitro*-RNA-Spaltung verifiziert, dass die sRNA Hpr10 ein Substrat für Rnc2 darstellt. Die iCLIP-Untersuchungen haben gezeigt, dass eine RNase-Bindungsstelle neben einer langen doppelsträngigen Region in der sRNA besteht, dort, wo die Prozessierung sehr wahrscheinlich stattfindet.

Zusammenfassend lässt sich festhalten, dass die iCLIP-Methode erfolgreich für die Untersuchung von RNase-RNA Interaktionen in Bakterien verwendet werden

kann. Die Verifizierung von iCLIP-Daten unter Verwendung der *in vitro*-Spaltungsuntersuchungen hat bestätigt, dass einige RNAs echte Ziele der untersuchten RNasen sind. Sicherlich sind zukünftig noch weitere umfassende Analysen erforderlich, um die spezifischen Funktionen der hier untersuchten Ribonukleasen in der post-transkriptionalen Genregulation besser zu verstehen.

List of abbreviations and symbols

<	less than
>	more than
^{0}C	degree Celsius
xg	times gravity
APC	allophycocyanin
approx.	approximately
APS	ammonium persulfate
AR	arginine-rich
asRNA	antisense RNA
ATPase	adenosine triphosphatase
bp	base pair
BCIP	5-bromo-4-chloro-3-indolyl phosphate
BL	blue light
BSA	bovine serum albumin
ca.	circa
cAMP	cyclic adenosine monophosphate
CBCR	cyanobacteriochrome
c-di-GMP	cyclic diguanylate
cDNA	complementary DNA
CDS	coding DNA sequence
cis-ncRNA	*Cis*-encoded ncRNA
CLIP	crosslinking and immunoprecipitation
cm	centimetre
Cm	Chloramphenicol
cpm	counts per minute
Cy3	cyanine dye
DMSO	dimethyl sulfoxide
DNA	deoxyribonucleic acid
DNase	deoxyribonuclease
DOC	sodiumdesoxycholate
ds	double-stranded
DTT	dithiothreitol
DUF	domain with unknown function
E. coli	*Escherichia coli*
EDTA	ethylenediaminetetraacetate
et al.	*et alia* (and others)
EtBr	ethidium bromide
FC	fold change
FPLC	fast protein liquid chromatography
FT	flow through
fw	forward
g	gram
Gent	Gentamicin
GST	glutathione-S-transferase
h	hour(s)
HEPES	4-(2-hydroxyethyl)-1-piperazineethanesulfonic acid
His	polyhistidine-tag
HITS	thigh-throughput sequencing
HL	high light
iCLIP	individual-nucleotide resolution crosslinking and immunoprecipitation

IPTG	isopropyl β-D-1-thiogalactopyranoside
kb	kilobases
kDA	kilodalton
Km	Kanamycin
l	liter
LB	lysogeny broth
M	molar
m	milli (10^{-3})
mA	milliampere
MEME	multiple Em for motif mlicitation
MEN	MOPS-EDTA-Natrium acetate buffer
min	minute(s)
miRNA	microRNA
MOPS	3-(N-morpholino) propanesulfonic acid
mRNA	messenger RNA
n	nano (10^{-9})
NBT	nitro blue tetrazolium
ncRNA	non-coding RNA
NL	normal light
nt	nucleotide(s)
OD	optical density
ORF	open reading frame
PAA	polyacrylamide
PAGE	polyacrylamide gel electrophoresis
PAZ	Piwi Argounaute Zwille
PC	phycocyanin
PCC	Pasteur Culture Collection
PCR	polymerase chain reaction
pH	*potentia Hydrogenii*
PK	proteinase K
PNK	polynucleotide kinase
PNPase	polynucleotide phosphorylase
RIII	RNase III domain
RACE	*rapid amplification of cDNA ends*
RBD	RNA-binding domain
RBP	RNA-binding protein
RBS	ribosome-binding site
rev	reverse
RIP	RNA immunoprecipitation
RL	red light
RNA	ribonucleic acid
RNase	ribonuclease
rpm	rounds per minute
rRNA	ribosomal RNA
RT	room temperature or reverse transcriptase
RT-PCR	reverse transcription-PCR
S. typhimurium	*Salmonella typhimurium*
S. aureus	*Staphylococcus aureus*
SDS	sodium dodecyl sulphate
sec	second(s)
seq	sequencing
sp.	species
sRNA	small RNA

SSC	saline-sodium citrate
Strep	Streptomycin
TBE	Tris/Borat/EDTA buffer
TBS	*Tris-buffered saline*
TBS-T	Tris-Buffered Saline buffer with Tween 20
TCA	trichloroacetic acid
TEMED	N,N,N´,N´-tetramethylene-diamine
TES	2-[[1,3-dihydroxy-2-(hydroxymethyl)propan-2-yl]amino]ethanesulfonic acid
trans-ncRNA	*Trans*-encoded ncRNA
Tricine	N-[Tris(hydroxymethyl)methyl]glycine
Tris	Tris(hydroxymethyl)aminomethane
tRNA	transfer RNA
TU	transcriptional unit
Tween 20	Polyoxyethylenesorbitan monolaurate
U	unit(s)
UTR	untranslated region
UV	ultraviolet
V	volt
V. anguillarum	*Vibrio anguillarum*
v/v	volume per volume
w/v	weight per volume
WCL	whole cell lysate
WT	wild type
ycf	hypothetical chloroplast open reading frame
α	alpha
β	beta
β-DM	n-dodecyl-β-D-maltoside
µ	micro (10^{-6})
γ	gamma
Δ	delta, without/lacking

1. Introduction

1.1 Overview

Cyanobacteria are Gram-negative bacteria that represent one of the oldest prokaryotic phyla and date back to approx. 3,5 billion years before present. They are responsible for oxygenation of the atmosphere and contributed to what is called the "Great Oxygenation Event" that occurred approx. 2,32 billion years ago (Schirrmeister *et al.*, 2011). Cyanobacteria occupy highly diverse marine, freshwater and terrestrial habitats, are capable of oxygenic photosynthesis and nitrogen fixation, which makes them major players in carbon and nitrogen turnover in aquatic environment (Whitton, 2012). Cyanobacteria are model organisms for studying photosynthesis and carbon and nitrogen assimilation. One of the best-studied representatives of this group is *Synechocystis* sp. PCC6803 (hereafter *Synechocystis*) that was isolated from a freshwater lake in California in 1968 by R. Kunisawa (Stanier *et al.*, 1971). It is a freshwater cyanobacterium capable of both phototrophic growth by oxygenic photosynthesis in the light and chemotrophic growth by glycolysis and oxidative phosphorylation during dark periods (Anderson and McIntosh, 1991). *Synechocystis* exhibits twitching motility (Stanier *et al.*, 1971) and is able to move towards or away from the light source with the help of type IV pili (Bhaya, 2004). Due to its natural competence for transformation *Synechocystis* is easy to manipulate genetically (Grigorieva and Shestakov, 1982). It was the first photosynthetic organism whose genome was completely sequenced (Kaneko *et al.*, 1996). The genome consists of multiple copies of the chromosome (3,57 Mbp in size), four large (44-120 kbp in size) and three small (2,3-5,2 kbp in size) plasmids (Kaneko *et al.*, 2003). All these properties made *Synechocystis* a model organism for the study of photosynthesis and gene regulation.
A rapidly changing environment pushes bacteria to develop quick responses to various conditions that in many cases are facilitated by post-transcriptional regulation on the level of RNA. Post-transcriptional control of gene expression is mostly determined by RNA degradation mechanisms. Prokaryotic mRNAs generally have shorter average half-lives than eukaryotic ones. It has been shown that average mRNA half-life for the cyanobacterium *Prochlorococcus* is as short as 2,4 minutes (Steglich *et al.*, 2010). RNA turnover has been vastly studied in *E. coli* and *Bacillus subtilis* (Arraiano *et al.*, 2010; Silva *et al.*, 2011); however, less is known about RNA degradation in cyanobacteria.

1.2 Ribonucleases: intriguing enzymes with dual function

RNA in bacteria is subjected to cleavage during either maturation, as in case of ribosomal RNA (rRNA), transfer RNA (tRNA) and some non-coding RNA (ncRNA), or degradation. Both processes are performed by ribonucleases (RNases). Many RNases are essential for cell viability, but there are also some RNases, whose functions overlap making them dispensable for the cell (Arraiano *et al.*, 2010). It is common to distinguish two major classes of RNases: exo- and endoribonuleases. The former digest RNA molecules one by one nucleotide from

the ends, the latter perform cleavage of RNA transcripts internally. For a long time it was thought that exoribonucleases in eubacteria degrade RNA only in 3' to 5' direction (Zuo and Deutscher, 2001). However, detailed investigation of RNA degradation machinery of *B. subtilis* revealed existence of a unique enzyme RNase J1, which possesses both endo- and 5'-to-3' exonucleolytic activity with the preference towards non- or monophosphorylated RNA (Mathy *et al*., 2007). Orthologs of this essential for *B. subtilis* RNase are widely spread among bacteria and archaea, including cyanobacteria (Even *et al*., 2005). This work however is focused on endoribonucleases, main of which are described in more detail below.
RNases are major contributors to post-transcriptional regulation of gene expression. RNA turnover provides basis for rapid adaptation to challenging growth conditions and insures versatility in conditions of small prokaryotic genome (Silva *et al.*, 2011). It is common for RNA decay in bacteria to follow the principle "all-or-none", meaning that after the initial rate-determining cleavage occurs, RNA molecule is being quickly degraded via joint action of endo- and exoribonucleases (Laalami *et al.,* 2014). This is not the case however for processing of polycistronic transcripts and maturation of rRNA and tRNA, where primary transcripts are being cleaved by RNases in order to obtain its mature functional form.
In many cases multiple RNases act together and the sequence of processing steps might then be determined simply by which enzyme binds and therefore cleaves first. Therefore two identical RNA molecules can undergo different order of cleavage events depending on which RNase acts first. However, frequently the structure of the precursor determines which enzyme cuts first depending on the specificity of the RNase. For instance, the presence of secondary structure at the 5' end of 16S rRNA precursor determines that maturation of the 3' end occurs first, leading to the release of double-stranded stem structure covering RNase E cleavage site at position +66 in the 5' region of the precursor. Only then single-strand specific RNase E is able to complete maturation of the 5' termini (Deutscher, 2015).
RNases are not only in charge of processing and decay of RNA molecules, they also function as RNA quality control instruments. In *E. coli* mRNAs containing premature stop codons are being cleaved by RNase E internally due to the exposure of cleavage sites as a result of premature release of ribosomes. The defective mRNAs are subsequently being degraded by other RNases (Baker and Mackie, 2003). Improperly folded tRNAs are also being eliminated. In this case degradation of defective tRNAs occurs at the precursor level and requires polyadenylation of the transcript to provide proper binding site for the RNase. Main players in this process are exoribonucleases RNase R and polynucleotide phosphorylase (PNPase) (Li *et al*., 2002). These two enzymes are also responsible for removal of mutant rRNAs in order to avoid accumulation of abnormal ribosomes (Cheng and Deutscher, 2003).
It is logical that RNases, being such a powerful tool in RNA metabolism, have to be strictly controlled. There are several ways developed by the cells to coordinate the activity of RNases, which include autoregulation of RNase E and RNase III, cross-regulation of PNPase and RNase II, and regulation of RNases by environmental conditions (Jain and Belasco, 1995; Bardwell *et al.*, 1989; Zilhão

et al., 1996; Silva *et al.*, 2011). Some of these control mechanisms are discussed in more detail below.

1.2.1 RNase E: a key player in RNA turnover in *E. coli*

Among 21 RNases found till now in *E. coli* RNase E plays an essential role in all aspects of RNA metabolism (Mackie, 2013). Analysis of RNase E activity *in vivo* using tiling microarrays showed that absence of RNase E leads to the change in steady-state levels of 60% of the annotated coding sequences and of at least 75% annotated ncRNAs in *E. coli* (Stead *et al.*, 2011). It has been shown that RNase E is in charge of rRNA processing, tRNA maturation and that cleavage of mRNA is also one of the essential functions of RNase E (Apirion and Lassar, 1978; Misra and Apirion, 1979; Li *et al.*, 1999; Li and Deutscher, 2002; Ow and Kushner, 2002; Hammarlöf *et al.*, 2015).

1.2.1.1 Structure of RNase E

RNase E in *E. coli* is an essential endoribonuclease that cleaves single-stranded RNA in AU-rich regions (McDowall *et al.*, 1994). It does not show any specific sequence preference, however, guanosine two nucleotides upstream of the cleavage site enhances reactivity (McDowall *et al.*, 1994; Redko *et al.*, 2001). The 1061 residues large RNase E protein can be divided into an N-terminal catalytic domain and a C-terminal scaffold domain. The amino-terminal part (residues 1-529) is in charge of the endonuclease activity; it is essential for viability and is highly conserved in prokaryotes including cyanobacteria (Kaberdin *et al.*, 1998). Crystal structure of the N-terminal half revealed that it consists of a large domain (residues 1-400), a Zn-link (residues 401-414) and a small domain (residues 415-529) (Figure 1); the monomers form a homotetramer, which is a dimer of dimers (Callaghan *et al.*, 2005a). Disruption of the tetramer leads to the loss of RNase E activity (Callaghan *et al.*, 2005b). The catalytic domain also possesses a 5'-sensing pocket, formed by Arg169, Thr170 and Val28, which facilitates formation of hydrogen bonds between the enzyme and its 5'-monophosphorylated RNA substrate and triggers a conformational change in the enzyme. This allows accommodation of the RNA substrate in the active site of RNase E, which is necessary for cleavage (Callaghan *et al.*, 2005a; Koslover *et al.*, 2008; Garrey *et al.*, 2009). As the downstream products of RNase E cleavage are monophosphorylated at the 5' end, the ability of the enzyme to sense 5' monophosphates aids to distinguish primary transcripts from the ones that have undergone at least one cleavage.
In contrast to the N-terminal domain the C-terminal half of RNase E (residues 530-1061) is unstructured and poorly conserved (Callaghan *et al.*, 2004). It is also dispensable for cell viability (Kido *et al.*, 1996). This non-catalytic domain aids interaction between RNase E and RNA, other proteins or cell components. Segment-A (residues 568-582) is in charge of binding of RNase E to the inner cytoplasmic membrane (Khemici *et al.*, 2008). The arginine-rich (AR) segment (residues 601-700) is responsible for RNA binding *in vitro* (Ow *et al.*, 2000). Residues 701-1061 comprise a region that contains binding sites for the major degradosome components, such as DEAD-box RNA helicase RhlB (residues 734-

738), glycolytic enzyme enolase (residues 739-845), and 3'-5' exoribonuclease PNPase (residues 844-1045) (Figure 1) (Vanzo *et al.*, 1998).

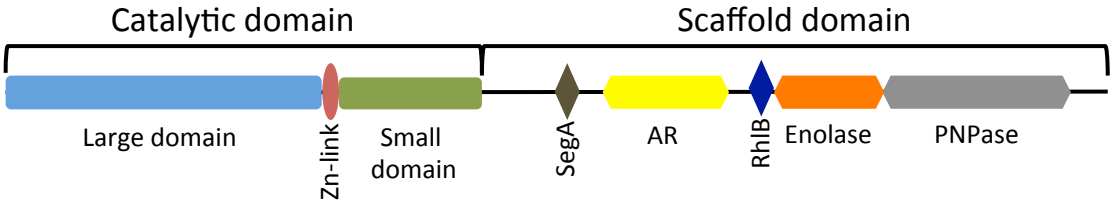

Figure 1: Schematic representation of the domain organization of RNase E in *E. coli*
Large and small domains together with Zn-link comprise the N-terminal catalytic half. The C-terminal scaffold domain consists of the membrane-binding region (Segment-A), an RNA-binding (arginine-rich) segment and binding sites for degradosome components (RhlB, enolase and PNPase).

The degradosome represents a multienzyme complex, in which the cooperative work of endo- and exoribonucleases together with RNA helicase aids rapid and effective degradation of RNA (Coburn *et al.*, 1999). Interestingly, under different growth conditions the composition of the degradosome may change resulting in multiple isoforms with interchangeable protein components, that affects RNA target spectrum of each particular isoform (Prud'homme-Genereux *et al.*, 2004; Gao *et al.*, 2006). Degradosomes have been found in various bacteria. For instance, *Rhodobacter capsulatus* possesses a degradosome that contains two DEAD-box RNA helicases and a transcription termination factor Rho (Jäger *et al.*, 2001); in *Pseudomonas syringae* PNPase is substituted by another exoribonuclease RNase R (Purusharth *et al.*, 2005). However, there is till now no evidence of degradosome existence in *Synechocystis*, which is probably explained by the structure of its RNase E homolog (see section 1.3.1).
RNase E homologs can be divided into five enzyme types according to their structure (Lee and Cohen, 2003; Ait-Bara and Carpousis, 2015). Type I enzymes are similar in their primary structure to *E. coli* RNase E and possess a highly conserved N-terminal catalytic domain as well as a small domain that is necessary for the formation of the tetrameric holoenzyme. Type I RNase E homologs are ubiquitous in cyanobacteria and are also found in β- and ϒ-proteobacteria. Type II enzymes are very similar to type I enzymes but they contain an arginine-proline-rich region of approx. 60 to 180 residues as part of the large domain of the catalytic half. This type of RNase E homologs is characteristic for α-proteobacteria. Type III RNase E homologs are found in actinobacteria and contain the same elements as type I enzymes with the difference that their catalytic domain is flanked by relatively long N- and C-terminal extensions. They are actually more similar to RNase G of *E. coli* that represents the class IV of RNase E homologs, but unlike the latter they are able to form multienzyme complexes (Lee and Cohen, 2003). Type V enzymes are present in the chloroplast of many plants and resemble the structure of type II RNase E homologs with the addition of an N-terminal extension, which includes a chloroplast transit peptide (Ait-Bara and Carpousis, 2015).

1.2.1.2 Mode of action of RNase E

RNase E has two major modes of action: the first one involves recognition of the 5'-monophosphorylated end of an RNA substrate; the second pathway bypasses this requirement and is therefore called "direct entry" (Figure 2).

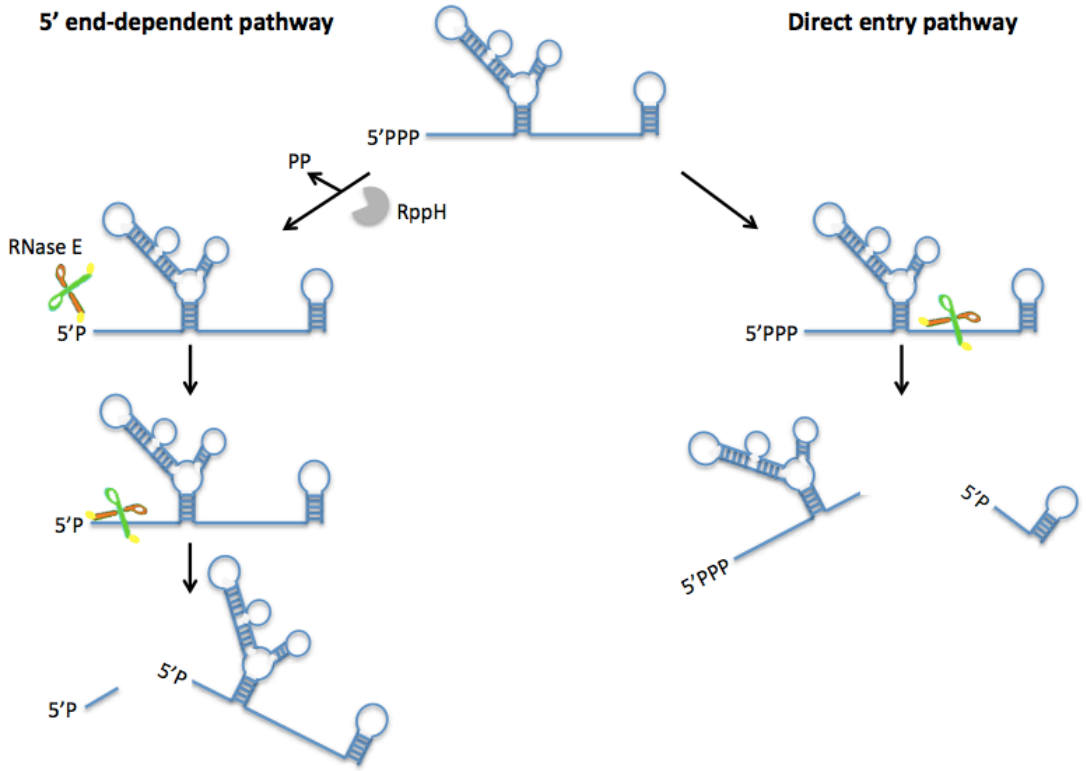

Figure 2: RNase E cleavage pathways
5' end-dependent pathway (left panel): the triphosphate at the 5' end of the RNA molecule is converted to monophosphate by RppH; 5' monophosphate is being recognized by the 5' sensing pocked of RNase E (yellow circle); RNA is getting cleaved.
Direct entry pathway (right panel): RNase E recognizes a single-stranded region within RNA in a 5'-independent manner and RNA is getting cleaved.

Preference of RNase E towards 5'-monophosphorylated substrates in comparison to transcripts with 5' triphosphorylated ends can be explained by the presence of the 5' sensing pocket in the catalytic domain (see section 1.2.1.1). This structure is too shallow to accommodate triphosphorylated substrates and therefore RNA molecules with a monophosphate at the 5' end are identified and cleaved. Binding to the RNA substrate increases the catalytic activity of RNase E (Garrey *et al.*, 2009). *E. coli* possesses a pyrophosphohydrolase RppH that converts RNA 5' triphosphates to 5' monophosphates and initiates mRNA decay (Figure 2, left panel) (Celesnik *et al.*, 2007; Deana *et al.*, 2008). RppH is not essential for cell viability, however deletion mutants exhibit an increase in half-lives of a subset of mRNAs (Deana *et al.*, 2008). It has also been shown that

mutation in Arg169 of the 5' sensing pocked leading to the loss of 5'-monophosphate-stimulated RNase E activity is dispensable *in vivo*; mutant cells however display a decline in doubling time and colony size combined with accumulation of immature 5S rRNA (Garrey *et al.*, 2009). These findings suggest that the 5' end-dependent pathway is not essential.
Another mechanism of RNase E cleavage, the so called direct entry pathway, does not require presence of the 5' monophosphate group (Figure 2, right panel). RNase E is able to recognize multiple single-stranded segments within RNA (in addition to the region in which cleavage occurs) and interacts with two or more of them facilitating rapid cleavage of RNA in a 5' end-independent manner (Kime *et al.*, 2009). Direct entry is central for maturation of tRNA in *E. coli* and is mediated by specific adjacent single-stranded regions within the precursor. Cleavage at a site on the 5' side of precursors generates a cascade of 5' monophosphate-dependent cleavage events (Kime *et al.*, 2014). However, the direct entry pathway is not limited to tRNA maturation, playing a role in mRNA and rRNA decay as well, and therefore can be considered as a major pathway for RNA processing and degradation in *E. coli* (Clarke *et al.*, 2014).

1.2.1.3 Localization of RNase E

As mentioned in section 1.2.1.1, the non-catalytic domain of RNase E contains Segment A that serves as a membrane anchor. Together with flanking proline-rich regions it facilitates tethering of N- and C-terminal parts of RNase E to the inner cytoplasmic membrane (Khemici *et al.*, 2008). The N-terminal half of RNase E alone can interact with anionic liposomes. It encompasses four putative membrane-binding sites: amino acids 20-40, 111-160, 216-279, and 280-400. These positively charged regions mediate RNase E – membrane interaction. Binding of RNase E to the membrane triggers change in protein's secondary structure and leads to increased enzymatic activity, heightened affinity to RNA substrates and stabilization of protein structure, preventing thermally induced unfolding (Murashko *et al.*, 2012). Some of the other RNases, such as RNase III and RNase P, were shown to associate with RNase E on the inner membrane which suggests that RNA degradation and processing are compartmentalized in bacteria (Miczak *et al.*, 1991; Khemici *et al.*, 2008). Membrane binding is a common feature among RNase E homologs including Rne of *Synechocystis* (Murashko *et al.*, 2012).

1.2.1.4 Regulation of RNase E activity

As RNase E is a key player in RNA turnover in *E. coli* levels of its cellular concentration and activity are subject to complex regulation. Excess of RNase E can be toxic for the cells. That is why it is of vital importance to have effective mechanisms of its regulation. RNase E is able to regulate its own synthesis by controlling the degradation rate of its mRNA. Due to such autoregulation the half-life of RNase E mRNA varies from 40 seconds to 8 minutes depending on enzyme activity in the cell. What is more, the 5' untranslated region (5' UTR) of the gene is essential for RNase E-mediated cleavage of its message (Jain and Belasco, 1995). The 5' UTR of mRNA encoding RNase E in *E. coli* is 361 nucleotide

long and contains six RNA secondary structure elements, two of which (simple stem-loop hp2 and branched stem-loop hp3) contribute to feedback regulation of RNase E gene expression (Diwa *et al.*, 2000). It has been shown that RNase E binds directly to the hp2 stem-loop in the 5' UTR of RNase E coding gene and facilitates cleavage elsewhere in the RNase E gene transcript (Schuck *et al.*, 2009). Besides autoregulation RNase E activity is also affected by protein inhibitors, which directly interact with the C-terminal half of the enzyme. Such regulatory proteins include ribosomal protein L4, regulator of RNase activity A (RraA) and RraB (Singh *et al.*, 2009; Gao *et al.*, 2006; Lee *et al.*, 2003). These regulators control RNase E activity during altered growth conditions and provide acute stress response (Mackie, 2013). Efficiency of RNase E cleavage also depends on the structure of its RNA substrate including accessibility of cleavage sites and monophosphorylated 5' ends (Mackie, 1998). RNase E activity towards specific mRNA targets is mediated by binding to RNA chaperone Hfq and small RNAs (sRNAs) (Wagner *et al.*, 2002). This type of regulation of RNase E action is discussed in more detail in section 1.4.3.

1.2.2 RNase G – a "light" version of RNase E in *E. coli*

RNase G is an endoribonuclease that is paralogous to RNase E, but in comparison to the latter is not essential in *E. coli* (Wachi *et al.*, 1991; Li *et al.*, 1999). It has 49.5% amino acid sequence similarity and 34.1% sequence identity to the N-terminal catalytic region of RNase E (McDowall *et al.*, 1993). However, RNase G possesses only a short non-catalytic C-terminal extension and lacks a small domain (that is in charge of a tetramer formation) characteristic to RNase E. RNase G cannot form a tetramer as RNase E does and functions as a dimer (Briant *et al.*, 2003). Due to partial relation in structure of these two enzymes there have been attempts to confer the viability of RNase E deletion mutants by overexpression of RNase G in *E. coli* (Lee *et al.*, 2002). Nevertheless, further studies showed that it is not possible to complement strains lacking RNase E with RNase G, which is probably due to inability of RNase G to process tRNA (Ow *et al.*, 2003). RNase G participates in degradation of several mRNAs including the ones that are part of glycolysis (Lee *et al.*, 2002). RNase G and RNase E share similar properties *in vitro* and are both necessary for 16S rRNA maturation (Li *et al.*, 1999; Wachi *et al.*, 1999). RNase G cleaves RNA in AU-rich regions and has a high preference for monophosphate at the 5' end of its substrate (Tock *et al.*, 2000). Stimulation of cleavage by 5' monophosphate is a result of enhanced substrate binding (Jourdan and McDowall, 2008). RNA-seq data revealed that RNase G has a prominent role in initial cleavage of some transcripts by removing the 5' end (Clarke *et al.*, 2014).

1.2.3 RNase III – a double strand-specific endoribonuclease

RNase III was the first discovered endoribonuclease that specifically targets double-stranded RNA (dsRNA) in *E. coli* (Robertson *et al.*, 1968). It generates monophosphates at the 5' end and a hydroxyl group with a two-base overhang at the 3' end of cleaved transcripts (Meng and Nicholson, 2008). It is dispensable for cell viability in *E. coli*; however, RNase III deletion mutants exhibit a slow

growth phenotype and accumulation of 30S rRNA precursors (Studier, 1975; Babitzke *et al.*, 1993). On the other hand, in *B. subtilis* RNase III is essential and cannot be knocked out (Herskovitz and Bechhofer, 2000). RNase III plays an important role in tRNA and rRNA maturation. In *E. coli* it processes the 30S rRNA precursor to 16S and 23S rRNA (Babitzke *et al.*, 1993). In α-ptoteobacteria the pattern of rRNA cleavage by RNase III is different and includes processing of intervening sequences in helix 9 of 23S rRNA (Evguenieva-Hackenberg and Klug, 2000). RNase III is also involved in degradation of mRNA as well as small RNAs (sRNAs) (Babitzke *et al.*, 1993; Drider and Condon, 2004; Stead *et al.*, 2011). Involvement of RNase III in sRNA-modulated regulation of gene expression is discussed in more detail in section 1.4.3. Analysis of a deletion mutant of RNase III using tiling microarray analysis revealed that 12% annotated coding sequences and 22% annotated non-coding RNAs (ncRNAs) in *E. coli* show significant fold change in the mutant. Affected coding sequences include genes involved in cysteine metabolism, iron transport, enterobactin production and in the heat shock pathway. However, it is possible that observed changes in mRNA abundance are secondary effects caused by changes in the steady-state levels of regulatory sRNAs. Interestingly, there was an overlap between the transcripts affected by the absence of RNase III and RNase E: changes in RNA abundance shared by both mutants constituted 10% of the coding sequences and 21% of annotated ncRNAs. This points out possible cooperation between these two major ribonucleases in *E. coli* (Stead *et al.*, 2011). Ability of RNase III to remove protective stem-loop structures makes it an effective regulator of gene expression. Similarly to RNase E RNase III can control its own synthesis by cleaving its message near the 5' end. This removal of the stem-loop structure promotes decay of RNase III mRNA (Bardwell *et al.*, 1989; Matsunaga *et al.*, 1996). Interestingly, autoregulation of PNPase in *E. coli* also requires presence of RNase III (Portier *et al.*, 1987). Another way of regulation of gene expression by RNase III involves sRNAs, as antisense RNA (asRNA)-mRNA duplexes are optimal substrates for RNase III cleavage (see section 1.4.3) (Viegas and Arraiano, 2008). What is more, RNase III can regulate gene expression not only by dsRNA-cleaving, but also as a dsRNA-binding protein, in which case it binds to RNA substrates in a site-specific manner, but does not process it (Dasgupta *et al.*, 1998; Blaszczyk *et al.*, 2004).

1.2.3.1 Structure of RNase III

RNase III belongs to the most conserved RNases throughout the eubacterial kingdom (Condon and Putzer, 2002). Endoribonucleases comprising RNase III family could be divided into four classes according to their polypeptide structure (Blaszczyk *et al.*, 2001; Olmedo and Guzman, 2008). Members of class 1 possess a dsRNA-binding domain (dsRBD) at the C-terminal region and a catalytic domain called RNase III domain (RIII) at the N-terminus. Catalytic domain contains a 9 amino acid signature motif ERLEFLGDS (Blaszczyk *et al.*, 2001). Class 1 RNase III homologs are ubiquitous in bacteria, bacteriophages and some fungi (MacRae and Doudna, 2007). RNase III is active as a homodimer and dimerization of the catalytic domains is necessary for enzyme's activity (Gan *et al.*, 2006). Class 2 of RNase III family is exemplified by Drosha protein from *Drosophila melanogaster*.

It is comprised of an N-terminal extension, followed by two RIII domains and one dsRBD (Filippov *et al.*, 2000). Members of class 3, represented by human Dicer protein, have the most complex structure. It encompasses an ATPase/helicase domain at the N terminus, a domain with unknown function (DUF 283), a Piwi Argounaute Zwille (PAZ) domain and two RIII domains together with dsRBD characteristic for class 2 enzymes (Fillipov *et al.*, 2000; MacRae and Doudna, 2007). Class 4 of RNase III homologs is represented by Mini-RNase III of *B. subtilis*. This enzyme lacks dsRBD and possesses only the RIII catalytic domain and is involved in 23S rRNA maturation (Redko *et al.*, 2008). Interestingly, Mini-RNase III homologs were found recently in cyanobacteria including *Synechocystis* (Cameron *et al.*, 2015).

1.2.3.2 Mode of action of RNase III

Substrate selection and site-specific cleavage are necessary determinants of effective and precise functioning of RNA processing and maturation machineries. In case of RNase III substrate selectivity is dictated by the combination of structural and sequence elements called reactivity epitopes. They include helix length, internal loops and bulges. Base pair sequence elements also take part in substrate selectivity. Occurrence of specific nucleotide pairs located at positions -4, -5 and -6 (referred to as proximal box) and at positions -11 and -12 (termed distal box) relative to the cleavage site was proven to influence cleavage. By comparing multiple RNase III substrates it was observed that certain nucleotides are excluded from proximal and distal boxes and if they are placed in these positions via mutagenesis the cleavage rate by RNase III decreases in *E. coli* due to weakened substrate affinity (Zhang and Nicholson, 1997; Pertzev and Nicholson, 2006). In other words reactive sites are determined by the absence of specific inhibitory sequences within proximal and distal boxes while other RNA regions are protected by those inhibitory sequences.
As mentioned above RNase III functions as a dimer, in which each monomer contains four RNA binding motifs (Zhang *et al.*, 2004). Two dsRBDs are in charge of substrate binding whereas RIII domains facilitate substrate specificity (Gan *et al.*, 2006). Typical dsRNA substrates are cleaved at both strands with each catalytic site cutting one strand of dsRNA substrate. The distance between the two cleavage sites is responsible for creating a two-nucleotide overhang at the 3' end (Zhang *et al.*, 2004).

1.3 RNA degradation and maturation machinery of *Synechocystis*

The RNA turnover and maturation machinery of *Synechocystis* combines components of RNA maturation and degradation systems of *E. coli* and *B. subtilis*. The genome of this model cyanobacterium contains genes that resemble high homology to RNase E/G, RNase II/R, RNase J, RNase III (including Mini-III) and PNPase (Rott *et al.*, 2003; Cameron *et al.*, 2015). It is interesting that *Synechocystis* has homologs for both RNase E/G and RNase J, whereas *E. coli* and *B. subtilis*, in which these enzymes were extensively studied, possess only RNase E/G or RNase J respectively. RNase J in *B. subtilis* has functional homology to RNase E in *E. coli*, however, RNase J was the first enzyme shown to possess endo-

and exoribonuclease activity. 5' – 3' exoribonuclease activity has a preference towards 5'-monophosphorylated or 5'-hydroxylated RNA substrates and is more robust (Mathy *et al.*, 2007). In contrast to *B. subtilis* that contains multiple RNase J enzymes, *Synechocystis* carries only a single protein homologous to RNase J; disruption of the gene encoding RNase J is lethal for the cells (Even *et al.*, 2005; Cameron *et al.*, 2015). As cyanobacteria are believed to be the ancestors of chloroplasts of higher plants, there has been a study comparing RNA polyadenylation and degradation mechanisms of cyanobacteria with those in *E. coli* and in the chloroplast. This work revealed that polyadenylation and degradation of RNA in *Synechocystis* is more similar to that in the chloroplast than in *E. coli.* Polyadenylation in *Synechocystis* is performed by PNPase, which is essential for cell viability (Rott *et al.*, 2003). Interestingly, chloroplasts as well as *Synechocystis* contain homologs for both RNase E and RNase J (Sharwood *et al.*, 2011).

1.3.1 RNase E/G of *Synechocystis*

Homologs of RNase E are found in every available cyanobacterial genome (Zhang *et al.*, 2014). In *Synechocystis* RNase E homolog (hereafter Rne) is encoded by *slr1129*, which gene product is 674 amino acids long and has 34,9% identity to the N-terminal catalytic domain (residues 1-498) of *E. coli* RNase E. The highest sequence similarity was observed in two regions corresponding to residues 41-222 in *E. coli* RNase E (residues 37-213 in *Synechocystis* Rne) and residues 278-398 in *E. coli* RNase E (residues 271-391 in *Synechocystis* Rne). The former is responsible for RNA binding and the latter is involved in endonucleotic activity in *E. coli.* Due to this high level of similarity it is possible that corresponding regions in Rne of *Synechocystis* have similar functions (Kaberdin *et al.*, 1998). The N-terminal region of the S*ynechocystis* Rne was shown to interact with the cytoplasmic membrane (Murashko *et al.*, 2012). Two cysteine residues that raise possibility of zinc-link formation were also found in Rne (Horie *et al.*, 2007).
In contrast to the highly conserved N-terminal half, the C-terminal non-catalytic domain of *Synechocystis* Rne is much shorter than the one of *E. coli* and shows no detectable conservation (Kaberdin *et al.*, 1998; Zhang *et al.*, 2014). Nevertheless alignment of protein sequences of all available genomes of cyanobacteria revealed presence of four conserved (C1 – C4) and three variable (V1 – V3) subregions within the C-terminal part of Rne. Motifs C1 (approx. 20 residues) and C2 (approx. 9 residues, highly positively charged) are relatively less conserved, whereas subregions C3 (approx. 50 residues) and C4 (9 residues with the consensus sequence GRRRRRSSA) are found in all cyanobacterial RNase E proteins. The presence of these conserved motifs suggests their importance in enzyme's function. Variable subregions differ a lot among various cyanobacteria implying that they might be involved in some species-specific activities (Zhang *et al.*, 2014). Because of its structure Rne of *Synechocystis* belongs to type I RNase E enzymes according to the classification proposed by Lee and Cohen (Lee and Cohen, 2003). Because Rne of *Synechocystis* has high sequence similarity in its N-terminal region to RNase E of *E. coli* and because Rne as RNase G of *E. coli* lacks the C-terminal scaffold domain the RNase E homolog of *Synechocystis* is commonly called RNase E/G.

Rne is essential for cell viability in *Synechocystis*. It was possible to confer viability of *E. coli* mutants deficient in RNase E via introduction of *Synechocystis* Rne to the cells. Normal maturation of 16S rRNA was also reconstituted by expression of *Synechocystis* Rne in the *rne* and *rng* temperature-sensitive mutants of *E. coli*. These findings prove that Rne can fulfill the functions of RNase E and RNase G in *E. coli* (Horie *et al.*, 2007).
Similar to *E. coli* RNase E and G *Synechocystis* Rne cleaves single-stranded RNA substrates in AU-rich regions *in vitro*. Investigation of cleavage patterns of different substrates also showed that often guanine is present at position -2 relative to the cleavage site or around it. Preference to 5'-monophosphorylated substrates was also observed. It has been shown that Rne participates in light-responsive gene regulation by contributing to mRNA instability in darkness (Horie *et al.*, 2007).
The fact that *Synechocystis* Rne resembles lots of attributes of RNase E of *E. coli* and that *Synechocystis* possesses PNPase (Sll1043), a light-induced DEAD-box helicase (Slr0083) and an enolase (Slr0757) – the main components of RNA degradosome – prompted that *Synechocystis* could also form degradosomes (Kaberdin *et al.*, 1998; Horie *et al.*, 2007). However, when *Synechocystis* Rne was expressed in *E. coli* it was purified without being associated with above-mentioned proteins (Rott *et al.*, 2003). Nevertheless, it has been shown that Rne and PNPase interact with each other. The key element responsible for this interaction is the conserved subregion C4 of the non-catalytic domain of Rne. The last three neutral residues in C4 (SSA) are critical for PNPase recognition by Rne. Association of Rne and PNPase in *Synechocystis* demonstrates tight interconnection between the processes of RNA cleavage (performed by the former), RNA polyadenylation and RNA phosphorolysis (both performed by the latter) where the Rne – PNPase complex acts as a highly effective RNA degradation machine (Zhang *et al.*, 2014).

1.3.2 RNase III of *Synechocystis*

The genome of *Synechocystis* contains two RNase III homologs. One is encoded by *slr0346* (hereafter *rnc1*); the gene product is 244 amino acids long. The second homolog of RNase III encoded by *slr1646* (hereafter *rnc2*) is 231 amino acids long. Both types of RNase III possess one RIII domain and a dsRBD (Cameron *et al.*, 2015). Simultaneous disruption of both RNase III copies is lethal for the cells suggesting importance of this enzyme in the RNA degradation machinery of *Synechocystis*. Mutants in which only one copy of RNase III is deleted are viable and do not show any specific phenotype. Both types of RNase III posses slightly modified RNase III signature motif within N-terminal catalytic domain. For Rnc1 it consists of QQLEFVGDA amino acids and for Rnc2 it is represented by DRLEFLGDA residues (compared to ERLEFLGDS in *E. coli*; Cameron *et al.*, 2015).
Recently a homolog of Mini-RNase III encoded by *slr0954* was found in *Synechocystis*. Mini-RNase III of *Synechocystis* is almost twice as small than a typical RNase III and is comprised of 143 amino acids including a unique motif VALAYLGDA. It also contains one catalytic RIII domain and no dsRBD (Cameron *et al.*, 2015).

1.4 Regulatory noncoding RNAs in bacteria

Bacteria occupy versatile habitats and therefore possess various mechanisms including horizontal gene transfer and relatively high mutation rate to be able to rapidly respond to changing environmental conditions. What is more, bacteria developed an intricate regulatory system that aids successful survival in which ncRNA molecules play a significant role. Regulatory ncRNAs are relatively short (approx. 50 – 300 nucleotides long), and therefore they are also called small RNAs (sRNAs) (Storz *et al.*, 2011). However, recent finding showed that ncRNAs could cover several ORFs and achieve length of 7 kb as in case of *Prochlorococcus* MED4 (Stazic *et al.*, 2011). In most cases sRNAs do not code for any protein and act solely as modulators of various physiological responses. However, some sRNAs possess dual function meaning that besides regulatory role they also encode peptides. One of the examples of such dual function sRNAs is SgrS of *E. coli*. It not only regulates several mRNAs via base pairing but also encodes the SgrT peptide. Interestingly, both SgrS and SgrT are involved in glucose-phosphate stress response (Vanderpool *et al.*, 2011). ncRNAs facilitate rapid adaptation of gene expression by acting at the post-transcriptional level as well as by influencing degradation of target mRNAs. Advantages of regulation by ncRNAs include reduced energy costs for the cell and much faster speed compared to protein-based regulation (Beisel and Storz, 2010). In contrast to ncRNAs that fulfill housekeeping functions (for instance, RNase P RNA that is in charge of tRNA processing, or 4.5S RNA component of the signal recognition particle) regulatory sRNAs are mainly being enforced in response to a particular growth phase or to stress conditions (Kazantsev and Pace, 2006; Wassermann, 2002). Comparative transcriptome analysis of *Synechocystis* under 10 different conditions identified 191 true non-coding transcripts (Kopf *et al.,* 2014b). It is less compared to the previously discovered 429 non-coding transcripts due to protocol modification that reduced false positive results (Mitschke *et al.,* 2011). The vast majority of ncRNAs use base pairing with their mRNA target to regulate gene expression and therefore can be divided into two categories: *cis*- and *trans*-encoded sRNAs.

1.4.1 *Cis*- and *trans*-encoded ncRNAs

Cis-encoded ncRNAs (*cis*-ncRNAs) are highly structured RNA transcripts that are encoded in *cis* on the DNA strand opposite to their target RNA and share extended regions of perfect complementarity to their target (Brantl, 2007). Due to complete complementarity to their sense mRNA, the majority of *cis*-ncRNAs have only one specific target RNA. However, some *cis*-ncRNAs are also able to base pair with other distant mRNAs via limited complementarity (Waters and Storz, 2009).
Trans-encoded ncRNAs (*trans*-ncRNAs) are encoded at a different genomic location from their target mRNA. They share only limited complementarity with their target mRNAs (7-12 nucleotides called “seed region” because of the analogy with cognate regions of eukaryotic microRNAs). This property allows them to regulate multiple RNA targets (Waters and Storz, 2009; Lalaouna *et al.*, 2013; Bartel 2009). Whereas some *cis*-ncRNAs are expressed constitutively, most of the

trans-ncRNAs are highly expressed under specific growth conditions (De Lay *et al.*, 2013). Because of imperfect complementarity between *trans*-ncRNAs and their targets this type of sRNAs frequently (especially for Gram-negative bacteria) requires the help of the RNA-binding protein Hfq (Storz *et al.*, 2011).

1.4.2 RNA chaperone Hfq and its role in ncRNA-mediated regulation

The Hfq protein was first identified in *E. coli* as a host factor, which is needed for replication of RNA bacteriophage Qβ's (Franze de Fernandez *et al.*, 1968). Hfq belongs to Lsm (Sm-like) protein family that is present in all three domains of life. Hfq has a ring-shaped structure and acts as a homomultimer in bacteria (De Lay *et al.*, 2013). Hfq possesses an Sm fold consisting of an N-terminal α-helical domain followed by five antiparallel β strands (Figure 3A). Subunits formed by an Sm fold interact with each other via β4 and β5 strands and form a homohexameric structure in bacteria (Figure 3B) (Khusial *et al.*, 2005).

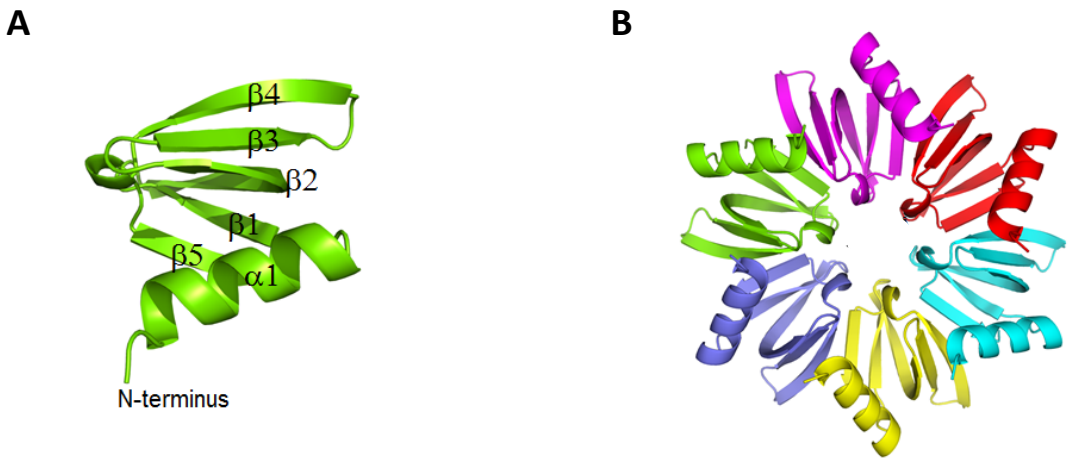

Figure 3: Schematic representation of Hfq structure
(A) Sm fold motif comprised of an α-helix and a 5-stranded β-sheet
(B) Ring-shaped homohexameric structure of bacterial Hfq. Figure from Bøggild *et al.*, 2009.

The doughnut-like shape of the Hfq multimeric complex provides proximal and distal faces to bind RNA. It has been shown that Hfq has a preference towards binding to AU-rich segments of RNA (Møller *et al.*, 2002). In *Staphylococcus aureus* the distal face is predominantly non-polar and the proximal face is highly charged with positively charged residues concentrated at the central pore. This was shown to be the region of binding of poly(U)-rich RNA in *S. aureus* (Schumacher *et al.*, 2002). Another study confirmed that the poly(U) region at the 3' end of sRNA and the adjusted stem-loop (Rho-independent terminator) are essential for Hfq function (Otaka *et al.*, 2011). Therefore, it is highly possible that the proximal face of Hfq protein is in charge for sRNA binding (Zhang *et al.*, 2013). In *E. coli* introduction of mutations in proximal and distal faces of Hfq and studies of the crystal structure of an Hfq-poly(A) RNA complex revealed that poly(A) RNA transcripts bind to the distal face of Hfq using specific binding motifs. Thus, Hfq preferably binds mRNAs at its distal face containing a binding

motif consisting of adenine (A), purine (R) and any nucleotide (N)(Link *et al.*, 2009). The outer rim of the doughnut-shaped Hfq hexamer also participates in RNA binding (Sauer *et al.*, 2012; Zhang *et al.*, 2013). Stoichiometry studies suggest that the Hfq hexamer can bind one sRNA and one mRNA molecule at a time (Updegrove *et al.*, 2011).
Hfq has various functions in bacteria the most important of which in light of sRNA-mediated regulation includes facilitating otherwise imperfect base pairing between *trans*-ncRNAs and their mRNA targets. This can be achieved via promoting changes in the secondary structure of the RNA that provides accessibility to complementary regions or via increasing local concentrations of two interacting RNAs (Morita and Aiba, 2011). What is more, Hfq can stabilize some sRNAs probably because it is able to protect sRNAs that are not paired with their mRNA from degradation by RNase E as both RNase E and Hfq have preference towards AU-rich regions (Moll *et al.*, 2003). Hfq interacts not only with RNAs but also with proteins, for instance, with RNase E. Hfq forms a stable association with the C-terminal scaffold domain of RNase E and facilitates sRNA-mRNA degradation by this endoribonuclease alone or as a part of the degradosome (Morita *et al.*, 2005; Ikeda *et al.*, 2011; De Lay *et al.*, 2013).

1.4.2.1 Hfq protein of *Synechocystis*

The *Synechocystis* Hfq (*Syn*-Hfq) homolog is encoded by *ssr3341* and the protein is 70 amino acids long. Cyanobacterial Hfq orthologs are conserved among cyanobacteria but vary a lot from Hfq proteins of other bacteria (Figure 4A). The most significant sequence difference is seen in the Sm2 motif that forms a part of the RNA interacting surface of the chaperone. Despite a distinct amino acid sequence *Syn*-Hfq still has a homohexameric doughnut-like structure. However, the charge distribution on proximal (more electropositive if compared to *S. aureus* Hfq) and distal sides (electronegative especially in the region of the central pore) does not favor strong RNA binding in the same manner as in *S. aureus* (Figure 4B). In support of this hypothesis *in vivo* experiments showed that *Syn*-Hfq has a very low affinity to known sRNAs from *E. coli* and it is also not able to complement an *E. coli Δhfq* mutant (Bøggild *et al.*, 2009).

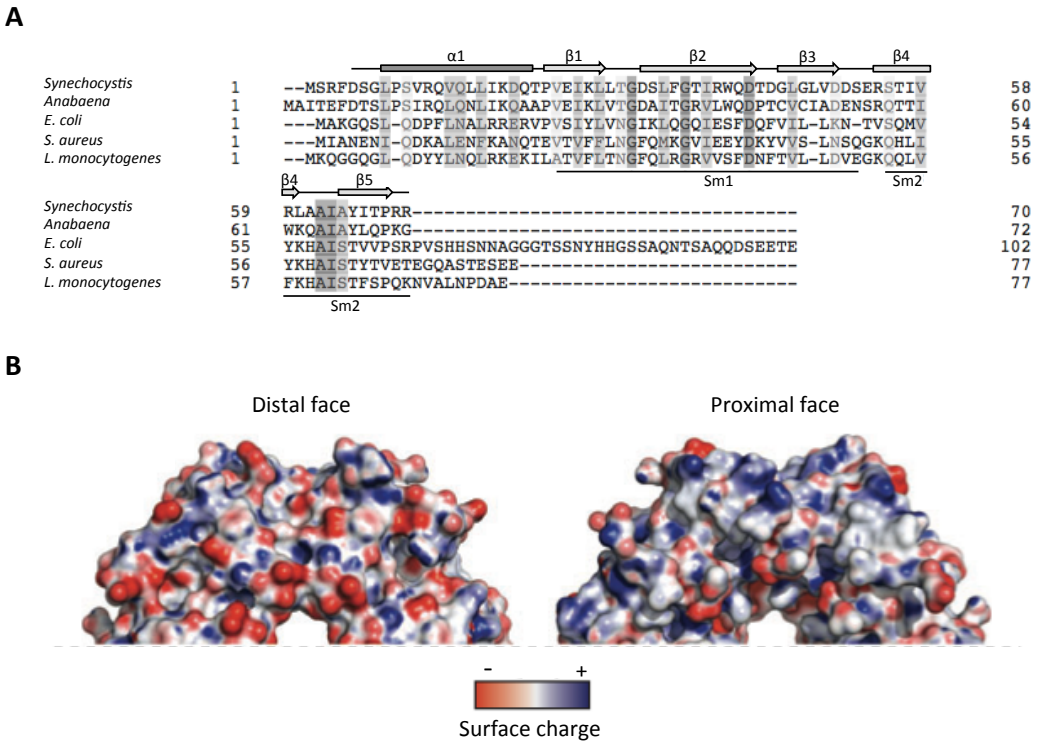

Figure 4: Sequence comparison and surface charge distribution of *Syn*-Hfq
(A) Sequence alignment of *Syn*-Hfq with Hfq orthologs from *Anabaena* sp., *E. coli*, *S. aureus*, and *Listeria monocytogenes*. Sequence similarity is depicted in grey scale. α-helical domain, five β strands as well as Sm1 and Sm2 motifs are marked accordingly. Sequence alignment was performed using Clustal Omega program.
(B) Surface charge distribution on proximal and distal faces of *Syn*-Hfq. Electropositive charges are depicted in blue and electronegative ones in red colour. Figure from Bøggild *et al.*, 2009.

Interestingly, disruption of the *hfq*-coding gene in *Synechocystis* leads to the loss of type IV pili and as a result to a non-transformable and non-motile phenotype (Dienst *et al.*, 2008). No RNA-interacting partners for *Syn*-Hfq have been reported so far. It has been shown, however, that *Syn*-Hfq interacts with the C-terminal domain of the type IV pili secretion ATPase PilB1 (Schürgers *et al.*, 2014).

1.4.3 Mode of action of ncRNAs

The majority of ncRNAs' functions fall under the category of negative regulation. sRNAs are able to attenuate transcription, inhibit translation and facilitate degradation of target mRNAs.
Transcription attenuation is a prerogative of *cis*-encoded antisense RNAs (asRNAs) (Georg and Hess, 2011). An example of such regulation is the differential gene expression in an operon *fatDCBAangRT* in the fish pathogen *Vibrio anguillarum* controlled by the RNAβ RNA (Figure 5). FatD, -C, -B, -A proteins are involved in ferric siderophore transport, AngR and AngT proteins are in charge of synthesis of the siderophore anguibactin. Together they are responsible for virulence of *V. anguillarum.* RNAβ is encoded antisense to the 3'

region of *fatA* and the 5' end of the *angR* gene. Binding of this sRNA to mRNA leads to transcription termination downstream of *fatA.* As a result the transcription level of the smaller *fatDCBA* message accumulates 17-fold higher than the one of the full *fatDCBAangRT* transcript (Figure 5) (Stork *et al.*, 2007).

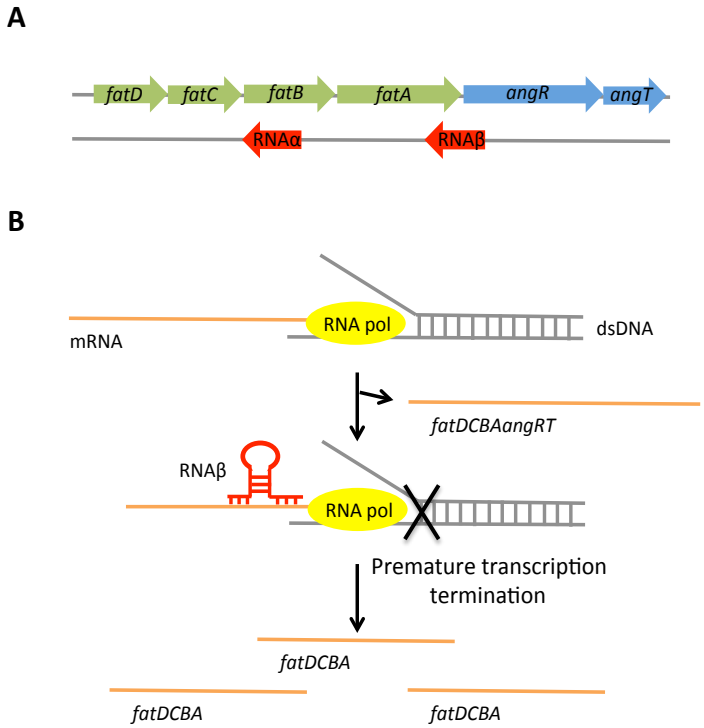

Figure 5: Transcription termination by RNAβ in *Vibrio anguillarum*
(A) Schematic representation of the *fatDCBAangRT* operon with the asRNA RNAβ.
(B) Transcription termination mechanism: in the absence of sRNA full *fatDCBAangRT* message is transcribed; when RNAβ binds to its target mRNA transcription gets prematurely terminated after *fatA* gene resulting in accumulation of shorter *fatDCBA* transcript.

The majority of studied ncRNAs regulate gene expression by blocking the ribosome-binding site (RBS) that leads to translation inhibition of target mRNAs (Lalaouna *et al.*, 2013). sRNAs normally base pair close to the RBS and mask it to prevent 30S ribosomes from initiating translation. However, binding to the regions up to 70 nucleotides upstream or 15 nucleotides downstream of the start codon can also result in blocking of translation (Storz *et al.*, 2011). A prominent example of ncRNA acting via translation inhibition is the *trans*-ncRNA RyhB that negatively regulates multiple mRNAs under iron stress conditions in *E. coli*. Genes that are controlled by RyhB include the ones encoding tricarboxylic acid cycle enzymes (*sdhCDAB, fumA* and *acnA*), superoxide dismutase (*sodB*), and iron storage proteins (*ftnA* and *bfr*). RyhB requires the RNA chaperone Hfq for its activity; it is also repressed by the ferric uptake regulator Fur (Masse and Gottesman, 2002). Under iron limiting conditions Fur is getting inactivated and transcription of RyhB occurs (Figure 6). RyhB then binds to target mRNAs via limited complementarity with the help of Hfq and represses their translation.

mRNA molecules together with sRNAs are then rapidly degraded in an RNase E dependent manner (Masse *et al.*, 2003; Morita *et al.*, 2005). This coupled RNA degradation happens so fast that at first it was not clear whether translation repression or mRNA destabilization causes target gene silencing. However, Morita *et al.* showed that inhibition of translation takes place also without mRNA destabilization and therefore is sufficient for target gene silencing (Morita *et al.*, 2006). What is more, it was demonstrated that blocking translation alone does not lead to *sodB* degradation, proving that collective action of RyhB, Hfq and RNase E is necessary for rapid mRNA degradation. The same study revealed that the RNase E cleavage site is located within *sodB*'s ORF 350 nucleotides downstream from the RyhB binding site. It is remarkable, as in most cases when regulatory sRNA binds in proximity to the RBS, cleavage of mRNA occurs in the nearby region. The authors explain the necessity for such a distant location of the cleavage site as the following: initial RNase E cleavage creates a 5'-monophosphorylated RNA transcript that is degraded very rapidly, therefore initial cleavage in close proximity to the RBS might lead to rapid mRNA degradation before the translation is completed resulting in trapping ribosomes in a prematurely terminated ORF. Distal cleavage site could prevent mRNA degradation before the ribosomes have cleared the upstream part of mRNA (Prevost *et al.*, 2011).

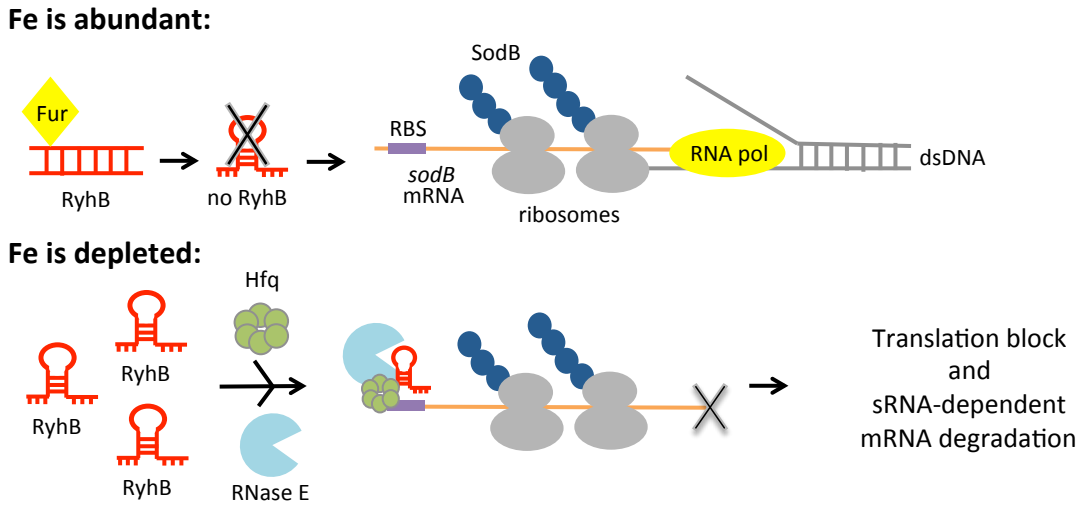

Figure 6: Translation block by RyhB in *E. coli*
Upon iron abundance Fur represses transcription of RyhB and *sodB* mRNA is translated. When iron is limited Fur is deactivated and RyhB production rapidly increases. RyhB forms a ribonucleoprotein complex with Hfq and RNase E, binds to target mRNA and blocks translation, which leads to rapid degradation of mRNA.

Despite that generally sRNA-mediated translation block is enough for gene silencing, it is frequently followed by destabilization of the targeted mRNA. A possible reason for mRNA degradation is to make gene silencing irreversible (Lalaouna *et al.*, 2013). Destabilization of RNA messages can be achieved by exposing cleavage sites, as upon translation inhibition mRNA is getting cleared from the ribosomes which before protected it from nucleolytic attack (Figure 7A) (Wagner, 2009). Another mechanism of sRNA-mediated mRNA degradation

involves increase in local concentration of RNase E near the target mRNA by formation of a ribonucleoprotein complex which includes Hfq, sRNA and RNase E as described above for RyhB. Base pairing of ncRNAs to its target can also actively stimulate RNase E-mediated cleavage. In this case sRNA bound to its target mRNA activates RNase E by presenting its 5'-monophosphorylated end to enzyme's 5' sensing pocket resulting in conformational change facilitating cleavage of the accommodated mRNA (for RNase E structure see section 1.2.1.1). This was proved on the example of MicC-regulated degradation of *ompD* in *Salmonella typhimurium* (Bandyra *et al.*, 2012). MicC is a *trans*-encoded Hfq-dependent ncRNA that downregulates expression of the outer membrane protein OmpC via translation inhibition mechanism (as described above for RyhB) (Vogel and Papenfort, 2006; Pfeiffer *et al.*, 2009). However, it has a second target *ompD*, which also encodes an outer membrane protein. In this case MicC interacts with the coding sequence of *ompD* (codons 23-26) far downstream from the RBS, its 5' end is being recognized by RNase E leading to its activation. As a result the target mRNA is being cleaved downstream of the base pairing region and consequently is rapidly degraded. Hfq is required for optimal RNase E activity (Figure 7B) (Bandyra *et al.*, 2012). Thus, sRNAs are able not only to recruit and guide RNase E, but also to activate the enzyme and promote destabilization of RNA messages.

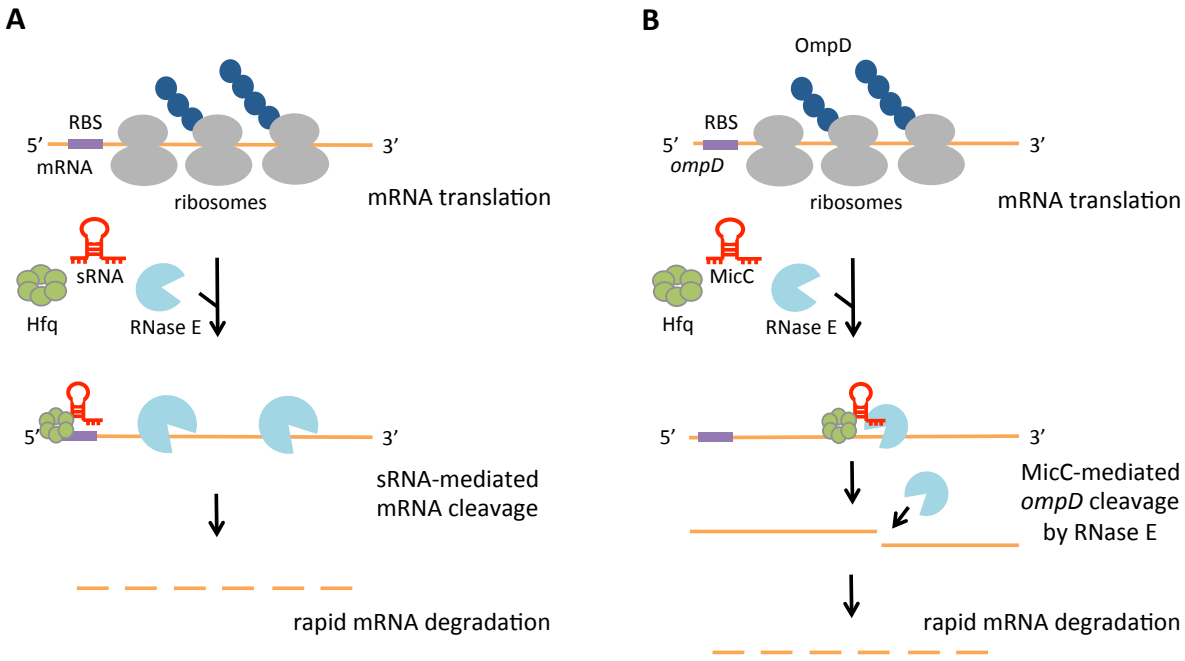

Figure 7: sRNA-mediated destabilization of target mRNAs
(A) Upon binding of sRNA-Hfq-RNase E complex in close proximity to the RBS, translation is being blocked; mRNA is getting cleared from the ribosomes leading to exposure of RNase E cleavage sites and mRNA degradation.
(B) Regulation of *ompD* expression by MicC in *S. typhimurium*: MicC together with Hfq and RNase E binds within the ORF of *ompD*; MicC activates RNase E leading to cleavage of mRNA downstream from the binding site by RNase E and further endo- and exonucleolytic mRNA degradation.

Another example of sRNA-mediated regulation of gene expression leading to destabilization of target mRNA includes IsrR ncRNA of *Synechocystis*. It is a *cis*-ncRNA that is encoded antisense to the gene *isiA.* Its product IsiA is responsible for the formation of antenna ring structure around photosystem I trimer, enhancing absorption of light under iron stress conditions. Because IsrR is fully complementary to its target mRNA, IsrR forms a duplex with *isiA,* which is probably being degraded by RNases (Dühring *et al.*, 2006). Thus, IsiA protein is only being produced once the number of *isiA* mRNA molecules exceeds the number of IsrR transcripts (Legewie *et al.*, 2008). Because of this fine-tuning IsrR prevents premature synthesis of IsiA and aids cells to distinguish between short- and long-term stresses.
ncRNAs are also able to positively regulate gene expression by activating translation. Interestingly, some sRNAs can do both: they act as repressors on one target and activate the other. Example for such multiple-function ncRNA is RyhB that is expressed under iron depletion conditions and downregulates about 20 genes involved in iron metabolism in *E. coli* (see above). However, RyhB also activates translation of *shiA,* which encodes permease necessary for import of shikimate, important for biosynthesis of siderophores (Prevost *et al.*, 2007; Herrmann and Weaver, 1999). The 5' UTR of *shiA* contains an inhibitory structure that blocks RBS and impedes translation initiation. When iron is limited RyhB binds to the 5' UTR of *shiA* and unfolds the inhibitory structure thus promoting translation initiation (Figure 8). RyhB also increases mRNA stability. As in the case of negative regulation by RyhB, Hfq is needed to facilitate interactions between sRNA and mRNA during translation activation (Prevost *et al.*, 2007).

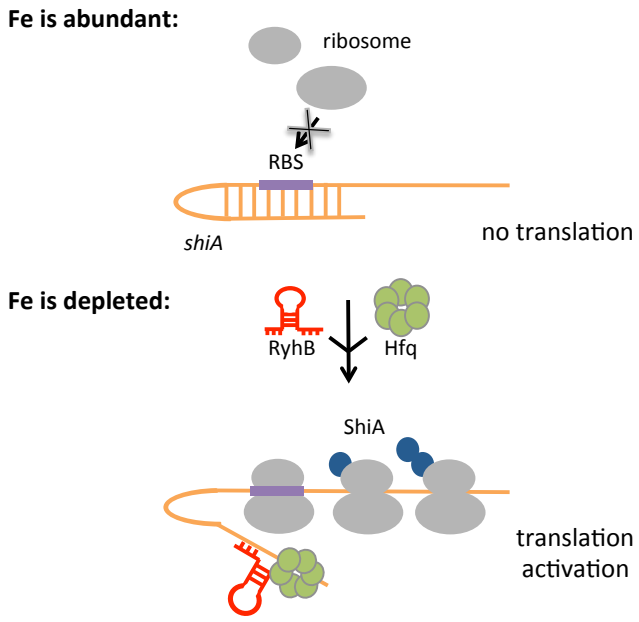

Figure 8: Translation activation by RyhB in *E. coli*
Under normal conditions the *shiA* mRNA is not translated because RBS is sequestered by an inhibitory structure. When iron gets depleted RyhB production rapidly increases; it binds together with Hfq to the 5' UTR of *shiA* and unfolds the inhibitory structure, liberating the RBS and therefore initiating translation.

Another way of ncRNA-mediated positive regulation is stabilization of target mRNAs. It was reported that *cis*-ncRNA GadY positively regulates transcript levels of *gadX* and *gadW* in *E. coli*. GadY is encoded antisense to the intergenic region between *gadX* and *gadW*, whose products are transcriptional regulators of glutamate-dependent acid stress response (Opdyke *et al.*, 2004; Ma *et al.*, 2002). The bicistronic *gadX-gadW* mRNA does not accumulate. Upon extensive base pairing of GadY to its complementary region processing within the intergenic region occurs and more stable separate *gadX* and *gadW* transcripts are produced (Figure 9A). In order to reveal which RNases are responsible for *gadX-gadW* mRNA cleavage series of experiments were conducted using strains lacking one or more RNases. Obtained results indicated that RNase III participates in the described processing event together with some unidentified (other than RNase E, G, BN and P) RNase (Opdyke *et al.*, 2011).
sRNAs are also able to stabilize target mRNAs by masking recognition sites of RNases and therefore protecting mRNA from nucleolytic attack. *Synechocystis* possesses such kind of regulatory mechanism represented by the low abundant asRNA PsbA2R. It is located antisense to the light-responsive *psbA2* gene, which encodes the D1 reaction center protein of photosystem II. Similar to its target mRNA PsbA2R is highly expressed under high light conditions and is down-regulated in darkness (Sakurai *et al.*, 2012). It has been shown that RNase E has cleavage sites within the RBS and the upstream located AU-box of the 5' UTR of *psbA2* gene (Horie *et al.*, 2007). Upon growth in the light PsbA2R binds to the 5' UTR of *psbA2* and forms a duplex masking the AU box; the RBS on the other hand is protected via loaded ribosomes *in vivo* (Sakurai *et al.*, 2012). Thus, under normal to high light conditions both RNase E cleavage sites within the 5' UTR of *psbA2* are masked and the mRNA is stabilized (Figure 9B).

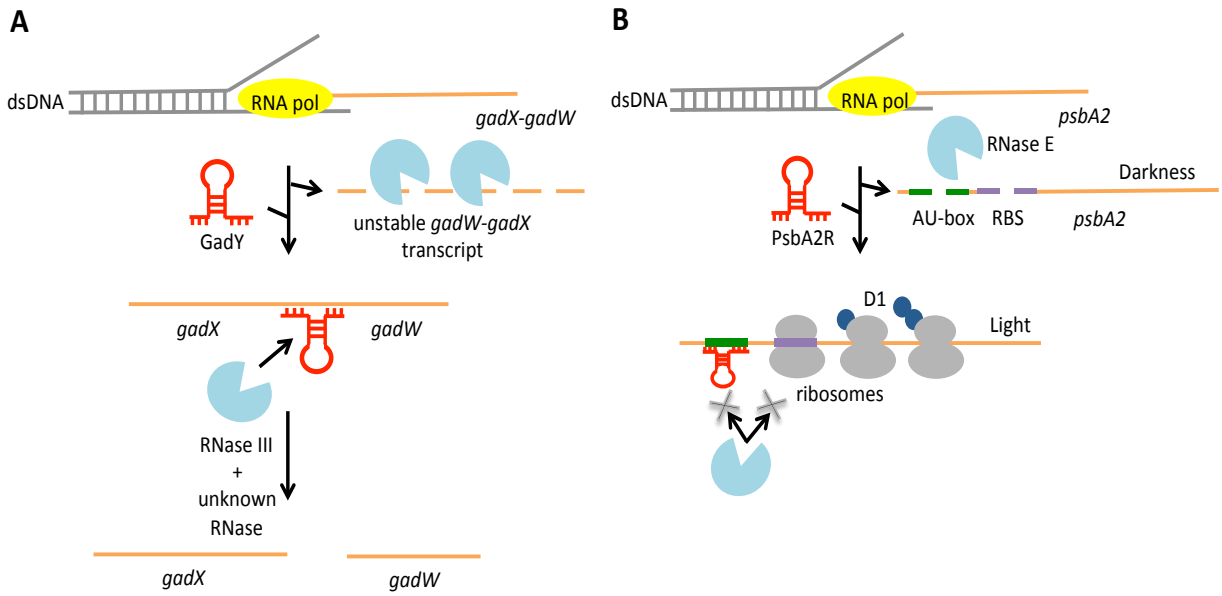

Figure 9: sRNA-mediated stabilization of target mRNAs
(A) The *gadX-gadW* transcript in *E. coli* does not accumulate. Upon binding of the GadY RNA to the intergenic region between *gadX* and *gadW* an RNA-RNA duplex is

formed; it is then degraded by RNase III and some other unidentified RNase. Processing leads to production of two stable transcripts *gadX* and *gadW*.
(B) The 5' UTR of the *psbA2* gene of *Synechocystis* is being cleaved by RNase E at the AU-box and the RBS. In the light PsbA2R masks cleavage site at the AU-box; the cleavage site located at the RBS is protected by translating ribosomes and the whole mRNA is being stabilized.

1.5 Individual-nucleotide resolution crosslinking and immunoprecipitation (iCLIP)

Importance of studying protein-RNA interactions cannot be overstated. Several methods exist that attempt to identify targets of RNA-binding proteins (RBPs). In order to determine binding sites of an RBP on a genome-wide scale ultraviolet (UV) crosslinking and immunoprecipitation (CLIP) method was developed. This *in vivo* approach was initially developed to investigate neuron-specific splicing factor Nova in mouse brain (Ule *et al.*, 2003). Brain tissue was directly irradiated with UV light creating covalent bonds between proteins and RNA that directly interact with each other. The interaction region (60-100 nucleotides) was isolated by partial RNase digestion, RNA was ligated to a linker at the 3' end and radioactively labeled, after which protein-RNA complexes were purified by SDS-PAGE and free RNA was removed during nitrocellulose membrane transfer. Proteins were then digested and a linker was ligated to the 5' end of RNA, followed by reverse transcription-polymerase chain reaction (RT-PCR) with primers complementary to 3' and 5' linkers. Amplified fragments were then cloned, sequenced and analyzed bioinformatically (Ule *et al.*, 2003). This approach was then technically improved which allowed avoiding false results because of bacterial RNA contamination during experimental procedures (Ule *et al.*, 2005). This modified method was applied to study other eukaryotic RBPs, as well as to investigate involvement of Ro autoantigen ortholog (Rsr) in rRNA degradation in the eubacterium *Deinococcus radiodurans.* Using CLIP it was shown that the Rsr protein has binding sites within 16S and 23S rRNA molecules. Authors also revealed that Rsr together with PNPase and additional nucleases play an important role in rRNA degradation during starvation (Wurtmann and Wolin, 2010). However, CLIP has certain limitations due to time-consuming and costly cloning and Sanger sequencing. Logically, next enhancement of the method was combining CLIP with high throughput sequencing methods (HITS-CLIP). It was utilized to create genome-wide protein-RNA interaction maps for Nova splicing factor. Interactions discovered by HITS-CLIP not only enriched previously obtained results but also revealed that Nova protein binds next to polyadenylation sites and therefore plays a role in regulation of alternative polyadenylation in the brain (Licatalosi *et al.*, 2008). Another study used HITS-CLIP to investigate miRNA-mRNA interactions in the mouse brain. HITS-CLIP approach determined that Argonaute proteins crosslink to two RNA populations: miRNA and mRNA. With the help of bioinformatic analysis these data revealed miRNA-target mRNA interaction sites (Chi *et al.*, 2009).
Despite the fact that different CLIP variations provide information about protein-RNA binding sites, determination of precise crosslink sites using these approaches remained challenging. Solution for this problem was found by König

et al., who developed individual-nucleotide resolution CLIP (iCLIP) and performed it to study heterogenous nuclear ribonucleoprotein C-dependent splicing regulation in human cells (König *et al.*, 2010). One of the main disadvantages of classic CLIP method is a creation of prematurely truncated cDNAs by reverse transcriptase, as the enzyme frequently stops at the crosslink site due to covalently attached amino acid remaining after protein-RNA crosslink (Urlaub *et al.*, 2002). This limitation was used as the base for iCLIP, in which these truncated cDNAs are captured. Truncated cDNAs are circularized and linearized which results in linker addition at the 5' end (the linker is initially introduced via an overhang in the primer used for reverse transcription). Thus, the end of the CLIP tag marks the initial binding site. What is more, introduction of a barcode system allowed quantification of cDNAs (discrimination between unique cDNA products and PCR duplicates) (König *et al.*, 2010). The iCLIP method has been used to investigate various human RBPs, including heterogeneous nuclear ribonucleoprotein L, which regulates transcription, translation and RNA stability; chromatin scaffold protein SAFB1, which is involved in coordination of RNA processing and neuronal function; T-cell intracellular antigens which regulate alternative splicing, and many others (Rossbach *et al.*, 2014; Rivers *et al.*, 2015; Wang *et al.*, 2010). However, iCLIP has never been utilized for studying prokaryotic protein-RNA interactions. Investigation of RNase E binding sites in *Synechocystis* using iCLIP approach is one of the main topics of this thesis and is discussed in detail in sections 2.6.8 and 3.2.2.

2. Materials and Methods

2.1 Materials

2.1.1 Chemicals

If not specified otherwise, the chemicals and reagents used for laboratory work were purchased from CARL ROTH GmbH (Karlsruhe), SIGMA-ALDRICH GmbH (Taufkirchen) and AppliChem GmbH (Darmstadt).
Radiochemicals used in this work were purchased from Hartmann Analytic GmbH (Braunschweig) and include the following:
[γ^{32}P]-ATP, specific activity: 3000 Ci/mmol
[α^{32}P]-UTP, specific activity: 3000 Ci/mmol

2.1.2 Molecular Weight Markers

Molecular Weight Markers used for gel electrophoresis of nucleic acids and proteins are summarized in Table 1.

Table 1: Molecular Weight Markers for Gel Electrophoresis

Marker	Supplier
Protein Markers	
Protein Marker VI (10-245) prestained	AppliChem
PageRuler Prestained Protein Ladder	Thermo Fisher Scientific
DNA Markers	
GeneRuler 1 kb Plus DNA Ladder	Thermo Fisher Scientific
GeneRuler Low Range DNA Ladder	Thermo Fisher Scientific
GeneRuler Ultra Low Range DNA Ladder	Thermo Fisher Scientific
RNA Markers	
RiboRuler High Range RNA Ladder	Thermo Fisher Scientific
RiboRuler Low Range RNA Ladder	Thermo Fisher Scientific

2.1.3 Antibodies

In order to perform immunological detection of proteins via Western blot (section 2.5.4) antibodies summarized in Table 2 were used.

Table 2: Antibodies

Antibody	Supplier
Anti-Digoxigenin-AP, Fab fragments	Roche Applied Science
Monoclonal anti-FLAG- HRP antibody produced in mouse	Sigma-Aldrich
Monoclonal anti-FLAG-AP antibody produced in mouse	Sigma-Aldrich
Monoclonal Anti-Glutathione-S-	Sigma-Aldrich

Transferase (GST) antibody produced in mouse	
Histidine Tag (6xHis) Monoclonal antibody produced in mouse	Life Technologies

2.1.4 Plasmids

In table 3 the plasmids used for constructing the mutants described in this work are summarized.

Table 3: Plasmids

Vector	Description	Reference
pJET1.2/blunt Cloning Vector	Blunt cloning vector, Amp^r; 2974 bp	Thermo Fisher Scientific
pDrive	TA-based cloning vector, Amp^r, Km^r; 3851 bp	Qiagen
pGEX-6P-1	Vector for heterologous expression of GST-tagged proteins in *E.coli;* Amp^r*;* 4984 bp	GE Healthcare
pVZ321	Shuttle-vector for protein expression in *Synechocystis*, Km^r, Cm^r; 9231 bp	Zinchenko *et al.* (1999)
pVZ322	Vector used as the source of $Gent^r$ resistance cassette	Zinchenko *et al.* (1999)
pVZ321-Strep	pVZ321 derivative with aadA-cassette in XbaI; IncQ, mob^+, Km^R, Cm^R, $Strep^R$	Unpublished
pUR	Derivative from the pVZ321 with P_{petJ} promotor and 3xFLAG tag on the 5' end of the insertions site of the gene of interest; IncQ, mob^+, Km^R, $Strep^R$	Wiegard *et al*., 2013
pUC4K	Vector used as the source of Km resistance cassette; Amp^r, Km^r	GE Healthcare
RP4	conjugative helper-plasmid, Amp^r, Km^r, Tet^r ; 60099 bp	Haase *et al*. (1995)
pQE*SlrRne*	C-terminal hexahistidine fusion of *Synechocystis* 6803 *rne*; Km^R, Amp^r	courtesy of M. Asayama; Horie *et al.,* 2007

2.1.5 Synthetic Oligonucleotides

Synthetic oligonucleotides were obtained from Sigma-Aldrich, Eurofins MWG Operon and Thermo Fisher Scientific. To achieve required storage solution

concentration (100 µM) the lyophilized DNA was dissolved in MQ-H_2O according to the manufacture's instructions. The sequences and special features of the synthetic oligonucleotides are given in Table 4.

Table 4: Synthetic DNA Oligonucleotides

Name	Sequence	Purpose of application	Special features
Eco-*slr1129*-fw	GTCGAATTCCCAAAACAAATTGTCATTGCTG	Cloning of *rne*	Underlined: EcoRI recognition site
slr1129-BamHI-rev	AGTGGATCCCTACTCCGCTGAAGAACG	Cloning of *rne*	Underlined: BamHI recognition site
RNaseE_fw_new	GTTGCAATTCCTTTTGGC	Cloning of *rne*	
RNaseE_rev_new V2	GTGGACCGGGCTACTCAATCTG	Cloning of *rne*	
slr1129-SalI-rev	AGTGTCGACCTACTCCGCTGAAGAACG	Cloning of *rne*	Underlined: SalI recognition site
slr1129-NdeI-fw	GTCATATGCCAAAACAAATTGTCATTGCTG	Cloning of *rne*	Underlined: NdeI recognition site
slr1129-XhoI-rev	TACTCGAGCTCCGCTGAAGAACG	Cloning of *rne*	Underlined: XhoI recognition site
slr1129-2-fw	ATGGGAATTGGTGCAACAACAGGC	Sequencing	
slr1129-3-fw	GCTGCTTGGAAACGGATAAGGC	Sequencing	
slr1129-4-fw	GCCATGACAACGTTGGAGCAG	Sequencing	
RNaseEoperon-probe-rev	CAGTGAACTATTCCCGTCATC	Southern blot hybridization	
EcoRI-*slr0346*-fw	GTCGAATTCTCTCTGCTTCCCCATCGT	Cloning of *rnc*1	Underlined: EcoRI recognition site
slr0346-BamHI-rev	AGTGGATCCTTAATTTATTTTGGGCATGGGTA	Cloning of *rnc*1	Underlined: BamHI recognition site
slr0346-SalI-rev	AGTGTCGACTTAATTTATTTTGGGCATGGGTA	Cloning of *rnc*1	Underlined: SalI recognition site
slr0346-k/o-fw	GCCACGGATTACCTCCATTG	Cloning of *rnc*1	
slr0346-rev-StuI	CCAAATTAATAGGCCTCAGAGACATGGAAGCTTA	Cloning of *rnc*1	Underlined: StuI recognition site

Name	**Sequence**	**Purpose of application**	**Special features**
slr0346-fw-StuI	GCTTCCATGTAGGCCTATTAATTTGGTTAGATAG	Cloning of *rnc*1	Underlined: StuI recognition site
slr0346-k/o-rev	CTGAGGAGTATTATCCTTTGAC	Cloning of *rnc*1	
EcoRI-*slr1646*-fw	GTCGAATTCGTGAACCATCCCGATTTC	Cloning of *rnc*2	Underlined: EcoRI recognition site
slr1646-BamHI-rev	AGTGGATCCTTATTGCAATAGCCCCAAAC	Cloning of *rnc*2	Underlined: BamHI recognition site
slr1646-SalI-rev	AGTGTCGACTTATTGCAATAGCCCCAAAC	Cloning of *rnc*2	Underlined: SalI recognition site
slr1646-k/o-fw	GCGATCGGTCTGACGGCCTG	Cloning of *rnc*2	
slr1646-StuI-rev	CTTTGCTTATAGGCCTATCGGGATGGTTCACACG	Cloning of *rnc*2	Underlined: StuI recognition site
slr1646-StuI-fw	CCATCCCGATAGGCCTATAAGCAAAGCAGAATCCAC	Cloning of *rnc*2	Underlined: StuI recognition site
slr1646-k/o-rev	ATCACCACCAGGGCGTAACCCA	Cloning of *rnc*2	
slr1214-EcoRI-fw	GTCGAATTCACTGCTGTGATCACCCGCCA	Overexpression of *slr1214*	Underlined: EcoRI recognition site
slr1214-SalI-rev	AGTGTCGACCTAGGGACAAAGAACAGGGAC	Overexpression of *slr1214*	Underlined: SalI recognition site
slr1213-fw	GCTCCATCAAAAATCAACGAA	Cloning of Hpr8	
slr1213-salI-rev	GCATGTTTGGAAAGTCGACAAAAATTCCCAACCCTGTCC	Cloning of Hpr8	Underlined: SalI recognition site
slr1214-salI-fw	GTTGGGAATTTTTGTCGACTTTCCAAACATGCAAAGGAG	Cloning of Hpr8	Underlined: SalI recognition site
slr1214-rev	GACAAATTTGGAATCACTCAATCA	Cloning of Hpr8	
P*petJ*-fw	GGAATTGCTCTGGCAACTG	Cloning of Hprs	
Hpr8-P*petJ*-rev	GCTCACCAGCACGAAGGTATTATGGGAGG	Cloning of Hpr8	
P*petJ*-Hpr8-fw	TAATACCTTCGTGCTGGTGAGCGAC	Cloning of Hpr8	
Oop-Hpr8-rev	AATAAAAAACGCCCGGCGGCAACCGAGCGTTGGATAAGGAGACCTAGGGC	Cloning of Hpr8	Underlined: Oop-terminator

Name	Sequence	Purpose of application	Special features
PHpr8-MluI-fw	TGTACACGCGTAGGAAATGGGATGTTC CCCCTATC	Cloning of Hpr8	Underlined: MluI recognition site
Hpr8-MluI-rev	TGTATACGCGTGGAAACTCCTTTGCAT GTTTGGAAA	Cloning of Hpr8	Underlined: MluI recognition site
slr1214-Fus-fw	TCCAAACATGCAAAGGAGTTTCCCATG ACTGCTGTGATCACCCGC	Cloning of Hpr8	
slr1214-MluI-rev	AGTATACGCGTCCACAGATTACAAAGT TCCCTCTAG	Cloning of Hpr8	Underlined: MluI recognition site
PHpr8-Fus-rev	GGGAAACTCCTTTGCATGTTTGGACAG TCCCATCCTAGGAAAAA TTCC	Cloning of Hpr8	
sll1834-fw	TGAGCGCAACTACGAAACTG	Cloning of Hpr10	
sll1834-BglII-rev	GGGATTTTTGGGAAGATCTCAGTTTTT CCTGCCGACATT	Cloning of Hpr10	Underlined: BglII recognition site
slr1915-BglII-fw	GCAGGAAAAACTGAGATCTTCCCAAAA ATCCCATTTTCA	Cloning of Hpr10	Underlined: BglII recognition site
slr1915-rev	GGGGAACCTACTCCCATCAT	Cloning of Hpr10	
Hpr10-P*petJ*-rev	CCATGGAGTTGAAGGTATTATGG	Cloning of Hpr10	
P*petJ*-Hpr10-fw	TAATACCTTCAACTCCATGGCAC	Cloning of Hpr10	
Hpr10-P-fw	TTTTACAATGGGAAGAACTCCA	Northern blot hybridization	
Hpr10-rev-T7	TAATACGACTCACTATAGGGAGTCGAA TCGTGCCCAAC	Northern blot hybridization	Underlined: T7-promoter
hpr10-rev	CTCAGTCGAATCGTGCCCA	*In vitro* transcription	
5S-new-T7-fw	TAATACGACTCACTATAGGGTTATTCT TCATTTTTCTTTCTCTTTTC	*In vitro* transcription	Underlined: T7-promoter
5S-tr-rev	ACTTGGCATCGGACTATTG	*In vitro* transcription	
ho1-T7-fw	TAATACGACTCACTATAGGGCAAGCCT ATGTGGACCGAGTC	*In vitro* transcription	Underlined: T7-promoter
ho1-tr-rev	CAGGTTGCCTTCAAGTTCGTTG	*In vitro* transcription	
cpcA-tr-T7-fw	TAATACGACTCACTATAGGGGCTGGTA TGTTGAAGCTCTGA	*In vitro* transcription	Underlined: T7-promoter
cpcC2-tr-rev	ATCCACCTCTTCCTCTGTACT	*In vitro* transcription	
psaA-T7-fw	TAATACGACTCACTATAGGGCTACCCC AGCTTTGCCCAAG	*In vitro* transcription	Underlined: T7-promoter

Name	**Sequence**	**Purpose of application**	**Special features**
psaA-rev	CGAGGATCTCTTTCATGCTATGG	*In vitro* transcription	
23S-T7.R.sp.-fw	TAATACGACTCACTATAGGATGTCCGAATGGGGAAACCC	*In vitro* transcription	Underlined: T7-promoter
23S-R.sp.-rev	CTTAGATGTTTCAGTTCC	*In vitro* transcription	
NC423-T7-fw	TAATACGACTCACTATAGGGAGTTAAATATTGCTTGCCATTG	*In vitro* transcription	Underlined: T7-promoter
NC423-tr-rev	CTCCTATCCTCTTTTCTTTATAT	*In vitro* transcription	
T7-SyR12-fw	*TAATACGACTCACTATAGGG*AAGACATAAAGTCAATATCACCC	*In vitro* transcription	Underlined: T7-promoter
SyR12-rev	AAAAAGAAAGCCGCCACTG	*In vitro* transcription	
Oop-Hpr10-rev	AATAAAAAACGCCCGGCGGCAACCGAGCGTTCTCAGTCGAATCGTGCCCA	Cloning of Hpr10	Underlined: Oop-terminator
ssr2153-probe-fw	TCTGTCCGTCGGGCGCTGCGCTC	Northern blot hybridization	
ssr2153-probe-rev	TAATACGACTCACTATAGGGAGATCACCGGGGCATTTGCCGTTA	Northern blot hybridization	Underlined: T7-promoter
5S-fw	ACTTGGCATCGGACTATTGTGC	Northern blot hybridization	
5S-T7-rev	CTAATACGACTCACTATAGGGAGATCTTGGTGTCTTTAGCGTCAT	Northern blot hybridization	Underlined: T7-promoter
t19probe-fw	TAGTGTTATAAATCGTCAGGTAAACGA	Northern blot hybridization	
t19probe-rev	CTAATACGACTCACTATAGGGAGACGGGCTTGGAGGGACTCGA	Northern blot hybridization	Underlined: T7-promoter
t16probe-fw	TATGTTGTTAATGCGCTAAAAAAGCCG	Northern blot hybridization	
t16probe-rev	CTAATACGACTCACTATAGGGAGATGCCAGGAGGCGGACTTGA	Northern blot hybridization	Underlined: T7-promoter
tRNA13-fw	GGGTCTGTAGTTCAATTGGTTAG	Northern blot hybridization	
tRNA13-rev	CGGGTCTGACGGGGCTC	Northern blot hybridization	
tRNA26-fw	CTATAGCTCAGTTGGTAGAGCA	Northern blot hybridization	
tRNA26-rev	GGAGCTAAGCGGGCTCGA A	Northern blot hybridization	
Hpr10-P-fw	TTTTACAATGGGAAGAACTCCA	Northern blot hybridization	

Name	Sequence	Purpose of application	Special features
Hpr10-rev-T7	TAATACGACTCACTATAGGGAGTCGAATCGTGCCCAAC	Northern blot hybridization	Underlined: T7-promoter
T7-Hpr8-fw	TAATACGACTCACTATAGGGTGCTGGTGAGCGACGGGC	*In vitro* transcription	Underlined: T7-promoter
Hpr8-tr-rev	AAGGAGACCTAGGGCCGAGTA	*In vitro* transcription	
T7-isrR-fw	TAATACGACTCACTATAGGGGATAACCATAAATAACCA	*In vitro* transcription	Underlined: T7-promoter
iCLIP-RT1	P-NNAACCNNNAGATCGGAAGAGCGTCGTGGATCCTGAACCGC	iCLIP	Underlined: BamHI recognition site
iCLIP-RT2	P-NNACAANNNAGATCGGAAGAGCGTCGTGGATCCTGAACCGC	iCLIP	Underlined: BamHI recognition site
iCLIP-RT3	P-NNCTAANNNAGATCGGAAGAGCGTCGTGGATCCTGAACCGC	iCLIP	Underlined: BamHI recognition site
iCLIP-RT4	P-NNCATTNNNAGATCGGAAGAGCGTCGTGGATCCTGAACCGC	iCLIP	Underlined: BamHI recognition site
iCLIP-RT5	P-NNGCCANNNAGATCGGAAGAGCGTCGTGGATCCTGAACCGC	iCLIP	Underlined: BamHI recognition site
Solexa P3	CAAGCAGAAGACGGCATACGAGATCGGTCTCGGCATTCCTGCTGAACCGCTCTTCCGATCT	iCLIP	
Solexa P5	AATGATACGGCGACCACCGAGATCTACACTCTTTCCCTACACGACGCTCTTCCGATCT	iCLIP	
Cut_oligo	GTTCAGGATCCACGACGCTCTTCAAAA	iCLIP	
3'-RNA-linker	P-UGAGAUCGGAAGAGCGGUUCAG-Puromycin	iCLIP	
3RACE_Tm55	GTGCTCTAGTCGTACAGAAGTG	3' RACE	
5S-Race-1	CATTTTTCTTTCTCTTTTCTTGTGC	3' RACE	
5S-Race-2	GTGCAGTCTTCTGGGTTTC	3' RACE	
5S-Race-3	GCGTCATGGAACCACTCCG	3' RACE	
5S-Race-4	GGTTGCCCCACGGCAC	3' RACE	
3' linker	P-AAGAUGAAUGCAACACUUCUGUACGACUAGAGCA(dd)C	3' RACE	

2.1.6 Software/Databanks

Software and databases used to obtain and analyse DNA and protein sequences as well as RNA structures are summarized in Table 5.

Table 5: Software and databanks

Name	Internet address/Reference	Purpose of application
Artemis	Rutherford *et al.,* 2000	Visualization and annotation of genomes
CyanoBase	http://genome.microbedb.jp/cyanobase	Databank for genome sequences of Cyanobacteria
Expasy-ProtParam	http://web.expasy.org/protparam/	Computation of various physical and chemical parameters for a given protein
Clustal Omega UniProt	http://www.uniprot.org/align/	Protein sequence alignment tool
Mfold	http://unafold.rna.albany.edu/?q=mfold/RNA-Folding-Form	Nucleic acid folding and hybridization prediction
Multalin	http://multalin.toulouse.inra.fr/multalin/	Multiple sequence alignment
NCBI-BLAST	http://blast.ncbi.nlm.nih.gov/Blast.cgi Altschul *et al.*, 1990	Search for homologous sequences for DNA and proteins
OligoCalc	http://www.basic.northwestern.edu/biotools/oligocalc.html Kibbe *et al.,* 2007	Oligonucleotide Properties Calculator
DoubleDigest Calculator	https://www.lifetechnologies.com/de/de/home/brands/thermo-scientific/molecular-biology/thermo-scientific-restriction-modifying-enzymes/restriction-enzymes-thermo-scientific/double-digest-calculator-thermo-scientific.html	Optimal reaction conditions determination for double digest reaction
Multiple Em for Motif Elicitation (MEME) tool	http://meme-suite.org/tools/meme	Discovery of novel binding motifs
WebLogo	http://weblogo.berkeley.edu/	Generation of sequence logo

2.1.7 Microorganisms

Strains of *Synechocystis* and *Escherichia coli* (*E. coli*) used in this work are summarized in Table 6.

Table 6: Microorganisms

Name	Description/ Genotype	Reference
Synechocystis sp. PCC6803 WT	Naturally transformable motile wild-type strain originated from Prof. S.V. Shestakov (Department of Genetics, Lomonosov Moscow State University, Russia)	Kaneko *et al.,* 1996 Trautmann *et al.,* 2012
Synechocystis sp. PCC6803 *Δhfq*	*ssr3341* knockout mutant, Cm^r	Dienst *et al*., 2008
E. coli DH5α	F-, φ80*lac*ZΔM15, Δ(*lacZYA-argF*)U169, *deoR, recA1*, *endA1, sdR17*(r_{k^-}, m_{k^+}), *phoA, supE44, thi-1, gyrA96, relA1*, λ-	Hanahan *et al*., 1983
E. coli J53 (RP4)	R+, *met*, *pro* (RP4: Amp^r, Tc^r, Km^r, Tra+, IncP)	Wolk *et al*., 1984
E. coli BL21 (DE3)	F-, *ompT*, *hsdSB* (r_B-m_B-), *gal*	Studier und Moffat 1986
E. coli ArcticExpress (DE3)	B F– *ompT hsdS*(r_{B^-} m_{B^-}) *dcm*+ Tet^r *gal* λ(DE3) *end*A Hte [*cpn10 cpn60* $Gent^r$]	Agilent Technologies
E. coli M15 (pREP4)	NaI^S, Str^S, Rif^S, Thi^-, Lac^-, Ara^+, Gal^+, Mtl^-, F^-, $RecA^+$, Uvr^+, Lon^+; Km^r	Qiagen
E. coli TOP 10 F'	F- mcrA Δ(*mrr-hsdRMS-mcrBC*) φ80*lac*ZΔM15 Δ*lacX74 nupG recA1 araD139 Δ(ara-leu)7697 galE15 galK16 rpsL*(Strep) A1 λ	Invitrogen

2.2 General and physiological methods

2.2.1 Cultivation conditions for *Synechocystis*

Liquid cultures were grown in BG11 medium (Rippka *et al.*, 1979) supplemented with 10 mM TES pH 8,0 under constant illumination with white light at 50 µmol photons m^{-2} s^{-1} (Phillips MASTER TL-D Super 80 18W/840 or Osram EL40 SS W/37) at 30°C. Liquid cultures were grown either in Erlenmeyer flasks under constant shaking (ca. 150rpm) or in glass fermenters under constant gassing with sterile air.
For cultivation of mutants expressing different gene products controlled by the *petJ* promoter, that is induced by the lack of Cu^{2+}, BG11 medium without $CuSo_4$ was used. Selection of mutants as well as the culture collection was carried out in cell culture dishes in BG11 medium containing 0,75% w/v Bacto-Agar (Difco, Becton Dickinson GmbH, Heidelberg) and 0.15% w/v $Na_2S_2O_3$. Depending on the selectable marker used to generate particular mutants the following antibiotics

were added to the medium: Chloramphenicol (Cm), 7 µg ml^{-1}; Kanamycin (Km), 40 µg ml^{-1}; Streptomycin (Strep), 15 µg ml^{-1} and Gentamicin (Gent), 2 µg ml^{-1}. For the long-term conservation aliquots of newly generated mutants were resuspended in 1 ml Cryo medium (0,5 x BG11; 8% (v/v) DMSO), frozen in liquid nitrogen and stored at -80°C.

1 x BG11 medium, autoclaved:

10 ml l^{-1}	100 x BG11
1 ml l^{-1}	Na_2CO_3
1 ml l^{-1}	K_2HPO_4 x 3 H_2O
1 ml l^{-1}	Fe (III) $(NH_4)_2$ citrate
1 ml l^{-1}	Trace metal mix
10 ml l^{-1}	TES-Puffer (pH 8,0)

100 x BG11, autoclaved:

25 mM	$CaCl_2$ x 2 H_2O
3 mM	$C_6H_8O_7$ (Citric acid)
1,77 M	$NaNO_3$
30 mM	$MgSO_4$ x 7 H_2O
0,3 mM	Na_2-EDTA (pH 8,0)

Trace metal mix, sterile filtered:

2,86 g l^{-1}	H_3BO_3
1,81 g l^{-1}	$MnCl_2$ x 4 H_2O
0,222 g l^{-1}	$ZnSO_4$ x 7 H_2O
0,390 g l^{-1}	Na_2MoO_4 x 2 H_2O
0,079 g l^{-1}	$CuSO_4$ x 5 H_2O
0,049 g l^{-1}	$Co(NO_3)_2$ x 6 H_2O

Other solutions:

190 mM	Na_2CO_3 (autoclaved)
180 mM	K_2HPO_4 x 3 H_2O (autoclaved)
30 mM	Fe (III) $(NH_4)_2$ citrate (sterile filtered)
1 M	TES-Puffer (pH 8,0)
40 mg ml^{-1}	Kanamycin
7 mg ml^{-1}	Chloramphenicol
20 mg ml^{-1}	Streptomycin
10 mg ml^{-1}	Gentamicin

2.2.2 Cultivation conditions for *Escherichia coli*

Liquid cultures were grown in lysogeny broth (LB) medium at 37 °C under constant shaking (ca. 200 rpm). Mutants were also grown on cell culture dishes with LB agar. For the selection of mutants the following antibiotics depending on the used resistance genes were added to the medium: Ampicillin (Amp), 100 µg ml^{-1}, Cm, 25 µg ml^{-1}, Km, 20 µg ml^{-1}, Strep, 20 µg ml^{-1}.

LB-Medium : (Lennox), Carl Roth (autoclaved)
LB-Agar: (Lennox), Carl Roth (autoclaved)

Antibiotics' solutions:

20 mg ml^{-1}	Kanamycin (sterile filtered)
24 mg ml^{-1}	Chloramphenicol in 96% v/v Ethanol
20 mg ml^{-1}	Streptomycin (sterile filtered)
100 mg ml^{-1}	Ampicillin in 50% v/v Ethanol

2.2.3 Determination of optical density of the liquid cultures

Determination of optical density (OD) of liquid microbial cultures was carried out on the BioSpectrometer Basic (Eppendorf) at wavelength 600 nm for *E. coli* and 750 nm for *Synechocystis* in plastic cuvettes. As a reference the cultivation medium was used.

2.2.4 Measuring of the absorption spectra of *Synechocystis*

Absorption spectra of liquid cultures of *Synechocystis* were measured at room temperature (RT) in the wavelength range from 400 to 750 nm on the spectrophotometer (UV-2450, Shimadzu) in plastic cuvettes. Before the measurement a baseline against air was taken.

2.2.5 Phototaxis assay

Investigation of motility and phototaxis behaviour of different *Synechocystis* mutants was carried out in a light gradient on modified BG11 medium containing 0,5% w/v agar, 0,2% w/v glucose, 10mM TES, 0,15% w/v $Na_2S_2O_3$. 5 µl of cells resuspended in BG11 medium were dropped on squared cell culture dish forming a row of equally distant drops. The cultures were incubated under diffused light (ca. 50 µmol photons m^{-2} s^{-1}) for 2-3 days and then under unidirectional light (<5 µmol photons m^{-2} s^{-1}) for 7-10 days by putting the cell culture dishes in non-transparent boxes with the opening only on one side.

2.2.6 Pigment determination from *Synechocystis* cell extracts

Chlorophyll content was determined according to MacKinney (1941), 5 µl *Synechocystis* cell extract (section 2.5.1) was mixed with 995 µl 80 % v/v acetone (dilution factor 200) and incubated for 30 at 4°C in the darkness. Insoluble fraction was removed via centrifugation (5 min, 16000g, 4 ^{0}C) and the absorption of chlorophyll was measured at 665 nm (A_{665nm}) using 80 % v/v acetone as a reference. Chlorophyll content was then calculated using the following formula:

Chlorophyll [µg ml^{-1}] = dilution factor x A_{665nm} x 1000 / 86,86

Phycocyanin and allophycocyanin contents were determined from the absorption spectra of soluble protein fractions using the following formulas (de Marsac *et al.*, 1988):

Phycocyanin [mg ml^{-1}] = dilution factor x ($A_{PC/620nm}$-($A_{APC/650nm}$ x 0,7)) / 7,83

Allophycocyanin [mg ml^{-1}] = dilution factor x ($A_{APC/650nm}$-($A_{PC/620nm}$ x 0,19)) / 5,65

2.2.7 Bradford protein assay

To determine protein concentration in a solution 798 µl H_2O was mixed with 200 µl Bradford reagent (Sigma-Aldrich), then 2 µl of the sample was added to the

mixture and incubated for 1 h at RT. Afterwards absorption of the samples at 595 nm (A_{595nm}) was measured against 800 µl H_2O + 200 µl Bradford reagent, and protein concentration was determined using the following formula:

µg protein μl^{-1} = factor x A_{595nm} / µl sample

The factor value was calculated in advance with the help of BSA standard curve and equals 11,7.

2.3 Methods of Molecular Biology

2.3.1 Plasmid DNA extraction from *E. coli*

Plasmid DNA extraction was carried out according to the alkaline extraction method by Birnboim and Doly (1979). Cells from 5 ml of overnight culture are harvested by centrifugation (10 min, 3500g, 4 ^{0}C) and resuspended in 350 µl buffer P1. Afterwards 350 µl buffer P2 is added to the sample and mixed carefully. Following 5 min incubation on ice 350 µl buffer P3 is added and the sample is incubated for another 15 min. Chromosomal DNA, proteins and high molecular weight RNA are co-precipitated by centrifugation (15 min, 16000g, 4 ^{0}C). The supernatant is collected and plasmid DNA is recovered by isopropanol (0,7 volume) precipitation for 2 h at -20 ^{0}C. Following the centrifugation (15 min, 16000g, 4 ^{0}C) sedimented plasmid DNA is washed with 75% v/v ethanol. The DNA pellet obtained after centrifugation (5 min, 16000g, 4 ^{0}C) is air-dried, resuspended in 30 µl H_2O and stored at -20 ^{0}C.

Buffer P1: 50 mM Tris/HCl (pH 8,0); 10 mM EDTA; 100 µg ml^{-1} RNase A
Buffer P2: 200 mM NaOH; 1% (w/v) SDS
Buffer P3: 3M potassium acetate (pH 5,5)

2.3.2 Polymerase Chain Reaction (PCR)

Polymerase chain reaction was used for *in vitro* amplification of genomic DNA of *Synechocystis* as well as plasmid DNA. For cloning, generating of templates for *in vitro* transcription and radiolabeled probes and amplification of PCR fragments without A overhangs Phusion High-Fidelity DNA Polymerase (Thermo Fisher Scientific) was used because of its high accuracy in generating PCR products. For other PCR reactions DreamTaq DNA Polymerase (Thermo Fisher Scientific) or MyTaq DNA Polymerase (Bioline) were used. Reaction set up was performed according to the manufacturer's instructions taking into account melting temperatures of the primers and length of PCR products.
In most cases genomic or plasmid DNA was used to perform PCR. In case of colony PCR to check if the transformants are correct *E. coli* cells were added directly to the reaction mix, while *Synechocystis* cells were lysed in H_20 at 98 ^{0}C for 5 min and aliquots of the lysate were added to the PCR reaction mix.
PCR products were either purified with QIAquick PCR Purification Kit, The QIAEX II Gel Extraction Kit (both Qiagen) or in case of 5'RACE with The High Pure PCR Product Purification Kit (Roche).

2.3.3 Digestion of DNA by restriction enzymes

Plasmid DNA or PCR products generated by primers containing restrictions sites were digested with standard restriction enzymes (Thermo Fisher Scientific) according to the manufacturer's instructions. If a double digest was necessary, the optimal buffer conditions were selected using the DoubleDigest Calculator by Thermo Fisher Scientific (Table 5).

2.3.4 Dephosphorylation of DNA and RNA

In order to avoid recircularization of linearized plasmid DNA it was dephosphorylated using FastAP Thermosensitive Alkaline Phosphatase (Thermo Fisher Scientific) according to manufacturer's instructions.
To convert 5´-triphosphorylated RNA to 5´-monophosphorylated RNA for further use in *in vitro* cleavage assays RNA 5´ Polyphosphatase (Epicentre) was used according to manufacturer's instructions.

2.3.5 Ligation of DNA fragments

For cloning of DNA fragments, plasmid vector (25-100 ng) and insert DNA were digested as described in section 2.3.3 and mixed in a molar ratio of 1:5 using the following reaction set up: 1x T4 DNA Ligase buffer und 5 U T4 DNA Ligase (Thermo Fisher Scientific) in a 20 µl reaction volume. DNA ligation was performed at 16°C for 4 hours or overnight. For ligation of PCR products into pJET1.2 or pDrive cloning vector CloneJET PCR Cloning Kit (Thermo Fisher Scientific) or QIAGEN PCR Cloning Kit (Qiagen) were used according to manufacturer's instructions.

2.3.6 Gel electrophoresis and extraction of DNA

To analyse DNA samples, agarose gel electrophoresis was used as standard method. Agarose (0,8-1% w/v) was dissolved in 1× TBE by boiling in a microwave oven. For DNA fragments smaller than 250 bp 2% w/v NuSieve agarose (Lonza) gels were used. The dissolved agarose was supplemented with 0.2 µg ml^{-1} ethidium bromide (EtBr) and poured and run in a horizontal agarose gel system (PerfectBlue Gelsystem, Peqlab). DNA samples were mixed with 1x DNA loading buffer and separated on a gel at 5-10 V cm^{-1} in 1× TBE. Gels were analysed and documented under UV-irradiation in UV transilluminator MD-25/HD-25 (Wealtec). If needed DNA fragments were cut out of the gel with a scalpel and extracted from the gel using QIAEX II Gel Extraction Kits (Qiagen) according to manufacturer's instructions.
When small DNA molecules (<200 bp) had to be analysed at high resolution, e.g. for analysis of the iCLIP library preparation PCR (section 2.6.8) or 5'RACE PCR (section 2.6.9), polyacrylamide (PAA) gel electrophoresis was used. A solution of 10% acrylamide/bisacrylamide (19:1) was prepared in 1× TBE, and polymerization was initiated by adding 1:125 volumes of 10% ammonium persulfate (APS) and 1:1,250 volumes of N,N,N´,N´-tetramethylene-diamine (TEMED). The SE250 small vertical electrophoresis system (Hoefer) was used.

Gels were run at 7 mA for 45-120 min, stained with a 5 µg ml^{-1} EtBr solution in 1× TBE for 10 min, and destained for 2 min in deionized water. Gels were analysed as described above for agarose DNA gels. If needed DNA fragments were cut out of the PAA gel with a scalpel, placed in 400 µl Tris-EDTA buffer, crushed with syringe plumber, put through Illustra MicroSpin G-25 column (GE Healthcare) and ethanol precipitated at -20 ^{0}C overnight, followed by centrifugation (30 min, 16000g, 4 ^{0}C), ethanol wash, air-drying and dissolving in H_2O.

10x TBE buffer:	Rotiphorese 10x TBE Buffer (Roth)
6x DNA loading buffer:	0,25% (w/v) bromphenol blue; 0,25% (w/v) xylencyanol; 30% (v/v) glycerol
Tris-EDTA buffer:	10 mM Tris/HCl (pH 8.0); 1 mM EDTA

2.3.7 Determination of concentration of nucleic acids

In order to determine concentrations of DNA and RNA in water solutions absorption at 260 nm was measured with *NanoDrop* 2000 (Thermo Fisher Scientific) spectrophotometer. Each time 1 µl of DNA (or RNA) solution was taken for the measurement. Additionally the quality of nucleic acids was evaluated via estimation of the ratio of OD_{260nm} to OD_{280nm} (optimal values have the ration 1,8-2,0). MQ-H_2O was taken as the reference.

2.3.8 Production of chemically competent *E. coli* cells

Chemically competent cells were produced according to Hanahan (1983). 5 ml of an overnight *E. coli* culture (DH5α or BL21) was diluted 1:50 with SOB medium and grown at RT under constant shaking (180 rpm) till OD_{660nm} 0,4. Following 10 min incubation on ice cells were sedimented by centrifugation (1000g, 15 min, 4 ^{0}C). Cells were resuspended in 17 ml pre-chilled CCMB solution and incubated for another 10 min on ice. After sedimentation by centrifugation (1000g, 15 min, 4 ^{0}C) cells were resuspended in 4 ml pre-chilled CCMB solution. 200 µl aliquots were frozen in liquid nitrogen and stored at -80 ^{0}C).

CCMB solution:	80 mM $CaCl_2x2H_2O$; 20 mM $MnCl_2x4H_2O$; 10 mM $MgClx6H_2O$; 10 mM potassium acetate; 10% v/v glycerol
SOB medium:	2% w/v Trypton; 0,5% w/v yeast extract; 10 mM NaCl; 2,5 mM KCl; 10 mM $MgCl_2x6H_2O$; 10 mM $MgSO_4x7H_2O$

2.3.9 Transformation of *E. coli*

Transformation of chemically competent *E. coli* DH5α or BL21 (DE3) was carried out via the heat shock method (Mandel und Higa, 1970). Competent cells were thawed on ice and mixed with the ligation mix (section 2.3.5). After 15 min incubation on ice the cells were heat shocked at 42 ^{0}C for 2 min. Following another 5 min incubation on ice the cells were mixed with 0,8 ml LB medium and incubated for 45 (for high-copy plasmids) and 90 min (for low-copy plasmids) at 37 ^{0}C under constant shaking (200rpm). 50-150 µl of cell culture was inoculated on cell culture dishes with LB agar supplemented with necessary antibiotics and

cultivated overnight at 37 ^{0}C. Transformants were analysed via colony PCR (section 2.3.2).

2.3.10 Transformation of *Synechocystis*

Transformation of *Synechocystis* was carried out according to Grigorieva and Shestakov (1982). 10 ml of the cell culture in the exponential growth phase (OD_{750nm} 0,6-0,8) were harvested by centrifugation (3000g, 5 min, RT), mixed with 1 µg plasmid DNA and resuspended in ca. 100 µl of BG11 media. Following 4 h incubation under constant indirect daylight the cells were inoculated on BG11 agar (1% w/v) medium and incubated for 2 days under moderate light (ca. 50 µmol photons m^{-2} s^{-1}) at 30 ^{0}C. Afterwards 400 µl of selective antibiotics in the concentration 1/5 of the standard concentration listed in section 2.2.1 was added under the agar layer on one side of the cell culture dish to create a concentration gradient. After 10-15 days resistant transformants could be detected, which were several times inoculated on BG11 agar medium cell culture dishes with growing concentration of selective antibiotics until the desired standard antibiotic concentration was reached. Afterwards correct homologous recombination and full segregation of the mutants was confirmed via PCR.

2.3.11 Conjugation of *Synechocystis*

Conjugation of *Synechocystis* with plasmid DNA based on the self-replicating vector pVZ321 from *E. coli* DH5α cell line was carried out according to the method of triparental mating with the help of conjugating plasmid RP4 from *E. coli* J53-RP4 cell line. 250 µl of each *E. coli* overnight culture were diluted in 10 ml LB medium without antibiotics and cultivated for 3 h at 37 ^{0}C. The cells were harvested by centrifugation (1000g, 5 min, RT) and gently resuspended in 1 ml LB medium. Both *E. coli* cultures were mixed together 1:1, centrifuged (1000g, 5 min, RT), resuspended in 100 µl LB medium and incubated for 1 h at 30 ^{0}C without shaking. Afterwards 1,5 ml of *Synechocystis* culture (OD750nm = 0,6-0,8) was added to the *E. coli* suspension, centrifuged (1000g, 5 min, RT) and resuspended in 30 µl BG11 medium. The conjugation mixture was inoculated on a HAFT nitrocellulose membrane placed on the cell culture dish with BG11 agar medium supplemented with 5% LB medium without antibiotics. After 2 days incubation under constant light (ca. 40 µmol photons m^{-2} s^{-1}) the cells were washed from the membrane with 200 µl BG11 medium. The conjugants were selected on the BG11 agar medium with half of the standard antibiotic concentration. After ca. 2 weeks resistant clones were transferred to the cell culture dishes with BG11 agar medium supplemented with selective antibiotics in the standard concentration.

2.4 Cloning strategies and construction of plasmids

2.4.1 General strategy for construction of FLAG-tagged RNases in *Synechocystis*

In order to create N-terminally FLAG-tagged variants of different RNases in *Synechocystis* their open reading frames (ORFs) were amplified using *Synechocystis* genomic DNA and the following primer combinations:

rne (*slr1129*): Eco-*slr1129*-fw
slr1129-BamHI-rev
*rnc*1 (*slr0346*): EcoRI-*slr0346*-fw
slr0346-BamHI-rev
*rnc*2 (*slr1646*): EcoRI-*slr1646*-fw
slr1646-BamHI-rev
(Table 4)

PCR fragments were purified from the agarose gel, digested using EcoRI and BamHI restriction enzymes (both Thermo Fisher Scientific), purified accordingly and ligated into previously restricted with the same restriction enzymes pUR plasmid. The pUR plasmid contains a controllable promoter, 3xFLAG and terminator sequences for expression of tagged proteins in *Synechocystis*. Ligation mixture was used for the transformation of *E. coli* DH5α. After selection of positive transformants via colony PCR and confirming the correct sequence of the extracted plasmid DNA by sequencing, plasmid DNA was transferred to *Synechocystis* WT cells via conjugation. Positive conjugants were selected on BG11 agar medium with Km and Strep and checked via colony PCR.

2.4.2 General strategy for construction of GST-tagged RNases in *E. coli*

In order to construct N-terminally GST-tagged RNases in *E. coli* their ORFs were amplified using *Synechocystis* genomic DNA and the following primer combinations:

rne (*slr1129*): Eco-*slr1129*-fw
slr1129-SalI-rev
*rnc*1 (*slr0346*): EcoRI-*slr0346*-fw
slr0346-SalI-rev
*rnc*2 (*slr1646*): EcoRI-*slr1646*-fw
slr1646-SalI-rev
(Table 4)

PCR fragments were purified from the agarose gel, digested using EcoRI and SalI restriction enzymes (both Thermo Fisher Scientific), purified accordingly and ligated into previously restricted with the same restriction enzymes pGEX-6P-1 cloning vector. Ligation mixture was used for the transformation of *E. coli*. For GST-*slr0346* and GST-*slr1646 E. coli* BL21 (DE3) strain was used, whereas GST-*slr1129* was transformed into *E. coli* ArcticExpress (DE3) competent cells.

Positive transformants were selected via colony PCR and the correct sequence of the extracted plasmid DNA was confirmed by sequencing.

2.4.3 General strategy for construction of knockout mutants of small ncRNAs

In order to create knockout strains of Hfq-dependent putative sRNAs (Hprs) in *Synechocystis* upstream and downstream genome regions were amplified using *Synechocystis* genomic DNA and then fused together via a third PCR, which resulted in omission of the sRNA. The following primer combinations were used:

Hpr8: 1.PCR *slr1213*-fw
slr1213-salI-rev
2.PCR *slr1214*-salI-fw
slr1214-rev
3.PCR *slr1213*-fw
slr1214-rev

Hpr10: 1.PCR *sll1834*-fw
sll1834-BglII-rev
2.PCR *slr1915*-BglII-fw
slr1915-rev
3.PCR *sll1834*-fw
slr1915-rev
(Table 4)

PCR products were ligated into the pJet 1.2 (in case of Hpr8) and pDrive (for Hpr10) cloning vectors. Recombinant vector was transferred into competent *E. coli* DH5α, positive transformants harbouring the respective recombinant vector were selected on LB agar medium supplemented with Amp and checked via colony PCR. Plasmid vector DNA was then extracted and digested with SalI and BglII restriction enzymes (both Thermo Fisher Scientific) respectively. The Km resistance gene cassette was obtained from the pUC4K vector, restricted with SalI or BamHI, respectively. The Km resistance gene cassette was then ligated into the digested pJet vector. Competent *E. coli* DH5α were transformed with recombinant vector, positive transformants were selected on LB agar medium supplemented with Amp and Km and checked via colony PCR. Then the plasmid vector was extracted, sequenced and used to transform *Synechocystis.* Positive transformants were selected on BG11 agar medium supplemented with Km and checked via colony PCR.

2.4.4 General strategy for construction of overexpression mutants of small ncRNAs

In order to create overexpression strains of sRNAs in *Synechocystis* their ORFs were amplified using *Synechocystis* genomic DNA and primer combinations leading to the introduction of copper-regulated *petJ* promoter in front of the sRNA followed by the *oop*-terminator from phage Lambda:

Hpr8: 1.PCR P*petJ*-fw
Hpr8-P*petJ*-rev
2.PCR P*petJ*-Hpr8-fw
Oop-Hpr8-rev
3.PCR P*petJ*-fw
Oop-Hpr8-rev
Hpr10: 1.PCR P*petJ*-fw
Hpf10-P*petJ*-rev
2.PCR P*petJ*-Hpr10-fw
Oop-Hpr10-rev
3.PCR P*petJ*-fw
Oop-Hpr10-rev
(Table 4)

Final PCR products were ligated into the pDrive cloning vector. Recombinant vector was transformed into competent *E. coli* DH5α cells, positive transformants harbouring recombinant vector were selected on LB agar medium supplemented with Amp and checked via colony PCR. Plasmid vector was then extracted and digested with PstI and SalI restriction enzymes (both Thermo Fisher Scientific) and inserted into the conjugative, self-replicating vector pVZ321-Strep digested with the same restriction enzymes. It was then transformed into competent *E. coli* DH5α cells, positive transformants were selected on LB agar medium supplemented with Km and Strep and checked via colony PCR and sequencing. Then the extracted plasmid vector was transferred into *Synechocystis* WT and *Δhfq* mutant by conjugation. Positive conjugants were selected on BG11 agar medium supplemented with Km and Strep and checked via colony PCR.

2.4.5 Construction of *slr1214*-rescue and hpr8-rescue mutants in *Synechocystis*

Hpr8-rescue and *slr1214*-rescue strains on the basis of the *Δhpr8* mutant were constructed by Jasper Matthiessen (AG Hess, Institute of Biology III, Albert-Ludwigs University Freiburg) by introducing the self-replicating plasmid pVZ322, modified to carry the native *hpr8* locus containing native *hpr8* promoter in front of *hpr8* (PHpr8>Hpr8). *hpr8* locus was amplified by PCR using the primers P-Hpr8-MluI-fw and SyR14-MluI-rev (Table 4) that introduce MluI restriction sites on both ends of the PCR product. The PCR product and pVZ322 were then digested with MluI, thus removing the Km resistance gene cassette from pVZ322. Following that, the fragments were ligated and transformed into *E. coli* TOP10F'. Positive clones were selected with Gent and verified by colony PCR and sequencing. Recombinant plasmid was then transferred via conjugation into *Δhpr8* and positive clones were selected using Km and Gent.
In order to create *slr1214*-rescue strain *hpr8* promoter was fused directly to the coding sequence of *slr1214* (PHpr8>*slr1214*), omitting the *hpr8* sequence in between the two. This was executed by introducing the self-replicating plasmid pVZ322 carrying the PHpr8>*slr1214* construct into the *Δhpr8* knockout mutant. The promoter of *hpr8* was amplified using the primers PHpr8-MluI-fw and PHpr8-Fus-rev (Table 4), introducing a MluI restriction site on the 5'-end and a

complementary region for fusion-PCR on the 3'-end of the PCR product. The coding region of *slr1214* was amplified using the primers *slr1214*-Fus-fw and *slr1214*-MluI-rev, thus introducing MluI restriction site on the 3'-end and a complementary region for fusion-PCR on the 5'-end of the PCR product. The two products were fused together by PCR. This final product and pVZ322 vector were then digested with MluI, ligated and transformed into *E. coli* TOP10F'. Positive clones were selected with gentamycin and verified by colony PCR and sequencing. Finally the correct, recombinant plasmid was conjugated into the *Δhpr8* knockout mutant and positive clones selected using kanamycin and gentamycin.

2.4.6 General strategy for construction of RNaseIII conditional knockout mutants in *Synechocystis*

First step in creation of conditional knockout strain of RNaseIII in *Synechocystis* was to construct a complementation mutant of RNaseIII in the existing knockout mutant. For that purpose FLAG-*slr0346* plasmid was transferred to *Synechocystis Δslr0346*(Cm^r) via conjugation and FLAG-*slr1646* plasmid was transferred to *Synechocystis Δslr1646*(Cm^r) also via conjugation. Both mutants were grown on BG11 medium without copper, thus inducing the expression of the respective RNasesIII controlled by the *petJ* promoter. In the next step knockout strains of RNasesIII (*slr0346* and *slr1646*) were created using the following strategy: upstream and downstream genome regions were amplified using *Synechocystis* genomic DNA and then fused together via a third PCR, thereby skipping RNaseIII. The following primer combinations were used:

*rnc*1 (*slr0346*):	1.PCR	*slr0346*-k/o-fw
		slr0346-rev-StuI
	2.PCR	*slr0346*-fw-StuI
		slr0346-k/o-rev
	3.PCR	*slr0346*-k/o-fw
		slr0346-k/o-fw
*rnc*2 (*slr1646*):	1.PCR	*slr1646*-k/o-fw
		slr1646-StuI-rev
	2.PCR	*slr1646*-StuI-fw
		slr1646-k/o-rev
	3.PCR	*slr1646*-k/o-fw
		slr1646-k/o-rev

(Table 4)

PCR products were ligated into the pJet 1.2 cloning vector. Recombinant vector was transformed into competent *E. coli* DH5α, positive transformants harbouring recombinant vector were selected on LB agar medium supplemented with Amp and checked via colony PCR and sequencing. Plasmid vector was then extracted and digested with StuI restriction enzyme (Thermo Fisher Scientific). Gent resistance cassette was obtained from the pVZ322 vector, restricted with StuI and HincII restriction enzymes (both Thermo Fisher Scientific). Gent resistance cassette was then ligated into the digested pJet. Recombinant vector was transformed into competent *E. coli* DH5α, positive transformants were selected

on LB agar medium supplemented with Amp and Gent and checked via colony PCR and sequencing.
In the final step *Δslr1646*(Gent^r) plasmid was transformed in *Synechocystis* FLAG-*slr0346* + *Δslr0346*(Cm^r), as well as *Δslr0346*(Gent^r) plasmid was transformed in *Synechocystis* FLAG-*slr1646* + *Δslr1646*(Cm^r). Positive transformants were selected on BG11 agar medium supplemented with Gent, Cm, Km and lacking copper. Thus when these mutants were transferred to the growth medium with normal copper concentration the expression of RNaseIII under the control of *petJ* promoter was abolished and conditional knockout of both RNasesIII was achieved.

2.5 Methods of Biochemistry

2.5.1 Harvesting *Synechocystis* cells and preparing the cell extract

Harvesting the *Synechocystis* cells was performed via centrifugation for 10 min at 6000g, 4 ^{0}C. Cell pellets were frozen at -80 ^{0}C until further use.
For preparation of cell extracts the pellets were resuspended in the extraction buffer (4 x cell pellet volume), 1 ml aliquots were placed in 2 ml Eppendorf tubes and mixed with 0,8 x volume glass beads (0,1- 0,11 und 0,25-0,5 mm). The cells were disrupted in a cell mill (type MM400, Retsch) at 4 ^{0}C and 30 Hz for 15 min. Following centrifugation (5 min, 1000g, 4 ^{0}C) the supernatant (whole cell extract) was collected, the sediment was mixed again with 0,5 ml extraction buffer and extraction was repeated. The whole cell extract was stored at -20 ^{0}C until further use.

Extraction buffer: 50 mM HEPES/NaOH (pH 7,0); 5 mM $MgCl_2$; 25 mM $CaCl_2$; 10% (v/v) glycerol

Determination of protein concentration in the cell extracts was performed following modified Lowry approach (Bensadoun and Weinstein, 1976) or by performing Bradford protein assay (Section 2.2.7).

2.5.2 Denaturing polyacrylamide/SDS gel electrophoresis of proteins

For gel electrophoresis of proteins (SDS-PAGE) the discontinuous Laemmli Tris-glycine buffer system (Laemmli, 1970) or continuous Schägger Tris-tricine buffer system (Schägger and von Jagow, 1987) was used. In case of Laemmli system 8-12% acrylamide/bisacrylamide solution (depending on the protein size) was prepared in separating gel buffer. Polymerization was initiated by adding 1:125 volumes 10% APS and 1:1,250 volumes of TEMED. Stacking gels were poured after complete polymerization of the separating gel, using 4% acrylamide/bisacrylamide solution in stacking gel buffer, adding similar dilutions of 10% APS and TEMED. Schägger gels were prepared as described in table 7. Protein samples were mixed with 1× SDS sample buffer and heated up to 95 ^{0}C for 5 min in a water bath. The insoluble fraction was separated via centrifugation (5 min, 1000g, RT) and the soluble supernatant was loaded on the gel. For Tris-glycine system electrophoresis was performed in SDS running

buffer (25 mM Tris/HCl, 192 mM glycine, 0.1% SDS) for 60-90 min at 150 V. When Tris-tricine system was utilized gels were run at constant current of 20 mA per gel in cathode and anode buffers. Afterwards the gels were either used for immunoblot analysis (section 2.5.4) or stained with Coomassie or silver (section 2.5.3).

Table 7: Schägger SDS-PAA gel

	4% stacking gel	**10% separating gel**	**16% separating gel**
AB-3 mix, ml	0,166	1	1,66
3x gel buffer, ml	0,5	1,66	1,66
50% (v/v) glycerol, ml	1,33	0,8	0,8
ddH_2O, ml		1,54	0,88
TEMED, µl	2,5	2,5	1,66
10% (w/v) APS, µl	15	25	16,6

3x gel buffer:	3M Tris (pH 8,45); 0,3 % (w/v) SDS
AB-3 mix:	50 % (w/v) acrylamide/bisacrylamide (49,5 % T/ 3 % C)
Separating gel buffer:	1.5M Tris/HCl (pH 8,8); 0,4 % (w/v) SDS
Stacking gel buffer:	0.5M Tris/HCl (pH 6,8); 0,4 % (w/v) SDS
4x SDS sample buffer:	250 mM Tris/HCl pH 6.8, 40 % (v/v) glycerol, 8 % (w/v) SDS, 0.4 % (w/v) bromphenol blue
Cathode buffer:	100 mM Tricin; 100 mM Tris (pH 8,25); 0,1 % (w/v) SDS
Anode buffer:	100 mM Tris/HCl (pH 8,9)

2.5.3 Coomassie and silver staining of proteins

For unspecific detection of proteins, PAA gels after SDS-PAGE (section 2.5.2) were stained by shaking overnight in Coomassie solution and destained by alternating washing in fixing solution and 7 % acetic acid until the protein bands were well distinguished from the background. The gels were then packed in a plastic foil and documented by scanning.

Coomassie dye solution:	0,2 % (w/v) Coomassie Brilliant Blue R250 (Serva); 40 % (v/v) methanol; 10 % (v/v) acidic acid
Fixing solution:	50 % (v/v) ethanol; 10 % (v/v) acetic acid

For more sensitive detection silver staining of proteins in PAA gels was performed. The gels were fixed for 30 min in fixing solution, then washed twice with 50 % v/v ethanol and placed in freshly prepared sodium thiosulfate solution for 1 min. After washing 3 times (5 sec each) with water the gels were stained with freshly prepared silver nitrate solution for 15 min. After washing with water (3x 5 sec) the gels were placed in developing solution until the protein bands were properly visible. Staining was terminated by adding the stop solution to the gel. The gels were then packed in a plastic foil and documented by scanning.

Fixing solution:	50 % (v/v) methanol; 12 % (v/v) acetic acid; 0.5 ml l^{-1} formaldehyde

Sodium thiosulfate solution:	0.2 g l^{-1} $Na_2S_2O_3*5H_2O$
Silver nitrate solution:	2 g l^{-1} $AgNO_3$
Developing solution:	30 g Na_2CO_3; 0.25 ml formaldehyde; 10 ml sodium thiosulfate solution; H_2O till 500 ml
Stop solution:	50mM EDTA

2.5.4 Western blot analysis

For specific detection of proteins, Western blot analysis was performed via electrophoretic transfer of proteins to nitrocellulose (Schleicher & Schuell) or PVDF (Bio-Rad) membrane using Mini Trans-Blot cell (Bio-Rad). After SDS-PAGE as described in section 2.5.2, the transfer sandwich consisting of blotting paper (Whatman), membrane, and the gel was assembled in blotting buffer according to manufacturer's instructions. If PVDF membrane was used it was activated for 2 min in methanol and then washed with H_2O prior to assembly. Transfer was performed for 90 min at the constant current of 6,5 mA cm^{-2} gel. The membrane was blocked for 90 min at RT in blocking solution. After washing the membrane in TBS-T buffer (3x 10 min) primary antibodies were added at the necessary dilutions and incubated at 4 ^{0}C overnight on the shaker. If the primary antibodies with the conjugated alkaline phosphatase for direct detection were used, the membrane was washed in TBS-T buffer (2x 5min) and detection was performed using 5-bromo-4-chloro-3-indolyl phosphate (BCIP) and nitro blue tetrazolium (NBT). In other cases secondary antibodies (conjugated with horseradish peroxidase) were applied for 1 h at RT and the membrane was washed with TBS-T buffer (3x 10 min). Chemiluminescent detection of immobilized proteins was performed using CheLuminate-HRP PicoDetect Extended kit (AppliChem) according to manufacturer's instructions. In both cases the signal was detected with the help of Chemiluminescence system Fusion SL (Peqlab).

Blotting buffer:	48 mM Tris/HCl, (pH 9,2); 39 mM glycine; 20% (w/v) methanol; 0,0375% (w/v) SDS
TBS-T:	100 mM Tris/HCl, (pH7,5); 150 mM NaCl; 0,1% (v/v) Tween 20
Blocking solution:	5% (w/v) milk powder in TBS-T

2.5.5 Overexpression and purification of FLAG-tagged proteins from *Synechocystis*

To achieve the necessary level of expression of FLAG-tagged proteins the corresponding mutant strains were grown in BG11 medium (ca. 800 ml) without copper for 7-8 days. The cultures were sedimented by centrifugation 15 min, 6000g, 4 ^{0}C), then the pellet was resuspended in FLAG-buffer with Protease inhibitor solution and sedimented again (15 min, 6000g, 4 ^{0}C). Cell pellets were stored at -80 ^{0}C until further use or used immediately. The pellet was resuspended in 10-15 ml of FLAG-buffer with Protease inhibitor solution and destroyed in the cell mill as described in section 2.5.1. After performing chlorophyll determination (section XXX), the necessary amount of n-dodecyl-β-D-maltoside (β-DM) was calculated and β-DM in the ratio 20:1 β-DM to chlorophyll was added to the cell extracts in order to dissolve membrane proteins. Following 10 min incubation at 4 ^{0}C the cells were sedimented (30 min,

25000g, 4 ^{0}C), the whole cell lysate collected and the soluble fraction was incubated with 400 µl ANTI-FLAG M2 Affinity Gel (Sigma-Aldrich) at 4 ^{0}C overnight. Afterwards the affinity gel was packed in the Poly-Prep Chromatography Column (Biorad) and the flow through was collected at 4 ^{0}C for further analysis. The column was washed 5 times with 2 ml FLAG-buffer (washing fractions were collected for further analysis) after which 200 µl 3x FLAG-Peptide (Sigma-Aldrich) in a concentration of 100 µg/ml was added to the column and it was incubated for 20 min at RT. Following centrifugation (5 min, 3000g, 4 ^{0}C) the supernatant was collected (elution fraction 1) and the column was washed two more times with 100µl 3xFLAG-peptide (elution fractions 2 and 3, analysed together with elution fraction 1). For the next elution step 400 µl 1% (w/v) SDS was used and the matrix was incubated with it for 5 min at RT. After centrifugation (5 min, 3000g, 4 ^{0}C) the supernatant (elution fraction 4) was collected and the matrix was washed with 400 µl 10% (w/v) SDS, incubated for 20 min at RT and centrifuged again (5 min, 3000g, 4 ^{0}C) to obtain elution fraction 5.
Extracted proteins were used for further analysis by SDS-PAGE (section 2.5.2) and Western blot (section 2.5.4).

FLAG-buffer:	50 mM HEPES/NaOH (pH 7,0); 5 mM $MgCl_2$; 25 mM $CaCl_2$; 150 mM NaCl; 10% (v/v) glycerol
Protease inhibitor solution:	5 mg/ml 6-amino-hexaonic acid; 1 mM AEBSF 4-(2-aminoethyl) benzenesulfonyl fluoride hydrochloride; 4 mM p-benzamidine

2.5.6 Overexpression and purification of His-tagged RNaseE/G from *E. coli*

An overnight culture of *E. coli* M15 (pREP4) pQE*Slr1129* was diluted with 1 l of LB supplemented with Amp and Km and grown at 37 ^{0}C on the shaker till OD_{600nm} 0.5-0.8. Then heterologous expression was induced with 1mM isopropyl β-D-1-thiogalactopyranoside (IPTG) and the cells were cultivated at 22 ^{0}C with constant shaking for additional 24 h. The cells were sedimented by centrifugation (10 min, 6000g, 4 ^{0}C) and the pellet was used immediately or stored at -80 ^{0}C until further use. Cell pellet was resuspended in lysis buffer A containing protease inhibitor PMSF (0.2 mM) at 2–5 ml per g wet weight. The cells were disrupted by sonication on ice using ultrasonic homogenizer Bandelin Sonopuls GM 70 (Sigma-Aldrich) with the following parameters: 5 times 1 minute at power 70 with a 10 s cooling period between each burst. Afterwards the cells were sedimented by centrifugation (30 min, 10000g, 4 ^{0}C). In the meanwhile 1 ml of Ni-NTA matrix was equilibrated with buffer A and the whole cell lysate was added to the matrix and incubated for 15 min at 4 ^{0}C with gentle shaking (200 rpm on a rotary shaker). Afterwards the Ni-NTA matrix was packed in the chromatography Column (Qiagen) and the flow through was collected for further analysis. The column was washed 60 volumes of buffer B (washing fractions were collected for further analysis). The proteins were eluted 4 times with 0.5 ml elution buffer containing 250mM imidazole (elution fractions 1-4) and then with elution buffer containing 500mM imidazole (elution fractions 5-8). Extracted proteins were used for further analysis by SDS-PAGE (section 2.5.2).

Buffer A (pH 8.0):	50 mM NaH_2PO_4; 300mM NaCl; 20mM imidazole
Buffer B (pH 8.0):	50 mM NaH_2PO_4; 500mM NaCl; 50mM imidazole; 0.1% (v/v) Triton X-100; 8% (v/v) glycerol
Elution buffer (pH 8.0):	50mM NaH_2PO_4; 300mM NaCl; 250/500 mM imidazole

2.5.7 Overexpression and batch-purification of GST-tagged RNases from *E. coli*

Overnight culture of the corresponding mutant strain was mixed with 1200 ml LB and incubated at 37 ^{0}C on a shaker (200 rpm) till OD_{600nm} 0,4-0,6. Expression of recombinant proteins GST-Slr0346 and GST-Slr1646 was induced by adding 1,5 mM IPTG followed by further incubation for 3 h at 37 ^{0}C. Overexpression of GST-*slr1129* was held in *E. coli* ArcticExpress (DE3) strain where the protein expression was induced by adding 1 mM IPTG; the cells were grown for additional 24 h at 11,5 ^{0}C. Afterwards all cultures were subjected to centrifugation (20 min, 6000g, 4 ^{0}C) and the pellets were used immediately or stored at -80 ^{0}C until further use. Cell pellets were resuspended in 15 ml of NaK-phosphate buffer, 1 mg/ml lysozyme and 2 µl benzonase nuclease were added (both Sigma-Aldrich) followed by 30 min incubation on ice. The cells were disrupted in the cell mill. 500 µl Glutathion Sepharose (GE Healthcare) matrix was equilibrated with 5 ml NaK-phosphate buffer and the whole cell lysate was added to the matrix and incubated 1 h at RT on a rotary shaker. After binding the matrix was sedimented by centrifugation (5 min, 4000g, 4 ^{0}C) and the supernatant (flow through) was collected for further analysis. The matrix was then washed 3 times with 1 ml NaK-phosphate buffer (washing fractions 1-3 are collected for further analysis) and two more times with 1 ml PreScission cleavage buffer (washing fractions 4-5). In order to cleave the GST tag 500 µl PreScission cleavage buffer with 25 µl of PreScission protease (GE Healthcare) was added to the sepharose and incubated on the rotator overnight at 4 ^{0}C. Afterwards the sample was centrifuged (3 min, 4000g, 4 ^{0}C) and the supernatant (elution fraction 1) was collected for further analysis. The proteins were then eluted 3 more times with 300 µl PreScission cleavage buffer (elution fractions 2-4).
Extracted proteins were used for further analysis by SDS-PAGE (section 2.5.2).

NaK-phosphate buffer:	20 mM Na-K-phosphate buffered solution (pH 7,6); 20 mM NaCl; 200 mM KCl, 2 mM $MgCl_2$; 10% (v/v) glycerol.
Na-K-phosphate buffered solution (pH 7,6):	13 ml 0,5 M KH_2PO_4; 87 ml 0,5 M Na_2HPO_4
PreScission-Cleavage buffer:	50 mM Tris/HCl (pH 7,0); 150 mM NaCl; 1 mM EDTA; 1mM DTT.

2.5.8 FPLC purification of GST-tagged RNases

Fast protein liquid chromatography (FPLC) was performed using ÄKTA Pure and corresponding Unicorn 6 Software (both GE Healthcare) according to manufacturer's instructions. For size exclusion chromatography batch-purified proteins (section 2.5.7) were applied to the HiLoad 16/600 Superdex 200 prep grade column (GE Healthcare) equilibrated with NaK-phosphate buffer. The

proteins were eluted with constant flow rate set to 0,5 ml/min and with measuring absorption at 280 nm. Elution fractions were collected for further analysis, concentrated by DOC-TCA treatment (section 2.5.9) and used for SDS-PAGE (section 2.5.2).
For direct purification of GST-tagged RNAses from whole cell lysate (WCL) GSTrap FF prepacked glutathione sepharose fast flow column (GE Healthcare) was utilized. The WCL was first centrifuged (20 min, 16000g, 4 °C) and put through the PVDF syringe filter (pore size 0,22 µm, Merck Millipore), then the sample was applied with the peristaltic pump 0,2-1 ml min^{-1}) to the equilibrated with NaK-phosphate buffer GSTrap FF column. The column was washed with NaK-phosphate buffer, connected to ÄKTA Pure and elution was performed by applying a gradient (2, 10, 20, 40, 70 and 100%) of glutathione elution buffer. Elution fractions were collected and analysed by SDS-PAGE (section 2.5.2).

Glutathione elution buffer: 10mM reduced glutathione; 50 mM TrisHCl (pH 8.0)

2.5.9 DOC-TCA treatment of proteins

If the concentration of extracted proteins after FPLC was not sufficient they were concentrated by sodiumdesoxycholate (DOC) – trichloroacetic acid (TCA) treatment (Bensadoun & Weinstein, 1976) prior to SDS-PAGE. The volume of the probes was adjusted to 1 ml by adding ddH_2O, then 25 µl 2 % (w/v) DOC was mixed with the samples and 30 µl 40 % (v/v) TCA were added. The solution was mixed and the proteins were precipitated for 15 min on ice. After centrifugation (10 min, 16000g, 4 °C) the sedimented proteins were resuspended in 3 volumes of 30 µl ChuaA buffer and mixed with 2 volumes of ChuaB buffer. The concentrated protein samples were then subjected to SDS-PAGE (section 2.5.2).

ChuaA buffer:	0,1 M Na2CO3; 0,1 M DTT
ChuaB buffer:	5 % (w/v) SDS; 30 % (w/v) sucrose; 0,1 % (w/v) bromphenol blue

2.6 RNA methods

To avoid contamination of the samples with RNases and to prevent autocatalytic degradation of RNA sterile disposable tubes, filter pipet tips and DEPC-treated H_2O were used. All the surfaces and pipets were wiped with ethanol and RNase AWAY (Roth). For preparation of *in vitro* transcripts and in further manipulations with them Ribolock (Thermo Fisher Scientific) was always added to the reaction mixture to prevent unspecific RNA degradation.

2.6.1 Extraction of total RNA from *Synechocystis*

For isolation of total RNA from *Synechocystis* ca. 30 ml of liquid culture in exponential growth phase (OD_{750nm} ≈ 0,4) was put through the Supor-450 Membrane Filter (47 mm, 0.45 µm pore size, Pall). The filter was rolled carefully with the forceps, put into the 15ml falcon tube with 1,2ml PGTX solution, destroyed by vortexing for 10-15 sec and frozen in liquid nitrogen. Afterwards

the samples were heated up to 95°C in a water bath for 7 minutes (with vortexing the tubes from time to time). Then the samples were chilled on ice for 5 minutes following addition of 120 µL prechilled 1-bromo-3-chloropropane, vortexing twice for 15 sec and incubation at room temperature for 10 min. Separation of phases was achieved via centrifugation (15 min, 16000g, 4 ^{0}C) after which the upper aqueous phase containing the RNA was transferred in a new pre-chilled 2 mL safe lock Eppendorf tube. After adding an equal volume of phenol:chloroform:isoamylalcohol (25:24:1; Roth) and vortexing for 10 sec the phases were separated again via centrifugation (7 min, 16000g, 4 ^{0}C). RNA was precipitated from the upper phase with and equal volume of isopropanol at -20 °C overnight. After centrifugation (30 min, 16000g, 4 ^{0}C) the pellet was carefully washed with 1 ml of pre-chilled 75% ethanol, centrifuged (15 min, 16000g, 4 ^{0}C), air-dried, resuspended in 30 µL H_2O and stored at -20°C.

PGTX solution: 396 g l^{-1} phenol; 69 ml l^{-1} glycerol; 1 g l^{-1} 8-hydroxyquinoline; 5,8 g l^{-1} EDTA; 8 g l^{-1} sodium acetate; 95 g l^{-1} guanidine thiocyanate; 46 g l^{-1} guanidine hydrochloride; 20 ml l^{-1} Triton x-100

2.6.2 Denaturing polyacrylamide-urea gel electrophoresis of RNA and electroblotting

For analysis of sRNAs and other transcripts smaller than 500nt denaturing polyacrylamide-urea gel electrophoresis of the total RNA was performed using **a** small vertical electrophoresis system (Hoefer) or a custom gel system (21 cm × 18 cm × 0.5 mm) for better resolution. A solution of 10% acrylamide/bisacrylamide (19:1) was prepared in 1× TBE with 7M urea, and polymerization was initiated by adding 1:125 volumes of 10% APS and 1:1,250 volumes of TEMED. Prior to loading the RNA samples on the gel they were mixed with 1x RNA loading dye, denatured for 5 min at 95 ^{0}C and chilled on ice for 5 min. Gels were run in 1× TBE at 7 mA for 45-120 min (or at 480V for 60-80 min for bigger gels), stained with 5 µg ml^{-1} EtBr solution in 1× TBE for 10 min, and destained for 2 min in deionized water. Gels were analysed under UV light as described in section 2.3.6.
To transfer RNA to the nylon membrane (Hybond N+, GE Healthcare) 'Semi-Dry' Electroblotter (*Perfect Blue Semi-Dry SEDEC M,* PEQLAB) was used with the following settings: 90 min in 0,5 x TBE buffer at RT under constant current of 0,8 mA cm^{-2}. Afterwards RNA was crosslinked to the membrane using Stratalinker UV crosslinker (Stratagene) with 120 mJ cm^{-2}.
For detection of specific RNAs from an RNA mixture, Northern hybridization was utilized (section 2.6.5).
When radioactively labeled *in vitro* transcripts for performing *in vitro* cleavage assays were used the PAA gels (21 cm × 18 cm × 0.5 mm) were dried on the gel dryer (GD-5040, Scie-Plas) for 90 min at 80 °C and then wrapped in a plastic foil, packed into a cassette with the phosphor screen and exposed for 24-48 h depending on the strength of the signal. Detection was performed using PharosFX phosphorimager and QuantityOne software (both Bio-Rad).

2.6.3 Denaturing electrophoresis of RNA in formaldehyde-agarose gels and capillary blotting

Total RNA was analysed via electrophoresis in formaldehyde containing agarose gels (1,3% w/v agarose, 5% v/v formaldehyde solution (37%), 1x MEN buffer) at constant voltage 5 V cm^{-1} in 1x MEN buffer using PerfectBlue gelsystem (Peqlab). Prior to loading the RNA samples on the gel they were mixed with 1x RNA loading dye, denatured for 5 min at 95 ^{0}C and chilled on ice for 5 min. Gels were analysed under UV light as described in section 2.3.6.
RNA was transferred to the nylon membrane (Hybond N+, GE Healthcare) by capillary blotting in 20× saline-sodium citrate (20x SSC) buffer overnight at RT. Afterwards the membrane was washed in 2x SSC buffer and RNA was crosslinked to the membrane using Stratalinker UV crosslinker (Stratagene) with 120 mJ cm^{-2}.
For detection of specific RNAs from an RNA mixture, Northern blot hybridization was utilized (section 2.6.5).

10x MEN buffer (pH7,0):	200 mM MOPS; 10 mM EDTA; 50 mM sodium acetate
2x RNA loading dye:	2,5% w/v SDS; 95% v/v formamide (deionized); 0,5 mM Na_2-EDTA; 0,1% w/v xylene cyanol; 0,1% w/v bromophenol blue; 0,4% w/v EtBr
20x SSC:	3 M NaCl; 0,3 M sodium citrate

2.6.4 Synthesis of radiolabeled and DIG-labeled probes

Radioactively labeled with [α^{32}P]-UTP RNA probes were made using MAXIScript Kit (Invitrogen) according to manufacturer's instructions. As a template for *in vitro* transcription gene specific PCR fragments generated in a way that T7 promoter was added to the sequence at the 3' end were used. After *in vitro* transcription template DNA was removed via 15 min digestion at 37 ^{0}C with Turbo DNase from the same kit. Radiolabeled probes were then purified with Illustra MicroSpin G-25 column (GE Healthcare) according to manufacturer's instructions.
For non-radioactive probes RNA was labeled with digoxigenin-UTP by *in vitro* transcription with T7 polymerase using DIG RNA Labeling Kit (Roche) according to the instructions. Gene specific DNA sequence fused to a T7 promoter was used as a template for *in vitro* transcription.

2.6.5 Northern blot hybridization

Northern blot analysis was performed following denaturing polyacrylamide-urea (section 2.6.2) or formaldehyde-agarose gel electrophoresis (section 2.6.3). After crosslinking the membrane was equilibrated in Church buffer for 45 min at 65 ^{0}C in a hybridization oven with rotation. Afterwards radioactively labeled probe was added to the Church buffer followed by hybridization of the membrane at 65 ^{0}C in a hybridization oven with rotation overnight. The membrane was then washed with washing solution I in a hybridization oven with rotation for 15 min at RT, then for 15 min at 65 ^{0}C and eventually for 15 min at 65 ^{0}C with washing

solution II. After sealing the membrane in a plastic bag, it was placed into a cassette with the phosphor screen and exposed for 1-48 h depending on the strength of the signal. Detection of the hybridization signals was performed using PharosFX phosphorimager and QuantityOne software (both Bio-Rad).
For Dig labeled probes the washing and detection procedures were the following: after overnight hybridization RNA probe solution was replaced with P1 buffer and incubated with constant rotation for 5 min at RT twice, then incubation with P2 buffer for 20 min at 68 °C in the hybridisation oven with rotation was performed twice. After equilibration of the membrane in 1x Dig P1 buffer for 5 min at RT it was blocked in 1 X Px buffer (DigP1 buffer with 1% blocking solution) for 30 min followed by 30 min incubation in 1 X Py buffer (DigP1 buffer with 1% blocking solution and Anti-Dig antibody [1:10.000], Roche). Afterwards the membrane was washed with P1 buffer for 15 min 3 times and placed into P3 buffer for 5 min. Detection was performed using CDP-*Star* chemoluminescence substrate (Sigma-Aldrich) diluted 1:100 in P3 buffer and visualized under UV-irradiation in UV transilluminator MD-25/HD-25 (Wealtec).

Church buffer:	0,25 M Na_2HPO_4/NaH_2PO_4 (pH 7,2); 1mM EDTA; 7% (w/v) SDS; 250mM NaCl; 50% (v/v) formamide (deionized)
Washing solution I:	2 x SSC; 0,5 % (w/v) SDS
Washing solution II:	0,1 x SSC; 0,1 % (w/v) SDS
P1 buffer:	2 x SSC; 0.1% SDS
P2 buffer:	0.1 SSC; 0.1% SDS
P3 buffer (pH 9,5):	100 mM Tris; 100 mM NaCl;
10 x Dig P1 buffer (pH 7,5):	1 M maleic acid; 1.5 M NaCl
10% blocking solution:	5 g blocking reagent (Roche) in 50 ml 1 X Dig P1

2.6.6 Microarray

Prior to hybridization total RNA was treated with Turbo DNase (Invitrogen) according to manufacturer's instructions, precipitated with sodium acetate/ethanol at -20 °C overnight, washed with ethanol and resuspended in H_2O. 3 µg of total RNA was taken for labeling with 2,4 µl ULS-Cy3 dye using ULS fluorescent labeling kit for Agilent arrays (Kreatech) at 85 °C for 15 min and then the reaction mixture was put on ice in the darkness. Afterwards the dye was removed using KREApure Columns (same kit) according to manufacturer's instructions. 1,65 µg RNA was then fragmented and hybridized using 4x44k one colour microarray (Agilent) according to manufacturer's instructions. After 17 h hybridization at 65 °C in a hybridization oven with rotation the array was washed and analysed using Feature extraction software of the G2565CA Microarray scanner (Agilent).

2.6.7 *In vitro* cleavage assay

For *in vitro* cleavage assays *in vitro* transcription was performed with T7 polymerase and PCR fragments generated in a way that T7 promoter was added to the sequence at the 5' end as templates using MEGAshortscript T7 Kit

(Thermo Fisher Scientific) according to manufacturer's instructions. Residual DNA was removed via 15 min digestion at 37 ^{0}C with Turbo DNase from the same kit. If needed the transcripts were radioactively labeled with [α^{32}P]-UTP and then purified with Illustra MicroSpin G-25 column (GE Healthcare) according to manufacturer's instructions. If dephosphorylation of the transcript was needed it was performed prior to the assay using 5' RNA polyphosphatase (Epicentre) according to the manufacturer's instructions. Afterwards the transcripts were purified using RNA Clean & Concentrator-5 kit (Zymo Research) according to manufacturer's instructions. Then the ionizing radiation of the transcripts was measured in counts per minute (cpm) on the LS6500 Multi Purpose Scintillation Counter (Beckman Coulter). The transcripts were diluted in a way that ca. 1500 cpm per well was loaded on the gel.
In vitro cleavage assay was carried out for 15 min at 30 ^{0}C in 10 µl reaction mixture containing cleavage buffer, 1,5 pmol RNA transcript and 7 pmol affinity-purified RNase. Endoribonuclease activity was abolished by addition of 1 µl 0.5 M EDTA and 1 volume RNA loading dye. Finally, samples were heated to 95 ^{0}C for 5 min, briefly chilled on ice and cleavage reactions were analysed by employing electrophoretic separation on 6-10% PAA gel (section 2.6.2) followed by detection and analysis of radioactive signals (section 2.6.5) or by EtBr staining (section 2.6.2) and visualization under UV light (2.3.6).

Cleavage buffer: 25 mM Tris–HCl (pH 8.0); 60 mM KCl; 5 mM $MgCl_2$; 100 mM NH_4Cl; 0,1 mM DTT; 5% (w/v) glycerol

2.6.8 Individual-nucleotide resolution crosslinking and immunoprecipitation (iCLIP)

The iCLIP protocol was established with the kind help of Dr. Oliver Rossbach (Institute of Biochemistry, Justus-Liebig University, Giessen) and Dr. Nils Schürgers (Institute of Biology III, Albert-Ludwigs University Freiburg). The methodology is similar to that described in König *et al* (2010). All the work was performed on ice using precooled buffers.
First the cultures (100 ml) of RNase overexpression *Synechocystis* mutant strains and the WT were grown in BG11 medium without copper and supplemented with the necessary antibiotics, then the cells were harvested (10 min, 6000g, 4 ^{0}C), the pellet was resuspended in in 10x volume RIPA-Buffer, transferred to cell culture dish on ice and irradiated 3 times with 450 mJ cm^{-2} UV-C light (at 254 nm) in the Stratalinker UV crosslinker (Stratagene). Cells were then sedimented (10 min, 3000g, 4 ^{0}C), pellet resuspended in 500µl RIPA-buffer supplemented with 3 µl Ribolock (Thermo Fisher Scientific) and the cells were disrupted in the cell mill (see section 2.5.1). The cell extract was cleared by centrifugation (20 min, 20000g, 4 ^{0}C) and the supernatant was collected. In order to determine the necessary amount of β-DM needed for solubilisation, chlorophyll determination was performed (see section 2.2.6). After adding β-DM in the ratio 20:1 β-DM to chlorophyll, solubilisation was performed by gentle agitation on ice for 40 min. Insolubilized material was removed by centrifugation (20 min, 20000g, 4 ^{0}C). Solubilized supernatant was subjected to DNase and RNase treatments: cell extract was diluted 1:2 with RQ1 buffer, mixed with 1:500 vol TURBO DNase (2

U/µl). Different dilutions of RNase I (100 U/µl) from 1:10 to 1:1000 in RQ1 buffer were prepared. These dilutions were added to the extract at a 1:1000 dilution. After incubation for 3 min at 37 °C with shaking (800 rpm), reactions were put on ice immediately for 5 min, followed by addition of 1:42 volumes of 5 M NaCl to a final concentration of 170 mM NaCl.
For co-immunoprecipitation 50µl ANTI-FLAG M2 affinity gel (Sigma-Aldrich) washed prior to use with FLAG buffer with Protease inhibitor solution (supplemented with Ribolock) was added to the extract and incubated for 2h (or overnight) at 4 °C on the rotator. After sedimentation (4 min, 4000g, 4 ^{0}C) the beads were washed 4 times with 1 ml TBS600-T buffer. After washing 80 µl pre-mixed phosphatase reaction was added to beads:

8 µl	10× phosphatase-buffer
3 µl	shrimp alkaline phosphatase (1 U/µl) (Roche)
1 µl	Ribolock (40 U/µl)
68 µl	H_2O (RNase free)

The reaction mixture was incubated for 20 min at 37°C, and washed twice with TBS600-T and twice with T4 polynucleotide kinase buffer (PNK-buffer) (Thermo Fisher Scientific).
Then 50µl pre-mixed RNA-linker ligation reaction was added to the beads:

3 µl	100 µM 3'-RNA-linker (Table 4)
5 µl	10× T4 RNA-ligase buffer
5 µl	10 mM ATP
1,25 µl	T4 RNA-ligase (10 U/µl) (Thermo Fisher Scientific)
0,5 µl	Ribolock (40 U/µl)
12,5 µl	Poly (ethylene glycol) (M_n 380-420) (Sigma-Aldrich)
22,75µl	H_2O

The reaction mixture was incubated overnight at 16 °C and washed twice with PNK-buffer.
Afterwards radioactive 5' end-labeling was performed by adding 20µl pre-mixed PNK labeling reaction to the beads:

2 µl	10× PNK-buffer (Thermo Fisher Scientific)
5 µl	[γ-^{32}P]-ATP (12.5 µM; 800 Ci/mmol)
1 µl	T4 polynucleotide kinase (10 U/µl) (Thermo Fisher Scientific)
0,5 µl	Ribolock (40 U/µl)
11,5 µl	H_2O

The reaction mixture was incubated for 20 min at 37 °C and washed once with TBS-T and once with PNK-buffer. The beads were mixed 1:1 with SDS loading buffer supplemented with reducing reagent (DTT) and the protein-RNA complexes were eluted by shaking at 1000 rpm for 10 min at 70 °C. The NuPAGE Novex 4-12% Bis-Tris gel (Thermo Fisher Scientific) was run for 75 min at 200 V, and the transfer to nitrocellulose membrane was performed for 1 h at 30 V using the NuPAGE electrophoresis and blotting system (Thermo Fisher Scientific). The membrane was then sealed in a plastic foil, placed into a cassette with the phosphor screen and exposed overnight.

The regions above the crosslinked bands were cut from the membrane (smear) and the proteins were digested via proteinase K (PK) treatment by adding 10 µl PK, 20 mg/ml (Sigma-Aldrich) in 200 µl PK-buffer to nitrocellulose membrane pieces and incubation at 37 °C for 20 min with shaking (1000 rpm). Afterwards 200 µl of urea-buffer was added followed by incubation for 20 min at 55 °C. The phenol-chlorophorm extraction was performed by adding 400µl of phenol/chloroform/isoamylalcohol (25:24:1; Roth), shaking for 5 min at 30 °C and separation of the phases for 5 min at 16000g, 4 °C. Aqueous phase was ethanol-precipitated at -20°C overnight. After centrifugation (15 min, 16000g, 4 ^{0}C) air-dried RNA pellet was diluted in 6 µl H_2O and reverse transcription was performed using one of the 5'-phosphorylated reverse transcription primers with distinct experimental barcode to filter for experiments/controls after sequencing. For that SuperscriptIII first strand synthesis supermix (Invitrogen) was utilized with the following reaction setup:

6 µl RNA solution
1 µl 2 µM iCLIP-RT primer (Table 4)
1 µl annealing buffer

Pre-incubation was performed in a thermocycler:

35 °C 5 min
25 °C hold

Then reverse transcription mix was added:

2 µl Superscript III / RNaseOUT enzyme mix
10 µl 2x first strand reaction mix

Incubation was performed in a thermocycler:

25 °C 5 min
45 °C 20 min
50 °C 50 min
85 °C 5 min

The reaction mixture was placed on ice after which ethanol precipitation was performed overnight at -20 °C as described above.
Samples were mixed 1:1 with 2× TBE-urea loading buffer (Invitrogen) and incubated at 70 °C for 3 min directly before loading on a 6% TBE PAA-urea gel (section 2.6.2). The gel was run at 180 V for 40 min, the slice of the gel with the marker was cut out, stained with EtBr and aligned back together with the rest of the gel to be able to distinguish the sizes of the bands and not to damage the samples by EtBr staining. Three different size regions were cut from the gel (70-85 nt, 85-110 nt and 110-200 nt) and cDNA was purified by crushing the gel pieces with a syringe plumber in 400 µl Tris-EDTA-buffer. Following purification with Illustra MicroSpin G-25 column (GE Healthcare) according to manufacturer's instructions, the samples were ethanol-precipitated at -20°C overnight. RNA pellet was diluted in 8 µl circligation mix:

0,8 µl	10× circligase II buffer (Epicentre)
0,4 µl	50 mM $MnCl_2$
0,5 µl	1 mM ATP
0,3 µl	circligase II (100 U/µl) (Epicentre)
6 µl	H_2O

Reaction mixture was incubated for 1 h at 60 °C. As the next step 30 µl of a pre-mixed reaction mixture containing an oligonucleotide (Table 4) that is complementary to the single-stranded BamHI restriction site was added to create a double-stranded restriction site:

3 µl	10x fast digest buffer (Thermo Fisher Scientific)
1 µl	10 µM cut oligo
26 µl	H_2O

To anneal the oligonucleotide incubation was performed for 2 min at 95 °C then decreasing the temperature by 1°C every 10 sec, holding at 25°C in a termocycler. Linearization was achieved by adding 2 µl fast digest BamHI (Thermo Fisher Scientific), and incubation for 30 min at 37 °C. Samples were ethanol- precipitated at -20°C overnight, RNA pellet was diluted in 25 µl H_2O.
The cDNA was amplified by PCR in several different reactions with varying cycle number (25, 27 and 30 cycles) to estimate the optimal conditions for preparative PCR, using the following reaction setup:

0,25 µl	primer mix Solexa P5/P3 (10 µM each) (Table 4)
0,5 µl	cDNA solution
5 µl	2× accuprime supermix 1 (Thermo Fisher Scientific)
4,25 µl	H_2O

PCR temperature profile:

2 min	94 °C	initial denaturation	
15 sec	94 °C	denaturation	] 25-30 cycles
30 sec	65 °C	annealing	
30 sec	68 °C	elongation	
3 min	68 °C	final elongation	
hold	4 °C	storage	

5 µl of the PCR reaction was analysed on a 6% PAA-urea gel (see section 2.6.2). 27 cycles seemed to be optimal.
PCR for Solexa library preparation was performed using the same temperature profile as described for analytical PCR, with three cycles less than the optimal cycle number estimated (27-3=24 cycles), because cDNA used for it was more concentrated (Huppertz *et al.,* 2014). The following reaction setup was used:

1 µl	primer mix Solexa P5/P3 (10 µM each) (Table 4)
10 µl	cDNA solution
20 µl	2× accuprime supermix 1 (Thermo Fisher Scientific)
9 µl	H_2O

The samples were pooled together in the following way:

for RNaseE/G (*slr1129*):	20 µl of 70-85 nt fraction
	25 µl of 85-110 nt fraction
	15 µl of 110-200 nt fraction
for RNaseIII-2 (*slr1646*):	18 µl of 70-85 nt fraction
	20 µl of 85-110 nt fraction
	22 µl of 110-200 nt fraction

PCR mix was purified using illustra GFX PCR DNA and gel band purification kit (GE Healthcare) according to manufacturer's instructions (elution with 80 µl of water) and checked on the fragment analyzer using PROSize software (both Advanced Analytical). Afterwards cDNA was sent for sequencing to Max Planck-Genome-centre Cologne.

RIPA Buffer:	50 mM Tris/HCl (pH 7,5); 1% NP-40; 0.1% (w/v) SDS; 150mM NaCl; 5 mM EDTA
RQ1 buffer:	40 mM Tris/HCl (pH 8); 10 mM $MgSO_4$; 1 mM $CaCl_2$
PK buffer:	100 mM Tris/HCl (pH 7,5); 50 mM NaCl; 10 mM EDTA; 1% (w/v) SDS
Urea buffer:	100 mM Tris/HCl (pH 7,5); 50 mM NaCl; 10 mM EDTA, 1% (w/v) SDS; 7M Urea
Tris-EDTA buffer:	10 mM Tris/HCl (pH 8.0); 1 mM EDTA
TBS600-T:	50mM Tris-HCl (pH 7,5); 600mM NaCl; 0,05% (v/v) 20% Tween 20
PNK buffer:	70 mM Tris-HCl (pH 7,5); 10 mM $MgCl_2$; 0,05% (w/v) NP-40

2.6.9 3' rapid amplification of cDNA ends (3' RACE)

The 3' RACE was performed with the mixture of RNA transcripts obtained after performing *in vitro* cleavage assay (2.6.7). First, the RNA was dephosphorylated using FastAP thermo sensitive alkaline phosphatase (Thermo Fisher Scientific) according to the manufacturer's instructions. Afterwards the volume of the reaction mixture was brought to 200 µl with H_2O, mixed with 1 volume of phenol/chloroform/isoamylalcohol (25:24:1; Roth), vortexed shortly and the phases were separated by centrifugation (3 min at 4000g, RT). The upper aqueous phase containing the RNA was transferred in a new 1,5 mL Safe Lock Eppendorf tube. Then 1 volume of 1-Bromo-3-chloropropane was added, followed by vortexing and centrifugation (3 min at 4000g, RT). The aqueous phase was transferred to a new 1,5 mL Safe Lock Eppendorf tube, mixed with 1:10 volume of sodium acetate and 3 volumes of 100% ethanol and incubated at -20 ^{0}C overnight. After centrifugation (30 min, 16000g, 4 ^{0}C) the pellet was air-dried and resuspended in 15 µL H_2O. As the next step linker was ligated to the 3' end with the following reaction setup:

15 µl	RNA solution
2,5 µl	10x T4 RNA ligase buffer (Epicentre)
2 µl	10 mM ATP
1 µl	Ribolock (40 U/µl)
0,2 µl	10 pmol μl^{-1} 3' linker (Table 4)

0,8 µl T4 RNA ligase (5 U/µl) (Epicentre)

Reaction mixture was incubated for 1 h at 37 °C, the volume was brought to 200 µl with H_2O, mixed with 1 volume of phenol/chloroform/isoamylalcohol (25:24:1; Roth), vortexed shortly and the phases were separated by centrifugation (3 min at 4000g, RT). The upper aqueous phase containing the RNA was transferred in a new 1,5 mL Safe Lock Eppendorf tube. Then 1 volume of 1-Bromo-3-chloropropane was added, followed by vortexing and centrifugation (3 min at 4000g, RT). The aqueous phase was transferred to a new 1,5 mL Safe Lock Eppendorf tube, ethanol precipitated at -20 ^{0}C overnight, followed by centrifugation (30 min, 16000g, 4 ^{0}C), air-drying and dissolving in 5 µl H_2O. Then in vitro transcription was utilized using Superscript III first strand synthesis supermix (Invitrogen) with the following reaction setup:

5 µl RNA solution
1 µl 2 pmol µl^{-1} 3RACE_RTrev primer (Table 4)
30 µl H_2O

Reaction mixture was incubated for 5 min at 95 °C in the thermocycler, then slowly cooled down at RT and finally placed on ice. 10 µl 5x first strand buffer and 2 µl Superscript III / RNaseOUT enzyme mix (both Invitrogen) were added and the reaction mixture was incubated for 2 h at 42 °C. For inactivation of the enzyme 5 min incubation at 95 °C was performed. cDNA was amplified by PCR using MyTaq DNA polymerase (Bioline) and the following primer combinations:

3RACE_Tm55 – 5S RACE1
3RACE_Tm55 – 5S RACE2
3RACE_Tm55 – 5S RACE3
3RACE_Tm55 – 5S RACE4
(Table 4)

The PCR products were separated via gel electrophoresis on a 3% NuSieve 3:1 agarose (Biozym) gel and stained with EtBr for visualization under UV light. PCR bands contatining products of interest were excised from the gel, PCR products were purified using QIAEX II gel extraction kit (Qiagen) according to manufacturer's instructions and cloned into pJET1.2 cloning vector utilizing CloneJET PCR cloning kit (Thermo Fisher Scientific) according to manufacturer's instructions. Ligation mixture was used for the transformation of *E. coli* DH5α competent cells (section 2.3.9). Plasmid DNA was then extracted and subjected to sequencing.

3. Results

The aim of this work was to investigate the RNA degradation machinery in *Synechocystis*. We started with the research of the main players in RNA decay in *Synechocystis* involving *rne* (*slr1129*) and two types of *rnc*: *rnc*1 (*slr0346*) and *rnc*2 (*slr1646*) with the further focus on *rne*. We were interested which RNases are responsible for the RNA cleavage in *Synechocystis*. As there has been extensive work done with the study of the function of the RNA chaperone Hfq in *Synechocystis* by AG Wilde we decided to have a closer look on sRNAs that are differently processed in an *hfq*-knockout strain. Thus, the first part of the results is devoted to the study of Hfq-dependent sRNAs Hpr8 and Hpr10, whereas the second part is based on the investigation of putative RNase targets in *Synechocystis* with the main focus on the iCLIP-based analysis of Rne binding to RNA.

3.1 Analysis of Hfq-dependent sRNAs

Extensive studies of the function of the Hfq protein in *Synechocystis* and its properties done by Dr. D. Dienst and Dr. N. Schürgers (AG Wilde) inspired further investigation of involvement of Hfq in RNA regulation. Microarrays and tiling array (Dienst *et al*, 2008, 2010; Schürgers, 2014) shed light on the differential transcript accumulation in *Δhfq* mutant in comparison to the WT. As the intergenic regions were also included in the analysis it was possible to detect Hfq-dependent putative sRNAs (Hprs) that were differently accumulated in the mutant.

3.1.1 General characteristics of Hpr8

The coding sequence for Hpr8 is located on the chromosome between *slr1213* (two-component response regulator AraC subfamily) and *slr1214* (two-component response regulator PatA subfamily) in the same orientation (Figure 10A). Hpr8 is not conserved among cyanobacteria even in closely related organisms (Kopf *et al*., 2015). However the high number of reads in the RNA-seq data (Mitschke *et al*., 2011) suggests its importance at least for *Synechocystis*. Northern blot analysis of the transcript accumulation in the WT revealed 3 fragments of approx. 360, 160 and 80 nt length detected after the hybridization with radioactively labelled Hpr8 probe, which indicates post-transcriptional processing. In *Δhfq* mutant however only a faint band for the largest (full length Hpr8) transcript and a slightly brighter band corresponding to the medium-size transcript are visible (Figure 10B). Thus we can see that Hpr8 processing is different in the *Δhfq* mutant and therefore is Hfq-dependent. The secondary structure of Hpr8 contains several terminal loops. Such loop structures can be important for RNA-RNA interactions and therefore facilitate functioning of Hpr8 as *trans*-ncRNA (Figure 10C). Also the presence of single-stranded AU-rich region (Figure 10C, magnified; nt 58-86) suggests that Hpr8 might be cleaved by Rne. The possible cleavage site position also fits to the results obtained by Northern blot analysis (Figure 10B).

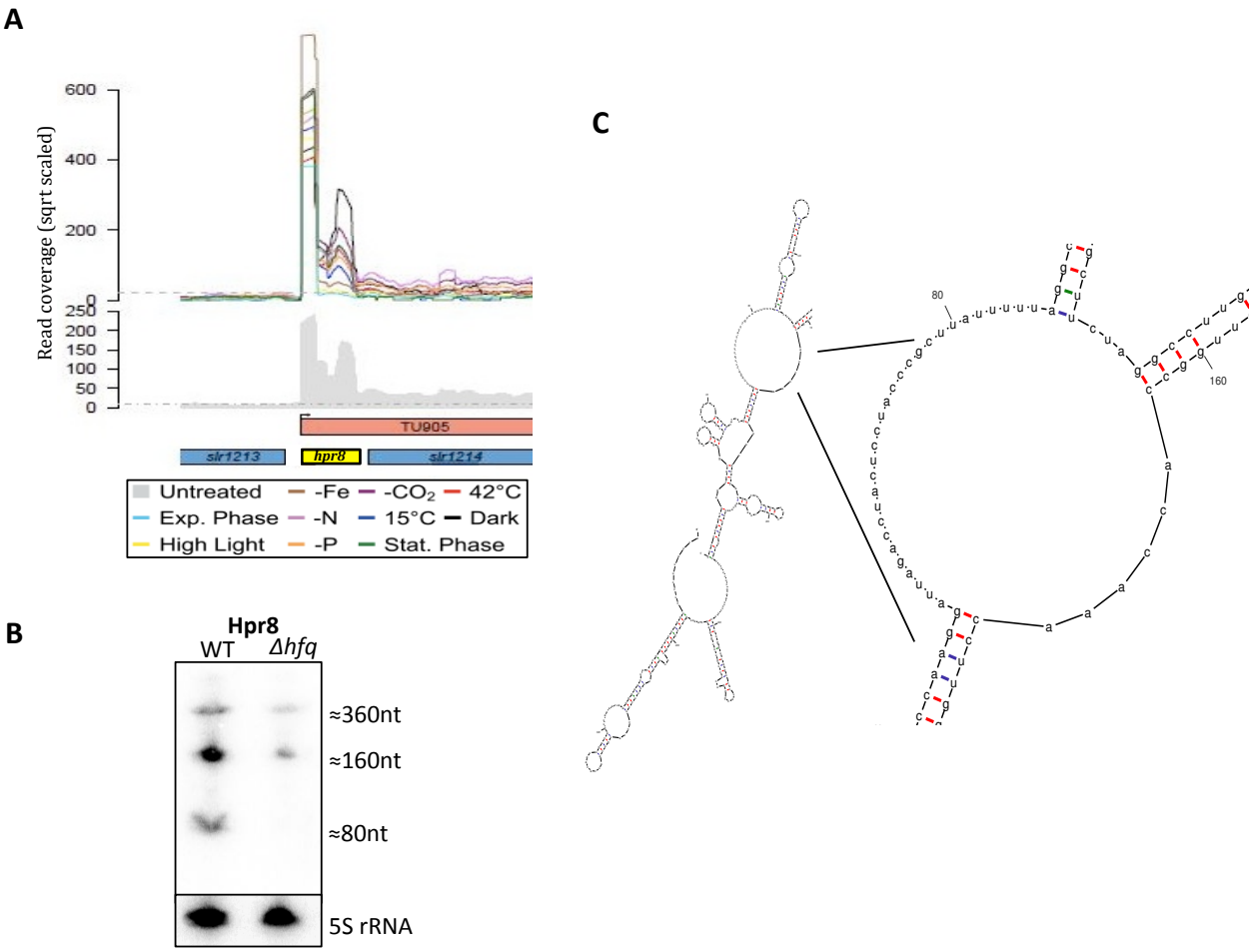

Figure 10: Northern blot verification of Hfq-dependent accumulation of Hpr8 and its predicted secondary structure

(A) Transcriptional organization of the *hpr8* locus. The color-coded graphs represent the accumulation of primary reads in the dRNA-seq analysis for the ten compared conditions (listen in black box). Secondary read coverage is depicted in grey; transcriptional units are depicted in orange; protein-coding genes are displayed in blue; Hpr8 is depicted in yellow. Figure from Kopf *et al.*, 2015; modified.

(B) Northern blot hybridization with the radioactively labelled Hpr8 probe. 5 µg RNA extracted from exponentially growing liquid culture (OD_{750nm} 0,6) was subjected to PAA-urea gel electrophoresis, transferred to nylon membrane and hybridized with Hpr8 probe as well as with 5S rRNA for loading control. Transcript sizes were estimated by overlapping the pictures of the membrane with the one from the EtBr-stained gel containing Low Range Riboruler RNA Ladder.

(C) Prediction for the secondary structure of Hpr8 corresponding to the respective minimum free energy state using mfold web server; the region containing a possible cleavage site is magnified.

3.1.1.1 Characterization of Hpr8 knockout, overexpression and complementation mutants

In order to investigate functions of Hpr8 *in vivo* knockout (as described in section 2.4.3), overexpression (see section 2.4.4) and complementation strains were generated. Complementation of *Δhpr8* was achieved by transferring the

Hpr8 overexpression plasmid in the *Δhpr8* strain via conjugation. The created mutant strains were verified by Northern blot analysis using radioactively labelled Hpr8 probe (Figure 11).

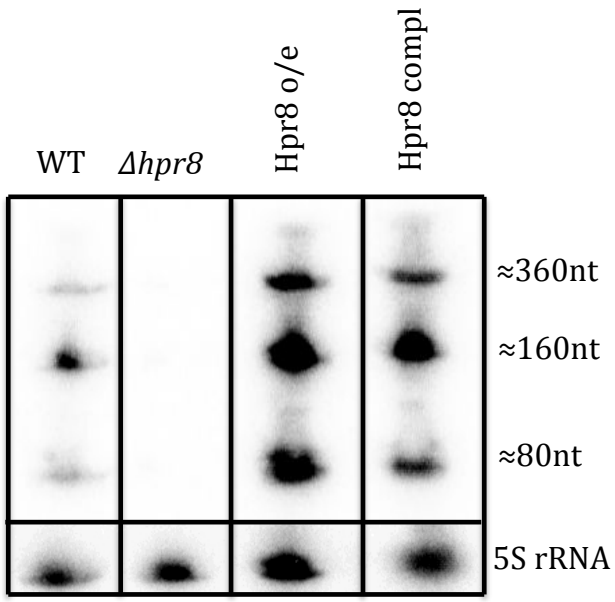

Figure 11: Northern blot verification of Hpr8 knockout, overexpression and complementation mutants
WT and the mutants (overexpression and complementation were achieved by introducing a self-replicating vector pVZ321 containing Hpr8 under the control of *petJ* promoter that is induced by the lack of copper in the media) were grown on BG11 medium without copper for 7 days to induce the expression of Hpr8 in the overexpression and complementation strains. 5 µg RNA was separated on 10% PAA-urea gel and transferred to PVDF membrane followed by hybridization with Hpr8 probe. Hybridization with 5S rRNA was made for loading control. The presented image was combined of the lanes cut out from the initial image of the hybridized membrane; the samples were analysed together in one experiment.

Analysis of the phenotype of the aforementioned strains did not show a remarkable difference in pigment content when compared to the WT (Figure 12A). In the absorption spectrum of whole cells, there was only a slightly lower phycocyanin content detected in the mutants expressing Hpr8 from the *petJ* promoter. It seems, that the complementation strain of Hpr8 is more similar to the overexpression one than to the WT in its phenotype because complementation mutant was constructed via introduction of pVZ321-*hpr8* to *Δhpr8* mutant and expression of Hpr8 integrated in this vector is higher than the natural expression of Hpr8. Hpr8 was expected to be involved in light-dependent motility (see below), hence we decided to check phototaxis behaviour of *Δhpr8* under different light conditions. However it did not differ from phototaxis behaviour of the WT (Figure 12B).

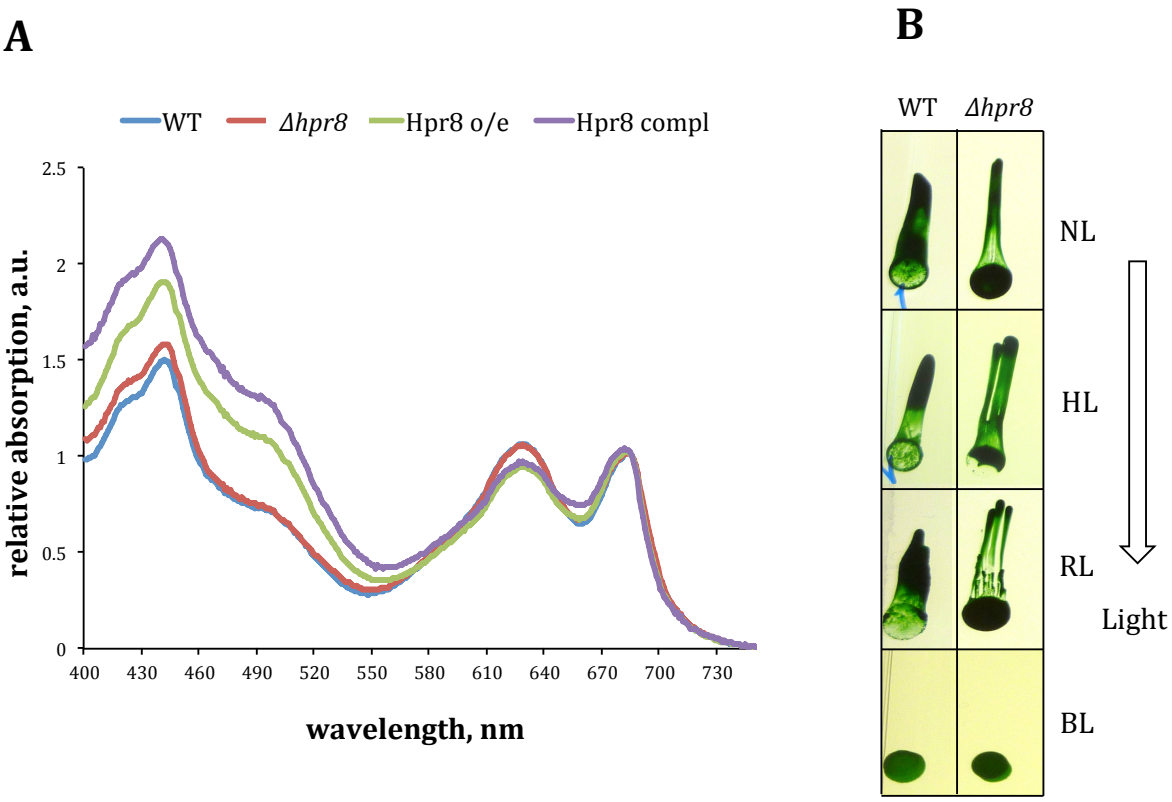

Figure 12: Phototaxis behaviour of Hpr8 knockout mutant
(A) Absorption spectra of liquid cultures of WT and Hpr8 knockout, overexpression and complementation strains grown for 8 days on BG11 without copper under normal light conditions. The spectra were normalized to chlorophyll *a* absorption at 685 nm and OD_{750nm}.
(B) Phototaxis assay on 0,5 % BG11 plates under normal light (NL), high light (HL), red light (RL) and blue light (BL); cells were grown in a special chamber with unidirectional illumination for 7 days. *Δhpr8* mutant behaved exactly like the WT under all tested light conditions. The presented image was combined of the lanes cut out from the initial image of the phototaxis plate; the samples were analysed together in one experiment.

In order to identify targets of Hpr8 we decided to monitor changes in abundance of putative target mRNAs by performing microarray analysis. For the microarray experiment RNA from the Hpr8 overexpression strain cultivated till logarithmic growth phase (OD_{750nm} 0,6) in BG11 medium with and without copper (each time 2 biological replicates) was extracted. Hpr8 overexpression strain under non-induced (BG11 with copper) conditions was taken as an equivalent instead of the WT to have a more accurate comparison and to avoid possible artefacts. Northern blot analysis of RNA samples taken immediately before (0h) and 6, 24 and 30 h after copper depletion showed that induction of Hpr8 after 6 h was possibly strong enough to detect changes in gene expression of targets (Figure 13). That is why in order to minimize the number of false positives that may result from secondary or pleiotropic effects upon longer overexpression of Hpr8 time point of 6 h after copper step down was chosen for the microarray assay. Transcripts with a $\log_2$ fold change (FC) ≥1 (for upregulated) and FC ≤ -0,45 (for

downregulated) transcripts and a P value ≤ 0.03 were taken as significantly differentially expressed. The results are summarized in Table 8.

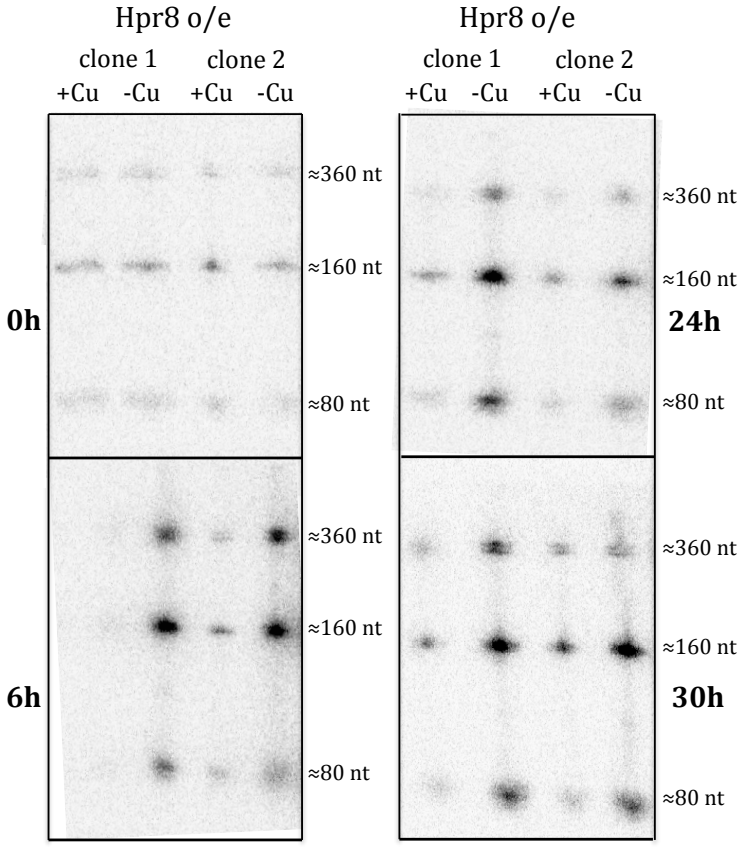

Figure 13: Northern blot analysis of RNA used for the microarray
5 µg RNA isolated from exponentially grown cultures of Hpr8 overexpression strain was separated on PAA-urea gel and transferred to nylon membrane. RNA samples were taken 0, 6, 24 and 30 hours after copper step down. Non-induced (BG11 with copper) cultures were treated in the same way as the induced (BG11 without copper) ones. Hybridization was performed with radioactively labelled Hpr8 probe.

Table 8: Microarray results of downregulated and upregulated transcripts responsive to overexpression of Hpr8. Compared to Hpr8 overexpression strain grown on BG11 containing copper (hence the overexpression of Hpr8 is not induced). Co-transcribed genes from known operons as well as similarly regulated genes (putative operons) were grouped together.
*FC of the transcripts in WT after 24h copper limitation compared to the WT grown under standard conditions in the presence of copper. NA stands for not annotated in the microarray design. The microarray analysis was performed by Dr. Jens Georg (Department of Genetics and Experimental Bioinformatics, Institute of Biology III, Albert-Ludwigs University Freiburg)

Gene name	Synonym	Gene product / description	FC	-Cu*
Downregulated				
sll0788	*copM*	hypothetical protein	-3.14	-0.9

Gene name	Synonym	Gene product / description	FC	-Cu*
sll0789	*copR, rre34, rreC*	two-component response regulator OmpR subfamily	-2.33	-0.2
sll0790	*hik31, copS, hikC, chk31*	two-component sensor histidine kinase	-1.35	-0.05
sll0381		hypothetical protein	-2.97	-1.13
sll0382		hypothetical protein	-2.14	-1
sll0383	*cbiM*	cobalamin biosynthesis protein M	-1.32	-1.3
sll0384	*cbiQ*	unknown protein	-1.28	-1.01
sll0385	*cbiO*	ATP-binding protein of ABC transporter	-0.62	-0.67
sll0036		hypothetical protein	-1.05	-0.46
sll0037	*cbiX*	hypothetical protein	-1.14	-0.62
NC-520		hypothetical 5'UTR	-0.79	NA
sll0199	*petE*	Plastocyanin	-0.68	-2.02
NC-175		located upstream of *petE*	-0.65	NA
NC-173		located upstream of *petE*	-0.63	NA
NC-544			-0.57	NA
ssr0692		hypothetical protein	-0.54	0.5
slr2015	*pilA9*	type IV pilin-like protein	-0.53	-0.36
slr2016	*pilA10*	type IV pilin-like protein	-0.47	-0.42
slr2017	*pilA11*	type IV pilin-like protein	-0.46	-0.45
sll1924	*sycrp2*	cAMP receptor protein sycrp1 homolog	-0.53	-0.01
Upregulated				
sll1796	*petJ*	cytochrome c_{553}	2.19	2.99
NC-425		Hpr8	2.15	NA
NC-109		located downstream of *petJ*	1.96	NA
NC-1136			1.86	NA
NC-1134			1.66	NA
slr0601		unknown protein	1.09	1.81
NC-380		located upstream of *sll1077*	1.04	NA

Microarray results showed that in Hpr8 overexpression mutant 21 RNA features presented reduction in transcript quantity and 7 RNA features (including Hpr8) illustrated increase in accumulation. Most of the affected downregulated genes are parts of operons. The genes with the strongest downregulation are organized in *copMRS* operon (*sll0788-sll0790*) that encodes two-component system *hik31-rre34* (*sll0789* and *sll0790*) and ORF (*sll0788*) containing two DUF305 domains of unknown function (Giner-Lamia *et al.*, 2012). This two-component system is responsible for copper resistance in *Synechocystis* and it also controls its own induction in response to copper in the medium (Giner-Lamia *et al.*, 2012) and therefore downregulation observed in the microarray is most likely a consequence of cell response to the lack of copper and not to the overexpression of Hpr8. *petE* is probably also downregulated due to copper limitation in the growth media. *petE* encodes plastocyanin that together with cytochrome c_{553} (encoded by *petJ*) mediates electron transport between cytochrome b_6f and

photosystem I complexes. Cells grown in the presence of copper synthesize plastocyanin, whereas under copper deprivation cytochrome c_{553} is produced. The mechanisms of copper regulation of synthesis of plastocyanin and cytochrome c_{553} were investigated by Zhang *et al*., and it has been demonstrated that copper regulates expression of both of *petE* and *petJ* prior to translation (Zhang *et al*., 1992). This also explains why *petJ* showed strong upregulation in our microarray results. It is likely that *NC-173* and *NC-175* located upstream from *petE* and *NC-109* located downstream from *petJ* present similar behavior to the adjacent genes due to the lack of copper and not to overexpression of the sRNA. Up- and downregulation of *petJ* and *petE* respectively is also seen from the microarray results comparing behaviour of the WT strain grown with and without copper (Table 8, last column). Another downregulated gene cluster *sll0381-sll0385* encodes for two cobalt transport proteins (CbiM and CbiO) suggesting that its possible role is related to metal homeostasis (Qiao *et al*., 2012). These results likewise overlap with the –Cu microarray and therefore are due to absence of copper in the media and not to overexpression of Hpr8 (Table 8, last column). It is hard to speculate on the possible effect of Hpr8 on the hypothetical proteins the functions of which are not well understood.

In response to overexpression of Hpr8 *slr2015, slr2016* and *slr2017* were downregulated. These genes are also organized in an operon (Yoshimura *et al*., 2002a). N-terminal regions of corresponding proteins are homologous to type IV prepilin and therefore they were called PilA9 (Slr2015), PilA10 (Slr2016) and PilA11 (Slr2018) (Yoshimura *et al*., 2002b). The aforementioned genes are involved in phototactic motility in *Synechocystis* (Bhaya *et al*., 2001; Panichkin *et al*., 2006). They were also repressed in the *Δhfq* mutant (Dienst *et al*, 2008, 2010; Schürgers, 2014). Because of this correlation and possible connection to Hfq we decided to choose this possible Hpr8 target for Northern blot verification. However, verification of *pilaA9* being a target of Hpr8 performed by Jasper Matthiessen (AG Hess, Institute of Biology III, Albert-Ludwigs University Freiburg) in the framework of his Diploma thesis, was unsuccessful. It is therefore likely that downregulation of *pilA9* – *pilA11* represents response to copper absence in the growth media as well.

sll1924 encoding the cAMP receptor protein homolog Sycrp2 seems to be one of the few targets, whose downregulation is not related to copper depletion. Cyclic AMP (cAMP) is a universal signalling molecule in prokaryotes (Botsford and Harman, 1992). In cyanobacteria intracellular cAMP levels fluctuate as a reaction to changing environmental conditions and exogenous cAMP stimulates gliding motility of *Synechocystis* (Ohmori, 1989; Terauchi and Ohmori, 1999). It has been shown that Sycrp2 in contrast to Sycrp1 does not bind cAMP (Yoshimura *et al*., 2000). However, it cannot be excluded that Sycrp2 is able to bind another bacterial second messenger, such as c-di-GMP, which has been shown to be involved in regulation of phototaxis in *Synechocystis* under blue light (Savakis *et al*., 2012). Therefore, downregulation of *sycrp2* due to overexpression of Hpr8 might hint to an involvement of this sRNA in regulation of motility in *Synechocystis*.

3.1.1.2 Hpr8 does not directly participate in response to UV light

In the WT the expression of Hpr8 is induced after exposure to high light and under UV light that suggests its involvement in stress response (Kopf *et al*., 2014) (Figure 10A; Figure 14).

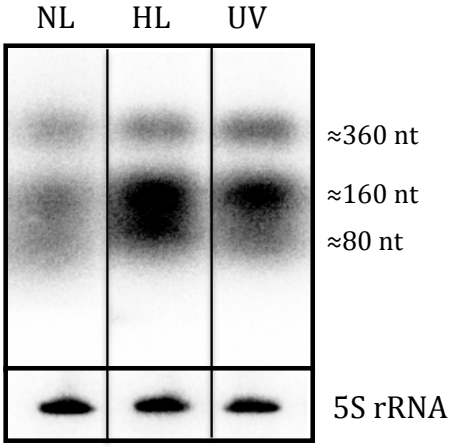

Figure 14: Northern blot verification of Hpr8 induction under high light and UV light
5 µg RNA isolated from exponentially grown WT cultures grown under normal light (NL), high light (HL) and ultraviolet light (UV) was separated on PAA-urea gel and transferred to nylon membrane followed by hybridization with Hpr8 probe. Hybridization with 5S rRNA was made for loading control. The presented image was combined of the lanes cut out from the initial image of the hybridized membrane; the samples were analysed together in one experiment, which was performed by Dr. Nils Schürgers (AG Wilde, Institute of Biology III, Albert-Ludwigs University Freiburg).

It has also been shown that the genes surrounding Hpr8 are involved in negative phototaxis under UV light (Song *et al*., 2011). The *slr1212-slr1214* gene cluster encodes for a two-component signalling system that consists of a cyanobacteriochrome (CBCR) (locus *slr1212* or *uirS*) and two adjacent response regulators (*slr1213* or *uirR* and *slr1214* or *lsiR*). This system is responsible for negative phototaxis under UV-A light (wavelength =355 ± 28.6 nm). The authors propose that UirS is a UV sensor that belongs to the CBCR photoreceptor family. It binds to UirR that transmits UV light signal perceived by UirS. UirR is being released and acts as transcription activator of the *lsiR* gene that encodes the PatA-family response regulator LsiR. That somehow triggers differential response on the proximal (irradiated) and distal (shaded) sides of the cell that leads to negative phototaxis under UV light (Song *et al*., 2011). Schematic representation of this model is presented in Figure 6. However, Song *et al*. did not mention the presence of sRNA (Hpr8) in the intergenic region between *slr1213* and *slr1214*, but they proved that the whole intergenic region from the *slr1213* stop codon to the translation initiation start site of *slr1214* is needed for *slr1214* transcription activation by UirR. That is why we decided to conduct phototaxis assays with the Hpr8 mutant strains under UV-A light (Figure 15). Hpr8 knockout mutants moved towards UV light, whereas WT and

overexpression strain slightly moved away from the light source. However the Hpr8 complementation mutants also moved towards UV light and the phenotype with the positive phototaxis towards UV light was not restored to the WT phenotype. This led us to the assumption that probably due to deletion of *hpr8* in the *Δhpr8* strain transcription of *slr1214* was affected. Despite that *in silico* data (Jasper Matthiessen**,** AG Hess, Institute of Biology III, Albert-Ludwigs University Freiburg; personal communication) suggested the presence of an independent *slr1214* promoter and also despite it was not possible to detect a co-transcript of Hpr8 and *slr1214* it seems that insertion of Km resistance cassette to knockout Hpr8 also affected *slr1214*.

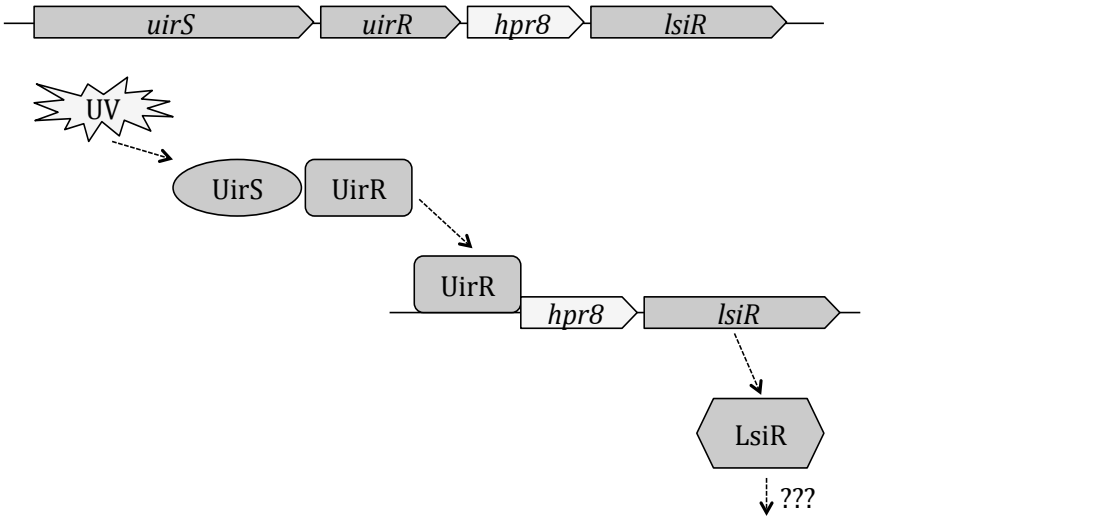

Figure 15: Schematic representation of the model of UirS/UirR/LsiR-based negative UV phototaxis signaling pathway in *Synechocystis* as proposed by Song *et al.*, 2011.

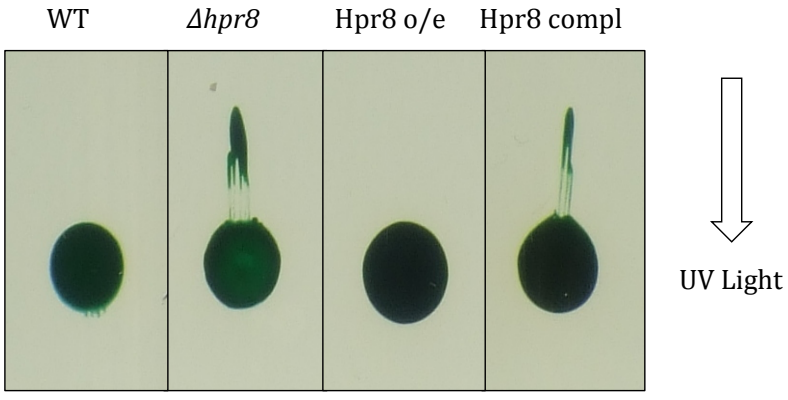

Figure 16: Phototaxis assay with different Hpr8 mutants under UV-A light
Cells were grown on 0,5% BG11 medium in a special chamber with unidirectional UV-A light illumination for 2 weeks. WT showed slightly negative phototaxis under UV light; Hpr8 knockout and complementation strains presented positive phototaxis under UV light; Hpr8 overexpression strain moved neither away nor towards the light source. The

presented image was combined of the lanes cut out from the initial image of the phototaxis plate; the samples were analysed together in one experiment.

In order to distinguish the effects of *hpr8* and *slr1214* knockouts separately two mutant strains: *hpr8*-rescue and *slr1214*-rescue on the basis of *Δhpr8* were constructed by Jasper Matthiessen (AG Hess, Institute of Biology III, Albert-Ludwigs University Freiburg) as described in section 2.4.5. These constructs were used to perform new phototaxis assays to investigate if the previously seen effect of positive phototaxis towards UV light in *Δhpr8* strain was really due to the knockout of *hpr8* or due to unintended knockout of *slr1214* (Figure 17). As discovered in the experiment *hpr8*-rescue does not alter the *Δhpr8* phenotype observed previously (Figure 16). Only when natural expression of *slr1214* was reconstituted in the *Δhpr8* knockout mutant its phenotype with positive phototaxis under UV light was restored to the WT phenotype and the cells started to move away from the UV light source (Figure 17). Thus we could conclude that Hpr8 does not directly participate in response to UV light and the model proposed by Song *et al*. was confirmed to be feasible. It is likely therefore that Hpr8 is the 5'UTR of *slr1214*.

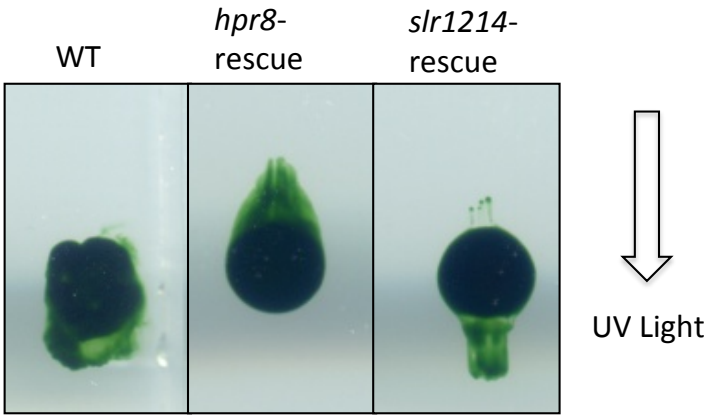

Figure 17: Phototaxis assay with *hpr8*-rescue and *slr1214*-rescue mutants under UV-A light
Cells were grown on 0,5% BG11 medium in the special chamber with unidirectional UV-A light illumination for 2 weeks. WT cells were moving away from the light source; *hpr8*-rescue strain performed positive phototaxis under UV light. Only expression of *slr1214* in *Δhpr8* background restored the mutant to the WT phenotype. The presented image was combined of the lanes cut out from the initial image of the phototaxis plate; the samples were analysed together in one experiment.

3.1.2 General characteristics of Hpr10

Hpr10 is another Hfq-dependent putative sRNA that was discovered in the microarray analysis of the Δ*hfq* mutant (Dienst *et al.*, 2008, 2010) The coding sequence for Hpr10 is located on the chromosome upstream of *slr1915* in the same orientation (Figure 18A). Hpr10 is not conserved among cyanobacteria even in closely related organisms. Its secondary structure (Figure 18B) contains a vast double-stranded region that suggests that it might be processed by RNase III.

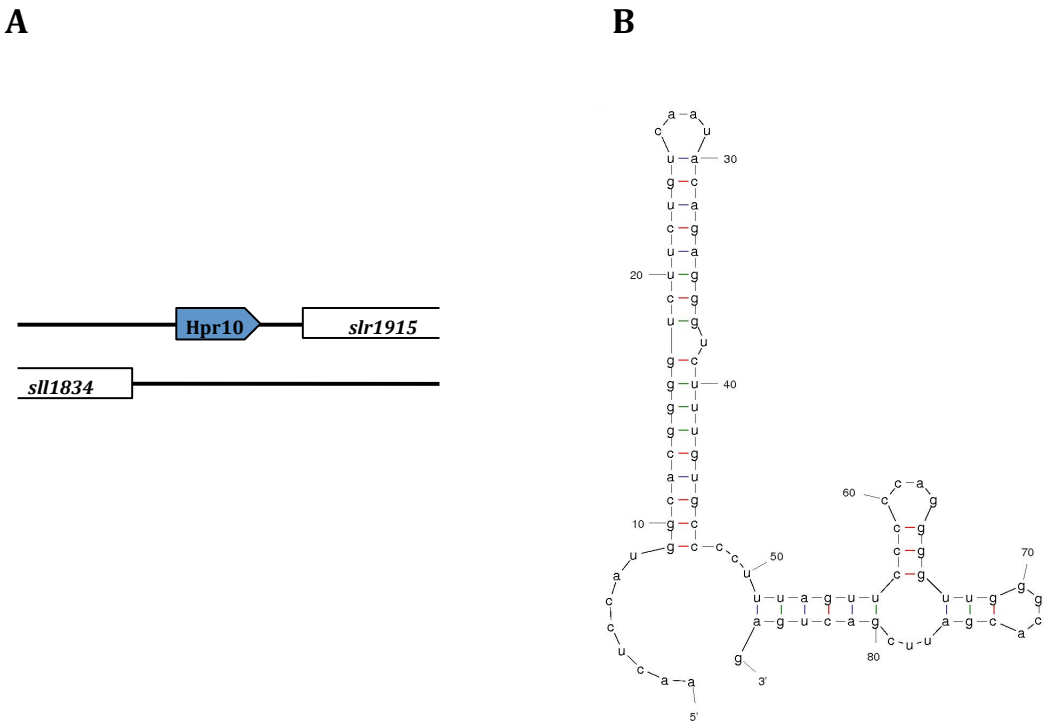

Figure 18: Hpr10 and its predicted secondary structure
(A) Schematic representation of the *hpr10* locus.
(B) Predicted secondary structure of Hpr10 corresponding to the respective minimum free energy state using mfold web server.

3.1.2.1 Characterization of Hpr10 knockout, overexpression and complementation mutants

In order to investigate functions of the Hpr10 knockout (section 2.4.3), overexpression (section 2.4.4) and complementation strains were generated. Complementation of *Δhpr10* was achieved by transferring the Hpr10 overexpression plasmid in the *Δhpr10* strain via conjugation. The created mutant strains were verified by Northern blot analysis using radioactively labelled Hpr10 probe (Figure 19).

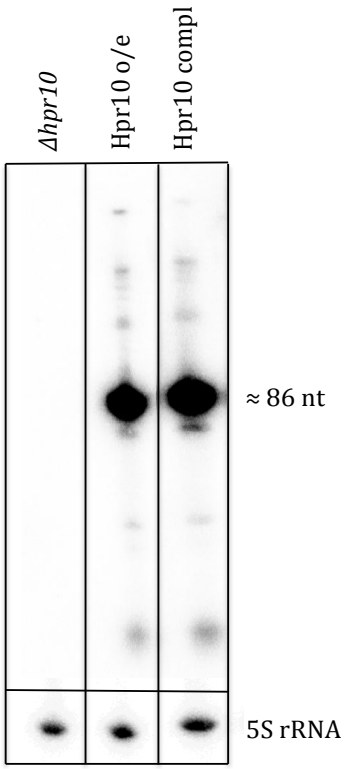

Figure 19: Northern blot verification of Hpr10 knockout, overexpression and complementation mutants
The mutants were grown on BG11 medium without copper for 7 days to induce the expression of Hpr10 in the overexpression and complementation strains. 5 µg RNA was separated on 10% PAA-urea gel and transferred to PVDF membrane followed by hybridization with Hpr10 probe. Hybridization with 5S rRNA was made for loading control. Transcript sizes were estimated by overlapping the pictures of the membrane with the one from the EtBr-stained gel containing Low Range Riboruler RNA Ladder. The presented image was combined of the lanes cut out from the initial image of the hybridized membrane; the samples were analysed together in one experiment.

First we decided to study phototaxis behaviour of Hpr10 knockout, overexpression and complementation strains under different light conditions. However no differences in motility of Hpr10 mutants in comparison to the WT were observed (Figure 20).

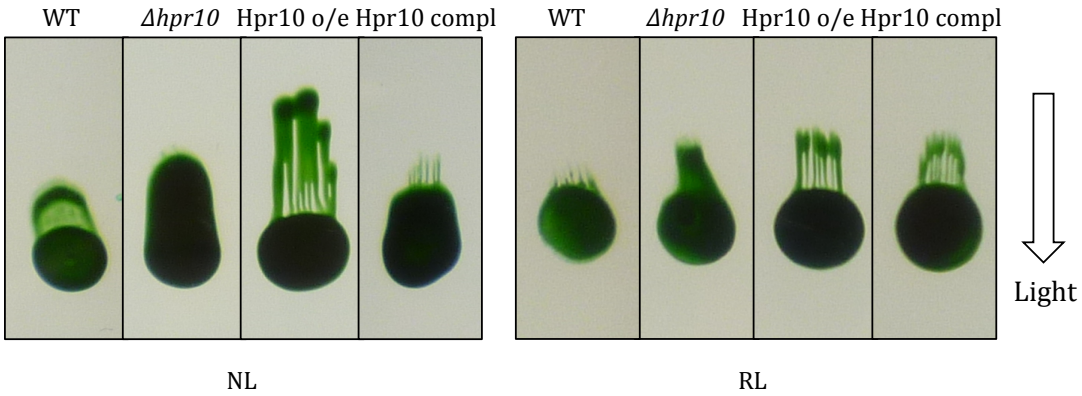

Figure 20: Phototaxis behaviour of Hpr10 mutants (previous page)
Phototaxis assay on 0,5 % BG11 plates under normal light (NL) and red light (RL); cells were grown in the special chamber with unidirectional illumination for 7 days. Hpr10 mutants behaved like the WT under all tested light conditions. The presented image was combined of the lanes cut out from the initial image of the phototaxis plate; the samples were analysed together in one experiment.

Then we analysed the growth of aforementioned mutants and discovered a slight reduction in pigment content in Hpr10 overexpression and complementation strains when compared to the WT (Figure 21). Complementation strain of Hpr10 is more similar to the overexpression one than to the WT in its phenotype because complementation mutant was constructed via introduction of pVZ321-*hpr10* to *Δhpr10* and expression of Hpr10 integrated in this vector is higher than the natural expression of Hpr10.

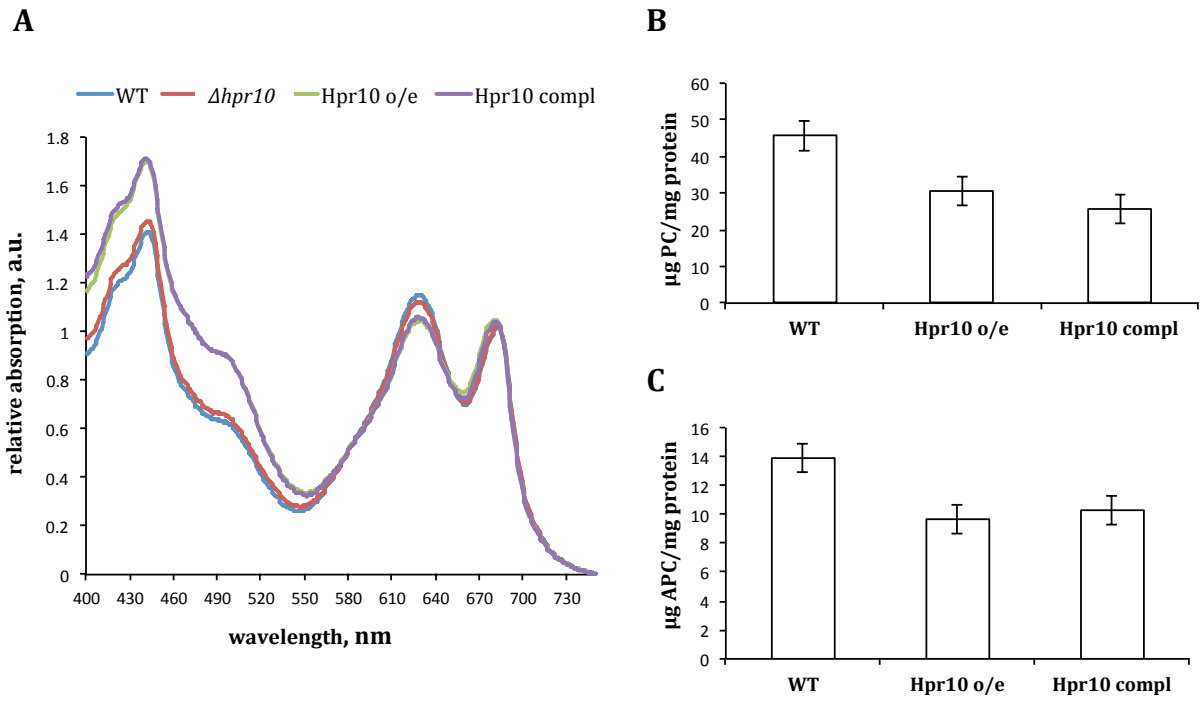

Figure 21: Phenotypical analysis of Hpr10 mutants
(A) Absorption spectra of liquid cultures of WT and Hpr10 knockout, overexpression and complementation strains grown for 8 days on BG11 without copper under normal light conditions. The spectra were normalized to chlorophyll *a* absorption at 685 nm and OD_{750nm}.
(B) Phycocyanin determination in liquid cultures of WT and Hpr10 overexpression and complementation strains grown for 8 days on BG11 without copper under normal light conditions.
(C) Allophycocyanin determination in liquid cultures of WT and Hpr10 overexpression and complementation strains grown for 8 days on BG11 without copper under normal light conditions.

In order to identify targets for Hpr10 we decided to monitor change in abundance of the target mRNA by performing microarray analysis. For the

microarray experiment whole RNA from *Δhpr10* mutant cultivated till logarithmic growth phase (OD_{750nm} 0,6) in BG11 medium (each time 2 biological replicates) was extracted. WT was taken as an equivalent. Transcripts with a log_2 FC ≥1,8 (for upregulated) and FC ≤ -1,8 (for downregulated) were taken as significantly differentially expressed.

Table 9: Microarray results of downregulated and upregulated transcripts responsive to knockout of Hpr10. Compared to the WT.

Gene name	Synonym	Gene product / description	FC
Downregulated			
slr1727-as1		asRNA	-3.41
sll0022		unknown protein	-2.53
slr1478		hypothetical protein	-2.04
sll0019	*dxr*	1-deoxy-d-xylulose 5-phosphate reductoisomerase	-2.02
sll1639	*ureD*	urease accessory protein D	-1.96
sll1446	*rfrL*	hypothetical protein	-1.95
sll0931		hypothetical protein	-1.93
slr1980		unknown protein	-1.84
sll0915	*pqqE*	periplasmic protease	-1.82
Upregulated			
NC-232/NC247		Hpr11	3.35
NC-65		*located upstream from sll0306 (sigB)*	2.11
sll1773	*pirA*	hypothetical protein	2.07
slr0444-5'UTR	*aroA*	3-phosphoshikimate 1-carboxyvinyltransferase	2.03
sll1006		unknown protein	1.98
sll1851		unknown protein	1.91
sll1666-5'UTR	dnaJ, dnaJ2, dnaJ3	DnaJ-like protein	1.91
slr2135	hupE, ureJ	hydrogenase accessory protein HupE	1.9
slr0449	*dnr*	probable transcriptional regulator	1.87
sll0609		hypothetical protein	1.86
ssl0331		hypothetical protein	1.83
sll1586-as1		asRNA	1.83
slr1789		unknown protein	1.81
slr1529	*ntrX*	nitrogen assimilation regulatory protein	1.81
sll0833	*appC*	probable oligopeptides ABC transporter permease protein	1.8

Microarray results showed that in Hpr10 knockout mutant 9 RNA features presented reduction in transcript quantity and 15 RNA features illustrated increase in accumulation. The most downregulated in *Δhpr10* is the asRNA *slr1727-as1*. However, a significant difference in transcript accumulation of the complementary (potentially target) mRNA was not detected. The same can be said about *sll1586-as1* that showed slight upregulation in the mutant, as its complementary mRNA was also not affected. Interestingly the most upregulated RNA feature was another Hfq-dependent sRNA Hpr11. It is located on the chromosome between *slr1822* and *slr1732* in the antisense orientation; in the *hfq* knockout strain Hpr11 transcript could not be detected (Schürgers, 2014). Most of the features with different transcript accumulation in *Δhpr10* in comparison to the WT corresponded to unknown or hypothetical proteins and could not be linked to the *hfq* mutant phenotype; therefore it has been decided not to proceed with the analysis of the microarray results and focus on the direct search for RNase targets.

3.2 Investigation of RNases in *Synechocystis*

3.2.1 Characterization of FLAG-tagged RNases in *Synechocystis*

In order to investigate RNA degradation machinery the following RNases were initially chosen for the analysis: Rne, Rnc1 and Rnc2. To study the functions of aforementioned ribonucleases FLAG-tagged variants of each of them were constructed as described in section 2.4.1. The expression of corresponding FLAG-tagged RNases was verified by western blot using anti-FLAG-alkaline phosphatase antibodies (Figure 22).

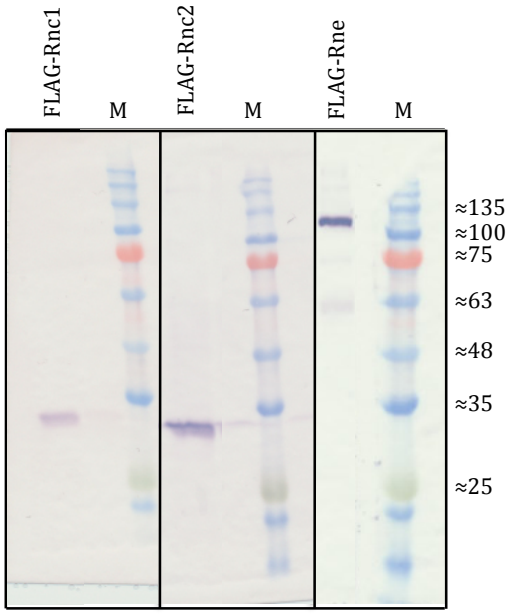

Figure 22: Western blot verification of the expression of FLAG-tagged RNases in *Synechocystis*
Strains of FLAG-tagged *rne*, *rnc*1 and *rnc*2 were grown on BG11 without copper to

induce the expression of the recombinant proteins. Whole cell extract was obtained, 10 µg protein was loaded on 10% SDS-PAA gel and subjected to SDS-PAGE. Afterwards the proteins were transferred on a nitrocellulose membrane and FLAG-tagged fusion proteins were detected using anti-FLAG-AP antibody. Sizes of the detected bands fit to the calculated sizes: 32 kDa for FLAG-Rnc1, 30 kDa for FLAG-Rnc2 and 82 kDa for FLAG-Rne. Marker: Protein Marker VI (AppliChem). Sizes of the marker bands are marked in kDA. The presented image was combined of the lanes cut out from the initial images of three nitrocellulose membranes, each of which contained FLAG-tagged RNase of interest and the marker.

FLAG-tagged *rnc* strains did not show any phenotype. FLAG-tagged *rne* overexpression strain however displayed a "bleaching" phenotype caused by the reduced amount of major pigments (Figure 23). This was most likely due to overexpression of the *rne* suggesting also that the FLAG-tag does not disturb Rne function.
We also studied motility under various light conditions of the overexpression strains of aforementioned RNases, however, no differences in phototaxis behaviour of the mutants compared to the WT were observed (data not shown).

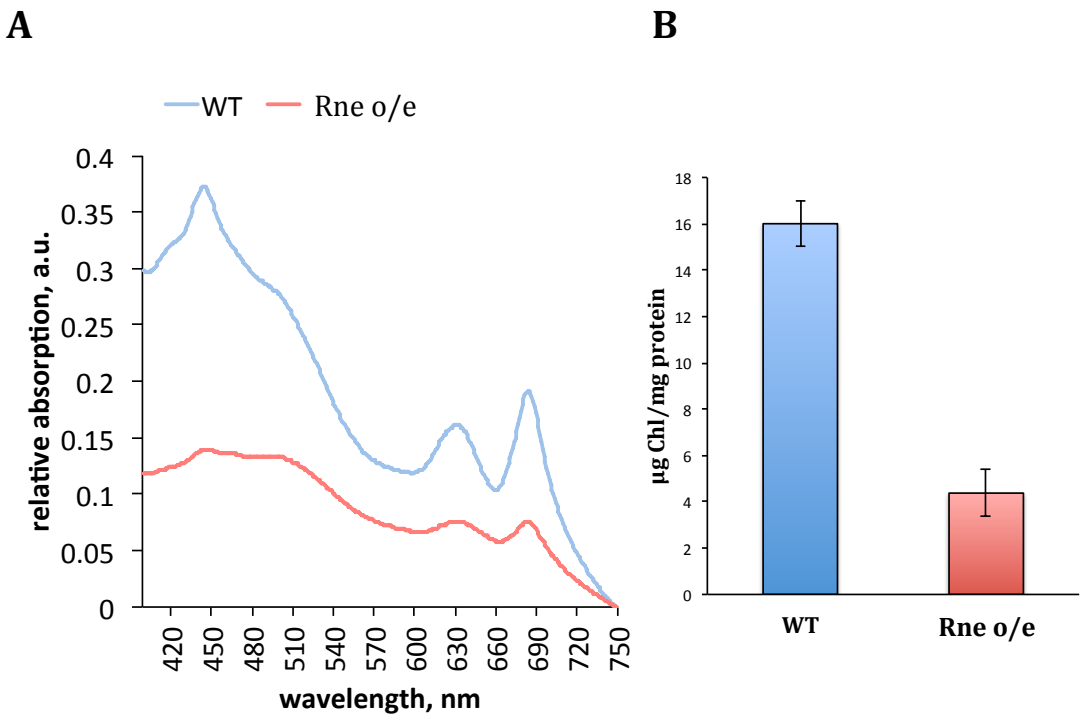

Figure 23: Phenotypical analysis of *rne* overexpression strain
(A) Absorption spectra of liquid cultures of WT and *rne* overexpression strain grown for 8 days on BG11 without copper under normal light conditions.
(B) Chlorophyll determination in liquid cultures of WT and *rne* overexpression strain grown for 8 days on BG11 without copper under normal light conditions.

3.2.2 iCLIP combined with high-throughput sequencing monitors genomewide binding of Rne and Rnc2

In order to search for the possible targets for investigated RNases we decided to implement a novel method: individual-nucleotide resolution crosslinking and immunoprecipitation (iCLIP) combined with Solexa high-throughput sequencing. The protocol was developed with the kind help of Dr. Oliver Rossbach (Institute of Biochemistry, Justus-Liebig University, Giessen) and Dr. Nils Schürgers (AG Wilde, Institute of Biology III, Albert-Ludwigs University Freiburg) and is similar to the technique described in König *et al.* (2010). Schematic representation of the method is presented in figure 24. First resuspended cell pellets of the overexpression strains of FLAG-*rne* and FLAG-*rnc*2 were irradiated 3 times with UV-C light at 254 nm to facilitate crosslinking of the proteins to nucleic acids (Figure 24-1). Then the cell extract was solubilized and treated with RNase I to partially digest long RNA molecules (Figure 24-2), and with DNase to degrade cellular DNA. This was followed by co-immunoprecipitation with ANTI-FLAG M2 antibodies bound to magnetic beads (Figure 24-3) and removal of 2',3'-cyclic phosphates introduced by RNase I digestion (Figure 24-4). Dephosphorylation facilitated 3' RNA-linker ligation, containing puromycin on its 3' end to avoid self-ligation (Figure 24-5). Self-ligation of the crosslinked RNA was also impeded due to the hydroxyl group on its 3' end. RNA was radioactively labelled on the 5' end to facilitate detection of protein-RNA complexes (Figure 24-6), which were eluted and subjected to denaturing gel electrophoresis and transferred to nitrocellulose membrane (Figure 24-7). Thus the protein-bound RNA was attached to the membrane and free non-crosslinked RNA was removed. Protein-RNA complexes were visualized using the phosphorimager and the regions above the expected molecular weight of the studied RNase (79 kDa for Rne and 27 kDa for Rnc2), corresponding to the RNase plus the CLIP tag and the RNA-linker (+approx. 80 kDa), were cut out from the membrane. In the next step proteinase K treatment led to the hydrolysis of the peptide bonds, thus crosslinked RNA was discharged, but the amino acid crosslinked to the RNA remained attached (Figure 24-8). This fact is essential for the experiment because it helps to reveal crosslink sites at the nucleotide resolution after sequencing. The reason for it is that reverse transcriptase during subsequent reverse transcription (Figure 24-9) often stalls at the remaining crosslinked amino acid producing cDNAs, which are truncated one nucleotide upstream of the crosslink site (Urlaub *et al*., 2002). The reverse transcription (RT) primer is designed in a way that its 3' end is complementary to the RNA-linker and most of the primer is compatible to the Solexa high-throughput sequencing primers. It also introduces the barcode system on the 5' end (Figure 25). It consists of „experimental barcode" that is a four nucleotide sequence which makes it possible to sequence several iCLIP samples (in our case they refer to the WT, *rne* and *rnc*2) in a single Solexa run. The second part of the barcode system introduced by the RT primer is called a "random barcode". It is a sequence of five nucleotides that helps to avoid PCR-bias during quantification of crosslinked RNA. PCR-bias is inevitable but comparing random barcodes makes it possible to distinguish the origin of several identical CLIP tags. If they contain indistinguishable nucleotide sequence at positions of the random barcode it

means that these CLIP tags result from PCR amplification of the same crosslinked and co-purified RNA molecule. If the nucleotide sequence at the randomized positions differs among the same tags it is reasonable to talk about distinctive crosslinking and co-immunoprecipitation events. It is known that during PCR short DNA molecules are most likely to be amplified than the longer ones, which creates another bias. To avoid this during the iCLIP experiment cDNAs were subjected to denaturing gel electrophoresis and three regions of different sizes were purified from the gel (Figure 24-10). This was followed by intramolecular cDNA circularization with the help of single-strand DNA-specific circLigase, annealing an oligo to create a double-stranded restriction site for BamHI and further linearization of the cDNA molecule by digestion with the restriction enzyme (Figure 24-11). This procedure resulted in creation of a linker at the 5' end of the cDNA molecule, which is compatible to the Solexa high-throughput sequencing primer. Afterwards cDNA was amplified by the PCR (Figure 24-12) and subjected to Solexa high-throughput sequencing (Figure 24-13). (Rossbach, 2012). Solexa sequencing was performed at Max Planck-Genome-centre Cologne.

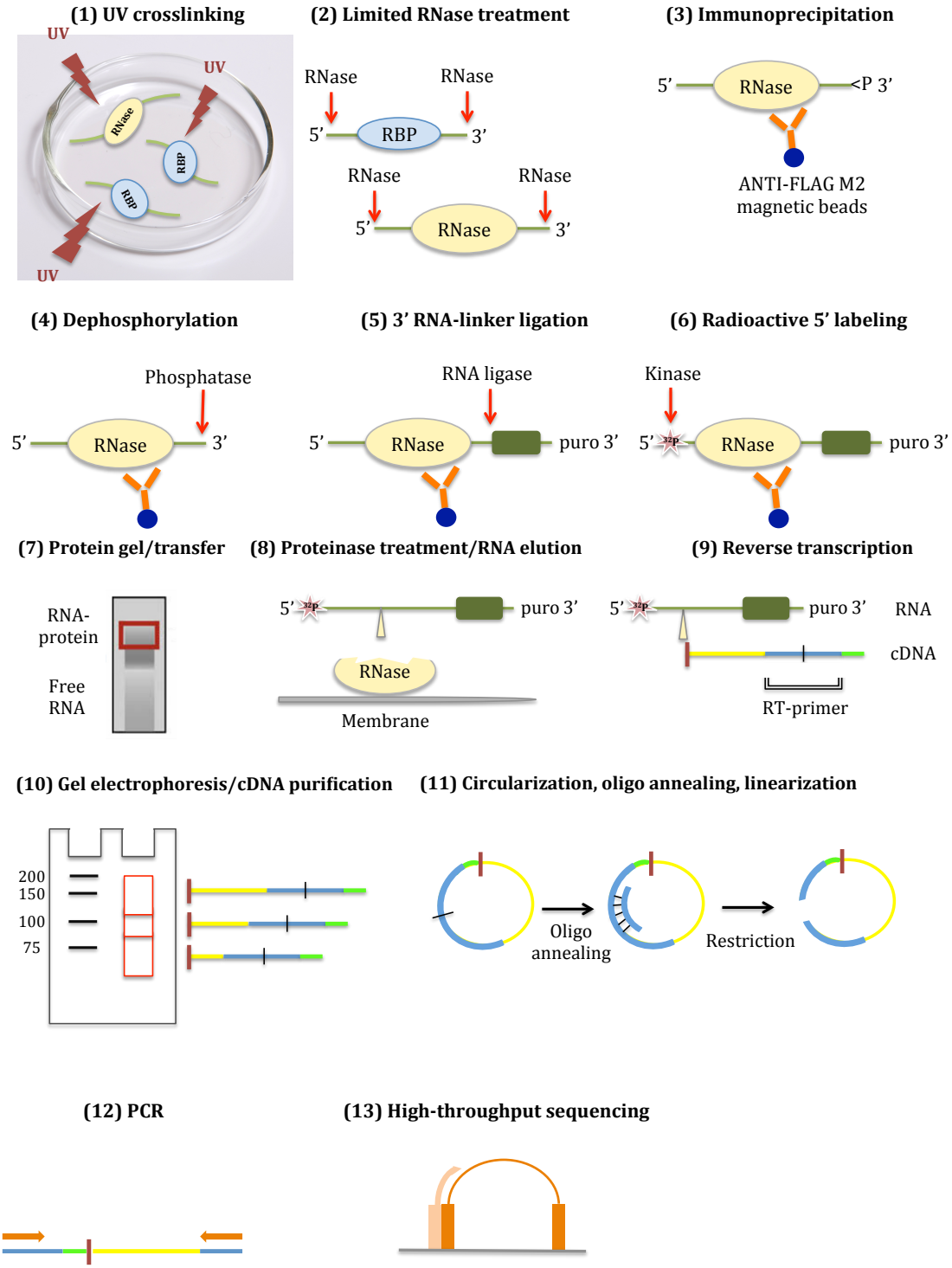

Figure 24: Schematic representation of the iCLIP procedure that allows to map genomewide binding sites of a specific RNA-binding protein at the nucleotide resolution

(**1**) Cultured cells are irradiated with UV light at 254 nm to crosslink RNA binding proteins (RBP) to cellular RNA (in green). (**2**) After cell lysis, the RNA is trimmed by limited RNase digestion. (**3**) The protein of interest (RNase) is immunoprecipitated with ANTI-FLAG M2 magnetic beads. (**4**) The 2',3'-cyclic phosphate produced by RNase digestion is removed by phosphatase treatment. (**5**) An RNA linker (dark green rectangle) is ligated to the 3' end of the RNA. The linker is protected by puromycin

(puro) on its 3' end to prevent self-ligation. (**6**) The RNA is radioactively 5' end-labelled with ^{32}P. (**7**) Free RNA is removed by gel electrophoresis followed by transfer to a nitrocellulose membrane, which binds proteins unspecifically. After visualization, the area with the covalent protein-RNA complexes of interest is cut from the membrane. (**8**) The RNA is eluted from the membrane by protein digestion with proteinase K, whereas a single amino acid remains at the crosslink site (yellow triangle). (**9**) The RNA is reverse-transcribed with an RT primer that introduces additional sequences to the 5'end of the cDNA: the region depicted in blue is compatible with high-throughput sequencing; a restriction site (vertical line); and a random barcode (light green). Frequently the reverse transcriptase stops one nucleotide prior to the crosslink site (bold red dash) producing truncated cDNA molecules. (**10**) The cDNA is size-selected via denaturing gel electrophoresis to avoid PCR bias and preserve DNA of any length. (**11**) The cDNA is circularized by an ssDNA-specific circLigase, and a short DNA oligonucleotide is annealed to complete the double-stranded restriction site. The cDNA is linearized, adding a 5' adapter sequence to the cDNA. (**12**) The cDNA is amplified by PCR with primers compatible with high-throughput sequencing. The 5' end of the PCR product (excluding linker sequence) marks the initial crosslink site (bold red dash). (**13**) The PCR product pool is subjected to Solexa high-throughput sequencing. From Rossbach (2012), modified.

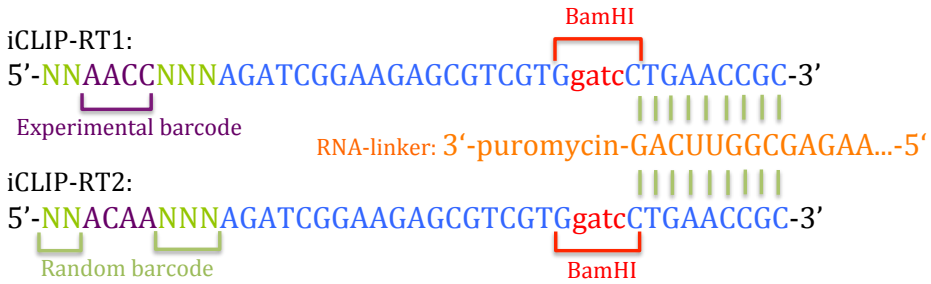

Figure 25: Schematic representation of the iCLIP reverse transcription primer with the barcode system
Experimental barcode (purple) consisted of four nucleotides is flanked by five random nucleotides (light green). Nucleotide sequence marked in blue is compatible with Solexa high-throughput sequencing. BamHI restriction site (GgatcC) is marked in red. 3' part is complementary to the RNA-linker (depicted in vertical lines).

In total four iCLIP experiments were conducted: for Rne+UV irradiation, Rnc2+UV irradiation, Rnc2-UV irradiation (negative control) and WT+UV irradiation (as control, to get rid of unspecific results possibly occurring due to purification procedures). First different dilutions of RNase I were tested to find out which concentration of the enzyme is appropriate for limited digestion of the RNA (Figure 26). It has been decided to use 10^{-4} dilution of RNase I for the experiment as in this lane the visible smear represented the variety of complexes of RNA with Rnc2. When higher RNase I concentrations were used the smear decreased as the RNA fragments became too short.

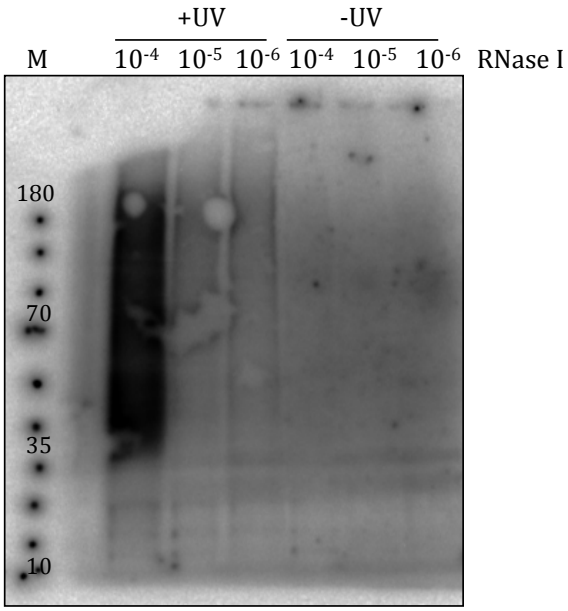

Figure 26: Nitrocellulose membrane with FLAG-Rnc2 treated by RNase I in different concentrations after visualization in the phosphorimager
FLAG-Rnc2 cultures were irradiated (+UV) with UV light; cell extract was solubilized and treated with different dilutions of RNase I (10^{-4}, 10^{-5}, 10^{-6}) to detect which enzyme concentration fits best. Non-irradiated cultures (-UV) were used as control. Protein marker (PageRuler Prestained Protein Ladder, Thermo Fisher Scientific) bands were marked with ^{32}P (dots on the membrane) to enable size estimation after membrane development. Sizes of the marker bands are marked in kDA. This test was performed by Dr. Nils Schürgers who kindly assisted me during the iCLIP experiment.

Figure 27 represents the image of nitrocellulose membrane with the smear from radioactively labelled RNA-protein complexes that was further cut out and subjected to proteinase K digestion. Lanes with UV-irradiated FLAG-tagged RNases (Rne+UV and Rnc2+UV) contain protein-RNA complexes visible as a smear on the membrane. In case of non-irradiated samples (Rne-UV and Rnc2-UV) no smear and therefore no protein-RNA complexes were detected. In every lane a slight signal at ca. 50 kDa and a stronger signal at ca. 25 kDa were detected. Judging by the sizes these signals most likely correspond to the heavy and light chain of the antibodies respectively. It could be due to phosphorylation of the protein by some kinase or incorporation of [γ-^{32}P]-ATP by the protein itself, or some unspecific RNA binding. The regions indicated by red boxes were cut out from the membrane and used for RNA elution and further cDNA library preparation. In order to estimate optimal conditions for preparative PCR cDNA was amplified by PCR in several different reactions with varying cycle number (Figure 28). 27 cycles seemed to be optimal for both iCLIP-processed RNases, as with 25 cycles the signal was too weak (indicating not high enough concentration of cDNA), and amplification with 30 cycles resulted in appearance of secondary bands corresponding to PCR artefacts. To avoid overamplification during the PCR preparative PCR for Solexa library preparation was performed with 24 cycles, because the cDNA used for it was more concentrated (Figure 29A). All PCR products were mixed together because thanks to the barcode

system it was possible to distinguish different samples after sequencing. cDNA was then checked on fragment analyzer (Figure 29B) and sent for sequencing to Max Planck-Genome-centre Cologne.

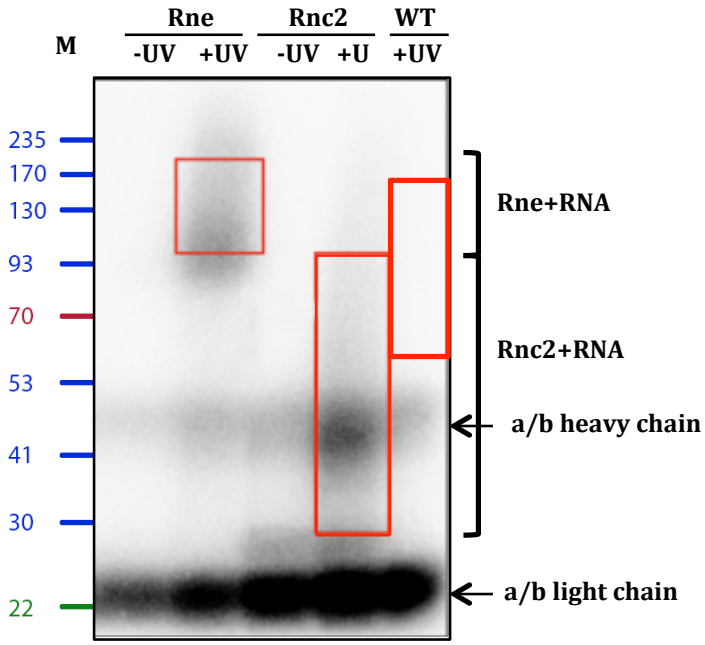

Figure 27: Nitrocellulose membrane with FLAG-Rne, FLAG-Rnc2 and WT after visualization in the phosphorimager

FLAG-Rne, FLAG-Rnc2 and WT cultures were irradiated (+UV) with UV light; cell extract was solubilized, digested with RNase and DNase, immunoprecipitated with ANTI-FLAG antibodies; RNA was dephosphorylated allowing 3' end linker ligation and radioactively labelled at the 5' end; RNA-protein complexes were subjected to SDS-PAGE and transferred to nitrocellulose membrane that was further developed and visualized using phosphorimager. Regions marked in red were cut out and subjected to RNA isolation and library preparation. Non-irradiated cultures (-UV) were used as control. Protein marker (Marker VI, AppliChem) is shown for better size evaluation. Sizes of the marker bands are marked in kDA.

Bioinformatic analysis was performed by Dr. Jan Mitschke (AG Wilde, Institute of Biology III, Albert-Ludwigs University Freiburg), and Karsten Voigt (AG Wilde, Institute of Biology III, Albert-Ludwigs University Freiburg). A bioinformatical pipeline was used to analyze the iCLIP data. In total approx. 100 000 reads were obtained. First, the raw reads were mapped using the *segemehl* package (Hoffmann *et al.*, 2009). Second, the mapped reads were merged and transformed into *grp*-files with SAMtools (Li *et al.*, 2009). All reads were subsequently mapped to predefined transcriptional units (TUs) (Kopf *et al.*, 2014) using own scripts created by Karsten Voigt. Signals were defined as clipping sites if the read-value at a certain position within the chromosome or a plasmid of *Synechocystis* excelled a number of 10. A clustering method was then used to summarize neighboring hits. The latter were clustered, if there were at least two of them (< 10 reads) within a window of 5 nucleotides. The hits were finally classified by their corresponding transcription units and their relative position according to the nearest annotated feature. Features were obtained by

the latest annotation of *Synechocystis* (Kopf *et al.*, 2014). iCLIP results exposed genomewide binding sites for Rne and Rnc2 in *Synechocystis*.

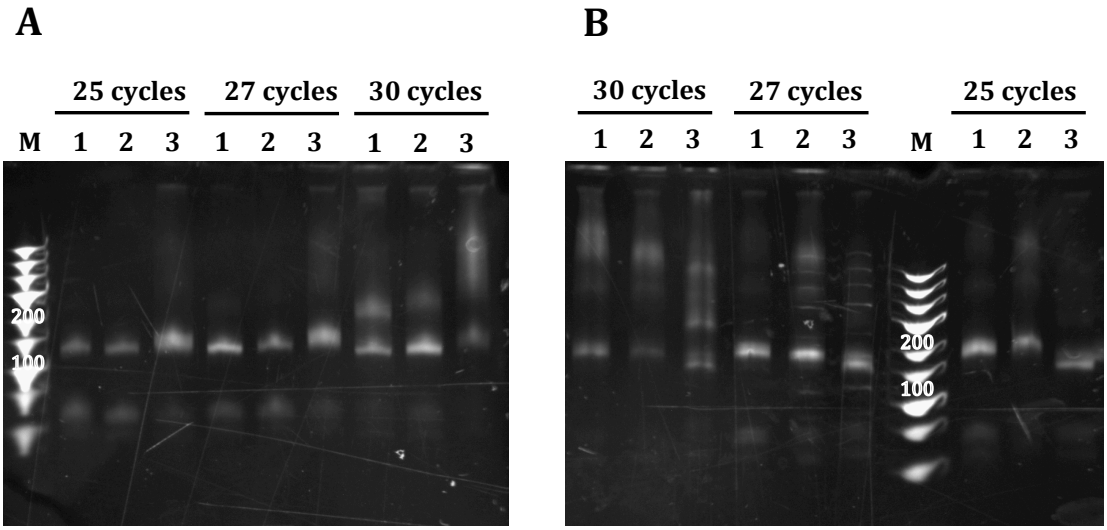

Figure 28: Analytical PCR of iCLIP-processed RNase purifications
(A) iCLIP-processed Rne: cDNA fractions 1-3 corresponding to three size regions cut out from the gel after denaturing gel electrophoresis were amplified by PCR using varying number of cycles. PCR products were separated on 6% PAA gel with 50% urea; gels were stained with EtBr and visualized under UV light. Marker: GeneRuler low range DNA ladder (Thermo Fisher Scientific). Sizes of the marker bands are marked in nt.
(B) iCLIP-processed Rnc2: cDNA fractions 1-3 corresponding to three size regions cut out from the gel after denaturing gel electrophoresis were amplified by PCR using varying number of cycles. PCR products were separated on 6% PAA gel with 50% urea; gels were stained with EtBr and visualized under UV light. Marker: GeneRuler low range DNA ladder (Thermo Fisher Scientific). Sizes of the marker bands are marked in nt.

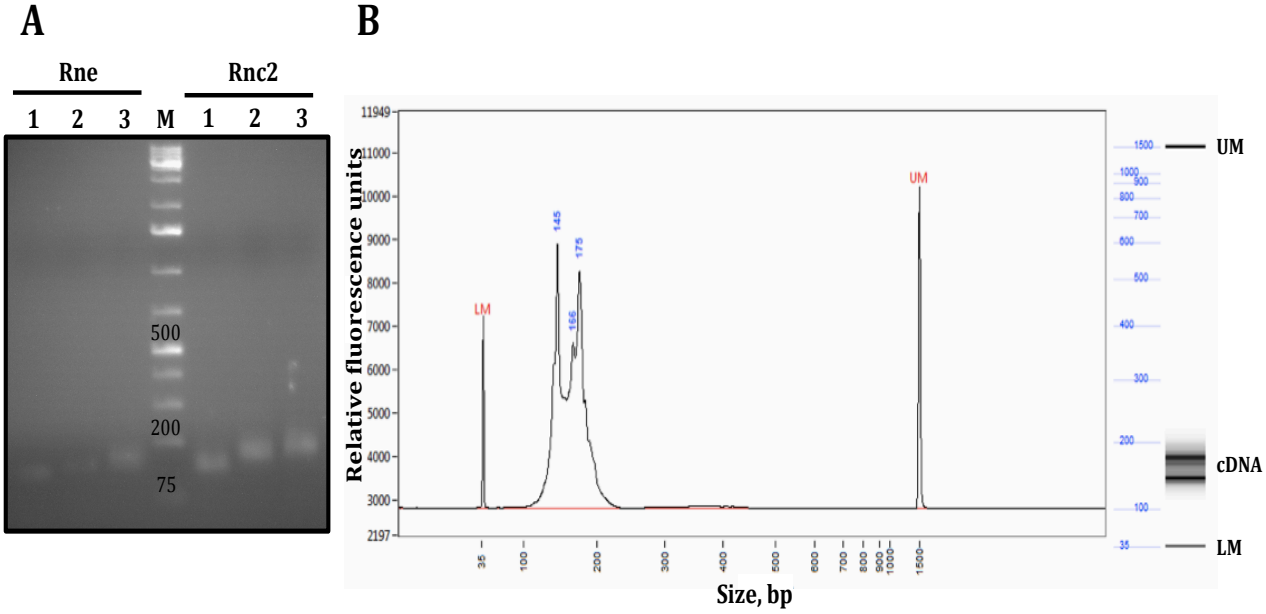

Figure 29: Preparative PCR and quality check of cDNA
(A) iCLIP-processed Rne and Rnc2 cDNA was amplified; PCR products were separated on 6% PAA gel with 50% urea; gels were stained with EtBr and visualized under UV

light. Marker: GeneRuler 1 kb Plus DNA ladder (Thermo Fisher Scientific). Sizes of the marker bands are marked in nt.
(B) Quality control of cDNA library (after pulling the samples together) on fragment analyzer. The concentration of cDNA was 30 ng μl^{-1}. The peak marked LM represents the Lower Alignment Marker (35 bp); the peak marked UM represents the Upper Alignment Marker (1500 bp); the peaks in between present analysed cDNA fractions with the corresponding sizes (145; 166 and 175 bp) depicted in blue. On the right side visualization of the gel is depicted with dark bands corresponding to the lower and upper markers and cDNA.

Annotation of sequencing results for *rne* revealed over 90 crosslink sites that were mapped to genes (including crosslink positions located within coding DNA sequences (CDSs), at 5'-UTRs and 3'-UTRs), ncRNAs (including asRNAs), and rRNAs (Table 10). The data was sorted according to the relative read value, crosslink hits with relative read value under 15 were excluded from the analysis. Crosslink positions for Rne were also mapped to 38 out of 43 tRNAs of *Synechocystis* (Table 11). For the majority of tRNAs more than one crosslink site was detected meaning possibly several binding sites. It is known that in *E. coli* RNase E plays a key role in mRNA turnover, however it is also in charge of maturation of rRNA and tRNA (Li *et al*., 1999; Li and Deutscher, 2002; Schuck *et al*., 2009). Therefore it was not surprising that our results revealed crosslink sites for *rne* in *Synechocystis* mostly within mRNA encoding genes as well as in rRNA and tRNA.

Table 10: iCLIP crosslink positions for Rne mapped to the genome of *Synechocystis*. Probable targets marked with an asterisk (*) were tested with *in vitro* cleavage assays. In case of multiple crosslink sites within one feature the highest relative read value is shown. Transfer RNAs are excluded from the table.

Name	Synonym	Gene product / description	iCLIP crosslink position	Relative read value
rrn16Sa		16S rRNA	internal	220
*rrn5Sa**		5S rRNA	5'-trailer	173
slr0108		unknown protein	5' UTR	92
sll1998	*ISY100d*	putative transposase	CDS	91
ncr0480		non-coding RNA	5'-trailer	85
sll1127as-2		antisense RNA	internal	75
ncr1320		non-coding RNA	5'-trailer	71
sll0260		hypothetical protein	CDS	68
sll1799	*rpl3, rplC*	50S ribosomal protein L3	5' UTR	59
ssaA		6Sa RNA	internal, 3'-trailer	57
*sll1184**	*ho1*	heme oxygenase	CDS (multiple crosslink sites), 5' UTR	52
sll0710		unknown protein	CDS	48
sll1251		hypothetical protein	5' UTR	48

Name	Synonym	Gene product / description	iCLIP crosslink position	Relative read value
SyR12*	NsiR4, *ncl0550, ncl0540, NC-225,*	non-coding RNA	internal	46
sll1577	*cpcB*	β-phycocyanin	5' UTR, CDS	45
sll1951	*HlyA, hlp*	unknown protein	CDS (multiple crosslink sites)	45
sll1070	*tktA*	transketolase	3' UTR	43
sll0765		hypothetical protein	CDS	40
sll1968	*pmgA*	photomixotrophic growth related protein	CDS	40
sll0535	*clpX*	ATP-dependent Clp protease ATPase subunit	CDS	39
sll0188		unknown protein	5' UTR	39
sll0517	*rbp1, rbpA*	putative RNA binding protein	5' UTR	39
sll1495		hypothetical protein	5' UTR	38
slr1524	*ISY100u*	putative transposase	5' UTR	38
SyR13*	*ncr0700*	non-coding RNA	internal (multiple crosslink sites)	37
slr1841		probable porin; major outer membrane protein	CDS (multiple crosslink sites)	37
slr0623	*trxA*	thioredoxin	CDS	35
slr1129	*rne*	RNase E/G	5' UTR	34
sll1981	*ilvB, gcl, alsS*	acetolactate synthase	CDS	34
sll0469	*prsA*	ribose-phosphate pyrophosphokinase	CDS (multiple crosslink sites)	33
slr1347	*icfA, ccaA, cab, cca*	beta-type carbonic anhydrase localized in the carboxysome	CDS	32
sll1949		unknown protein	3' UTR, CDS	31
sll1470	*leuC*	3-isopropylmalate dehydratase large subunit	CDS (multiple crosslink sites)	30
ncl0320		non-coding RNA	internal	29
slr1756	*glnA*	glutamate-ammonia ligase	CDS	28
ssr1399	*rpsR, rps18*	30S ribosomal protein S18	5' UTR	28
*slr1834**	*psaA*	P700 apoprotein subunit Ia, PsaA	CDS (multiple crosslink sites)	27
slr1679	*SynVanX*	hypothetical protein	CDS	27
slr0772	*chlB*	light-independent protochlorophyllide reductase subunit ChlB	CDS	26
rrn23Sa		23S rRNA	internal (multiple crosslink sites), 3'-trailer	25
sll1764		unknown protein	CDS	25
slr0993	*nlpD*	putative peptidase	CDS (multiple crosslink sites)	25
slr1204	*htrA, degP*	protease	5' UTR	24

Name	Synonym	Gene product / description	iCLIP crosslink position	Relative read value
sll1578	*cpcA*	phycocyanin α subunit	CDS	23
slr1471	*alb3, oxa1, synyidC*	hypothetical protein	CDS	23
sll1193		hypothetical protein	5' UTR	22
ncl1780		non-coding RNA	internal	22
SyR11	*ncr1160*	non-coding RNA	internal	21
slr1232		unknown protein	5' UTR	21
ssr1375		hypothetical protein	3' UTR	21
sll1268	*urf*	unknown protein	CDS	20
sll1349	*cbbZp*	phosphoglycolate phosphatase	5' UTR	20
slr0082	*rimO*	hypothetical protein	5' UTR	20
slr1227	*lAP75*	chloroplastic outer envelope membrane protein homolog	CDS (multiple crosslink sites)	20
ssr2799	*rpmA, rpl27*	50S ribosomal protein L27	3' UTR	20
sll1629	*phr, phrB, syn-cry, Ccry1*	bacterial cryptochrome	CDS	19
slr1530		hypothetical protein	CDS	19
slr1708		probable peptidase	CDS	19
sgl0002		hypothetical protein	CDS	19
rrn5Sb		5S rRNA	3'-trailer	18
sll0534	*clpP2*	ATP-dependent Clp protease proteolytic subunit 2	CDS	18
sll0819	*psaF, sll0819, psbF*	photosystem I reaction center subunit III precursor (PSI-F), plastocyanin (cyt c553) docking protein	CDS	18
sll1142		hypothetical protein	CDS	18
slr0749	*chlL*	light-independent protochlorophyllide reductase iron protein subunit ChlL	CDS	18
slr1945	*yibO, pgm*	2,3-bisphosphoglycerate-independent phosphoglycerate mutase	CDS	18
Yfr1		non-coding RNA	internal	18
sll1135	*ahp*	unknown protein	5' UTR	17
slr1838	*ccmK3*	carbon dioxide concentrating mechanism protein CcmK homolog 3, putative carboxysome assembly protein	5' UTR	17
slr2034	*ycf48*	putative homolog of plant HCF136, which is essential for stability or assembly of photosystem II	CDS	17
SyR5		non-coding RNA	internal	17
sll0821	*cph2*	phytochrome-like protein	CDS	16

Name	Synonym	Gene product / description	iCLIP crosslink position	Relative read value
sll1688	*thrC*	threonine synthase	CDS (multiple crosslink sites)	16
sll1949		unknown protein	CDS	16
slr0488		virulence factor MviN homolog	CDS	16
slr1204	*htrA, degP*	protease	5' UTR	16
slr1378		hypothetical protein	CDS	16
slr1629		ribosomal large subunit pseudouridine synthase D	CDS	16
ssr3307-as		antisense RNA	internal	15
slr1198		antioxidant protein	CDS (multiple crosslink sites)	15

Table 11: iCLIP crosslink positions for Rne mapped to tRNAs of *Synechocystis*. In case of multiple crosslink sites within one feature the highest relative read value is shown.

Name	Synonym	Gene product / description	number of iCLIP crosslink positions	Relative read value
trnR-ACG	*6803t19*	tRNA-Arg(ACG)	2	820
trnD-GUC	*6803t13*	tRNA-Asp(GTC)	3	439
trnF-GAA	*6803t16*	tRNA-Phe(GAA)	2	375
trnP-GGG	*6803t01*	tRNA-Pro(GGG)	2	254
trnN-GUU	*6803t24*	tRNA-Asn(GTT)	2	200
trnW-CCA	*6803t09*	tRNA-Trp(CCA)	2	190
trnC-GCA	*6803t35*	tRNA-Cys(GCA)	1	170
trnH-GUG	*6803t22*	tRNA-His(GTG)	1	158
trnV-UAC	*6803t05*	tRNA-Val(TAC)	2	146
trnK-UUU	*6803t27*	tRNA-Lys(TTT)	3	142
trnfM-CAU_3'		tRNA-fMet(CAT)3'	3	139
trnY-GUA	*6803t37*	tRNA-Tyr(GTA)	2	138
trnM-CAU	*6803t11*	tRNA-Met(CAT)	2	124
trnR-CCG	*6803t33*	tRNA-Arg(CCG)	2	110
trnA-GGC	*6803t26*	tRNA-Ala(GGC)	3	104
trnT-GUU	*6803t38*	tRNA-Thr(GGT)	3	95
trnQ-UUG	*6803t23*	tRNA-Gln(TTG)	2	94
trnG-GCC	*6803t36*	tRNA-Gly(GCC)	2	92
trnA-UGC	*6803t28*	tRNA-Ala(TGC)	2	81
trnE-UUC	*6803t14*	tRNA-Glu(TTC)	4	80
trnP-UGG	*6803t15*	tRNA-Pro(TGG)	1	80
trnL-GAG	*6803t10*	tRNA-Leu(GAG)	2	65
trnO-CGG	*6803t04*	tRNA-Pro(CGG)	1	58
trnV-GAC	*6803t42*	tRNA-Val(GAC)	1	38
trnS-GCU	*6803t21*	tRNA-Ser(GCT)	1	36
trnG-UCC	*6803t17*	tRNA-Gly(TCC)	1	33
trnL-UAG	*6803t07*	tRNA-Leu(TAG)	2	27
trnR-UCU	*6803t08*	tRNA-Arg(TCT)	2	27

Name	Synonym	Gene product / description	number of iCLIP crosslink positions	Relative read value
trnS-GGA	*6803t20*	tRNA-Ser(GGA)	1	26
trnL-CAA	*6803t12*	tRNA-Leu(CAA)	2	24
trnI-GAU(1)	*6803t29*	tRNA-Ile(GAT)	2	23
trnT-UGU	*6803t25*	tRNA-Thr(TGT)	2	21
trnL-CAG	*6803t41*	tRNA-Leu(CAG)	3	21
trnR-CCU	*6803t06*	tRNA-Arg(CCT)	2	13
trnI-CAU	*6803t18*	tRNA-Ile(CAT)	1	13
trnL-UAA	*6803t39*	tRNA-Leu(TAA)	2	13
trnT-CGU	*6803t03*	tRNA-Thr(CGT)	2	12
trnA-CGC	*6803t32*	tRNA-Ala(CGC)	1	6

Our iCLIP experiment revealed Rne binding site in the 5' UTR of *rne* gene (Table 10). The 5' UTR of *rne* in *Synechocystis* is extremely long and consists of 583 nt. Analysis of the predicted secondary structure of the 5' UTR of *rne* disclosed the location of the Rne binding site in the loop region (Figure 30). These data imply that Rne in *Synechocystis* might autoregulate its activity via mechanism analogous to the one shown for *E. coli* (Schuck *et al.*, 2009).

In order to have a better understanding of interaction of Rne with its targets biocomputational analysis of Rne binding motif identification was performed using Multiple Em for Motif Elicitation (MEME) tool (Bailey and Elkan, 1994). tRNAs were excluded from the analysis due to possibly different mechanism of RNase binding. In total 276 sequences were analysed. A window size comprised of 40 nt upstream and downstream the maximum iCLIP value was chosen for Rne binding motif search. Three most statistically significant motifs (according to the E-value) were discovered. The results were visualized with WebLogo application and are presented in Figure 31. As it is seen from Figure 31 the first two discovered motifs contain overlapping sequences (marked with the black frame). It suggests that this sequence might be the most promising candidate for Rne binding motif discovered by iCLIP using MEME.

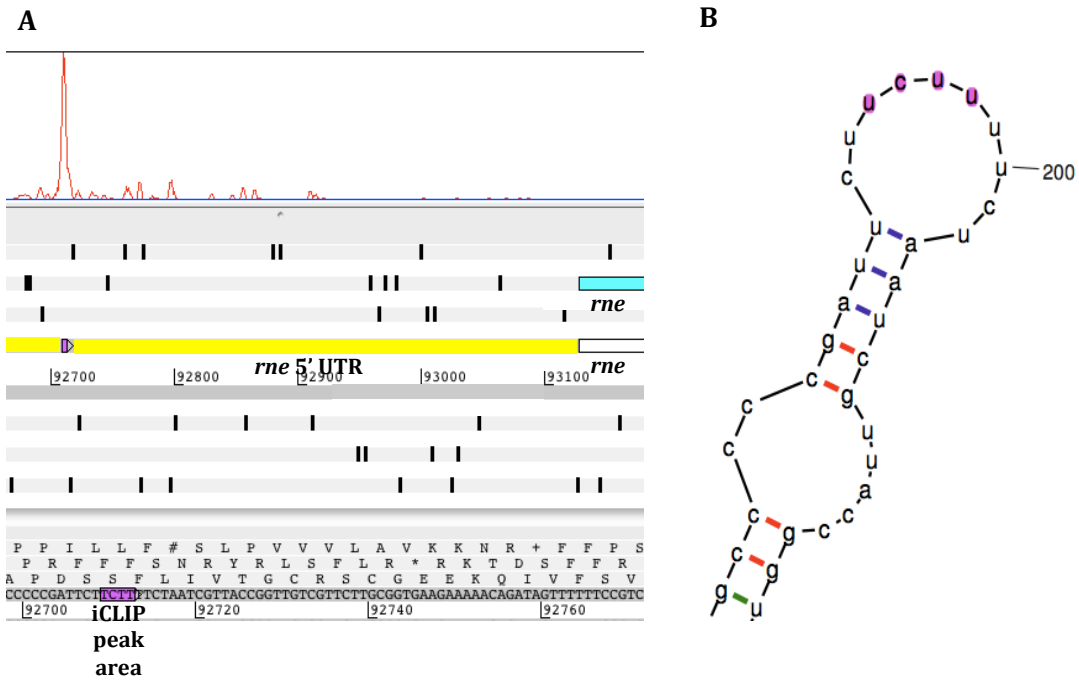

Figure 30: Depiction of the iCLIP peak at the 5' UTR of *rne*
(A) Image of the region of the iCLIP peak at the 5' UTR of *rne* (marked in yellow) obtained from the Artemis genome browser. iCLIP peak corresponding to the binding region of Rne is depicted on the graph in red; nucleotide sequence corresponding to the iCLIP peak area is marked in purple.
(B) Fragment of the secondary structure of the 5' UTR of *rne* created with mfold web server. Region marked in purple corresponds to the predicted iCLIP peak area.

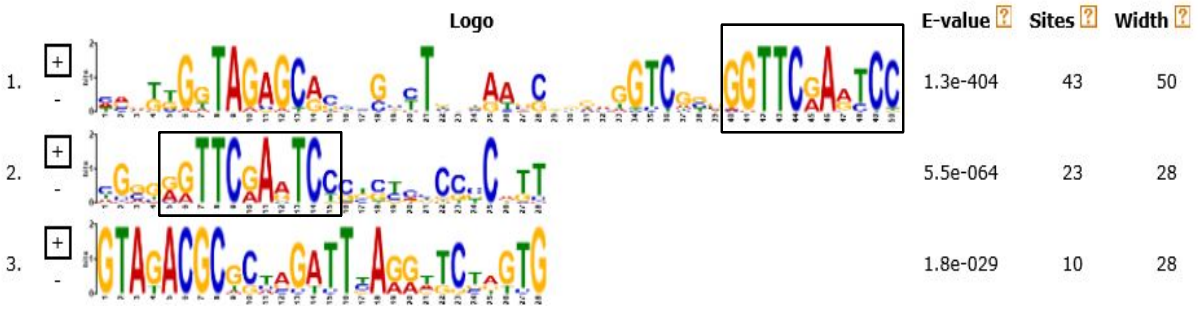

Figure 31: Consensus binding motifs for Rne generated by MEME
"Sites" value characterizes the number of sites contributing to the construction of the motif. Overlapping sequences in motifs 1 and 2 are marked with black frames.

As almost all tRNAs in *Synechocystis* were shown to contain one or more Rne binding sites according to the iCLIP data (Table 11) we decided to have a closer look at the location of the binding sites in some of them. tRNAs *trnY-GUA* and *trnT-GUU* are cotranscribed and therefore their precursor has to undergo certain processing steps in order for tRNAs to achieve mature functional forms. Figure 32 demonstrates the Rne binding sites within the *trnY-GUA* - *trnT-GUU* tRNA precursor. Presence of multiple iCLIP peaks suggests that Rne might simultaneously bind to multiple regions of the multimeric transcript, which

could lead to the cleavage of the precursor and facilitate maturation of *trnY-GUA* and *trnT-GUU.*

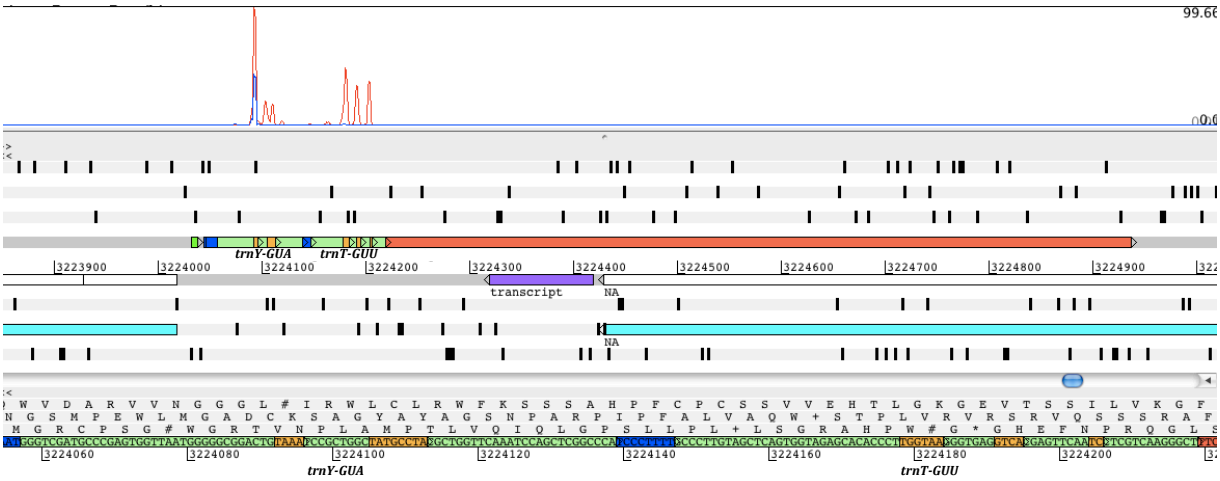

Figure 32: Depiction of the iCLIP peaks at the *trnY-GUA* - *trnT-GUU* tRNA precursor
Image of the region of the iCLIP peak at the *trnY-GUA* - *trnT-GUU* tRNA precursor obtained from the Artemis genome browser. Transcription unit encompassing both tRNAs (depicted in green) is depicted in orange. iCLIP peaks corresponding to the binding regions of Rne are depicted on the graph in red; nucleotide sequences corresponding to the iCLIP peak areas are marked in yellow.

In order to further investigate Rne interaction with tRNAs we analysed predicted with mfol web server secondary structures of tRNAs and the location of binding region discovered by iCLIP. We found that Rne was crosslinked to a site, which is located at the unpaired region of the anticodon loop (Figure 33A). However, in many cases an additional binding site was discovered at the variable loop of some tRNAs (Figure 33B).
As the next step we decided to check if some of the potential targets discovered by iCLIP as well as Hprs, previously assumed to be processed by the studied RNases, could be cleaved by Rne *in vitro*.

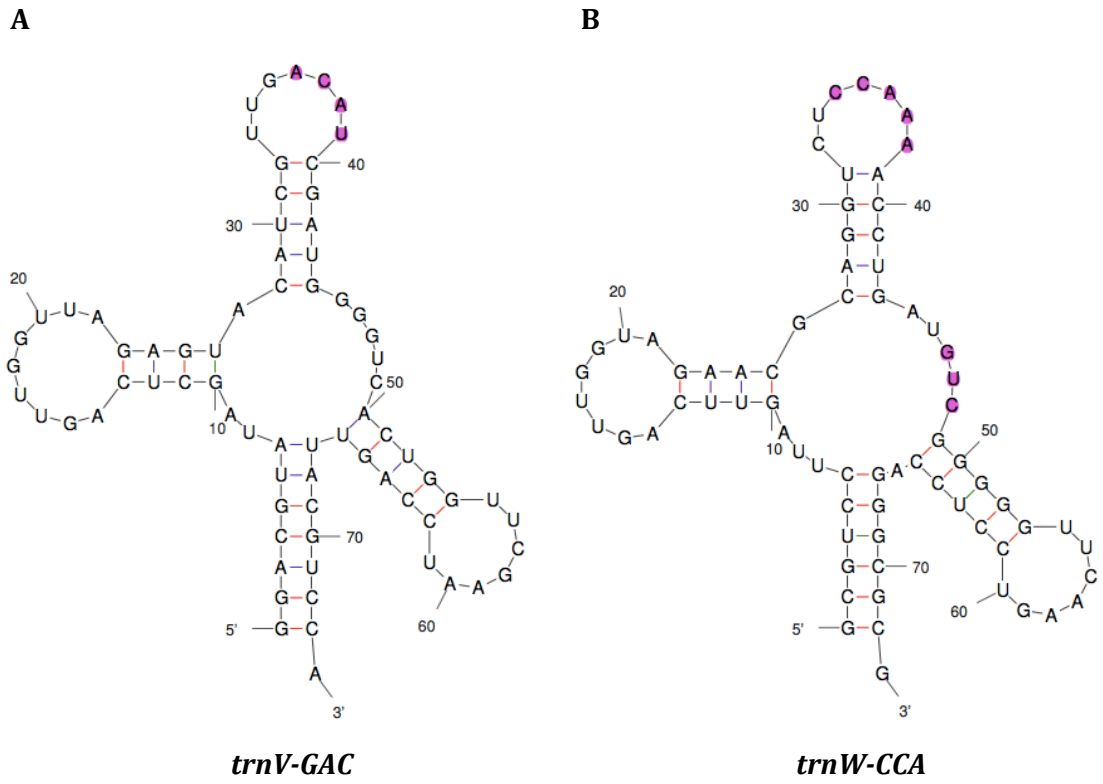

Figure 33: Depiction of the Rne binding sites for *trnV-GAC* and *trnW-CCA* tRNAs
(A) Predicted secondary structure of *trnV-GAC* tRNA created with mfold web server with the iCLIP peak area corresponding to Rne binding site marked in purple.
(B) Predicted secondary structure of *trnW-CCA* tRNA created with mfold web server with the iCLIP peak area corresponding to Rne binding site marked in purple.

Analysis of sequencing data from iCLIP experiment performed with Rnc2 revealed lower number of crosslink sites in comparison to the ones for Rne (Table 12). The majority of the crosslink sites were mapped to mRNAs (including crosslink positions located within CDSs, at 5'-UTRs and 3'-UTRs). However, binding of Rnc2 to rRNAs and some ncRNAs was also detected via iCLIP. Interestingly, one of the ncRNAs suggested to bind Rnc2 was Hpr10. Figure 34 represents the location of Rnc2 binding sites within Hpr10 (marked in blue). It was already proposed earlier that Hpr10 might be processed by Rnc due to the presence of extended double-stranded region (Figure 18), and identification of Rnc2 binding sites in close proximity to the possible cleavage site confirmed this hypothesis.

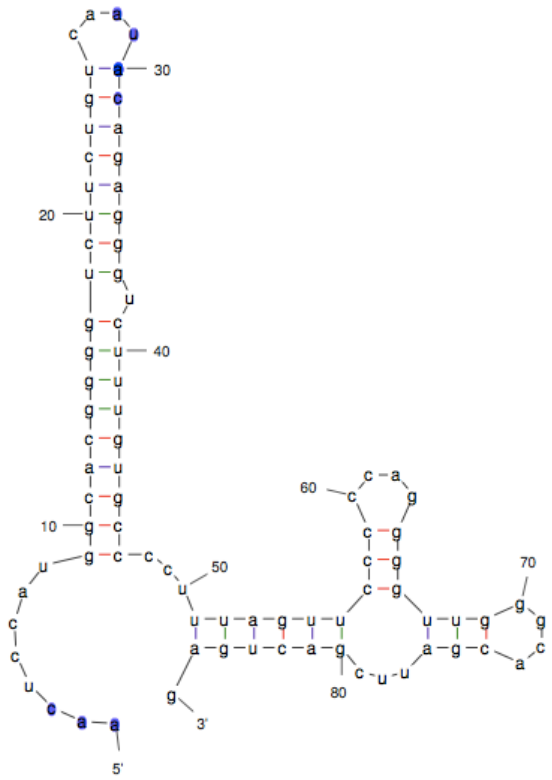

Figure 34: Depiction of the Rnc2 binding sites for Hpr10
Predicted secondary structure of Hpr10 corresponding to the respective minimum free energy state using mfold web server. iCLIP peak areas corresponding to Rnc2 binding sites are marked in blue.

Table 12: iCLIP crosslink positions for Rnc2 mapped to the genome of *Synechocystis*. Features marked with an asterisk (*) also appear to have probable binding sites for Rne (see Table 10); the exact binding sites however did not always coincide. In case of multiple crosslink sites within one feature the highest relative read value is shown. Transfer RNAs are excluded from the table.

Name	Synonym	Gene product / description	iCLIP crosslink position	Relative read value
slr1474		hypothetical protein	5' UTR (multiple crosslink sites)	220
*rrn16Sa**		16S rRNA	internal (multiple crosslink sites), 5'-trailer	198
*rrn5Sa**		5S rRNA	internal (multiple crosslink sites)	129
*slr1679**	*SynVanX*	hypothetical protein	CDS	94
slr1634		hypothetical protein	5' UTR (multiple crosslink sites)	62
*sll0260**		hypothetical protein	CDS	56
slr0093	*dnaJ, dnaJ4, dnaJ2*	DnaJ protein, heat shock protein 40, molecular chaperone	5' UTR	52

Name	Synonym	Gene product / description	iCLIP crosslink position	Relative read value
slr1634		hypothetical protein	5' UTR	46
slr0552		hypothetical protein	5' UTR	43
ncr1397		non-coding RNA	internal	42
*sll1577**	*cpcB*	β-phycocyanin	5' UTR (multiple crosslink sites), CDS	41
sll1579	*cpcC2*	phycobilisome rod linker polypeptide	5' UTR	24
slr0335	*apcE*	phycobilisome core-membrane linker polypeptide	CDS	38
slr0226		unknown protein	CDS	38
ncr0270	Hpr10	non-coding RNA	internal (multiple crosslink sites)	34
Yfr2a		non-coding RNA	internal	33
*Yfr1**		non-coding RNA	internal (multiple crosslink sites)	30
ssl1263		hypothetical protein	5' UTR	28
ssl3093	*cpcD*	phycobilisome small rod linker polypeptide	5' UTR	23
slr1187		unknown protein	CDS	21
*rrn23Sa**		23S rRNA	internal	21
SyR11*	*ncr1160*	non-coding RNA	internal (multiple crosslink sites)	20
slr1835	*psaB*	P700 apoprotein subunit Ib	3' UTR (multiple crosslink sites)	18
Syr13*	*ncr0700*	non-coding RNA	5'-trailer	18
ssr1552		hypothetical protein	CDS	18
slr0335	*apcE*	phycobilisome core-membrane linker polypeptide	CDS	17
slr1734	*opcA*	glucose 6-phosphate dehydrogenase assembly protein	CDS	16
ssr0757		hypothetical protein	CDS	15

Crosslink sites for Rnc2 were also mapped to almost all (41 out of 43) tRNAs of *Synechocystis* (Table 13). For the majority of tRNAs more than one crosslink site was detected meaning possibly several binding sites. In order to further investigate interaction of Rnc2 with tRNAs we analysed their secondary structures predicted with mfold web server. We discovered that Rnc2 binding site is always located in the D-loop of the tRNAs (Figure 35). The majority of tRNAs contained more than one Rnc2 binding site (Table 13). Frequently Rnc2 crosslink sites were mapped to the tRNAs, which also included binding sites for Rne. In these cases Rnc2 additional binding site spreading to the variable loop of tRNA overlapped with Rne crosslink site also located in that region (Figure 35).
There were a number of overlaps between the iCLIP sequencing data for Rne and Rnc2, however, even if the crosslink sites were found within the same feature they not always coincided. Involvement of RNase III in mRNA and sRNA processing as well as in rRNA and tRNA maturation was shown for different

bacteria (Babitzke *et al.*, 1993; Evguenieva-Hackenberg and Klug, 2000; Drider and Condon, 2004; Stead *et al.*, 2011). Our iCLIP data suggest that this might also be true for *Synechocystis*. Due to time limitations it has been decided to focus on experimental validation of probable targets for Rne. However, data obtained via iCLIP for Rnc2 provide some insights to involvement of this double-strand specific RNase in RNA processing in *Synechocystis.*

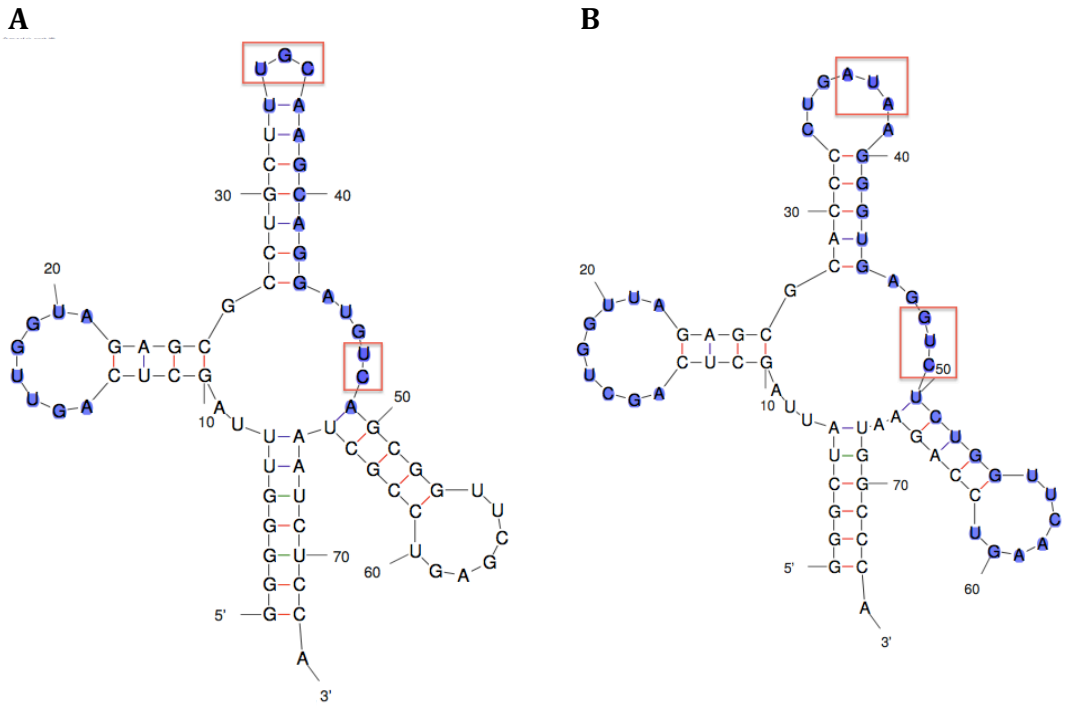

Figure 35: Depiction of the Rnc2 and Rne binding sites for *trnA-UGC* and *trnI-GAU(1)* tRNAs
(A) Predicted secondary structure of *trnA-UGC* tRNA created with mfold web server with the iCLIP peak areas corresponding to Rnc2 binding sites marked in blue; Rne binding sites overlap with Rnc2 binding site and are marked with red boxes.
(B) Predicted secondary structure of *trnI-GAU(1)* tRNA created with mfold web server with the iCLIP peak areas corresponding to Rnc2 binding sites marked in blue; Rne binding sites overlap with Rnc2 binding site and are marked with red boxes.

Table 13: iCLIP crosslink positions for Rnc2 mapped to tRNAs of *Synechocystis*. In case of multiple crosslink sites within one feature the highest relative read value is shown.

Name	Synonym	Gene product / description	number of iCLIP crosslink positions	Relative read value
trnR-ACG	*6803t19*	tRNA-Arg(ACG)	2	1057
trnF-GAA	*6803t16*	tRNA-Phe(GAA)	2	1025
trnE-UUC	*6803t14*	tRNA-Glu(TTC)	2	956
trnY-GUA	*6803t37*	tRNA-Tyr(GTA)	1	940
trnQ-UUG	*6803t23*	tRNA-Gln(TTG)	2	889

Name	Synonym	Gene product / description	number of iCLIP crosslink positions	Relative read value
trnL-UAA	*6803t39*	tRNA-Leu(TAA)	3	860
trnD-GUC	*6803t13*	tRNA-Asp(GTC)	2	818
trnK-UUU	*6803t27*	tRNA-Lys(TTT)	1	805
trnW-CCA	*6803t09*	tRNA-Trp(CCA)	2	787
trnL-CAA	*6803t12*	tRNA-Leu(CAA)	2	762
trnC-GCA	*6803t35*	tRNA-Cys(GCA)	2	758
trnV-UAC	*6803t05*	tRNA-Val(TAC)	2	726
trnN-GUU	*6803t24*	tRNA-Asn(GTT)	3	726
trnP-GGG	*6803t01*	tRNA-Pro(GGG)	3	666
trnfM-CAU_3'		tRNA-fMet(CAT)3'	2	606
trnL-UAG	*6803t07*	tRNA-Leu(TAG)	2	577
trnA-GGC	*6803t26*	tRNA-Ala(GGC)	3	566
trnS-GCU	*6803t21*	tRNA-Ser(GCT)	3	538
trnA-UGC	*6803t28*	tRNA-Ala(TGC)	1	532
trnL-GAG	*6803t10*	tRNA-Leu(GAG)	4	525
trnI-GAU(1)	*6803t29*	tRNA-Ile(GAT)	2	484
trnM-CAU	*6803t11*	tRNA-Met(CAT)	3	480
trnO-CGG	*6803t04*	tRNA-Pro(CGG)	2	453
trnG-UCC	*6803t17*	tRNA-Gly(TCC)	2	427
trnH-GUG	*6803t22*	tRNA-His(GTG)	2	409
trnR-CCG	*6803t33*	tRNA-Arg(CCG)	2	349
trnG-GCC	*6803t36*	tRNA-Gly(GCC)	3	326
trnP-UGG	*6803t15*	tRNA-Pro(TGG)	3	318
trnS-GGA	*6803t20*	tRNA-Ser(GGA)	2	296
trnT-GUU	*6803t38*	tRNA-Thr(GGT)	4	267
trnR-UCU	*6803t08*	tRNA-Arg(TCT)	3	245
trnT-UGU	*6803t25*	tRNA-Thr(TGT)	2	187
trnT-CGU	*6803t03*	tRNA-Thr(CGT)	1	154
trnA-CGC	*6803t32*	tRNA-Ala(CGC)	4	142
trnL-CAG	*6803t41*	tRNA-Leu(CAG)	3	139
trnI-CAU	*6803t18*	tRNA-Ile(CAT)	2	128
trnV-GAC	*6803t42*	tRNA-Val(GAC)	2	92
trnR-CCU	*6803t06*	tRNA-Arg(CCT)	2	57
trnG-CCC	*6803t30*	tRNA-Gly(CCC)	1	56
trnS-UGA	*6803t02*	tRNA-Ser(TGA)	3	51
trnS-CGA	*6803t31*	tRNA-Ser(CGA)	4	31

3.2.3 *In vitro* cleavage assays with GST-tagged RNases are insufficient to identify cleavage pattern of Hpr8 and Hpr10

In order to investigate which RNAs are degraded by the studied RNases we performed series of *in vitro* cleavage assays. However, it was decided to use GST-tagged RNases instead of FLAG-tagged RNases for the assays to exclude the possibility of disturbance caused by the FLAG tag. One of the biggest advantages of using pGEX system is that the GST-tag can be cleaved by PreScission protease during the purification of recombinant proteins so the affinity tag is not

hindering protein properties (section 2.5.7). The overexpression strains of GST-tagged RNases were created as described in section 2.4.2. Rne in large quantities might be toxic for the cells, so overexpression can result in production of large amounts of incorrectly folded inactive protein that aggregates forming inclusion bodies. To increase the yield of soluble protein lower cultivation temperatures can be used. However, normal *E. coli* chaperonins that facilitate proper protein folding by binding to and stabilizing unfolded or partially folded proteins lose activity under reduced temperatures. *E. coli* ArcticExpress cells were specially designed to overcome this problem as they contain cold-adapted chaperonins Cpn10 and Cpn60 from the psychrophilic bacterium, *Oleispira antarctica*, that show high protein refolding activities at temperatures of 4–12 °C (ArcticExpress Competent cells and ArcticExpress (DE3) competent cells Instruction manual, Agilent). For these reasons the *E. coli* ArcticExpress strain was used for overexpression of GST-*rne.* GST-tagged RNases were overexpressed and purified (Figure 36).

It was possible to overexpress all three RNases of interest as it is visible in the enrichment of the band corresponding to the size of GST-tagged RNases in the lane containing sample taken after induction of overexpression (Figure 36, "+" IPTG). As a result of purification of GST-tagged Rnc with the batch method (Figure 36A and 36B), as it is seen from Coomassie stained SDS-PAA gels and corresponding western blots with antibodies against GST tag, elution fractions contain not only Rnc, but also leftovers of cleaved GST tag, PreScission protease and even RNases with the GST tag still attached to them. Normally GST tag and PreScission protease were supposed to bind to the column and not get eluted together with the protein of interest. However, it seems that either the binding to the column was not strong enough or the elution conditions were not optimal. In case of Rne purification (Figure 36C) the same impurities were observed in the elution fractions. Despite that protein purification was not ideal it was decided to perform *in vitro* cleavage assays with these enzymes.

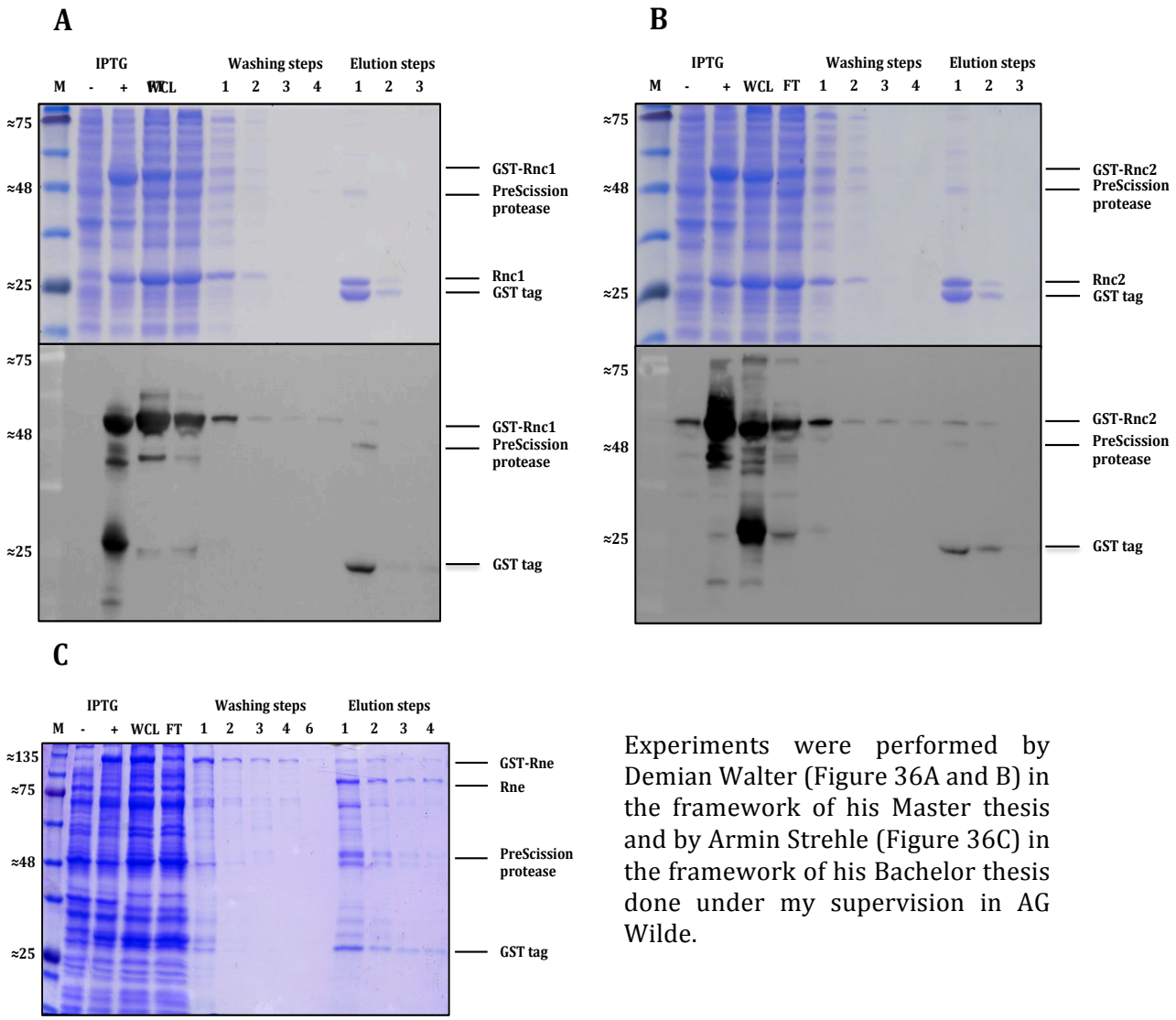

Experiments were performed by Demian Walter (Figure 36A and B) in the framework of his Master thesis and by Armin Strehle (Figure 36C) in the framework of his Bachelor thesis done under my supervision in AG Wilde.

Figure 36: Purification of GST-tagged RNases from *E. coli* with the batch-method

(A) Purification of GST-Rnc1 from 1,2 l *E. coli* BL21-GST-Rnc1 culture using glutathione sepharose and PreScission protease. Protein marker (Marker VI, AppliChem), samples taken before ("-" IPTG) and after ("+" IPTG) the induction of expression, whole cell lysate (WCL), flow through (FT), washing fractions 1-4 and elution fractions 1-3 were separated on 7,5% SDS-PAA gel and stained with Coomassie dye solution (top) and transferred to the nitrocellulose membrane. Immunological detection was performed using anti-GST antibody (bottom). Sizes of the detected bands fit to the calculated sizes: 54 kDa for GST-Rnc1, 46 kDa for PreScission protease, 29 kDa for Rnc1 and 25 kDa for GST tag. Sizes of the marker bands are marked in kDA.

(B) Purification of GST-Rnc2 from 1,2 l *E. coli* BL21-GST-Rnc2 culture using glutathione sepharose and PreScission protease. Protein marker (Marker VI, AppliChem), samples taken before ("-" IPTG) and after ("+" IPTG) the induction of expression, WCL, FT, washing fractions 1-4 and elution fractions 1-3 were separated on 7,5% SDS-PAA gel and stained with Coomassie dye solution (top) and transferred to the nitrocellulose membrane. Immunological detection was performed using anti-GST antibody (bottom). Sizes of the detected bands fit to the calculated sizes: 52 kDa for GST-

Rnc2, 46 kDa for PreScission protease, 27 kDa for Rnc2 and 25 kDa for GST tag. Sizes of the marker bands are marked in kDA.
(C) Purification of GST-Rne from 1,2 l *E. coli* ArcticExpres-GST-Rne culture using glutathione sepharose and PreScission protease. Protein marker (Marker VI, AppliChem), samples taken before ("-" IPTG) and after ("+" IPTG) the induction of expression, WCL, FT, washing fractions 1-4 and 6, and elution fractions 1-3 were separated on 10% SDS-PAA gel and stained with Coomassie dye solution. Sizes of the detected bands fit to the calculated sizes: 104 kDa for GST-Rne, 79 kDa for Rne, 46 kDa for PreScission protease and 25 kDa for GST tag. Sizes of the marker bands are marked in kDA.

As a substrate for *in vitro* cleavage assay Hpr8 *in vitro* transcript was used. It was assumed that this sRNA is processed by Rne because of the AU-rich single-stranded regions present in its secondary structure. Nevertheless we decided to check all three of the purified RNases on the ability to cleave Hpr8. *In vitro* cleavage assays were performed as described in section 2.6.7, the results are presented in Figure 37.

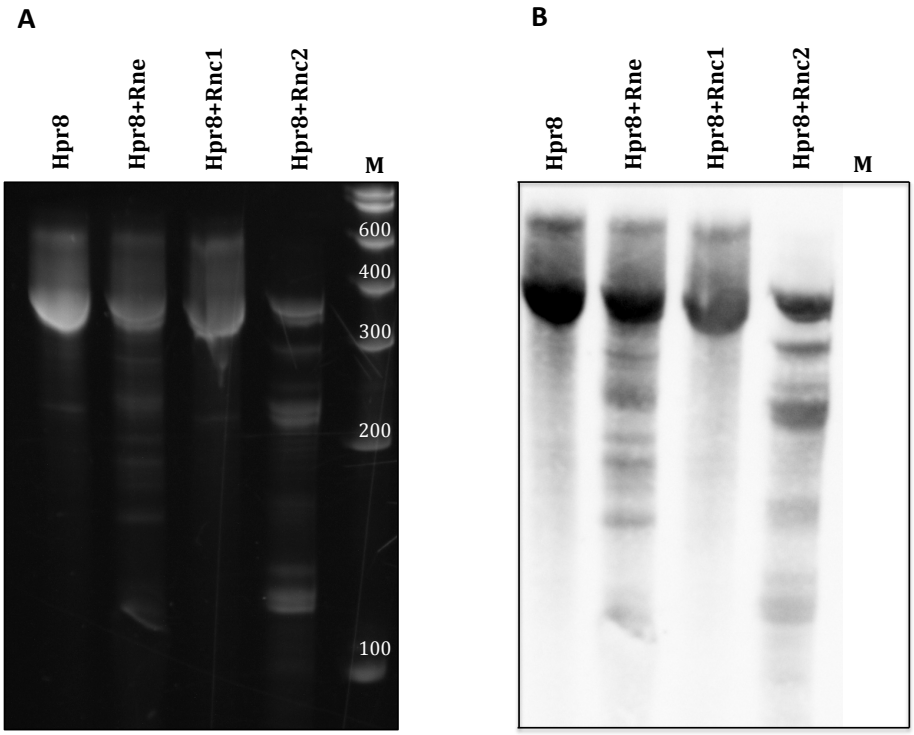

Figure 37: *In vitro* cleavage assay of Hpr8
(A) Hpr8 *in vitro* transcript was generated by *in vitro* transcription, cleaved with Rne and both types of Rnc; the cleavage products were separated on 6% PAA-urea gel that was stained with EtBr afterwards. Marker: RiboRuler low range RNA ladder (Thermo Scientific). Sizes of the marker bands are marked in nt. This experiment was performed by Armin Strehle in the framework of his Bachelor thesis done under my supervision in AG Wilde.
(B) Northern blot analysis of the cleavage pattern. RNA from *in vitro* cleavage assay was transferred to nylon membrane and hybridized with radioactively labelled Hpr8 probe.

Hpr8 transcript was incubated for 15 min at 30 ^{0}C in cleavage buffer alone (Hpr8; negative control for unspecific RNA degradation) or in the presence of Rne (Hpr8+Rne), Rnc1 (Hpr8+Rnc1) or Rnc2 (Hpr8+Rnc2). Endoribonuclease activity was abolished by adding EDTA and RNA loading dye. After electrophoretic separation of RNA in PAA-urea gel and Northern blot hybridization with Hpr8 probe it became evident that Hpr8 is cleaved by Rne and Rnc2, but not by Rnc1. Processing of this sRNA by Rnc2 was unexpected, but because the cleavage pattern by Rnc2, judging by the Northern blot image, is different from the one by Rne it is most likely not an artefact. However, the RNases used in the assay were not pure enough, so it is hard to conclude with certainty that Hpr8 is a true substrate for Rne and Rnc2 in *Synechocystis*.

In order to obtain purer proteins for *in vitro* cleavage assays we decided to use fast protein liquid chromatography (FPLC) on ÄKTA Pure chromatography system (GE Healthcare) as described in section 2.5.8. GST-*rnc*2 overexpression strain was cultivated as described in section 2.5.7. Recombinant proteins were purified directly from the cell lysate using GSTrap FF column (GE Healthcare) that was connected to ÄKTA Pure system and proteins were eluted (Figure 38A). Elution fractions number 5, 9, 18, 25 and 26 corresponding to the peaks on the chromatogram were selected for SDS-PAGE analysis with further silver staining of the gel (Figure 38B).

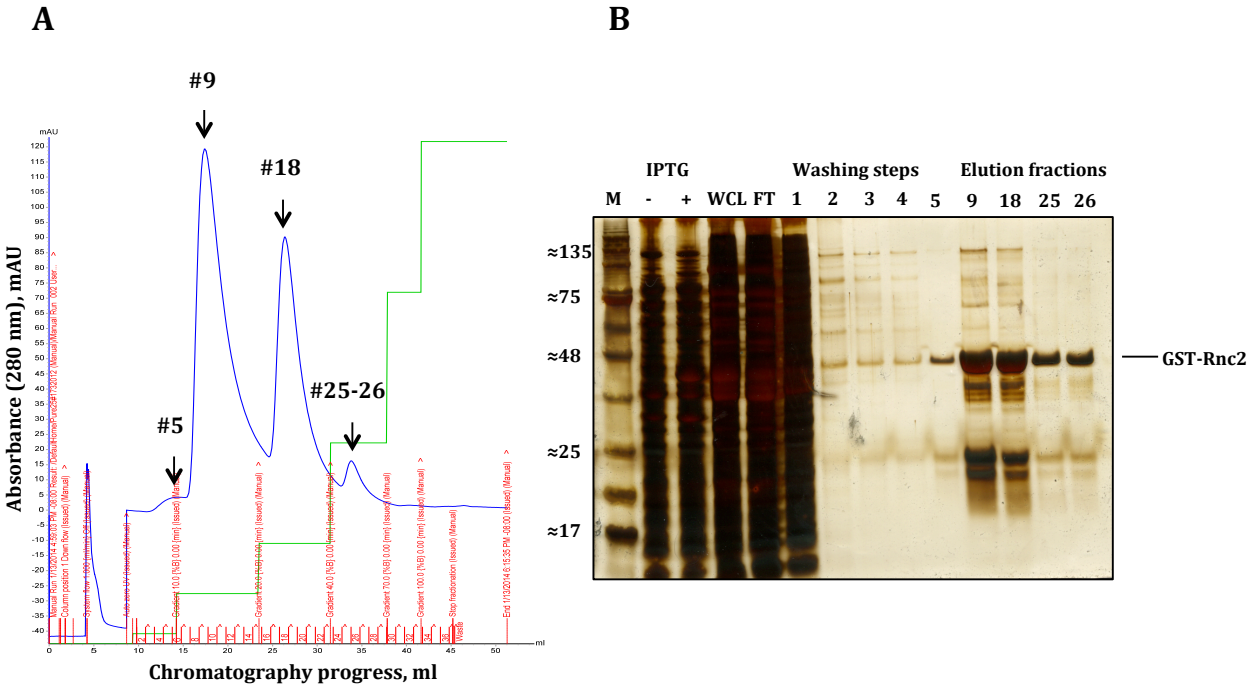

Figure 38: FPLC purification of GST-Rnc2

(A) Purification of GST-Rnc2 from 1,2 l *E. coli* BL21-GST-Rnc2 culture using GSTrap FF column connected to ÄKTA Pure. Peaks on the chromatogram (in blue) correspond to eluted proteins. Green graph corresponds to the elution buffer gradient. Fraction numbers are depicted in red on the x-axis.

(B) Protein marker (Marker VI, AppliChem), samples taken before ("-" IPTG) and after ("+" IPTG) induction of expression, WCL, FT, washing fractions 1-4 and elution fractions #5, 9, 18, 25 and 26 were separated on 10% Tris-Tricine SDS-PAA gel and stained with silver nitrate. Size of the detected band at ca. 50 kDa fits to the calculated size of 52 kDa for GST-Rnc2. Sizes of the marker bands are marked in kDA.

Separation of the eluted proteins by means of electrophoresis revealed that all the tested elution fractions contain GST-Rnc2, Rnc2 and GST tag. In order to get pure Rnc2 elution fractions #5, 25 and 26 were subjected to cleavage with PreScission protease (section 2.5.7) and put again through GSTrap column to get rid of cleaved affinity tag and PreScission protease. As a result only one distinct peak was visible on the chromatogram (Figure 39A). The column was then washed with 100% reduced glutathione buffer to elute the GST tag and PreScission protease that were used as a control for SDS-PAGE silver staining and western blot with anti-GST antibodies (Figure 39B).

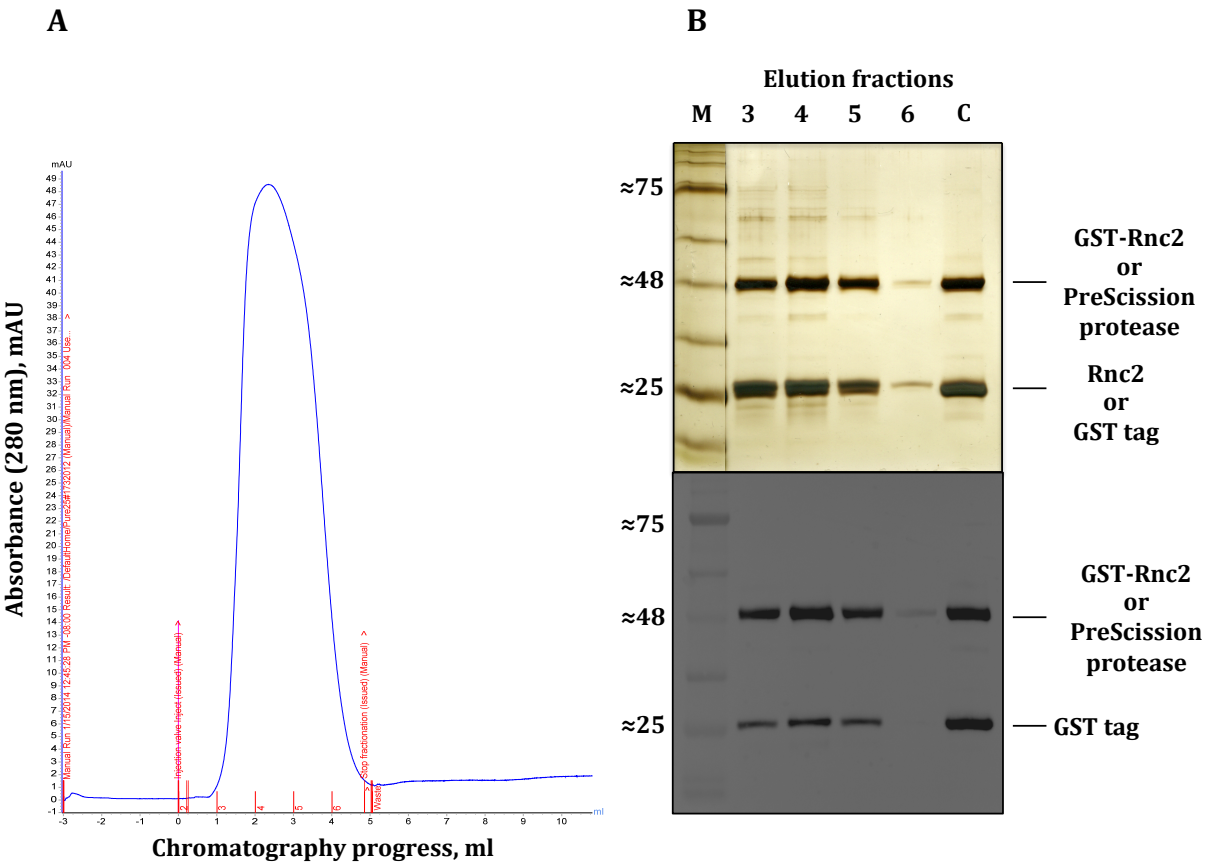

Figure 39: FPLC purification of GST-Rnc2 cleaved with PreScission protease
(A) After cleavage with PreScission protease elution fractions #5, 25 and 26 were put through GSTrap FF column connected to ÄKTA Pure. The peak on the chromatogram (in blue) corresponds to eluted proteins. Fraction numbers are depicted in red on the x-axis.
(B) Protein marker (Marker VI, AppliChem), elution fractions #3-6 and GST-elution were separated on 10% Schägger SDS-PAA gel and subjected to silver staining (top) and transferred to the nitrocellulose membrane. Immunological detection was performed using anti-GST antibody (bottom). Sizes of the detected bands fit to the calculated sizes: 52 kDa for GST-Rnc2, 46 kDa for PreScission protease, 27 kDa for Rnc2 and 25 kDa for GST tag. Sizes of the marker bands are marked in kDA.

On the silver stained SDS-PAA Tris-Tricine gel it is hard to distinguish if there are 2 bands of ca. 26 kDa size that would correspond to Rnc2 and GST tag or if only one of these proteins was eluted. It is also possible that the upper band of

approx. 50 kDa corresponds not to GST-Rnc2 but to PreScission protease as these two proteins are also quite close in size. Possible explanation for these results is that either (i) after cleavage of the affinity tag all four proteins (GST-Rnc2, PreScission protease, Rnc2 and GST tag) were eluted from the column but because they are too close in size it is hard to distinguish separated bands corresponding to all four of them; or (ii) only PreScission protease and GST tag are present in the analysed elution fractions after the cleavage, as Rnc2 got eluted before them and was not captured or got too strongly attached to the column (the latter is less likely as the affinity of GST tag alone and of PreScission protease is considered to be much stronger).
Despite this ambiguity about the quality of purified Rnc we still decided to make an *in vitro* cleavage assay to check if it is responsible for processing of Hpr8 and also Hpr10 that was considered a good candidate due to its secondary structure. FPLC-purified Rnc2 was used for this *in vitro* cleavage assays (Figure 40).

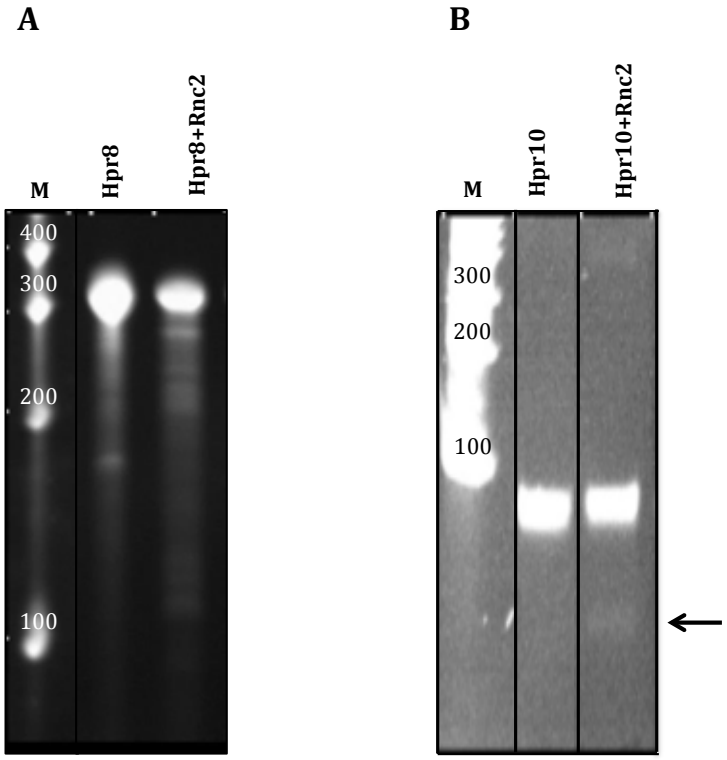

Figure 40: *In vitro* cleavage of Hpr8 and Hpr10 with Rnc2
(A) Hpr8 *in vitro* transcript (360 nt) was generated by *in vitro* transcription and cleaved with Rnc2; the cleavage products were separated on 6% PAA-urea gel that was stained with EtBr afterwards. Marker: RiboRuler low range RNA ladder (Thermo Scientific). Sizes of the marker bands are marked in nt.
(B) Hpr10 *in vitro* transcript (86 nt) was generated by *in vitro* transcription, cleaved with Rnc2; the cleavage products were separated on 12% PAA-urea gel that was stained with EtBr afterwards. Marker: RiboRuler low range RNA ladder (Thermo Scientific). Sizes of the marker bands are marked in nt. The presented image was combined of the lanes cut out from the initial image of the stained with EtBr PAA-urea gel; the samples were analysed together in one experiment. *In vitro* cleavage assay of Hpr10 was performed by Demian Walter in the framework of his Master thesis done under my supervision in AG Wilde.

Hpr8 transcript was incubated for 15 min at 30 ^{0}C in cleavage buffer alone (Hpr8; negative control for unspecific RNA degradation) or in the presence of Rnc2 (Hpr8+Slr1646). Endoribonuclease activity was abolished by adding EDTA and RNA loading dye. After electrophoretic separation of RNA in PAA-urea gel it became evident that there was a slight unspecific degradation of the substrate in the negative control, however cleavage pattern by Rnc2 differed from it proving specific degradation of Hpr8 by Rnc2. *In vitro* cleavage of Hpr10 was done analogously. In the lane Hpr10+Rnc2 there is a faint but clear band that is not present in the negative control (marked by an arrow in Figure 40B). This proves that Hpr10 is most likely processed by Rnc2 *in vitro*.

3.2.4 *In vitro* cleavage assays with His-tagged Rne confirmed *rne* target predictions made with iCLIP.

In order to obtain purer Rne for better performance of *in vitro* cleavage assays we put elution fractions #1 and 2 from the batch purification of GST-Rne (Figure 36C) through the HiLoad 16/600 Superdex 200 prep grade column (GE Healthcare) connected to ÄKTA Pure for gel filtration chromatography. Several peaks appeared on the elution profile. After silver staining of the gel we detected too many impurities in elution fractions, so purified GST-Rne was not really suitable for performing *in vitro* cleavage assays with it.
As the attempts to purify GST-tagged Rne were not absolutely satisfying we decided to use His-tagged Rne in further *in vitro* cleavage assays to verify possible *rne* targets discovered in the iCLIP experiment. The plasmid pQE*Rne* was kindly provided by Dr. Damir Stazic (AG Hess, Institute of Biology III, Albert-Ludwigs University Freiburg). His-Rne was overexpressed in *E. coli* M15 (pREP4) and purified as described in section 2.5.6 (Figure 41). Elution fraction 3 was used for further experiments.
In order to verify some of the targets predicted by iCLIP *in vitro* transcripts for *sll1184* (*ho1*, coding heme oxygenase), *slr1834* (*psaA*, coding P700 apoprotein subunit Ia), *rrn5Sa* (5S ribosomal RNA), SyR12 (NsiR4, non-coding RNA) and *NC-423* (non-coding RNA) were created as described in section 2.6.7. To avoid generating too long *in vitro* transcripts shorter versions were constructed. However, predicted secondary structures were checked with mfold web server and kept the same as in the original full-length versions, because it is highly important for cleavage. The transcripts were radioactively labelled with [α^{32}P]-UTP and subjected to dephosphorylation using 5' RNA polyphosphatase (Epicentre) to create a monophosphate at the 5' end as it facilitates cleavage by Rne (Mackie, 1998).

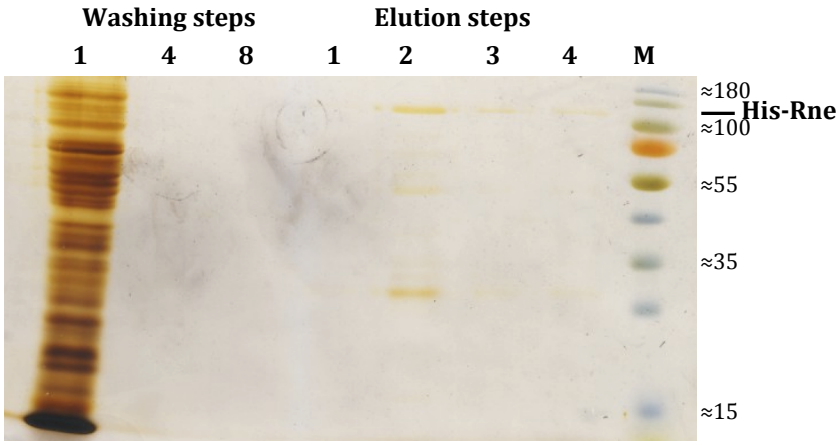

Figure 41: Purification of His-Rne
1 l of *E. coli* M15-pQE*Rne* culture was grown at 37°C, the overexpression of the heterologously expressed protein was induced by adding IPTG. His-tagged Rne was affinity purified using Ni-NTA, loaded on 10% SDS-PAA gel and subjected to SDS-PAGE. The gel was stained with silver nitrate. Protein marker: PageRuler Prestained Protein Ladder (Thermo Fisher Scientific). Sizes of the marker bands are marked in kDA.

In vitro cleavage assays with His-Rne were performed as described in section 2.6.7. We always compared the substrate incubated in the cleavage buffer without adding the RNase (negative control for unspecific RNA degradation) to the 5'-tri- and monophosphorylated substrates incubated in the presence of the enzyme (Figure 42). *In vitro* transcripts were incubated for 15 min at 30 ^{0}C in the cleavage buffer. Endoribonuclease activity was abolished by adding EDTA and RNA loading dye. After electrophoretic separation of RNA in 8% PAA-urea gel the gels were dried in the gel dryer, placed into a cassette with the phosphor screen and exposed overnight. The radioactive signals were detected using a phosphorimager.
In vitro cleavage assay with Rne and 5S rRNA as a substrate (Figure 42A) discovered specific cleavage pattern that accurately fits to the iCLIP data. The 5S rRNA *in vitro* transcript was created in a way that it includes the whole intergenic region between *rrn23Sa* and *rrn5Sa* and a full *rrn5Sa*. According to the sequencing results of the iCLIP experiment there is a strong peak directly in front of *rrn5Sa* depicting the binding site for Rne (Figure 43A). If we assume that cleavage site is located directly next to the binding site discovered by iCLIP, we could see that in the marked peak area there is a single-stranded AU-rich region in the loop (Figure 43B) that is a good candidate for Rne cleavage site. If the ribonuclease cuts the transcript at this predicted position 5S rRNA *in vitro* transcript gets divided into two parts of approx. 50 and 140 nt in length. This fits exactly to the cleavage pattern obtained by digestion of 5S rRNA with Rne (Figure 42A) and therefore confirms the iCLIP prediction.

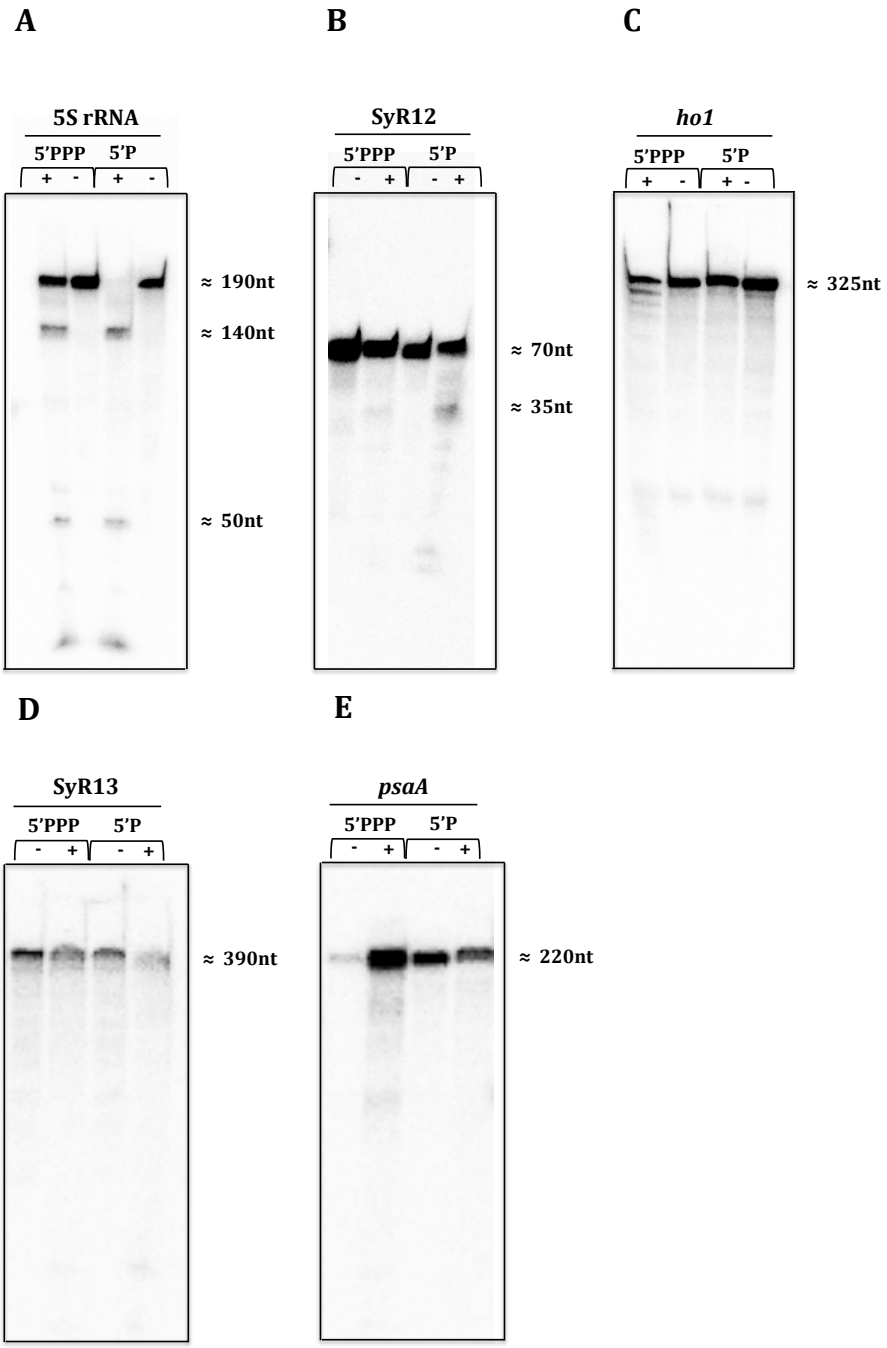

Figure 42: *in vitro* cleavage assays with His-Rne and various substrates
(A) Radioactively labelled *5S rRNA in vitro* transcript was dephosphorylated and subjected to *in vitro* cleavage by Rne for 15 min at 30 ^{0}C. Tri- (5'PPP) and monophosphorylated (5'P) versions of the transcript with ("+") and without ("-") Rne were separated on 10% PAA-urea gel using custom gel system. The gels were dried, exposed to the phosphor screen overnight and analysed on the phosphorimager. The sizes of the cleaved fragments were calculated from the comparison with the known sizes of the full transcripts loaded on the same gel.
(B) Radioactively labelled SyR12 *in vitro* transcript was treated as described in (A).
(C) Radioactively labelled *ho1 in vitro* transcript was treated as described in (A).
(D) Radioactively labelled SyR13 *in vitro* transcript was treated as described in (A).
(E) Radioactively labelled *psaA in vitro* transcript was treated as described in (A).

In order to determine exact location of the cleavage site in the 5S rRNA the mixture of RNA transcripts obtained after performing *in vitro* cleavage assay with Rne was subjected to 3' RACE as described in section 2.6.9. Obtained cDNA was amplified by PCR using 4 different primer combinations and PCR products were separated via gel electrophoresis on a 3% NuSieve 3:1 agarose (Biozym) gel and stained with EtBr (Figure 44). Lower PCR bands from lanes one and two contatining cleavage products were excised from the gel, PCR products were purified and cloned into pJET1.2 cloning vector. Ligation mixture was then used for the transformation of *E. coli* DH5α competent cells. Extracted plasmid DNA was subjected to sequencing. In total 26 clones were sequenced, which resulted in identification of 16 different 3' ends (Figure 45). The heterogeneous 3' ends may be explained by partial trimming by 3'-to-5' exoribonuclease. The majority of retrieved 3' ends were localized to a window 48-59 nt downstream of the 3' end of the 23S rRNA. According to the predicted secondary structure the cleavage site lies in the single-stranded loop area of the intergenic region between 23S and 5S rRNA (Figure 43B). However, 4 sequenced clones presented 3' ends in the adjacent single-stranded A-rich region, which makes it possible that Rne cleavage site is located at that position (Figure 43B).

A

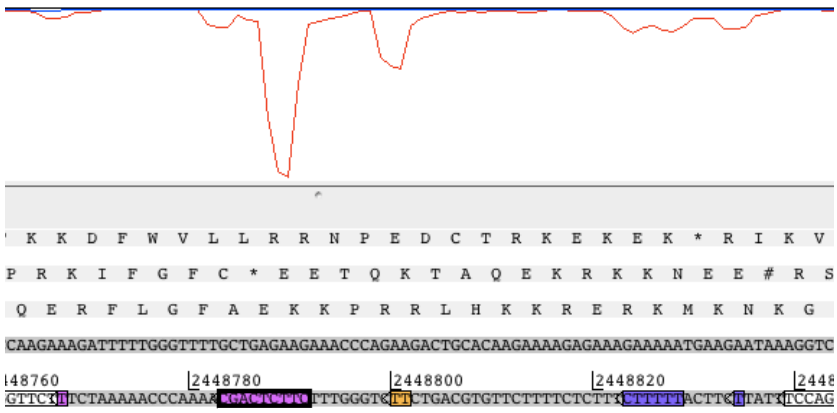

B

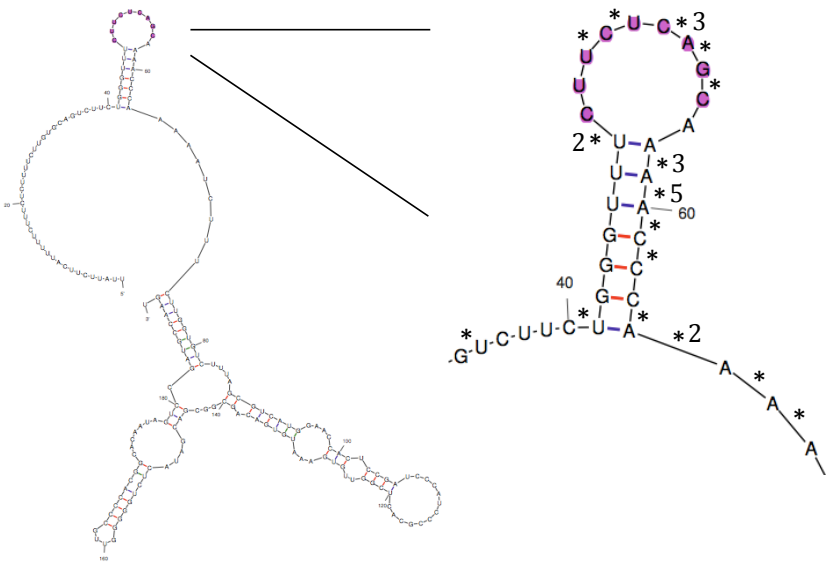

Figure 43: Depiction of the iCLIP peak at the 5' end of 5S rRNA (previous page)
(A) Image of the region of the iCLIP peak at the 5' end of 5S rRNA obtained from the Artemis genome browser. iCLIP peak corresponding to the binding region of Rne is depicted on the graph in red; nucleotide sequence corresponding to the iCLIP peak area is marked in purple.
(B) Secondary structure of 5S *in vitro* transcript created with mfold web server with the magnified iCLIP peak area (marked in purple). Asterisks indicate cleavage sites detected via 3' RACE. The number next to the asterisk indicates the number of sequenced clones containing that 3' end (no number for 1).

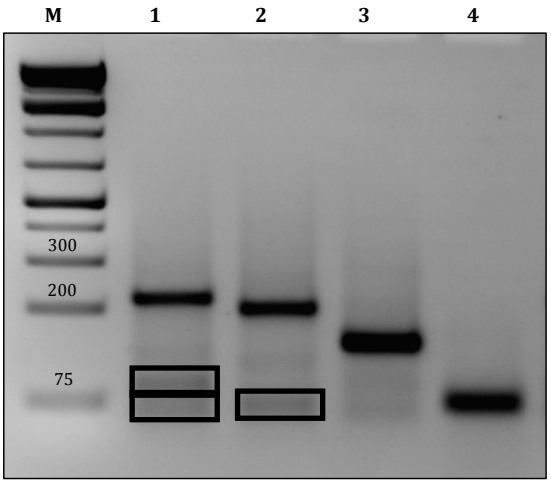

Figure 44: Gel electrophoresis of the cDNA amplification for the 3' RACE
Obtained cDNA was amplified by PCR using the following primer combinations:
lane 1: 3RACE_Tm55 + 5S-Race-1; expected PCR fragment length 218 bp;
lane 2: 3RACE_Tm55 + 5S-Race-2; expected PCR fragment length 197 bp;
lane 3: 3RACE_Tm55 + 5S-Race-3; expected PCR fragment length 140 bp;
lane 4: 3RACE_Tm55 + 5S-Race-4; expected PCR fragment length 69 bp.
Marker: GeneRuler 1 kb Plus DNA ladder (Thermo Fisher Scientific). Sizes of the marker bands are marked in nt. PCR bands marked with black boxes were excised from the gel, PCR products were purified and cloned into pJET1.2 cloning vector.

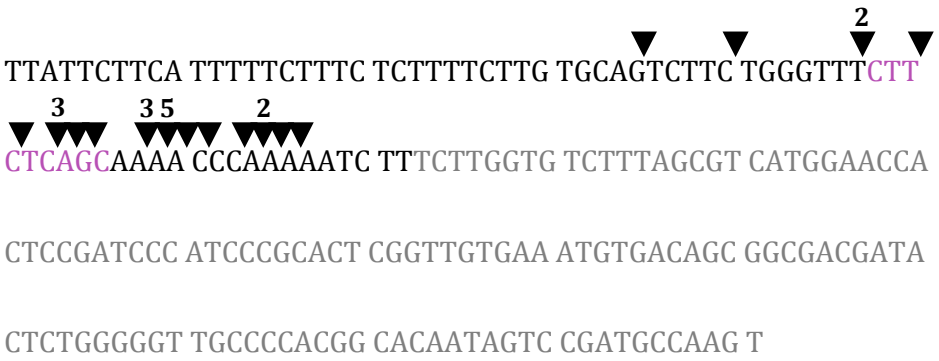

Figure 45: 3' end mapping of the cleavage product
Nucleotide sequence of the 5S *in vitro* transcript. Arrowheads indicate the identified via 3' RACE 3' termini. Number above the arrowheads indicate the number of sequenced clones containing that 3' end (no number for 1). iCLIP peak area is marked in purple. *rrn5Sa* sequence is marked in grey.

Another promising target for Rne binding and probable cleavage discovered by iCLIP was ncRNA SyR12 (NsiR4). The name comes from *Synechocystis* ncRNA12 (Voss *et al.*, 2009). It is a small ncRNA 70 nt in length; its coding sequence is located on the chromosome between *sll1697* and *sll1698* coding for hypothetical proteins in the same orientation. SyR12 *in vitro* transcript includes the entire ncRNA. iCLIP sequencing results revealed a very strong peak directly in SyR12 depicting the binding site for Rne (Figure 46A). The presence of the AU-rich single-stranded region in the predicted secondary structure of this ncRNA (Figure 46B) suggests that the cleavage site for Rne is located approximately in the middle of the transcript in the AU-rich single-stranded loop region.

A

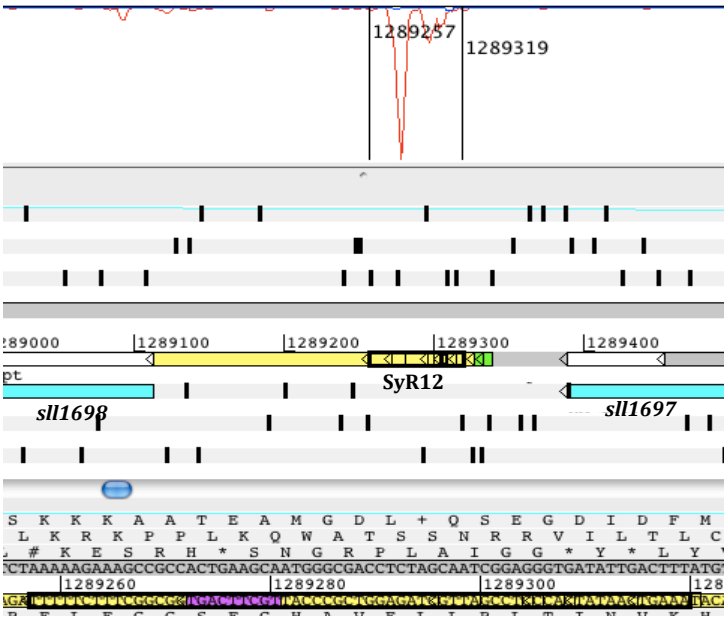

B

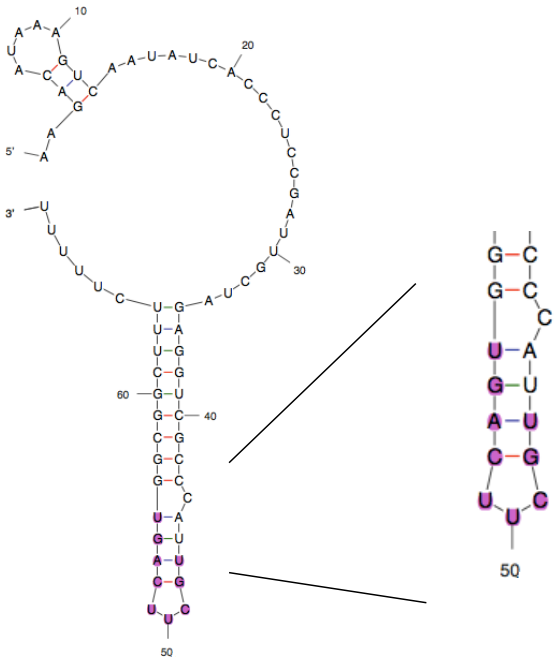

Figure 46: Depiction of the iCLIP peak in SyR12 (previous page)
(A) Image of the region of the iCLIP peak in SyR12 obtained from the Artemis genome browser. SyR12 nucleotide sequence is marked with a black box. iCLIP peak corresponding to the binding region of Rne is depicted on the graph in red; nucleotide sequence corresponding to the iCLIP peak area is marked in purple.
(B) Predicted secondary structure of SyR12 *in vitro* transcript created with mfold web server with the magnified iCLIP peak area (marked in purple).

In vitro cleavage assay (Figure 42B) showed that the monophosphorylated version of SyR12 is cleaved by Rne. The fact that after the separation of the cleaved products on the PAA-urea gel we saw only one band of approximately 35 nt size can be explained by the assumption that the transcript was most likely cut in the middle and on the gel there are actually two cleavage products that run on the same height and therefore are visible as one band.
From the iCLIP results we also chose two large mRNAs: *ho1* (*sll1184*) and *psaA* (*slr1834*) for validation. Constructed *in vitro* transcripts were slightly smaller (324 nt for *ho1* and 221 nt for *psaA*), however, the secondary structures of the resulted shorter versions were checked with mfold web server and appeared to be very similar to the original ones. *In vitro* cleavage assays with His-Rne did not show positive results. In case of *ho1* there was a slightly visible band of ca. 50 nt size (Figure 42C), but it appeared also in the negative control (lanes marked with "-") and therefore was unspecific. There was one more extra band running a bit lower than the main transcript, however, it also could not be determined as a specific product of the Rne cleavage because it was also present in the negative control. *In vitro* cleavage assay of *psaA* did not yield positive result as well. The smear visible in the 5'PPP+ lane most likely resulted from unspecific degradation of the transcript and was detected due to the general higher amount of the loaded cleaved substrate on the gel (Figure 42E).
Another ncRNA SyR13 that gave a strong peak on the iCLIP dataset was checked via *in vitro* cleavage assay. The second band below the full transcript at the height of approx. 370 nt was probably a result of unspecific RNA degradation as it appeared in every lane (Figure 42D).

4. Discussion

4.1 Hfq-dependent sRNAs in *Synechocystis*

Identification of Hfq-dependent sRNAs in *Synechocystis* via microarray and tiling arrays performed by Dr. D. Dienst and Dr. N. Schuergers (Dienst *et al.*, 2008, 2010; Schuergers, 2014) was the starting point of the present work. However, only few of identified ncRNAs were shown to be differentially expressed in an Δ*hfq* mutant (Dienst, 2010; Schürgers, 2014). In contrast, in *E. coli* all studied *trans*-ncRNAs co-immunoprecipitate with Hfq (Waters and Storz, 2009). Deep sequencing and bioinformatics terminator prediction revealed 40 Hfq-dependent sRNA candidates in the plant pathogen *Erwinia amylovora*, some of which were validated experimentally and are thought to play a role in virulence regulation (Zeng and Sundin, 2014). Analysis of Hfq-binding ncRNAs in the nitrogen-fixing α-proteobacterium *Sinorhizobium meliloti* in five growth conditions via RNA-seq determined 85 *trans*-ncRNAs and 83 asRNAs that are Hfq-bound. Interestingly, only 20 *trans*-ncRNAs and 13 asRNAs were expressed in the exponential growth phase, whereas the majority of Hfq-binding sRNAs were expressed under stress conditions (osmotic stress, cold shock, heat shock, stationary growth phase) (Torres-Quesada *et al.*, 2014). The fact that most of regulatory sRNAs participate in stress response and are therefore expressed only under specific growth conditions may explain the relatively low number of Hfq-dependent sRNAs identified so far in *Synechocystis*, because transcript accumulation was investigated under normal growth conditions (logarithmic growth phase).
For ncRNA Hpr8 it has been shown that its processing is disrupted in the Δ*hfq* mutant in *Synechocystis* (Figure 10B). Investigation of various *hpr8* mutants did not reveal any phenotype caused by knockout or overexpression of this sRNA. Microarray analysis of Hpr8 overexpression strain did not reveal probable functions of this ncRNA. It has been shown that Hpr8 (also called CsiR1: carbon-stress-induced RNA 1) is highly induced upon low carbon shift and totally repressed upon high carbon conditions, which may hint on its regulatory function during carbon depletion (Kopf *et al.,* 2014; Klähn *et al*., 2015). Induction of Hpr8 under high light and UV light as well as its location upstream of *slr1214* gene, which is a part of the operon (*slr1212-slr1214*) encoding two-component signalling system responsible for negative phototaxis under UV-A light, suggested its involvement in response to UV light (Figure 14). However, phototaxis assays with various *hpr8* mutants revealed that this sRNA is not directly in charge of UV light response in *Synechocystis*. Our data suggest that Hpr8 might be a 5' UTR of *slr1214*. In this case *slr1214* possesses only very weak or no promoter and results as a read-through of Hpr8 because of incomplete transcription termination. The fact that our attempts to knock out *hpr8* led to simultaneous knockout of *slr1214* also confirm that they are cotranscribed. sRNAs that accumulate as individual and abundant transcripts and also serve as 5' UTRs of the downstream genes were recently identified as a novel class of genetic elements called actuatons (Kopf and Hess, 2015). Hpr8 is not the only

example of an actuaton in *Synechocystis'* genome. Another sRNA that is cotranscribed with the adjacent mRNAs in *Synechocystis* is SyR9. This sRNA is located upstream of the aldehyde deformylating oxygenase gene (*ado*, *sll0208*), encoding the main enzyme of alkane synthesis. Despite that *sll0208* has its own promoter it also is cotranscribed with SyR9 (Klähn *et al*., 2014).
As the focus of present study is RNA degradation in *Synechocystis*, we also investigated processing of Hpr8. Its secondary structure contains a vast single-stranded AU-rich region, which makes this sRNA a possible target for Rne (Figure 10C). *In vitro* cleavage assays conducted with affinity purified Rne, Rnc1 and Rnc2 showed that Hpr8 is cleaved by Rne and Rnc2 (Figure 37). However, the degradation pattern was not specific enough to conclude with certainty that Hpr8 is a true substrate for either of the RNases. This might be explained by insufficient purity of the proteins. FPLC-purified Rnc2 was also used to perform *in vitro* cleavage assay with Hpr8 (Figure 40A); the cleavage pattern however looked slightly different in comparison to the previously described experiment, which also did not allow deducing, that Hpr8 is processed by Rnc2. iCLIP analysis did not expose any binding sites for Rne or for Rnc2 within Hpr8. This does not prove, however, that Hpr8 is not processed by either of the RNases, because the iCLIP experiment was performed under normal growth conditions and Hpr8 is highly expressed under high light and UV light (Figure 14). What is more, it is possible that proper cleavage of this sRNA requires additional adaptor protein *in vivo*. This has been shown for *E. coli* in respect to regulation of *glmS* expression mediated by two homologous sRNAs GlmY and GlmZ. *glmS* encodes glucosamine-6-phosphate synthase. Its translation is promoted directly by GlmZ, which is inactivated by RNase E processing. GlmY protects GlmZ from cleavage and therefore activates *glmS* indirectly. Interestingly, there is an additional factor in this regulatory system: the sRNA-binding protein RapZ serves as an adaptor for GlmZ and interacts with the catalytic domain of RNase E. As a result RapZ recruits GlmZ for degradation by this RNase. Because of sequence and structure similarity GlmY is able to sequester RapZ acting as an anti-adaptor (Göpel *et al.*, 2013). The fact that in *E. coli* an adaptor protein is required for cleavage of the sRNA GlmZ by RNase E supports our assumption that Hpr8 might still be cleaved by Rne if all the necessary factors are present.
Investigation of Hpr10 revealed a slight reduction in phycocyanin and allophycocyanin contents in Hpr10 overexpression strain (Figure 21). However, microarray analysis could not elucidate promising targets that could explain this phenomenon. The secondary structure of Hpr10 contains a relatively long double-stranded region, that hints on possible processing by double strand-specific Rnc. This assumption was supported via iCLIP results that showed multiple binding sites for Rnc2 within Hpr10 (Table 12). What is more, *in vitro* cleavage assay performed with FPLC-purified Rnc2 displayed specific degradation of Hpr10, which substantiates that Hpr10 is a target for Rnc2 (Figure 40B).

4.2 Genomewide analysis of binding sites for Rne in *Synechocystis* using iCLIP

RNases play an important role in regulation of gene expression by means of RNA processing and degradation. Mapping their interactions with target RNAs is crucial for understanding of their effect on the transcriptome. iCLIP is a novel approach that allows determination of natural RNA targets for RNA-binding proteins *in vivo*. In combination with high-throughput sequencing it provides identification of binding sites at a single nucleotide resolution. iCLIP method, as well as its predecessor classic CLIP approach, utilizes the property of UV light to specifically crosslink proteins and RNAs that are in direct contact. Because RNA and proteins become covalently bound the following immunoprecipitation steps can be held at highly stringent conditions that allows increased specificity. This method was first used to study RNA-binding Nova proteins and their role in regulation of neuronal pre-messenger RNA splicing in mice (Ule *et al.*, 2003). Classic CLIP was later combined with high-throughput sequencing (HITS-CLIP or CLIP-Seq) and used among others to investigate miRNA-target networks in cells infected with herpesviruses (Haecker and Renne, 2014). The next step in method modification was aimed to increase resolution of binding site prediction, which was achieved by utilization of the ability of reverse transcriptase to stop at the nucleotide that is crosslinked to the peptide and to produce truncated cDNAs. Truncated cDNAs were shown to constitute 82-95% of all cDNAs depending on RBPs studied (Sugimoto *et al.,* 2012). This approach was called individual nucleotide resolution CLIP (iCLIP) as it allows determining precise crosslink position, which is located one nucleotide upstream from the truncation site (König *et al*., 2010). Another advantage of iCLIP is that introduction of random barcode in the reverse transcription primer made it possible to distinguish between unique cDNAs and PCR duplicates. This raised the possibility of quantification of RNA-protein interactions. However, iCLIP reads do not directly represent the affinity of the RBP. Number of reads also depends on the level of expression of the particular RNA transcript. Therefore, for direct comparison of different binding sites within the transcriptome normalization of iCLIP data should be performed using expression profiles obtained by RNA-seq for example (König *et al*., 2012). iCLIP was used among others to study alternative splicing regulation mechanisms, *cis*- and *trans*-splicing in *Trypanosoma brucei*, protein-RNA interactions in HIV-1 infected cells (Rossbach *et al.*, 2014; Misra *et al.*, 2015; Preusser *et al.*, 2014; Apolonia *et al.*, 2015). However, iCLIP has never been used to investigate protein-RNA interactions in prokaryotes. Only the classic CLIP approach was utilized to elucidate the function of Ro autoantigen ortholog (Rsr) in rRNA degradation upon starvation in *Deinococcus radiodurans.* The authors conducted CLIP experiment in order to identify possible RNA targets for Rsr in stationary phase. It was shown that this RBP crosslinks to 16S and 23S rRNAs and together with PNPase and additional nucleases is involved in rRNA degradation upon starvation in stationary phase (Wurtmann and Wolin, 2010). However, performed CLIP analyses was not combined with high-throughput sequencing, so the quantity and quality of obtained data was quite low in comparison to high-throughput sequencing of cDNA libraries normally obtained by iCLIP. We on the other hand utilized slightly modified iCLIP method for

investigation of Rne targets in *Synechocystis* and shed light on RNA degradation machinery of this model cyanobacterium. In our iCLIP experiment we obtained only approx. 100 thousand reads that is relatively low compared to the other studies (König *et al.,* 2010; Rossbach, 2012). However, we still decided to proceed with the further analysis of this data, as resequencing the library was not possible due to time constrains.

4.2.1 Interaction of Rne with mRNAs

The majority of the binding sites (44%) for Rne were mapped to CDSs in *Synechocystis'* genome and were represented by 64 different genes, some of which contained two or more crosslink sites (Table 10). For some genes crosslink sites were mapped to the 5' UTR, others had crosslink sites positioned at the 3' UTR or contained one or more binding sites within the CDS itself. Interestingly, crosslink sites were detected in the 5' UTR of the *rne* gene. It has been shown that in *E. coli* RNase E autoregulates its activity by direct binding to the stem loop located at its 5' UTR (Schuck *et al.*, 2009). Our data demonstrated that Rne in *Synechocystis* also binds to the predicted loop region at its own 5' UTR (Table 10, Figure 30). 3' RACE experiment and *in vitro* cleavage assays aimed to investigate cleavage of the 5' UTR of *rne* by Rne demonstrated that Rne cleaves its mRNA in the U-rich region of the AU box (Dr. Damir Stazic, AG Computational Transcriptomics, Institute of Biology III, Albert-Ludwigs University Freiburg; unpublished data; personal communication). These findings suggest that in *Synechocystis* Rne autoregulates its synthesis by binding to the stem loop in the 5' UTR of *rne* and cleaving its mRNA in the similar way as in *E. coli*.

Two of the mRNAs containing predicted by iCLIP Rne binding sites were subjected to *in vitro* cleavage by purified Rne. The first one was heme oxygenase *ho1,* for which multiple crosslink sites were detected (Table 10). Ho1 is one of the two heme oxygenase isoforms that *Synechocystis* possesses (Cornejo *et al*., 1998). Ho1 is constitutively expressed and plays a major role in synthesis of bilin pigments (Aoki *et al.*, 2011). The cleavage assay did not yield positive results, as slight degradation was visible in all lanes including negative control (Figure 42C). However, this does not prove that obtained iCLIP data are wrong. Because in many cases Rne acts together with other RNases or the cleavage is facilitated by sRNAs or other factors that were not present in *in vitro* cleavage assay set up, we cannot conclude from this results that *ho1* is not a true substrate for Rne. What is more, it has been shown that cleavage by RNase E in *E. coli* in some cases requires interaction of the enzyme with multiple single-stranded regions, other than those that are cleaved, within the mRNA (Kime *et al.*, 2009). In other words there could be regions within the transcript that are poorly cleaved, but are bound to RNase E with high affinity. Studies of RNase G cleavage pattern also indicated that it could simultaneously interact with multiple single-stranded segments and subsequently cleave the RNA at another site (Jourdan *et al*., 2009). As iCLIP depicts interaction sites for Rne with RNAs it cannot be excluded that the tested transcripts are in fact Rne substrates, which could not be cleaved *in vitro* because the cleavage site was more distant from the binding site or because other Rne interaction sites that facilitate cleavage were not present because of

the shorter length of the *in vitro* transcript in comparison to target mRNA. The fact that multiple crosslink positions were mapped to *ho1* supports this assumption (Table 10).
Another large mRNA that was discovered via iCLIP as Rne target and tested for *in vitro* cleavage was *psaA*. It encodes the integral membrane protein PsaA that together with PsaB forms the heterodimeric core of photosystem I (Chitnis *et al*., 1995; Sun *et al*., 1997). We could not see cleavage with Rne in our *in vitro* cleavage assay (Figure 42E). However, as for *ho1* mRNA, it is possible that absence of other single-stranded regions necessary for promoting Rne cleavage, resulted in inability to detect any specific degradation in conducted *in vitro* cleavage assay. In favour of this explanation acts the fact that we detected multiple crosslink position within *psaA*. Another reason for negative result of *in vitro* cleavage assay might be involvement of other players in *psaA* cleavage together with Rne. It has been shown that mRNA encoding another component of photosystem I, namely reaction center protein subunit XI PsaL, is cleaved by Rne in an sRNA-dependent manner (Georg *et al.*, 2014). PsaL is necessary for the trimer formation of photosystem I (Chitnis and Chitnis, 1993). Its mRNA interacts with sRNA SyR1 (PsrR1) in its 5' region and the presence of SyR1 is necessary for cleavage of *psaL* by Rne (Georg *et al*., 2014). Thus, there is a possibility that degradation of *psaA* by Rne is also regulated by sRNA and therefore requires its presence. The fact that some of the known Rne targets, such as *psaL,* are not present in our iCLIP data is probably due to the setup of iCLIP experiment. Tested cell cultures were grown under standard conditions and SyR1 that is required for *psaL* cleavage is highly expressed under high light and iron and nitrogen depletion (Kopf *et al.,* 2014). Therefore, it cannot be excluded that Rne binds to *psaL* only when SyR1 is highly expressed. Another known Rne target *psbA2* is also cleaved by Rne only in the darkness, as upon growth in the light cleavage sites are protected due to duplex formation between *psbA2* and ncRNA PsbA2R (Horie *et al.*, 2007). It is possible that binding of Rne to *psbA2* is hindered under standard growth conditions as well.

4.2.2 Interaction of Rne with ncRNAs

Analysis of iCLIP data revealed that 9% of the crosslink sites were mapped to ncRNAs, among which were two asRNAs (Table 10). It has been shown for a number of sRNAs that termination of translation mediated by them is frequently followed by coupled degradation of the mRNA target making gene silencing irreversible. Examples of such negative regulation by sRNAs include translation termination by RyhB in *E. coli* leading to degradation of the target mRNA *sodB* by RNase E (Masse *et al.*, 2003; Morita *et al.*, 2005; Prevost *et al.*, 2011). In this case sRNA acts together with RNase E and RNA chaperone Hfq and facilitates cleavage of the mRNA transcript. Although, exact mechanism of the sRNA-Hfq-RNase E complex formation has not been elucidated it is possible that RNase E interacts directly with sRNA. This could explain why we were able to detect binding sites for Rne via iCLIP mapped to sRNAs in *Synechocystis*. It is also likely that Rne might not only bind to sRNAs, but cleave them as well. Therefore we investigated cleavage of two promising Rne target candidates via *in vitro* cleavage assays. SyR12 (NsiR4) is a highly abundant sRNA in *Synechocystis*, which is expressed

under various growth conditions, but it is induced to its maximum under nitrogen depletion, which is why it was also named NsiR4 (nitrogen-stress-induced RNA4). High expression level of SyR12 during nitrogen starvation suggests its regulatory function in response to nitrogen depletion (Kopf *et al.,* 2014). It is conserved in a distinct but closely related strain *Synechocystis* sp. PCC 6714 (Kopf and Hess, 2015). Despite SyR12 could be validated as an individual transcript, its transcription start site also drives the transcription of the downstream gene *sll1698*. Therefore, SyR12 is organized in an operon together with the protein-coding gene *sll1698* and represents another example of an actuaton (Kopf *et al.,* 2014). *In vitro* cleavage assay of the SyR12 transcript revealed 2 cleavage products of approx. 35 nt (Figure 42B). This goes in accordance with presence of single-stranded AU-rich region in the middle of the transcript, which favours Rne cleavage (Figure 46B). It is worth mentioning that 5' monophosphorylated version of SyR12 was cleaved much more effectively compared to the triphosphorylated one (Figure 42B). It was not surprising, as it is known for *E. coli* that RNase E prefers substrates with the monophosphate at the 5' end (Garrey *et al.*, 2009). The same was also shown for *Synechocystis* (Horie *et al.*, 2007). Results of the *in vitro* cleavage assay combined with the iCLIP binding site prediction not far away from the probable cleavage site (Figure 46B) prove that SyR12 is a true substrate for Rne in *Synechocystis*.
Another ncRNA that was tested *in vitro* for Rne cleavage was SyR13 (*ncr0700*). It is a relatively long (251 nt) ncRNA, which represents one of the most abundant transcripts in *Synechocystis*. It is highly expressed in darkness, after heat shock and during stationary phase (Kopf *et al.,* 2014). SyR13 is also conserved and appears to be a promising candidate for regulatory factor in response to darkness (Kopf and Hess, 2015). While accumulating as a discrete transcript SyR13 also serves as a 5' UTR for the downstream gene and therefore acts as another example of an actuaton. Interestingly, its ortholog in *Synechocystis* sp. PCC 6714 constitutes a free-standing transcription unit, which was rearranged by transposition in *Synechocystis* sp. PCC 6803 (Kopf *et al.,* 2015). Our attempt to prove that SyR13 is cleaved by Rne was performed with a slightly bigger *in vitro* transcript. However, predicted secondary structures of the synthesized transcript and original ncRNA were quite similar and therefore the overall length should not have been a problem for the cleavage. Nevertheless, we were not able to observe any specific degradation of SyR13 via *in vitro* cleavage assay (Figure 42D). This is probably due to the conditions in which the experiment was performed, namely the absence of other factors that might be important for effective cleavage.

4.2.3 Interaction of Rne with rRNAs and its role in 5S rRNA maturation

rRNAs are synthesized in the form of large precursors that have to be processed to a functional mature 23S, 16S and 5S rRNA molecules. Primary rRNA transcripts in *Synechocystis* are organized in the following order: Promoter-16S-tRNA-23S-5S-Terminator. Individual rRNAs and tRNA that are cotranscribed are getting separated from each other by endonucleolytic cleavage, followed by processing events aimed to produce mature 3' and 5' ends (Deutscher, 2006). In *E. coli* cells deficient of RNase E 9S RNA accumulates. It is a processing

intermediate that spans from the 23S rRNA till the 3' end of the 5S rRNA. It has been shown that 9S RNA is cleaved by RNase E in two positions: three nucleotides upstream of the 5' end of 5S rRNA and downstream from the 3' end of 5S rRNA (Roy *et al*., 1983). What is more, secondary structure of 9S RNA plays an important role in the efficiency of processing by RNase E. A hairpin structure upstream of the first cleavage site is required for recognition and binding of RNase E (Cormack and Mackie, 1992).
We discovered that 7% of the crosslink sites obtained from iCLIP experiment with Rne were mapped to rRNAs (Table 10). Interestingly, a very strong iCLIP peak was detected in the region between 23S and 5S rRNA. As it has been shown that this area includes RNase E cleavage site in *E. coli* we investigated it in detail. An *in vitro* transcript spanning from the 3' end of 23S rRNA till the 3' end of 5S rRNA was created and tested for cleavage with Rne *in vitro* (Figure 42A). It is worth mentioning that our 5S *in vitro* construct resembles 9S RNA of *E. coli*. *In vitro* cleavage assay demonstrated that the 191 nt long transcript is cleaved by Rne resulting in two fragments approx. 150 and 40 nt long (Figure 42A). The 5' monophosphorylated version of the transcript was processed more efficiently as it was also seen for SyR12 cleavage described above. To investigate the precise location of the cleavage site 3' RACE was conducted. The results indicated that Rne cleavage site lies in the window 48-59 nt downstream of the 3' end of 23S rRNA (Figure 45). Taking into account the predicted secondary structure of the 5S *in vitro* transcript (Figure 43B) and the fact that Rne prefers to cleave in single-stranded AU-rich regions, we could assume that the true cleavage site is located either in the hairpin region (residues 48-57) or in the A-rich single-stranded region following the loop structure (residues 64-67). In comparison to 9S RNA processing in *E. coli* the second cleavage site located 64-67 nt downstream of the 3' end of 23S rRNA (or 5-8 nt upstream of the 5' end of 5S rRNA) appears to be more feasible. It also suits to the model suggested by Cormack and Mackie, according to which recognition and binding site for RNase E resides in the hairpin structure upstream from the cleavage site (Cormack and Mackie, 1992). Thus, it is reasonable to conclude that iCLIP analysis provided accurate results for Rne binding site in between 23S and 5S rRNAs, which allows assuming that processing of rRNA precursor leading to mature 5S rRNA in *Synechocystis* is conducted in a similar manner as in *E. coli*.

4.2.4 Interaction of Rne with tRNAs

tRNAs as well as rRNAs are synthesized as part of long complex transcripts that have to undergo a number of endo- and exonucleolytic cleavage events in order to be converted to mature functional molecules. In *E. coli* RNase E plays a major role in maturation of tRNA precursors by performing the initial processing of the long transcript and preparing the substrate for other RNases that contribute to the generation of mature 3' and 5' tRNA termini (Li and Deutscher, 2002). What is more, initial processing by RNase E at the 3' terminus is required for the subsequent cleavage at the 5' end of tRNA transcript performed by RNase P (Ow and Kushner, 2002). It has been shown that in *E. coli* tRNAs are mostly processed via direct entry pathway (Kime *et al.,* 2014). This mechanism of action does not require the presence of 5' monophosphate for efficient RNase E cleavage.

However, for some substrates simultaneous interaction of two or more single-stranded regions with the enzyme was proven to be necessary for rapid cleavage via direct entry (Kime *et al.*, 2009). Processing of tRNA precursors by RNase E in *E. coli* also requires recognition of adjacent, but not contiguous, unpaired segments, which are bound but not cleaved by the enzyme (Kime *et al*., 2014).
Study of Rne binding sites via iCLIP revealed that 35% of the crosslink sites referred to tRNAs. Only 5 out of 43 tRNAs in *Synechocystis* did not contain Rne binding sites (Table 11). Most of the tRNAs were shown to encompass multiple crosslink positions. *trnY-GUA* and *trnT-GUU* are transcribed as a single transcript, so to achieve their functional form they have to be processed. We identified multiple Rne binding sites in both tRNAs, which fits to the model proposed for *E. coli* that RNase E interacts simultaneously with several single-stranded regions within the tRNA precursor in order to facilitate its cleavage (Figure 32; Kime *et al*., 2014). At this point it is not possible to conclude with certainty whether Rne also processes *trnY-GUA* - *trnT-GUU* tRNA precursor as there were no *in vitro* cleavage assays performed with this transcript.
In order to further investigate Rne interaction with tRNAs we analysed secondary structures of tRNAs and the position of Rne sites discovered by iCLIP. We discovered that Rne was always crosslinked to a site, which is located at the unpaired region of the anticodon loop (Figure 33A), with the presence of an additional binding site at the variable loop of some tRNAs (Figure 33B). As tRNAs together with rRNAs represent a stable RNA population in the cell, they are normally not degraded during exponential growth. tRNAs are protected from cleavage due to their extensive secondary structure, aminoacylation at the 3' end and short-term but continuous interaction with amino-acyl-tRNA synthetases, elongation factor, and ribosomes (Deutscher, 2003). However, various stress conditions, such as starvation or slow growth, as well as treatment of bacterial cells with agents altering membrane permeability lead to extensive RNA degradation including tRNAs (Deutscher, 2003; Deutscher, 2006). Another case in which tRNAs are purposely degraded involves RNA quality control. If errors occur during the process of synthesis or maturation of tRNA this defective tRNA has to be fixed or eliminated to avoid interference with the function of its normal counterparts. Example of such repair of tRNA is restoration of the terminal A residue at the 3' end of mature tRNA by tRNA nucleotidyltransferase, which may be lost due to RNase T exonucleolytic attack (Deutscher, 2003). Cells also have irreversible mechanisms of RNA quality control that include degradation of tRNA precursors, which cannot be effectively converted to their mature forms. These abnormal tRNA precursors are being polyadenylated, which indicates their suitability for degradation (Li *et al*., 1998). Experiments comparing accumulation, metabolism and stability of a defective mutant tRNA to its wild-type counterpart revealed that the mutant tRNA precursor is getting degraded in a poly(A) polymerase-dependent manner. The main RNase involved in this process was shown to be PNPase (Li *et al.,* 2002). However, the authors did not exclude that other RNases are involved in defective tRNA precursor degradation, which leaves a question, whether RNase E participates in stable RNA degradation, opened. Our data based on iCLIP analysis of Rne binding sites in *Synechocystis* indicate that this RNase interacts with almost all tRNAs present in

the model organism. However, at this point it is not possible to state whether Rne also cleaves investigated tRNAs or is only bound to them.

4.2.5 Possible Rne binding motif identification

Different modifications of the CLIP method were used previously to study binding sites for eukaryotic RBPs (Darnell, 2010; Ascano *et al.,* 2012; Ascano *et al.,* 2013). Investigation of protein-RNA interactions in prokaryotes is, however, not as vast. Lots of research has been done on analysing of Hfq binding properties. In *E. coli* this RNA chaperone facilitates sRNA-mRNA annealing by binding with its distal face to poly(A-R-N) triplets, where R is a purine and N is any nucleotide (Link *et al.*, 2009). Further studies implemented a variation of the CLIP method called CRAC, which involves UV-crosslinking and cDNA analysis by high throughput sequencing, to address transcriptome-wide targets of Hfq in enterohemorrhagic *E. coli* (EHEC) (Tree *et al*., 2014). Using this *in vivo* approach the authors confirmed recognition of A-R-N motifs in mRNAs by the distal face of Hfq and proposed that the consensus Hfq binding site for sRNAs is comprised of an U-rich single-stranded region (Tree *et al*., 2014). CLIP-seq analysis of Hfq RNA recognition patterns in *S. typhimurium* revealed that Hfq binds to a hairpin structure followed by a U-rich sequence (similar to Rho-independent terminator) at the 3' end of mRNAs. Consensus motif for Hfq binding in sRNAs was also shown to resemble Rho-independent terminator region. These results suggested that the general Hfq binding motif that is common for mRNAs and sRNAs involves a Rho-independent terminator (Holmqvist *et al.,* 2016).
We attempted to identify Rne binding motif based on the iCLIP data using biocomputational analysis with the help of MEME tool. We were able to discover three possible binding motifs, sequences of two of which overlapped (Figure 31). Despite that Rne does not show strong sequence specificity in terms of cleavage position and opts for cleavage within AU-rich single-stranded sequence, our data provide the first hint that Rne might have a certain sequence preference for the binding site. These are just the preliminary results. More detailed biocomputational analysis is certainly required for an accurate description of a consensus binding motif for Rne.

4.2.6 Interconnection between RNA binding and cleavage by Rne

Investigation of RNA degradation machinery is certainly aimed to determine cleavage targets for particular RNases. Our iCLIP approach implemented for analysis of Rne and Rnc2 of *Synechocystis* allowed discovering interaction RNA partners for the studied enzymes. However, in order to elucidate which RNA targets are being cleaved by Rne and Rnc2 and at which position the cleavage occurs, it is necessary to conduct further experiments. Nevertheless, some insight of the cleavage pattern of Rne could be drawn from the existing knowledge of interconnection between RNA binding and RNA processing by RNase E in *S. typhimurium* and *E. coli* (Bandyra *et al.*, 2012; Prevost *et al.*, 2011). Both studies focused on research of sRNA-mediated destabilization of target mRNAs in RNase E-dependent manner. It has been shown that the sRNA MicC guides RNase E to its cleavage site in the CDS of the target mRNA *ompD* in *S.*

typhimurium (Figure 7B). The MicC-Hfq-RNase E ribonucleoprotein complex is being tethered to the target mRNA, whereas MicC activates RNase E via interaction with its 5' sensing pocket, resulting in cleavage of *ompD* 6 nt downstream of the binding site (Bandyra *et al.*, 2012). In this case cleavage site is located in the close proximity to the binding site. However, Prevost *et al*. in their study of sRNA RyhB-mediated translation termination and subsequent degradation of target mRNA *sodB* by RNase E in *E. coli* discovered that cleavage site is located 350 nt downstream from the site, where RyhB-Hfq-RNase E complex interacts with *sodB* (Prevost *et al.*, 2011). Thus, despite that it is more likely that cleavage and binding sites of RNase E are located close to each other; it is also possible that the distance between the two can be relatively long. This might be another explanation why we could not observe any processing of *psaA* and *ho1 in vitro* transcripts, as they were much shorter than the corresponding mRNAs and if the cleavage site was located as far away from the binding site as for *sodB,* is was not possible to detect processing with our *in vitro* cleavage assay setup.
Figure 47 presents the possible model of Rne action based on our data.

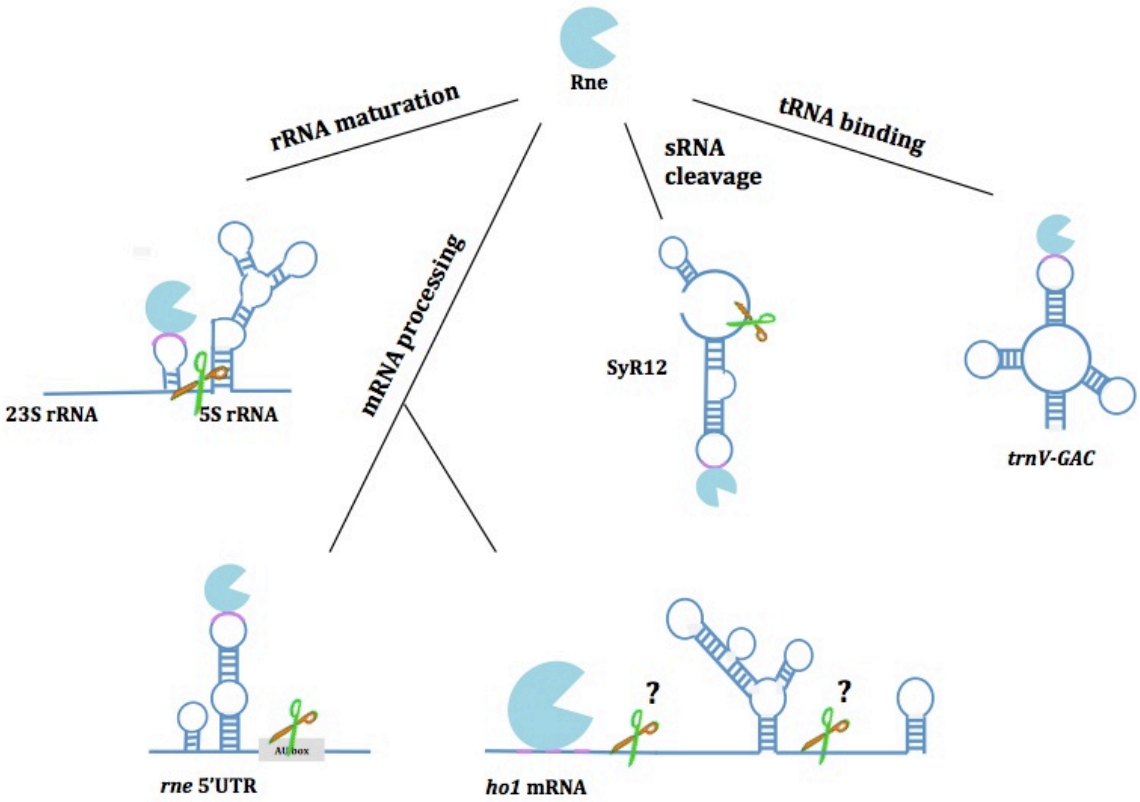

Figure 47: Schematic representation of binding and cleavage pattern of Rne
Binding sites for Rne are depicted in purple; discovered and possible cleavage sites are marked with the scissor symbol.

4.3 Genomewide analysis of binding sites for Rnc2 in *Synechocystis* using iCLIP

The vast majority of the binding sites (60%) for Rnc2 were mapped to tRNAs, for most of which more than one crosslink position was detected (Table 13). In total 31 out of 43 tRNAs in *Synechocystis* were shown to interact with Rnc2. We analysed tRNAs bound by Rnc2 and found out that Rnc2 binds to the D-loop of the tRNAs. However, in most cases multiple binding sites were detected via iCLIP, which partly overlapped with Rne binding sites (Figure 35). Many tRNAs are synthesized as part of mixed tRNA-mRNA polycistronic transcripts. In *E. coli metY-nusY-infB* operon, which encodes tRNA MetY, transcription termination factor NusA and translation initiation factor IF2 is processed by RNase III with the cleavage site located in between of tRNA and first mRNA. This cleavage step is essential for the maturation of tRNA (Régnier and Grunberg-Manago, 1989). In *S. aureus* maturation of tRNAs is initiated by the cleavage of rRNA precursor by RNase III (Lioliou *et al*., 2012). In *Synechocystis trnI-GAU(1)* is a part of a large rRNA precursor and is located in between 16Sa and 23Sa rRNAs. We also found Rnc2 binding sites within *trnI-GAU(1)* (Figure 35B), which hints that this tRNA might also be excised from the large precursor by Rnc2. As it is seen from Figure 35B *trnI-GAU(1)* also contains binding sites for Rne. It is not very surprising, as investigation of tRNA and rRNA maturation in *E. coli* revealed that tRNAs, which are part of longer transcripts together with rRNAs, are released from the precursor by RNase III with subsequent cleavage of 5S rRNA – tRNA fragment by RNase E (Deutscher, 2006). Investigation of RNase E and RNase III action via tiling microarrays discovered that many transcripts show overlapping effects of both RNases (Stead *et al.,* 2011).

5% of binding sites for Rnc2 discovered via iCLIP were mapped to rRNAs (Table 12). In *E. coli* the major role of RNase III is cleavage of the primary transcript of rRNA operons. It recognises double-stranded structures flanking 16S and 23S rRNAs and releases the precursors of these molecules (Srivastava and Schlessinger, 1990). In *S. aureus* cleavage of rRNA operon that leads to excision of 16S pre-RNA was proved experimentally (Lioliou *et al.,* 2012).

RNase III is also involved in ncRNA degradation. In *E. coli* deletion of RNase III affected 22% annotated ncRNAs (Stead *et al.,* 2011). Co-IP experiments revealed that 58 ncRNAs interact with RNase III in *S. aureus*, many of which are in charge of regulation of gene expression via antisense mechanism (Lioliou *et al*., 2012). It is known that duplexes formed between asRNAs and their target mRNAs are optimal substrates for RNase III (Viegas and Arraiano, 2008). In our investigation of Rnc2 binding sites we found out that 8% of crosslink positions were mapped to ncRNAs (Table 12). It is possible that some of them modulate gene expression via antisense mode of action. Interestingly, Hpr10 was also found to contain probable Rnc2 binding sites (Table 12; Figure 34). As this sRNA contains long double-stranded region next to the detected binding site we assumed that it is probably cleaved by Rnc2. *In vitro* cleavage assay confirmed this hypothesis and suggested that Hpr10 is a true target for Rnc2 (Figure 40B).

We also detected Rnc2 binding sites mapped to mRNAs and their 5' and 3' UTRs (Table 12). These crosslink positions constitute 21% of total number of Rnc2 binding sites mapped to *Synechocystis'* genome. For many transcripts iCLIP peak

position corresponds to the 5' UTR. In *E. coli* RNase III regulates its own synthesis by cutting the 5' UTR of the *rnc* gene, which leads to destabilizing of its mRNA. The RNase III cleavage site is located in the stem of the hairpin structure in the 5' UTR of *rnc* (Bardwell *et al*., 1989). Initiation of degradation of another RNase in *E. coli*, namely PNPase, is also triggered by cleavage of its mRNA at the 5' end by RNase III (Portier *et al.*, 1987). Thus, RNase III regulates gene expression in *E. coli* via removal of protective secondary structures at the 5' ends of some mRNAs. This might also be the case for *Synechocystis*.
We were able to find Rnc2 binding sites mapped to the *cpc* operon. This operon includes five genes: *cpcB* and *cpcA*, which encode α- and β-phycocyanin, and *cpcC2*, *cpcC1* and *cpcD* genes encoding rod linker polypeptides (Ughy and Ajlani, 2004). High relative read values corresponding to the crosslink positions in the 5' UTRs of *cpcB*, *cpcC2* and *cpcD* indicate binding sites for Rnc2 (Table 12). It is therefore possible that Rnc2 is in charge of processing of *cpc* operon in *Synechocystis*. As we also detected binding site for Rne within *cpcA* and *cpcB* CDSs as well as in the 5' UTR of *cpcB* (this binding site however does not overlap with the one for Rnc2), it cannot be excluded that both RNases act together in processing of *cpc* operon (Table 10).

4.4 iCLIP: limitations and perspectives

iCLIP is a novel tool for genomewide analysis of binding sites for RBPs, which represents the latest modification of CLIP method and provides greater sensitivity, precision and possibility to quantify obtained results. Main advantage of iCLIP is that it takes into account both truncated and read-through cDNAs, whereas previous modifications of CLIP only allow amplification of the latter (König *et al*., 2010). However, this gives rise to possible complications, as domination of read-through cDNA libraries might hinder the ability of iCLIP to identify binding sites at a single nucleotide resolution. The proportion of truncated and read-through cDNA libraries depends on the protein studied and can vary from 82 to 95% truncated cDNAs over longer counterparts (Sugimoto *et al.,* 2012). Despite the obvious prevalence of truncated cDNA in the iCLIP analysis of investigated RBPs, it is important to consider this possible limitation when studying new RBPs.
iCLIP library preparation involves a number of complex enzymatic reactions the efficiency of which has an impact on binding site determination. One of the crucial steps includes partial RNase digestion, where the concentration of the enzyme has to be adjusted for every protein studied. What is more, efficiency of crosslinking with UV-C light, which is used at the first stages of iCLIP experiment, varies for different proteins (Kishore *et al.,* 2011). The choice of RNA ligase is also important as it may affect the cloning of short RNAs (Hafner *et al*., 2011).
One of the greatest advantages of iCLIP is the ability to provide quantitative information. Because of introduction of a random barcode sequence it became possible to compare binding sites within the same RNA transcript. However, one must be cautious with comparing the binding sites on different transcripts, as they vary tremendously in their abundance (Sugimoto *et al.,* 2012). Therefore, additional normalization of the iCLIP results to control of transcript abundance is necessary for accurate quantification of the data (König *et al*., 2012).

iCLIP and its modifications have already been used to study protein-RNA interactions in fungi, yeast, worms and mammals and our study presents the possibility to use iCLIP in bacteria. It is certain that optimization of cDNA library preparation aimed to achieve higher complexity, improvement of quantification methods to compare binding sites across the transcriptome and also development of advanced computational algorithms to analyse the results are essential for elucidation of complex protein-RNA interactions in any organism.

5. References

Aït-Bara, S., and Carpousis, A.J. (2015) RNA degradosomes in bacteria and chloroplasts: classification, distribution and evolution of RNase E homologs. *Mol Microbiol* **97**: 1021-1135.

Anderson, S. L. and McIntosh, L. (1991) Light-activated heterotrophic growth of the cyanobacterium *Synechocystis* sp. strain PCC 6803: a blue-light-requiring process. *J Bacteriol* **173**: 2761-2767.

Aoki, R., Goto, T., and Fujita, Y. (2011) A Heme Oxygenase Isoform is Essential for Aerobic Growth in the Cyanobacterium *Synechocystis* sp. PCC 6803: Modes of Differential Operation of Two Isoforms/Enzymes to Adapt to Low Oxygen Environments in Cyanobacteria. *Plant Cell Physiol* **52**: 1744-1756.

Apirion, D., and Lassar, A.B. (1978) A conditional lethal mutant of *Escherichia coli* which affects the processing of ribosomal RNA. *J Biol Chem* **253**: 1738–1742.

Apolonia, L., Schulz, R., Curk, T., Rocha, P., Swanson, C. M., Schaller, T., Ule, J., and Malim, M. H. (2015) Promiscuous RNA Binding Ensures Effective Encapsidation of APOBEC3 Proteins by HIV-1. *PLoS Pathogens* **11**: e1004609.

Arraiano, C.M., Andrade, J.M., Domingues, S., Guinote, I.B., Malecki, M., Matos, R.G., Moreira, R.N., Pobre, V., Reis, F.P., Saramago, M., Silva, I.J., and Viegas, S.C. (2010) The critical role of RNA processing and degradation in the control of gene expression. *FEMS Microbiol Rev* **34**: 883-923.

Ascano, M., Gerstberger, S., and Tuschl, T. (2013). Multi-Disciplinary Methods to Define RNA-Protein Interactions and Their Regulatory Networks. *Current Opinion in Genetics & Development* **23**: 20–28.

Ascano, M., Hafner, M., Cekan, P., Gerstberger, S., and Tuschl, T. (2012) Identification of RNA–protein interaction networks using PAR-CLIP. *Wiley Interdisciplinary Reviews. RNA* **3**: 159–177.

Babitzke, P., Granger, L., Olszewski, J., and Kushner, S.R. (1993) Analysis of mRNA decay and rRNA processing in *Escherichia coli* multiple mutants carrying a deletion in RNase III. *J Bacteriol* **175**: 229–239.

Bailey, T.L., and Elkan, C. (1994) Fitting a mixture model by expectation maximization to discover motifs in biopolymers. *Proceedings of the Second International Conference on Intelligent Systems for Molecular Biology*, AAAI Press, Menlo Park, California, pp. 28-36.

Baker, K.E., and Mackie, G.A. (2003) Ectopic RNase E sites promote bypass of 5′-end-dependent mRNA decay in *Escherichia coli. Mol Microbiol* **47**: 75–88.

Bandyra, K.J., Said, N., Pfeiffer, V., Gorna, M.W., Vogel, J., and Luisi, B.F. (2012) The seed region of a small RNA drives the controlled destruction of the target mRNA by the endoribonuclease RNase E. *Mol. Cell* **47**: 943–953.

Bardwell, J.C., Regnier, P., Chen, S.M., Nakamura, Y., Grunberg-Manago, M., and Court, D.L. (1989) Autoregulation of RNase III operon by mRNA processing. *EMBO J* **8**: 3401–3407.

Bartel, D.P. (2009) MicroRNAs: target recognition and regulatory functions. *Cell* **136:** 215–233.

Beisel, C.L., and Storz, G. (2010) Base pairing small RNAs and their roles in global regulatory networks. *FEMS Microbiol. Rev* **34**: 866–882.

Bhaya, D. (2004) Light matters: phototaxis and signal transduction in unicellular cyanobacteria. *Mol Microbiol* **53**: 745-54.

Blaszczyk, J., Gan, J., Tropea, J.E., Court, D.L., Waugh, D.S., and Ji, X (2004) Noncatalytic assembly of ribonuclease III with double- stranded RNA. *Structure* **12**: 457–466.

Blaszczyk, J., Tropea, J.E., Bubunenko, M., Routzahn, K.M., Waugh, D.S., Court, D.L., and Ji, X. (2001) Crystallographic and modeling studies of RNase III suggest a mechanism for double-stranded RNA cleavage. *Structure* **9**: 1225–1236.

Bøggild, A., Overgaard, M., Valentin-Hansen, P., and Brodersen, D.E. (2009) Cyanobacteria contain a structural homologue of the Hfq protein with altered RNA-binding properties. *FEBS J* **276**: 3904-3915.

Botsford, J.L., and Harman, J.G. (1992) Cyclic AMP in prokaryotes. *Microbiol. Mol. Biol. Rev* **56**: 100-122.

Brantl, S. (2007) Regulatory mechanisms employed by cis-encoded antisense RNAs. *Curr Opin Microbiol* **10**: 102-109.

Briant, D.J., Hankins, J.S., Cook, M.A., and Mackie, G.A. (2003) The quaternary structure of RNase G from *Escherichia coli*. *Mol. Microbiol* **50**: 1381–1390.

Callaghan, A. J., Redko, Y., Murohy, L.M., Grossmann, J.G., Yates, D., German, E., Ilag, L.L., Robinson, C.V., Symmons, M.F., McDowall, KJ., and Luisi, B.F. (2005) "Zn-link": a metal sharing interface that organizes the quaternary structure and catalytic site of the endoribonuclease, RNase E. *Biochemistry* **44**: 4667–4675. Callaghan *et al*., 2005b.

Callaghan, A.J., Aurikko, J.P., Ilag, L.L., Günter Grossmann, J., Chandran, V., Kühnel, K., Poljak, L., Carpousis, A.Aj., Robinson, C.V., Symmons, M.F., and Luisi B.F. (2004) Studies on the RNA degradosome- organizing domain of the *Escherichia coli* ribonuclease RNase E. *J. Mol. Biol* **340**: 965–979.

Callaghan, A.J., Marcaida, M.J., Stead, J.A., McDowall, K.J., Scott, W.G., and Luisi, B.F. (2005) Structure of *Escherichia coli* RNase E catalytic domain and implications for RNA turnover. *Nature* **437**: 1187–1191. Callaghan *et al*., 2005a.

Cameron, J.C., Gordon, G.C., and Pfleger, B.F. (2015) Genetic and genomic analysis of RNases in model cyanobacteria. *Photosynth Res* **126**:171-83.

Celesnik, H., Deana, A., and Belasco, J.G. (2007) Initiation of RNA decay in *Escherichia coli* by 5′ pyrophosphate removal. *Mol Cell* **27**: 79–90.

Cheng, Z.F., and Deutscher, M.P. (2003) Quality control of ribosomal RNA mediated by polynucleotide phosphorylase and RNase R. *Proc Natl Acad Sci U S A* **100**: 6388–6393.

Chi, S.W., Zang, J.B., Mele, A., and Darnell, R.B. (2009) Argonaute HITS-CLIP decodes microRNA-mRNA interaction maps. *Nature* **460**: 479–486.

Chitnis, P.R., Xu, Q., Chitnis, V.P., and Nechushtai, R. (1995) Function and organization of Photosystem I polypeptides. *Photosynth Res* 1995 **44**: 23-40.

Chitnis, V.P., and Chitnis, P.R. (1993) PsaL subunit is required for the formation of photosystem I trimers in the cyanobacterium *Synechocystis* sp. PCC 6803. *FEBS Lett* **336**: 330-334.

Clarke, J.E., Kime, L., Romero, A.D., and McDowall, K.J. (2014) Direct entry by RNase E is a major pathway for the degradation and processing of RNA in *Escherichia coli. Nucleic Acids Res* **42**: 11733–11751.

Coburn, G.A., Miao, X., Briant, D.J., and Mackie, G.A. (1999) Reconstitution of a minimal RNA degradosome demonstrates functional coordination between a 30 exonuclease and a DEAD-box RNA helicase. *Gene Dev* **13**: 2594–2603.

Condon, C., and Putzer, H. (2002) The phylogenetic distribution of bacterial ribonucleases. *Nucleic Acids Res* **30**: 5339–5346.

Cormack, R.S. and Mackie, G.A. (1992) Structural requirements for the processing of *Escherichia coli* 5 S ribosomal RNA by RNase E *in vitro. J. Mol. Biol* **228**: 1078-1090.

Cornejo, J., Willows, R.D., and Beale, S.I. (1998) Phytobilin biosynthesis: cloning and expression of a gene encoding soluble ferredoxin-dependent heme oxygenase from *Synechocystis* sp. PCC 6803. *Plant J* **15**: 99-107.

Darnell, R. B. (2010) HITS-CLIP: panoramic views of protein-RNA regulation in living cells. *Wiley Interdisciplinary Reviews. RNA* **1**: 266–286.

Dasgupta, S., Fernandez, L., Kameyama, L., Inada, T., Nakamura, Y., Pappas, A., and Court, D.L. (1998) Genetic uncoupling of the dsRNA-binding and RNA cleavage activities of the *Escherichia coli* endoribonuclease RNase III – the effect of dsRNA binding on gene expression. *Mol Microbiol* **28**: 629–640.

De Lay, N., Schu, D.J., and Gottesman, S. (2013) Bacterial small RNA-based negative regulation: Hfq and its accomplices. *J Biol Chem* **288**: 7996-8003.

Deana, A., Celesnik, H., and Belasco, J.G. (2008) The bacterial enzyme RppH triggers messenger RNA degradation by 5′ pyrophosphate removal. *Nature* **451**: 355–358.

Deutscher, M. P. (2015) Twenty years of bacterial RNases and RNA processing: how we've matured. *RNA* **21**: 597–600.

Deutscher, M.P. (2003) Degradation of stable RNA in bacteria. *J Biol Chem* **278**: 45041-4.

Deutscher, M.P. (2006) Degradation of RNA in bacteria: comparison of mRNA and stable

RNA. *Nucleic Acids Res* **34**: 659-66.

Dienst, D. (2010) Untersuchungen zu Funktion und Struktur des Regulatorproteins Hfq in *Synechocystis* sp. PCC 6803. *Doctoral Thesis* Humboldt-Universität zu Berlin.

Dienst, D., Dühring, U., Mollenkopf, H.J., Vogel, J., Golecki, J., Hess, W.R., and Wilde, A (2008) The cyanobacterial homologue of the RNA chaperone Hfq is essential for motility of *Synechocystis* sp. PCC 6803. *Microbiology* **154**: 3134-3143.

Diwa, A., Bricker, A.L., Jain, C., and Belasco, J.G. (2000) An evolutionarily conserved RNA stem-loop functions as a sensor that directs feedback regulation of RNase E gene expression. *Gene Dev* **14**: 1249–1260.

Drider, D., and Condon, C. (2004) The continuing story of endoribonuclease III. *J Mol. Microbiol. Biotechnol* **8**: 195–200.

Dühring, U., Axmann, I.M., Hess, W.R., and Wilde, A. (2006) An internal antisense RNA regulates expression of the photosynthesis gene *isiA. Proc Natl Acad Sci U S A* **103**: 7054-7058.

Even, S., Pellegrini, O., Zig, L., Labas, V., Vinh, J., Brechemmier-Baey, D., and Putzer, H. (2005) Ribonucleases J1 and J2: two novel endoribonucleases in *B. subtilis* with functional homology to *E. coli* RNase E. *Nucleic Acids Res* **33**: 2141–2152.

Evguenieva-Hackenberg, E., and Klug, G. (2000) RNase III processing of intervening sequences found in helix 9 of 23S rRNA in the alpha subclass of Proteobacteria. *J Bacteriol* **182**: 4719–4729.

Filippov, V., Solovyev, V., Filippova, M., and Gill, S.S. (2000) A novel type of RNase III family proteins in eukaryotes. *Gene* **245**: 213-21.

Franze de Fernandez, M.T., Eoyang, L., and August, J.T. (1968) Factor fraction required for the synthesis of bacteriophage Qbeta-RNA. *Nature* **219**: 588-590.

Gan, J., Tropea, J.E., Austin, B.P., Court, D.L., Waugh, D.S., and Ji, X. (2006) Structural insight into the mechanism of double-stranded RNA processing by ribonuclease III. *Cell* **124**: 355–366.

Gao, J., Lee, K., Zhao, M., Qiu, J., Zhan, X., Saxena, A., Moore, C.J., Cohe, S.N., and Georgiou, G. (2006) Differential modulation of *E. coli* mRNA abundance by inhibitory proteins that alter the composition of the degradosome. *Mol. Microbiol* **61**: 394–406.

Garrey, S.M., Blech, M., Riffell, J.L., Hankins, J.S., Stickney, L.M., Diver, M., Hsu, Y.H., Kunanithy, V., and Mackie, G.A. (2009) Substrate binding and active site residues in RNases E and G: role of the 5′-sensor. *J Biol Chem* **284**: 31843–31850.

Georg, J., and Hess, W.R. (2011) *cis*-antisense RNA, another level of gene regulation in bacteria. *Microbiol Mol Biol Rev* **75**: 286-300.

Georg, J., Dienst, D., Schürgers, N., Wallner, T., Kopp, D., Stazic, D., Kuchmina, E., Klähn, S., Lokstein, H., Hess, W.R., and Wilde, A. (2014) The Small Regulatory RNA SyR1/PsrR1

Controls Photosynthetic Functions in Cyanobacteria. *The Plant Cell* **26**: 3661–3679.

Göpel, Y., Papenfort, K., Reichenbach, B., Vogel, J., and Görke, B. (2013) Targeted decay of a regulatory small RNA by an adaptor protein for RNase E and counteraction by an anti-adaptor RNA. *Genes & Development* **27**: 552–564.

Grigorieva, G. and Shestakov, S. (1982) Transformation in the cyanobacterium *Synechocystis* sp. 6803. *FEMS Microbiol Lett.***13**: 367-370.

Haecker, I., and Renne, R. (2014) HITS-CLIP and PAR-CLIP advance viral miRNA targetome analysis. *Critical Reviews in Eukaryotic Gene Expression* **24:** 101–116.

Hafner, M., Renwick, N., Brown, M., Mihailović, A., Holoch, D., Lin, C., Pena, J.T.G., Nusbaum, J.D., Morozov, P., Ludwig, J., Ojo, T., Luo, S., Schroth, J., and Tuschl, T. (2011) RNA-ligase-dependent biases in miRNA representation in deep-sequenced small RNA cDNA libraries. *RNA* **17**: 1697–1712.

Hammarlöf ,D.L., Bergman. J.M., Garmendia, E., and Hughes, D. (2015) Turnover of mRNAs is one of the essential functions of RNase E. *Mol Microbiol* **98**: 34-45.

Herrmann, K.M., and Weaver, L.M. (1999) The shikimate pathway. *Annu Rev Plant Physiol Plant Mol Biol* **50**: 473–503.

Herskovitz, M.A., and Bechhofer, D.H. (2000) Endoribonuclease RNase III is essential in *Bacillus subtilis. Mol Microbiol* **38**: 1027–1033.

Hoffmann, S., Otto, C., Kurtz, S., Sharma, C. M., Khaitovich, P., Vogel, J., Stadler, P.F., and Hackermüller, J. (2009) Fast mapping of short sequences with mismatches, insertions and deletions using index structures. *PLoS Computational Biology **5***: 1-10.

Holmqvist, E., Wright, P., Li, L., Bischler, T., Barquist, L., Reinhardt, R., Backofen, R., and Vogel, J. (2016) Global RNA recognition patterns of post-transcriptional regulators Hfq and CsrA revealed by UV crosslinking *in vivo*. *The EMBO Journal* **35**: 991-1011.

Horie, Y., Ito, Y., Ono, M., Moriwaki, N., Kato, H., Hamakubo, Y., Amano, T., Wachi, M., Shirai, M., and Asayama, M. (2007) Dark-induced mRNA instability involves RNase E/G-type endoribonuclease cleavage at the AU-box and SD sequences in cyanobacteria. *Mol Genet Genomics* **278**: 331-346.

Huppertz, I., Attig, J., D'Ambrogio, A., Easton, L. E., Sibley, C. R., Sugimoto, Y., Tajnik, M., König, J., and Ule, J. (2014) iCLIP: Protein–RNA interactions at nucleotide resolution. *Methods (San Diego, Calif.) **65***: 274–287.

Ikeda, Y., Yagi, M., Morita, T., and Aiba H. (2011) Hfq binding at RhlB-recognition region of RNase E is crucial for the rapid degradation of mRNAs mediated by sRNAs in *Escherichia coli*. *Mol. Microbiol* **79**: 419–432.

Jäger, S., Fuhrmann, O., Heck, C., Hebermehl, M., Schiltz, E., Rauhut, R., and Klug, G. (2001) An mRNA degrading complex in *Rhodobacter capsulatus*. *Nucleic Acids Res* **29**: 4581–4588.

Jain, C., and Belasco, J.G. (1995) RNase E autoregulates its synthesis by controlling the degradation rate of its own mRNA in *Escherichia coli*: unusual sensitivity of the *rne* transcript to RNase E activity. *Genes Dev* **9**: 84 – 96.

Jourdan, S.S., and McDowall, K.J. (2008) Sensing of 5' monophosphate by *Escherichia coli* RNase G can significantly enhance association with RNA and stimulate the decay of functional mRNA transcripts in vivo. *Mol Microbiol* **67**: 102-15.

Jourdan, S.S., Kime, L., and McDowall, K.J. (2009) The sequence of sites recognised by a member of the RNase E/G family can control the maximal rate of cleavage, while a 5'-monophosphorylated end appears to function cooperatively in mediating RNA binding. *Biochem Biophys Res Commun* **391**: 879-883.

Kaberdin, V.R., Miczak, A., Jakobsen, J.S., Lin-Chao, S., McDowall, K.J., and von Gabain, A. (1998) The endoribonucleolytic N-terminal half of *Escherichia coli* RNase E is evolutionarily conserved in *Synechocystis* sp. and other bacteria but not the C-terminal half, which is sufficient for degradosome assembly. *Proc Natl Acad Sci U S A* **95**:11637–11642.

Kaneko, T., Nakamura, Y., Sasamoto, S., Watanabe, A., Kohara, M., Matsumoto, M., Shimpo, S., Yamada, M., and Tabata, S. (2003) Structural analysis of four large plasmids harboring in a unicellular cyanobacterium, *Synechocystis* sp. PCC 6803. *DNA Res* **10**: 221-8.

Kaneko, T., Sato, S., Kotani, H., Tanaka, A., Asamizu, E., Nakamura, Y., Miyajima, N., Hirosawa, M., Sugiura, M., Sasamoto, S., Kimura, T., Hosouchi, T., Matsuno, A., Muraki, A., Nakazaki, N., Naruo, K., Okumura, S., Shimpo, S., Takeuchi, C., Wada, T., Watanabe, A., Yamada, M., Yasuda, M., and Tabata, S. (1996) Sequence analysis of the genome of the unicellular cyanobacterium *Synechocystis* sp. strain PCC6803. II. Sequence determination of the entire genome and assignment of potential protein-coding regions. *DNA Res* **3**: 109- 136.

Kazantsev, A.V., and Pace, N.R. (2006) Bacterial RNase P: a new view of an ancient enzyme. *Nat. Rev. Microbiol* **4**: 729–740.

Khemici, V., Poljak, L., Luisi, B.F., and Carpousis, A.J. (2008) The RNase E of *Escherichia coli* is a membrane-binding protein. *Mol Microbiol* **70**: 799–813.

Khusial, P., Plaag, R., and Zieve, G.W. (2005) LSm proteins form heptameric rings that bind to RNA via repeating motifs. *Trends Biochem Sci* **30**: 522-528.

Kido,M., Yamanaka,K., Mitani,T., Niki,H., Ogura,T. and Hiraga,S. (1996) RNase E polypeptides lacking a carboxyl-terminal half suppress a *mukB* mutation in *Escherichia coli. J. Bacteriol* **178**: 3917–3925.

Kime, L., Clarke, J.E., Romero, A.D., Grasby, J.A., and McDowall, K.J. (2014) Adjacent single-stranded regions mediate processing of tRNA precursors by RNase E direct entry. *Nucleic Acids Res* **42**: 4577–4589.

Kime, L., Jourdan, S.S., Stead, J.A., Hidalgo-Sastre, A., and McDowall, K.J. (2009) Rapid cleavage of RNA by RNase E in the absence of 5′-monophosphate stimulation. *Mol Microbiol* **76**: 590–604.

Kishore, S., Jackiewicz, L., Burger, L., Hausser, J., Khorshid, M., and Zavolan, M. (2011) A quantitative analysis of CLIP methods for identifying binding sites of RNA-binding proteins. *Nature Methods* **8**: 559–564.

Klähn, S., Baumgartner, D., Pfreundt, U., Voigt, K., Schön, V., Steglich, C., and Hess, W. R. (2014) Alkane Biosynthesis Genes in Cyanobacteria and Their Transcriptional Organization. *Frontiers in Bioengineering and Biotechnology* ***2***: 24.

Klähn, S., Orf, I., Schwarz, D., Matthiessen, J.K.F., Kopka, J., Hess, W.R., and Hagemann, M. (2015) Integrated transcriptomic and metabolomic characterization of the low-carbon response using an *ndhR* mutant of *Synechocystis* sp. PCC 6803. *Plant Physiol* **169**: 1540-1556.

König, J., Zarnack, K., Luscombe, N.M., and Ule, J. (2012) Protein-RNA interactions: new genomic technologies and perspectives. *Nature Reviews Genetics* **13**: 77-83.

König, J., Zarnack, K., Rot, G., Curk, T., Kayikci, M., Zupan, B., Turner, D.J., Luscombe, N.M., and Ule, J. (2010) iCLIP reveals the function of hnRNP particles in splicing at individual nucleotide resolution. *Nat Struct Mol Biol* **17**: 909–915.

Kopf, M., and Hess, W.R. (2015) Regulatory RNAs in photosynthetic cyanobacteria. *FEMS Microbiol Rev* **39**: 301-315.

Kopf, M., Klähn, S., Scholz, I., Hess, W.R., and Voss, B. (2015) Variations in the non-coding transcriptome as a driver of inter-strain divergence and physiological adaptation in bacteria. *Sci Rep* **5**: 9560.

Kopf, M., Klähn, S., Scholz, I., Matthiessen, J. K. F., Hess, W. R., and Voß, B. (2014) Comparative analysis of the primary transcriptome of *Synechocystis* sp. PCC 6803. *DNA Research : An International Journal for Rapid Publication of Reports on Genes and Genomes* ***21***: 527–539.

Koslover, D.J., Callaghan, A.J., Marcaida, M.J., Garman, E.F., Martick, M., Scott, W.G. and Luisi, B.F. (2008) The crystal structure of the *Escherichia coli* RNase E apoprotein and a mechanism for RNA degradation. *Structure* **16**: 1238–1244.

Laalami, S., Zig, L., and Putzer, H. (2014) Initiation of mRNA decay in bacteria. *Cellular and Molecular Life Sciences* **71**: 1799–1828.

Lalaouna, D., Simoneau-Roy, M., Lafontaine, D., and Massé, E. (2013) Regulatory RNAs and target mRNA decay in prokaryotes. *Biochim Biophys Acta* **1829**: 742-747.

Lee, K. and Cohen, S.N. (2003) A *Streptomyces coelicolor* functional orthologue of *Escherichia coli* RNase E shows shuffling of catalytic and PNPase-binding domains. *Mol Microbiol* **48**: 349–360.

Lee, K., Bernstein, J.A., and Cohen, S.N. (2002) RNase G complementation of *rne* null mutation identifies functional interrelationships with RNase E in *Escherichia coli*. *Mol Microbiol* **43**:1445-56.

Lee, K., Zhan, X., Gao, J., Qiu, J., Feng, Y., Meanathan, R., Cohe, S.N., and Georgiou, G. (2003) RraA: a protein inhibitor of RNase E activity that globally modulates RNA abundance in

E. coli. Cell **114**: 623–634.

Legewie, S., Dienst, D., Wilde, A., Herzel, H., and Axmann, I.M. (2008) Small RNAs establish delays and temporal thresholds in gene expression. *Biophys J* **95**: 3232-3238.

Li, H., Handsaker, B., Wysoker, A., Fennell, T., Ruan, J., Homer, N., Marth, G., Abecasis, G., Durbin, R., and 1000 Genome Project Data Processing Subgroup. (2009) The Sequence Alignment/Map format and SAMtools. *Bioinformatics **25***: 2078–2079.

Li, Z., and Deutscher, M.P. (2002) RNase E plays an essential role in the maturation of *Escherichia coli* tRNA precursors. *RNA* **8**: 97–109.

Li, Z., Pandit, S. and Deutscher, M.P. (1999) Maturation of 23S rRNA requires the exoribonuclease RNase T. *RNA* **5**:139–146.

Li, Z., Pandit, S., and Deutscher, M. P. (1998) Polyadenylation of stable RNA precursors *in vivo*. *Proceedings of the National Academy of Sciences of the United States of America* **95**: 12158–12162.

Li, Z., Reimers, S., Pandit, S., & Deutscher, M. P. (2002) RNA quality control: degradation of defective transfer RNA. *The EMBO Journal* **21**: 1132–1138.

Licatalosi, D.D., Mele, A., Fak, J.J., Ule, J., Kayikci, M., Chi, S.W., Clark, T.A., Schweitzer, A.C., Blume, J.E., Wang, X., Darnell, J.C., and Darnell, R.B. (2008) HITS-CLIP yields genome-wide insights into brain alternative RNA processing. *Nature* **456**: 464–469.

Link, T. M., Valentin-Hansen, P., and Brennan, R. G. (2009) Structure of *Escherichia coli* Hfq bound to polyriboadenylate RNA. *Proc. Natl. Acad. Sci. U S A* **106**: 19292–19297.

Lioliou, E., Sharma, C. M., Caldelari, I., Helfer, A.-C., Fechter, P., Vandenesch, F., Vogel, J., and Romby, P. (2012) Global Regulatory Functions of the *Staphylococcus aureus* Endoribonuclease III in Gene Expression. *PLoS Genetics* **8**: e1002782.

Ma, Z., Richard, H., Tucker, D.L., Conway, T., and Foster, J.W. (2002) Collaborative regulation of *Escherichia coli* glutamate-dependent acid resistance by two AraC-like regulators, GadX and GadW (YhiW). *J Bacteriol* **184**: 7001–7012.

Mackie, G.A. (1998) Ribonuclease E is a 50-end-dependent endonuclease. *Nature* **395**: 720–723.

Mackie, G.A. (2013) RNase E: at the interface of bacterial RNA processing and decay. *Nat Rev Microbiol* **11**:45-57.

MacRae, I.J., and Doudna, J.A. (2007) Ribonuclease revisited: structural insights into ribonuclease III family enzymes. *Curr Opin Struc Biol* **17**: 138–145.

Massé, E., and Gottesman, S. (2002) A small RNA regulates the expression of genes involved in iron metabolism in Escherichia coli. *Proc Natl Acad Sci U S A* **99**: 4620-4625.

Massé, E., Escorcia, F. E., Gottesman, S. (2003) Coupled degradation of a small regulatory RNA and its mRNA targets in *Escherichia coli*. *Genes Dev* **17**: 2374–2383.

Mathy, N., Benard, L., Pellegrini, O., Daou, R., Wen, T., and Condon, C. (2007) 5'-to-3' exoribonuclease activity in bacteria: role of RNase J1 in rRNA maturation and 5' stability of mRNA. *Cell* **129**: 681-692.

Mathy, N., Benard, L., Pellegrini, O., Daou, R., Wen, T., and Condon, C. (2007) 5′-to-3′ exoribonuclease activity in bacteria: role of RNase J1 in rRNA maturation and 5′ stability of mRNA. *Cell* **129**: 681–692.

Matsunaga, J., Simons, E.L., and Simons, R.W. (1996) RNase III autoregulation: structure and function of *rncO*, the posttranscriptional 'operator'. *RNA* **2**: 1228–1240.

McDowall, K.J., Hernandez, R.G., Lin-Chao, S., and Cohen, S.N. (1993) The *ams-1* and *rne-3071* temperature-sensitive mutations in the *ams* gene are in close proximity to each other and cause substitutions within a domain that resembles a product of the *Escherichia coli mre* locus. *J Bacteriol* **175**: 4245–4249.

McDowall, K.J., Lin-Chao, S., and Cohen, S.N. (1994) A+U content rather than a particular nucleotide order determines the specificity of RNase E cleavage. *J Biol Chem* **269**: 10790 – 10796.

Meng, W., and Nicholson, A.W. (2008) Heterodimer-based analysis of subunit and domain contributions to double-stranded RNA processing by *Escherichia coli* RNase III *in vitro*. *Biochem J* **410**: 39–48.

Miczak, A. Srivastava, R. A., and Apirion, D. (1992) Location of the RNA-processing enzymes RNase III, RNase E and RNase P in the *Escherichia coli* cell. *Mol. Microbiol* **5**: 1801–1810.

Misra, A., Ou, J., Zhu, L. J., and Green, M. R. (2015) Global analysis of CPSF2-mediated alternative splicing: Integration of global iCLIP and transcriptome profiling data. *Genomics Data* **6**: 217–221.

Misra, T.K., and Apirion, D. (1979) RNase E, an RNA processing enzyme from *Escherichia coli*. *J. Biol. Chem* **254:** 11154–11159.

Mitschke, J., Georg, J., Scholz, I., Sharma, C.M., Dienst, D., Bantscheff, J., Voss, B., Steiglich, C., Wilde, A., Vogel, J., and Hess, W.R. (2011) An experimentally anchored map of transcriptional start sites in the model cyanobacterium *Synechocystis* sp. PCC6803. *Proc Natl Acad Sci USA* **108**: 2124-2129.

Moll, I., Afonyushkin, T., Vytvytska, O., Kaberdin, R.V., and Blasi, U. (2003) Coincident Hfq bind- ing and RNase E cleavage sites on mRNA and small regulatory RNAs. *RNA* **9**: 1308–1314.

Møller, T., Franch, T., Højrup, P., Keene, D.R., Bächinger, H.P., Brennan, R.G., and Valentin-Hansen, P. (2002) Hfq: a bacterial Sm-like protein that mediates RNA-RNA interaction. *Mol Cell* **9**: 23-30.

Morita, T., and Aiba, H. (2011) RNase E action at a distance: degradation of target mRNAs mediated by an Hfq-binding small RNA in bacteria. *Genes Dev* **25**: 294-298.

Morita, T., Maki, K., and Aiba H. (2005) RNase E-based ribonucleoprotein complexes: mechanical basis of mRNA destabilization mediated by bacterial noncoding RNAs. *Genes Dev* **19**: 2176–2186.

Morita, T., Mochizuki, Y., and Aiba, H. (2006) Translational repression is sufficient for gene silencing by bacterial small noncoding RNAs in the absence of mRNA destruction, *Proc. Natl. Acad. Sci. U S A* **103**: 4858–4863.

Murashko, O.N., Kaberdin, V.R., and Lin-Chao, S. (2012) Membrane binding of *Escherichia coli* RNase E catalytic domain stabilizes protein structure and increases RNA substrate affinity. *Proc. Natl. Acad. Sci. U S A* **109**: 7019–7024.

Ohmori, M. (1989) cAMP in *Anabaena cylindrica*: rapid changes in cellular levels in response to changes in extracellular environments. *Plant Cell Physiol* **30**: 911-914.

Olmedo, G., and Guzman, P. (2008) Mini-III, a fourth class of RNase III catalyses maturation of the *Bacillus subtilis* 23S ribosomal RNA. *Mol Microbiol* **68**: 1073–1076.

Opdyke, J.A., Fozo, E.M., Hemm MR, and Storz, G. (2011) RNase III participates in GadY-dependent cleavage of the gadX-gadW mRNA. *J Mol Biol* **406**: 29–43.

Opdyke, J.A., Kang, J.G., and Storz, G. (2004) GadY, a small-RNA regulator of acid response genes in *Escherichia coli. J Bacteriol* **186**: 6698– 6705.

Otaka, H., Ishikawa, H., Morita, T., and Aiba, H. (2011) PolyU tail of rho-independent terminator of bacterial small RNAs is essential for Hfq action. *Proc. Natl. Acad. Sci. U S A* **108**: 13059–13064.

Ow, M.C, Perwez, T., and Kushner, S.R. (2003) RNase G of *Escherichia coli* exhibits only limited functional overlap with its essential homologue, RNase E. *Mol. Microbiol* **49**: 607–622.

Ow, M.C., and Kushner, S.R. (2002) Initiation of tRNA maturation by RNase E is essential for cell viability in *E. coli*. *Genes Dev* **16**: 1102–1115.

Ow, M.C., Liu, Q., and Kushner, S.R. (2000) Analysis of mRNA decay and rRNA processing in *Escherichia coli* in the absence of RNase E-based degradosome assembly. *Mol Microbiol* **38**: 854–866.

Pertzev, A.V., and Nicholson, A.W. (2006) Characterization of RNA sequence determinants and antideterminants of processing reactivity for a minimal substrate of *Escherichia coli* ribonuclease III. *Nucleic Acids Res* **34**: 3708–3721.

Pfeiffer, V., Papenfort, K., Lucchini, S., Hinton, J.C., and Vogel, J. (2009) Coding sequence targeting by MicC RNA reveals bacterial mRNA silencing downstream of translational initiation. *Nat. Struct. Mol. Biol* **16**: 840–846.

Portier, C., Dondon, L., Grunberg-Manago, M., and Regnier, P. (1987) The first step in the functional inactivation of the *Escherichia coli* polynucleotide phosphorylase messenger is a ribonuclease III processing at the 5′ end. *EMBO J* **6**: 2165–2170.

Preußer, C., Rossbach, O., Hung, L.-H., Li, D., and Bindereif, A. (2014) Genome-wide RNA-binding analysis of the trypanosome U1 snRNP proteins U1C and U1-70K reveals *cis*/*trans*-spliceosomal network. *Nucleic Acids Research* **42**: 6603–6615.

Prévost, K., Desnoyers, G., Jacques, J.F., Lavoie, F., and Masse, E. (2011) Small RNA-induced mRNA degradation achieved through both translation block and activated cleavage. *Genes Dev* **25**: 385-396.

Prévost, K., Salvail, H., Desnoyers, G., Jacques, J.F., Phaneuf, E., and Massé, E. (2007) The small RNA RyhB activates the translation of *shiA* mRNA encoding a permease of shikimate, a compound involved in siderophore synthesis. *Mol. Microbiol* **4**: 1260–1273.

Prud'homme-Genereux, A., Beran, R.K., Iost, I., Ramey, C.S., Mackie, G.A., and Simons R.W. (2004) Physical and functional interactions among RNase E, polynucleotide phosphorylase and the cold-shock protein, CsdA: evidence for a 'cold shock degradosome'. *Mol Microbiol* **54**: 1409 – 1421.

Purusharth, R.I., Klein, F., Sulthana, S., Jäger, S., Jagannadham, M.V., Evguenieva-Hackenberg, E., Ray, M.K., and Klug, G. (2005) Exoribonuclease R interacts with endoribonu- clease E and an RNA helicase in the psychrotrophic bacterium *Pseudomonas syringae* Lz4W. *J Biol Chem* **280**:14572–14578.

Redko, Y., Bechhofer, D.H., and Condon C (2008) Mini-III, an unusual member of the RNase III family of enzymes, catalyses 23S ribosomal RNA maturation in *B. subtilis. Mol Microbiol* **68**: 1096–1106.

Redko, Y., Tock, M.R., Adams, C.J., Kaberdin, V.R., Grasby, J.A., and McDowall, K.J. (2003) Determination of the catalytic parameters of the N-terminal half of *Escherichia coli* ribonuclease E and the identification of critical functional groups in RNA substrates. *J Biol Chem*. **278**: 44001–44008.

Régnier, P., and Grunberg-Manago, M. (1989) Cleavage by RNase III in the transcripts of the *met Y-nus-A-infB* operon of *Escherichia coli* releases the tRNA and initiates the decay of the downstream mRNA. *J. Mol. Biol* **210**: 293-302.

Rivers, C., Idris, J., Scott, H., Rogers, M., Lee, Y.B., Gaunt, J., Phylactou, L., Curk, T., Campbell, C., Ule, J., Norman, M., and Uney, J.B. (2015) iCLIP identifies novel roles for SAFB1 in regulating RNA processing and neuronal function. *BMC Biol* **13**: 111.

Robertson, H.D., Webster, R.E., and Zinder, N.D. (1968) Purification and properties of ribonuclease III from *Escherichia coli*. *J Biol Chem* **243**: 82–91.

Rossbach, O. (2012) Genomewide analyses of hnRNP L function: an autoregulatory mechanism amd novel roles in RNA processing. *Doctoral Thesis* Justus-Liebig-Universität Giessen.

Rossbach, O., Hung, L.H., Khrameeva, E., Schreiner, S., König, J., Curk, T., Zupan, B., Ule, J., Gelfand, M.S., and Bindereif, A. (2014) Crosslinking-immunoprecipitation (iCLIP) analysis reveals global regulatory roles of hnRNP L. *RNA Biol* **11**: 146-55.

Rott, R., Zipor, G., Portnoy, V., Liveanu, V., and Schuster, G. (2003) RNA polyadenylation and degradation in cyanobacteria are similar to the chloroplast but different from *Escherichia coli. J Biol Chem* **278**:15771–15777.

Roy, M.K., Singh, B., Ray, B.K. and Apirion, D. (1983) Maturatio of 5-S rRNA: Ribonuclease E Cleavages and Their Dependence on Precursor Sequences. *European Journal of Biochemistry* **131**: 119–127.

Sakurai, I., Stazic, D., Eisenhut, M., Vuorio, E., Steglich, C., Hess, W.R., and Aro, E.M. (2012) Positive regulation of *psbA* gene expression by *cis*-encoded antisense RNAs in *Synechocystis* sp. PCC 6803. *Plant Physiol* **160**: 1000-1010.

Sauer, E., Schmidt, S., and Weichenrieder, O. (2012) Small RNA binding to the lateral surface of Hfq hexamers and structural rearrangements upon mRNA target recognition. *Proc. Natl. Acad. Sci. U S A* **109**: 9396–9401.

Savakis, P., De Causmaecker, S., Angerer, V., Ruppert, U., Anders, K., Essen, L.-O. and Wilde, A. (2012) Light-induced alteration of c-di-GMP level controls motility of *Synechocystis* sp. PCC 6803. *Molecular Microbiology* **85**: 239–251.

Schirrmeister, B.E., Antonelli, A., and Bagheri, H.C. (2011) The origin of multicellularity in cyanobacteria. *BMC Evol Biol* **11**: 45-66.

Schumacher, M. A., Pearson, R. F., Møller, T., Valentin-Hansen, P., and Brennan, R. G. (2002) Structures of the pleiotropic translational regulator Hfq and an Hfq-RNA complex: a bacterial Sm-like protein. *EMBO J* **21**: 3546–3556.

Schürgers, N. (2014) Funktion und Lokalisation von Hfq in *Synechocystis* sp. PCC 6803. *Doctoral Thesis* Justus-Liebig-Universität Giessen.

Schürgers, N., Ruppert, U., Watanabe, S., Nürnberg, D.J., Lochnit, G., Dienst, D., Mullineaux, C.W., and Wilde, A. (2014) Binding of the RNA chaperone Hfq to the type IV pilus base is crucial for its function in *Synechocystis* sp. PCC 6803. *Mol Microbiol* **92**: 840-852.

Sharwood, R.E., Halpert, M., Luro, S., Schuster, G., and Stern, D.B. (2001) Chloroplast RNase J compensates for inefficient transcription termination by removal of antisense RNA. *RNA* **17**: 2165-2176.

Shuck, A., Diwa, A., and Belasco, J.G. (2009) RNase E autoregulates its synthesis in *Escherichia coli* by binding directly to a stem-loop in the *rne* 5'-untranslated region. *Mol. Microbiol* **72**: 470–478.

Silva, I.J., Saramago, M., Dressaire, C., Domingues, S., Viegas, S.C., and Arraiano, C.M. (2011) Importance and key events of prokaryotic RNA decay: the ultimate fate of an RNA molecule. *Wiley Interdiscip Rev RNA* **2**: 818-36.

Singh, D., Chang, S.J., Lin, P.H., Averina, O.V., Kaberin, V.R., and Lin-Chao, S. (2009) Regulation of ribonuclease E activity by the L4 ribosomal protein of *Escherichia coli. Proc. Natl Acad. Sci. U S A* **106**: 864–869.

Srivastava, A.K., and Schlessinger, D. (1990) Mechanism and regulation of bacterial

ribosomal RNA processing. *Annu. Rev. Microbiol* **44**: 105-129.

Stanier, R.Y., Kunisawa, R., Mandel, M., and Cohen-Bazire, G. (1971) Purification and properties of unicellular blue-green algae (order Chroococcales). *Bacteriol Rev* **35**: 171-205.

Stazic, D., Lindell, D., and Steglich, C. (2011) Antisense RNA protects mRNA from RNase E degradation by RNA-RNA duplex formation during phage infection. *Nucleic Acids Res* **39**: 4890-4899.

Stead, M.B., Marshburn, S., Mohanty, B.K., Mitra, J., Pena Castillo, L., Ray, D., van Bakel, H., Hughes, T.R., and Kuschner, S.R. (2011) Analysis of *Escherichia coli* RNase E and RNase III activity *in vivo* using tiling microarrays. *Nucleic Acids Res* **39**: 3188–3203.

Steglich, C., Lindell, D., Futschik, M., Rector, T., Steen, R., and Chisholm, S.W. (2010) Short RNA half-lives in the slow-growing marine cyanobacterium *Prochlorococcus*. *Genome Biol* **11**: R54.

Stork, M., Di Lorenzo, M., Welch, T.J., and Crosa, J.H. (2007) Transcription termination within the iron transport-biosynthesis operon of *Vibrio anguillarum* requires an antisense RNA. *J. Bacteriol* **189**: 3479–3488.

Storz, G., Vogel, J., and Wassarman, K.M. (2011) Regulation by small RNAs in bacteria: expanding frontiers. *Mol Cell* **43**: 880-891.

Studier, F.W. (1975) Genetic mapping of a mutation that causes ribonucleases III deficiency in *Escherichia coli*. *J Bacteriol* **124**: 307-16.

Sugimoto, Y., König, J., Hussain, S., Zupan, B., Curk, T., Frye, M., and Ule, J. (2012) Analysis of CLIP and iCLIP methods for nucleotide-resolution studies of protein-RNA interactions. *Genome Biology* **13**: R67.

Sun, J., Xu, Q., Chitnis, V.P., Jin, P., and Chitnis, P.R. (1997) Topography of the photosystem I core proteins of the cyanobacterium *Synechocystis* sp. PCC 6803. *J Biol Chem* **272**: 21793-21802.

Terauchi, K., and Ohmori, M. (1999) An adenylate cyclase, Cya1, regulates cell motility in the cyanobacterium *Synechocystis* sp. PCC 6803. *Plant Cell Physiol* **40**: 248-251.

Tock, M.R., Walsh, A.P., Carroll, G., and McDowall, K.J. (2000) The CafA protein required for the 5′-maturation of 16S rRNA is a 5′-end-dependent ribonuclease that has context-dependent broad sequence specificity. *J. Biol. Chem* **275**: 8726–8732.

Torres-Quesada, O., Reinkensmeier, J., Schlüter, J.-P., Robledo, M., Peregrina, A., Giegerich, R., Toro, N., Becker, A., and Jiménez-Zurdo, J.I. (2014) Genome-wide profiling of Hfq-binding RNAs uncovers extensive post-transcriptional rewiring of major stress response and symbiotic regulons in *Sinorhizobium meliloti*. *RNA Biology* **11**: 563–579.

Tree, J. J., Granneman, S., McAteer, S. P., Tollervey, D., and Gally, D. L. (2014) Identification of Bacteriophage-Encoded Anti-sRNAs in Pathogenic *Escherichia coli*. *Molecular Cell* **55**: 199–213.

Ughy, B., and Ajlani, G. (2004) Phycobilisome rod mutants in *Synechocystis* sp. Strain PCC6803. *Microbiology* **150**: 4147-4156.

Ule, J., Jensen, K., Mele, A., and Darnell, R.B. (2005) CLIP: a method for identifying protein-RNA interaction sites in living cells. *Methods* **37**: 376–386.

Ule, J., Jensen, K.B., Ruggiu, M., Mele, A., Ule, A., and Darnell, R.B. (2003) CLIP identifies Nova-regulated RNA networks in the brain. *Science* **302**: 1212–1215.

Updegrove, T. B., Correia, J. J., Chen, Y., Terry, C., and Wartell, R. M. (2011) The stoichiometry of the *Escherichia coli* Hfq protein bound to RNA. *RNA* **17**: 489–500.

Urlaub, H., Hartmuth, K., and Lührmann, R. (2002) A two-tracked approach to analyze RNA-protein crosslinking sites in native, nonlabeled small nuclear ribonucleoprotein particles. *Methods* **26**: 170–181.

Vanderpool, C.K., Balasubramanian, D., Lloyd, C.R. (2011) Dual-function RNA regulators in bacteria. *Biochimie* **93**: 1943-1949.

Vanzo, N.F., Li, Y.S., Py, B., Blum, E., Higgins, C.F., Raynal, L.C., Krish, H.M., and Carpousis, A.J. (1998) Ribonuclease E organizes the protein interactions in the *Escherichia coli* RNA degradosome. *Gene Dev* **12**: 2770–2781.

Viegas, S.C., and Arraiano, C.M. (2008) Regulating the regulators: How ribonucleases dictate the rules in the control of small non-coding RNAs. *RNA Biol* **5**: 230–243.

Vogel, J., and Papenfort, K. (2006) Small non-coding RNAs and the bacterial outer membrane. *Curr Opin Microbiol* **9**: 605-611.

Wachi, M., Umitsuki, G., and Nagai, K. (1997) Functional relationship between *Escherichia coli* RNase E and the CafA protein. *Mol. Gen. Genet* **253**: 515–519.

Wachi, M., Umitsuki, G., Shimizu, M., Takada, A., and Nagai, K. (1999) *Escherichia coli cafA* gene encodes a novel RNase, designated as RNase G, involved in processing of the 5′ end of 16S rRNA. *Biochem. Biophys. Res. Commun* **259**: 483–488.

Wagner, E.G. (2009) Kill the messenger: bacterial antisense RNA promotes mRNA decay, *Nat. Struct. Mol. Biol* **16**: 804–806.

Wagner, E.G., Altuvia, S., and Romby, P. (2002) Antisense RNAs in bacteria and their genetic elements. *Adv Genet* **46**: 361–398.

Wang, Z., Kayikci, M., Briese, M., Zarnack, K., Luscombe, N.M., Rot, G., Zupan, B., Curk, T., and Ule, J. (2010) iCLIP predicts the dual splicing effects of TIA-RNA interactions. *PLoS Biol* **8**: e1000530.

Wassarman, K.M. (2002) Small RNAs in bacteria: diverse regulators of gene expression in response to environmental changes. *Cell* **109**:141-144.

Waters, L.S., and Storz, G. (2009) Regulatory RNAs in bacteria. *Cell* **136**: 615-628.

Whitton, B.A., and Potts, M. (2012) Introduction to the cyanobacteria. In: Ecology of cyanobacteria II. *Springer, Dordrecht* 1–13.

Wurtmann, E.J., and Wolin, S.L. (2010) A role for a bacterial ortholog of the Ro autoantigen in starvation-induced rRNA degradation. *Proc Natl Acad Sci U S A* **107**: 4022–4027.

Yoshimura, H., Hisabori, T., Yanagisawa, S., and Ohmori, M. (2000) Identification and characterization of a novel cAMP receptor protein in the cyanobacterium *Synechocystis* ap. PCC 6803. *The Journal of Biological Chemistry* **275**:6241-6245.

Zeng, Q., and Sundin, G.W. (2014) Genome-wide identification of Hfq-regulated small RNAs in the fire blight pathogen *Erwinia amylovora* discovered small RNAs with virulence regulatory function. *BMC Genomics* **15**: 414-433.

Zhang, A., Schu, D. J., Tjaden, B. C., Storz, G., and Gottesman, S. (2013) Mutations in interaction surfaces differentially impact *E. coli* Hfq association with small RNAs and their mRNA targets. *J. Mol. Biol* **425**: 3678-3697.

Zhang, H., Kolb, F.A., Jaskiewicz, L., Westhof, E., and Filipowicz, W. (2004) Single processing center models for human Dicer and bacterial RNase III. *Cell* **118**: 57–68.

Zhang, J.Y., Deng, X.M., Li, F.P., Wang, L., Huang, Q.Y., Zhang, C.C., and Chen, W.L. (2014) RNase E forms a complex with polynucleotide phosphorylase in cyanobacteria via a cyanobacterial-specific nonapeptide in the noncatalytic region. *RNA* **20**: 568-579.

Zhang, K., and Nicholson, A.W. (1997) Regulation of ribonuclease III processing by double-helical sequence antideterminants. *P Natl Acad Sci U S A* **94**: 13437–13441.

Zilhão, R., Cairrão, F., Régnier, P., and Arraiano, C.M. (1996) PNPase modulates RNase II expression in *Escherichia coli*: implications for mRNA decay and cell metabolism. *Mol Microbiol* **20**: 1033–1042.

Zuo, Y., and Deutscher, M. P. (2001) Exoribonuclease superfamilies: structural analysis and phylogenetic distribution. *Nucleic Acids Research* **29**: 1017–1026.